Prateek Gupta

Ship Performance Monitoring using In-service Measurements and Big Data Analysis Methods

Doctoral thesis

Prateek Gupta

NTNU
Norwegian University of
Science and Technology
Thesis for the degree of
Philosophiae Doctor
Faculty of Engineering
Department of Marine Technology

NTNU
Norwegian University of
Science and Technology

NTNU
Norwegian University of
Science and Technology

NTNU

Prateek Gupta

Ship Performance Monitoring using In-service Measurements and Big Data Analysis Methods

Thesis for the degree of Philosophiae Doctor

Trondheim, March 2022

Norwegian University of Science and Technology
Faculty of Engineering
Department of Marine Technology

NTNU
Norwegian University of
Science and Technology

Abstract

Ship performance monitoring is quite important for ship owners as well as charter parties to optimize their profits. Moreover, the regulatory organizations, like IMO, has also become interested here in order to maintain the economic growth around the world while reducing the green house gas (GHG) emissions, primarily to hinder the effects of global warming. IMO has set several emission reduction targets until 2050 to limit the rise of global temperature. The performance of ships, therefore, needs to be optimized if these targets are to be achieved, and to ensure optimal performance for a ship over its entire life, it is required to develop reliable methods to continuously monitor its performance.

The current work focuses on developing data-driven methods for ship performance monitoring using the high frequency in-service data recorded onboard the ships. The data-driven methods, namely, Principal Component Regression (PCR), Partial Least Squares Regression (PLSR) and probabilistic Artificial Neural Network (probabilistic ANN), are calibrated using the in-service data. Linear methods, PCR and PLSR, are enhanced with some non-linear transformations, obtained from the domain knowledge, to capture the non-linearities in the ship's hydrodynamic model.

A data processing framework is developed and streamlined to process the in-service data. Principal Component Analysis (PCA) is used for preliminary data analysis tasks, like correlation study, variable selection and outlier detection. A statistical hydrodynamic performance indicator, in the form of generalized admiralty coefficient ($\Delta^m V^n / P_s$), for ships is established. The performance indicator is further used in the data-driven models to formulate a fouling growth factor (FGF), accounting for the fouling growth on the ship's hull and propeller.

The calibrated data-driven models are used to predict the change in performance for two ships over several propeller and hull cleaning events. The results indicate improvement in the performance of at least one of the ships for almost all

the cleaning events, with the highest improvement predicted for the hull cleaning event, which is as expected. Moreover, the linear methods with non-linear transformations produced comparable results with the fully non-linear method, indicating that the problem can be solved using transparent and interpretable linear methods.

Acknowledgements

List of Publications

The following papers are included as part of this thesis:

1. Gupta P., Kim Y.-R., Steen S., Rasheed A. Data Processing Framework for Ship Performance Analysis. Submitted to Ocean Engineering.
   DOI: 10.13140/RG.2.2.35775.38567.

2. Gupta P., Steen S., Rasheed A. Big Data Analytics As a Tool to Monitor Hydrodynamic Performance of a Ship. Proceedings of the ASME 2019 38th International Conference on Ocean, Offshore and Arctic Engineering. Volume 7A: Ocean Engineering. Glasgow, Scotland, UK. June 9-14, 2019.
   DOI: 10.1115/OMAE2019-95815.
   The copy of this article attached here (Article 2) includes some minor corrections which are not incorporated in the published version available at the given DOI.

3. Gupta P., Taskar B., Steen S., Rasheed A. Statistical Modeling of Ship's Hydrodynamic Performance Indicator, Applied Ocean Research 111 (2021) 102623.
   DOI: 10.1016/j.apor.2021.102623.

4. Gupta P., Rasheed A., Steen S. Ship Performance Monitoring using Machine-learning. Accepted for publication in Ocean Engineering.
   DOI: 10.13140/RG.2.2.18166.52809.

Contents

Introduction

This chapter presents the motivation of the study along with the background. Further, the structure of this thesis is outlined.

1.1 Background & Motivation

In line with the Paris agreement on climate change (2015), the International Maritime Organization (IMO) proposed a set of short-, mid- and long-term targets in 2018 to reduce the impact of maritime transport on the climate change. It is the aim of IMO to bring down the total annual greenhouse gas (GHG) emissions by 2050 to at least half of the emissions in 2008, where the carbon intensity is supposed to be at least 40% lower by 2030 and 70% lower by 2050. The transportation of goods by ships, i.e., the maritime transport work is projected to increase by 40-100% between 2018 and 2050, according to the simulated scenarios presented in the fourth IMO GHG study (2020). Thus, to achieve IMO's emission targets, the industry needs to consider all possible emission abatement technologies, including energy-saving technologies, use of renewable energy and alternative fuels, and reducing the speed of ships.

Such extreme targets may only be achieved if shipping as a complete process is optimized. The reason for this is quite clear from a broader perspective. As of 2018, it is reported in the fourth IMO GHG study that shipping only contributes to about 2.89% of the global anthropogenic emissions. Owing to this small share and a limited supply of renewable energy and green alternative fuels, the shipping industry would have to heavily bank upon the other alternatives for emission abatement, i.e, energy-saving technologies and reducing the speed of ships. In other words,

shipping as a process has to become far more energy efficient. The energy efficiency of shipping can be increased to a certain extent by designing and operating energy efficient ships. In order to increase the operational efficiency of an individual ship as well as recognize an energy efficient design for a ship, it is required to develop reliable systems to continuously monitor the operational performance of sea-going ships. A continuous performance monitoring system would not only enable the stake holders to make well informed decisions regarding the scheduled maintenance of their ships, but it would also help them identify the energy efficient ship designs by analyzing the data from their fleet.

In today's fast-moving industrial world, it is nearly impossible to micro-manage valuable industrial assets like ships, and therefore, it can be challenging to continuously monitor their performance and energy efficiency. Fortunately, with the advancements in science and technology, it is now possible to obtain a fairly continuous stream of in-service data from a sea-going ship, enabling us to imagine and develop concepts like digital twin. With the help of digital twin technology, it seems possible to develop digitized systems which can empower the industry and provide effective solutions to manage fleets of ships with ease. To ensure high energy efficiency, the digital twin of a ship can be used to establish autonomous or semi-autonomous (depending on the capability of the digital twin) data-driven systems for continuous performance monitoring as well as predictive maintenance of the ship. The current research can be seen as a step towards realizing the digital twin for ships, by developing some of the building blocks required to create the digital twin for a sea-going ship.

As mentioned above, the in-service data recorded onboard a sea-going ship can be utilized to develop continuous ship performance monitoring systems. The in-service data is generally recorded by a number of sensors installed onboard the ship. The data collected from individual sensors can be collected, assimilated and sent to shore-based control centers, with the help of data acquisition (DAQ) systems, for further processing and analysis. The primary aim of the current research is to establish data-driven methods for ship performance monitoring using the in-service data. Even though it may be possible to integrate some simple data processing within the DAQ system, the data obtained at the control center would still need a good amount of cleaning and processing to carry-out any further analysis. Therefore, a data processing framework is also established along with a set of data-driven methods, which can be used for ship performance monitoring.

1.2 Literature Review

A good amount of research has already been done to establish models for ship performance monitoring, some more reliable than the others. It has even been

attempted to standardize the procedure to measure the change in performance of the hull and propeller of a ship (ISO (2016)). The ISO standard suggests to use the near-calm-water filtered in-service data to estimate the speed-loss due to the degradation of ship's performance. Several researchers accepted ISO (2016) positively and implemented their models based on it, whereas other proposed their own methods and claimed improvement over ISO (2016). Koboević et al. (2019) used high frequency in-service data, filtered according to the procedure outlined in ISO (2016), for ship performance monitoring based on the ship's speed-loss and fuel consumption. Coraddu et al. (2019) reported an improvement over ISO (2016) using a data-driven approach based on the principles of digital twin to estimate the speed-loss of the ship due to fouling growth.

1.2.1   Key Performance Indices (KPIs)

The biggest weakness of ISO (2016) is, probably, its unilateral advocacy for speed-loss as a key performance indicator (KPI) to monitor the hydrodynamic performance of a ship. Using speed-loss as a KPI needs an accurate measure or estimate of the speed-through-water of the ship which may be difficult to achieve due to several problems, as cited by Dalheim and Steen (2021). Moreover, ISO (2016), in the current state, only suggests correcting the filtered data for the remaining wind loads, the correction for remaining wave loads are expected to be incorporated in future revisions. Therefore, it may be argued that there is a good scope for improvement here.

Looking at the KPIs, a wide range of alternatives have been tried-out. The second most obvious alternative, which is also acknowledged in ISO (2016), is the change in power demand. Carchen and Atlar (2020) suggested using the change in power demand along with three other KPIs, including two wake-based KPIs and the fouling coefficient, to monitor the hydrodynamic performance of ships. In a previous article, Carchen et al. (2017) demonstrated that power-based KPIs are robust, easy to interpret and have relatively low uncertainty. Moreover, it is the only KPI, out of the all four, which can be directly measured, and for estimating the other three KPIs, several other details regarding the ship are required with a good enough accuracy. Nevertheless, other viable options for KPIs, demonstrated in literature, include fuel consumption (Koboević et al. (2019)), resistance (or fouling) coefficient (Munk (2016); Foteinos et al. (2017); Carchen and Atlar (2020)), propeller law coefficient (Foteinos et al. (2017)), admiralty coefficient (Ejdfors (2019)), wake fraction (Carchen and Atlar (2020)), energy (or fuel) efficiency (Lu et al. (2015); Kim et al. (2021)) and sand-grain roughness height (k_s; Oliveira et al. (2020)).

1.2.2   Ship Performance Monitoring

Another important aspect of ship performance monitoring is the adopted methodology. Based on the methodology, ship performance monitoring methods can be characterized as one of the following three: physics-based, data-driven and hybrid methods. In case of physics-based methods, the KPIs are calculated using a well-known relationship using one or many physics-based and/or empirical models. A physics-based method is, generally, based on the resistance model. Here, the total resistance is divided into resistance components, like calm-water, added wind, added waves, fouling friction, etc. There are several ways to estimate these individual components. Tsujimoto and Orihara (2018) developed a simulation-based physics-based model, using the equations of motion, ship's hydrodynamic coefficients and empirical methods for the estimation of added wind and wave resistance, to monitor the performance of a ship in actual seas. Foteinos et al. (2017) presented a far simpler model where the individual resistance components were estimated using physics-based empirical methods. Lu et al. (2015) presented a more advanced but similar approach for ship performance monitoring, using the modified Kwon's method (Kwon (2008)) to estimate the added resistance in wind and waves.

Although a physics-based method may not need any historical in-service data for training the model, it surely needs a lot of information regarding the design and shape of the ship, which sometimes can be hard to get. Moreover, unless the ship specific information is obtained using model tests and so on, the physics-based models may introduce some errors due to several assumed generalizations and applicability of physics-based empirical methods. A data-driven method can be used, on the other hand, to address some of these problems, but it would need a good amount of historical in-service data to train and validate the model before it can be used to produce any fruitful results. The popularity of data-driven methods is increasing many-folds with the advancement in technology, due to the easy availability of high frequency in-service data recorded onboard the ships. It should be noted that, unlike the belief of some researchers, a data-driven method is not always uninterpretable or opaque, a data-driven method is just based on statistics rather than the true physics. For instance, a fully transparent and interpretable linear regression method is also a data-driven method.

In case of data-driven methods, the KPIs are estimated directly or in-directly using a statistics-based data-driven model. In the above cited work by Coraddu et al. (2019), data-driven Extreme Learning Machine (ELM; Cambria et al. (2013)) models were used to estimate the speed-loss for a ship due to the growth of marine fouling. Karagiannidis and Themelis (2021) used artificial neural network (ANN) models to estimate the fuel consumption and speed-loss for a ship. Laurie et al.

(2021) used several different data-driven machine-learning models to estimate the increase in power demand of five sister ships over a period of 1 year. Although the data-driven methods are immensely powerful, they lack on important characteristics like transparency, interpretability as well as estimation of uncertainty in the model predictions. In view of that, several researcher demonstrated using domain knowledge to improve the data-driven approach, resulting in the creation of hybrid methods.

A hybrid method may use domain knowledge in the form of known relationships between different variables from our understanding of the physical model. In a probability-based hybrid modeling approach, Yoo and Kim (2019) presented Gaussian process and simple polynomial models, based on physics-based formulations, to predict the ship's speed and power. Here, the uncertainty in model predictions were also reported. Kim et al. (2021) demonstrated using domain knowledge along with curve fitting technique to perform variable section for an artificial neural network (ANN) and multiple linear regression (MLR) model used to predict the fuel efficiency of a ship. The hybrid modeling approach seems promising but much has to be explored before a solid conclusion can be made regarding its dominance over physics-based and data-driven models.

1.3   Thesis Structure

Chapter 2 lists the objectives formulated to guide this research.

Chapter 3 presents the research strategy. The scope of the work and limitations are also included here.

Chapter 4 presents the summary of publications contributing to this thesis along with the contribution of this research to the corresponding field.

Chapter 5 presents the conclusion of this research and ideas for future work.

Research Objectives

This chapter lists the objectives formulated to guide this research.

The main objective of this work is to establish and demonstrate the use of data-driven methods for ship performance monitoring. A ship performance monitoring system based-on data-driven methods is developed using the in-service data recorded onboard sea-going ships. The raw in-service data collected from a ship is known to have several problems, and therefore, it needs to be processed before carrying-out any further analysis. Moreover, in order to implement a data-driven method, it is mandatory to study, analyse and understand the correlation between data variables. It is also important to introduce an additional feature in a data-driven model to account for performance degradation of a ship due to factors like marine fouling. Thus, the final objective is, here, achieved in the following four main steps:

1. Development of a data processing framework

2. Data analysis and correlation study

3. Establishing a hydrodynamic performance indicator

4. Developing a data-driven ship performance monitoring system

The data processing framework filters-out, corrects and converts the raw in-service data into a usable dataset, with a good-enough quality, suitable for further analysis.

The data processing framework also takes into account all essential modeling assumptions adopted by the forthcoming analysis. Along with tasks like data cleaning and validation, the data processing framework also gathers, assimilates and absorbs data from supplementary sources, like weather hindcast, which are required for further analysis. Any additional features, which may be required for the analysis, are also derived during the data processing steps. The data processing framework along with several examples from existing datasets is presented for publication in Article 1.

The correlation study is carried-out in order to understand the correlation between different data variables. Here, the knowledge from the actual physical model of the problem-at-hand is also verified. This step is instrumental in performing important tasks like variable selection, which forms the basis for creating a data-driven model. The correlation study also helps to understand if the given dataset is of good-enough quality so that a reliable data-driven model can be calibrated using it. Article 2[1] presents the conducted correlation study, variable selection and outlier detect using the Principal Component Analysis (PCA) on a small dataset.

A statistics-based hydrodynamic performance indicator (presented in Article 3), in the form of generalized admiralty coefficient ($\Delta^m V^n / P_s$), is established for ships. The performance indicator can be used to monitor the hydrodynamic performance of sea-going ships with the help of in-service data recorded onboard the ships. The generalized admiralty coefficient is statistically fitted on the near-calm-water in-service data to obtain the displacement and speed exponents, m and n, respectively. Unlike the well-known traditional performance indicator for ships, i.e., fouling friction coefficient (ΔC_F), the generalized admiralty coefficient can be obtained solely from the in-service data recorded onboard the specific ship, without the use of any physics-based and/or empirical methods.

Several data-driven methods are demonstrated and established for ship performance monitoring and analysis. Models based-on the data-driven methods are calibrated using the in-service datasets, processed with the help of above mentioned data processing framework. The model architecture is based on the selected set of variables resulting from the correlation study. An additional feature to account for fouling growth on ship's hull and propeller is introduced using the above established hydrodynamic performance indicator. The calibrated models are further used to monitor the hydrodynamic performance of ships over a period of time, through several propeller and hull cleaning events. The change in performance of the ships due to these cleaning activities is evaluated to demonstrate the established

---

[1]The copy of Article 2 attached here includes some minor corrections which are not incorporated in the published version available at the given DOI.

ship performance monitoring system. Article 4 presents the calibrated data-driven models along with the predicted change in performance for two sister ships.

CHAPTER 3

Research Design

This chapter presents the research strategy. The scope of the work and limitations are also included here.

3.1 Research Strategy

The first step of a data-driven approach is to explore the data, to assess its quality and understand its potential. While starting from scratch it may be a good idea to use an already established dataset, which would be instrumental in developing some basic understanding regarding the dataset. This would help the researcher to think from the perspective of a data scientist who can utilize the different components (features and correlations) available in the dataset to begin with the research and start picturing about how to ultimately fulfill the task-at-hand. A similar approach is used for this work. A small subset of the data (containing only a single voyage), further referred to as the pilot dataset, is used here for getting started with the analysis.

The physical understanding of the problem is quite helpful while validating the relationship between data variables, i.e., inferring the expected correlation between the data variables, and verifying it by visualizing and analyzing the dataset. The first part of this work is, therefore, dedicated to study the correlations and perform validation on the aforementioned small or pilot dataset. The primary aim here is to instantiate a deep understanding of the data and correlation between the variables. The pilot dataset contained very few samples which made the task of data cleaning and processing quite easy. Moreover, in the absence of any established or unanimously adopted data processing guidelines for the given problem, the data cleaning

and processing used for the pilot dataset is further built-upon and streamlined to finally establish a data processing framework, which is later proven to be applicable for substantially large datasets.

Another important thing to keep in mind, while pursuing a data-driven approach, is the physical understanding of the problem, specially if the problem is well-researched in that direction. The concept of ship performance monitoring is very old and several models has been suggested to perform it, some more reliable than the others. Moreover, several physics-based and/or empirical methods constitute components of most of these models. In other words, some of the ship performance monitoring models are purely based on physics-based and/or empirical components, whereas the others take a hybrid approach, using data-driven machine-learning models along with physics-based and/or empirical components. Although the initial idea for the current research was to establish a purely data-driven approach, some physics-based and/or empirical methods (or components) are used here to enhance the reliability of results.

3.1.1   Data Acquisition

The current research is part of the Smart Maritime (237917/O30) project undertaken by the Center for Research-based Innovation (SFI), funded by the Research Council of Norway (RCN). The SFI Smart Maritime project constitute several industry partners, having deep interest in the research topic. The onboard recorded in-service datasets used for the current work are also supplied by some of these industry partners. As these datasets contain sensitive business information, they are treated as confidential, and therefore, only limited details are provided regarding the specifications of the ships on which the datasets were recorded.

In order to account for the environmental loads experienced by the ships, the weather hindcast (or metocean) data is obtained from the following three publicly available sources: (a) European Centre for Medium-Range Weather Forecasts (ECMWF), (b) Hybrid Coordinate Ocean Model (HYCOM), and (c) Copernicus Marine Environment Monitoring Service (CMEMS). These sources provide data variables covering information regarding the three main environmental loads, i.e., wind (from ECMWF), waves (from ECMWF) and sea currents (from HYCOM or CMEMS), as well as the geoid depth at the sea (from CMEMS) around the globe. The data files containing the data required for all the in-service datasets is downloaded on a local computer for further processing.

3.1.2   Data Analysis & Correlation Study

Principal Component Analysis (PCA) is used here to perform the initial data analysis and correlation study. There are several reasons for adopting PCA as the

stepping-stone for the current work. PCA is a very powerful as well as highly useful statistics-based unsupervised machine-learning method, which is generally used for dimensionality reduction. Despite being a simple method, it can be used to perform most of the preparatory tasks, like variable selection and outlier detection, required to be done before calibrating a data-driven machine-learning model. It should not be considered an exaggeration if one calls PCA a one-stop shop for all the basic data analysis.

One of the main objectives of the correlation study is to understand the relationship between different data variables. As in the current case, if the physical model of the problem is well-studied, the correlation study can be used to verify the physical relationship between the data variables and even obtain new information in this regard. In case of a regression problem, the variable selection is performed by studying the correlation of individual variables with the target variables. The data variables showing strong correlation with the target variables must be included in the model as the input variables. PCA allows us to visualize the correlation between all the data variables in graphical as well as tabular format, as shown later in section 4.1.2 and Article 2[1] (figure 12 & table 3). Thus, the task of variable selection can be performed here quite conveniently.

Another important aspect of data analysis and preparation for data-driven modeling is outlier detection. Data samples deviating marginally from the expected trends, defined by the correlation between the data variables, are suspected as outliers. They should be further investigated to understand their abnormal behavior. Such a task can also be performed easily using PCA. PCA operates by factorizing the given data matrix into a number of Principal Components (PCs). Each of these PCs assigns loadings to each data variable and scores to each data sample, as shown in Article 2 (equation 4). A data sample with a very high or a very small score, as compared to the rest of the data, can be suspected as an outlier. Moreover, it is possible to create diagnostic plots, called influence plots, in PCA for detecting outliers, as shown later in section 4.1.2 and Article 2 (figure 10). Article 2 (pages 9-10) also demonstrates the procedure to detect outliers, carrying-out further investigation and dealing with them.

3.1.3   Data Processing

In case of the pilot dataset, processing or preparing the dataset for further analysis is quite easy, as there are only a handful of samples which can be analyzed and closely investigated visually as well as analytically. Moreover, the high frequency ship propulsion datasets are generally characterized by several substantially long

---

[1]The copy of Article 2 attached here includes some minor corrections which are not incorporated in the published version available at the given DOI.

periods of quasi-steady state, i.e., the propulsive state, and therefore, the data variables recorded onboard the ship almost remains constant in deep seas due to unchanged control parameters, like shaft rpm, rudder angle, etc., and slowly varying weather conditions. Figure 3.1 shows the pilot dataset used at the beginning of this work. The work presented in Article 2 is based on the same dataset.

To process a large dataset covering several trips (or voyages) an automatic or semi-automatic approach must be formulated such that the data processing step can be performed in a reasonable amount of time. Keeping this in mind, the processing steps used for the pilot dataset were further studied and refined to formulate a data processing framework (presented in Article 1), both on paper and in terms of an executable piece of code. The major difference between the large dataset and the pilot dataset (used here) is that the latter contains only one trip, whereas the former is a continuous time-series of several trips. Thus, the first primary step suggested to process a large dataset is to divide the dataset into individual trips so that further processing steps can be carried-out, validated and visualized in trip-wise manner, making it easier for the user to handle the large amount of data.

The usual practice followed here is to create and save the trip-wise validation plots for all the critical data processing steps and later visually inspect the plots to detect any errors. Figure 3.1, in fact, shows the validation plots created during the trip division step for the same trip that constitutes the pilot dataset. Such validation practice ensures obtaining a high fidelity dataset for further analysis as well as detecting bugs in the executable code and algorithms written to process the data.
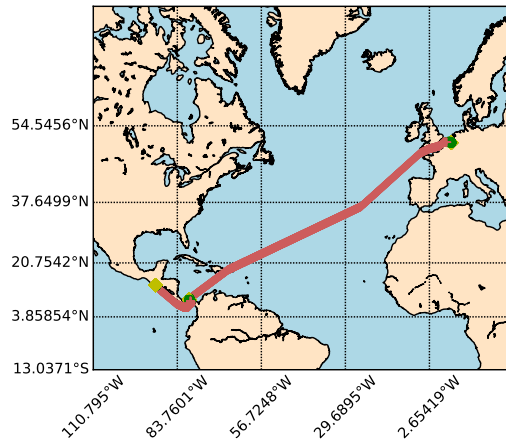
(a) Ship's trajectory.
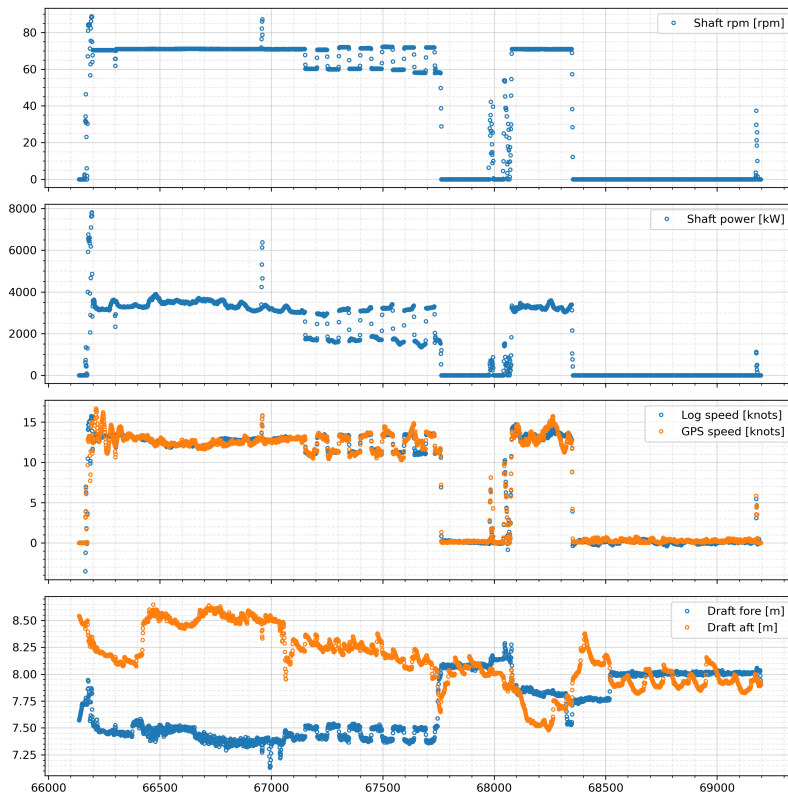
(b) Recorded time-series data.

Figure 3.1: The pilot dataset used at the beginning of the current work and for Article 2.

3.1.4 Methods & Techniques

Method selection is an important step in a data-driven approach. The field of machine-learning is known to have a wide variety of methods and algorithms, which can be used to solve several different problems. Thus, the method selection step can only be carried-out after briefly formulating the problem. In order to formulate the problem, the final objective of the task is considered and a research plan is constructed so that the problem can be solved using the available data.

Assessing the performance of a sea-going ship using the onboard recorded in-service data is a challenging task, mainly due to the varying environmental loads, vessel draft and even the control parameters (rpm, rudder angle, etc.). According to the research plan conceptualized here, first, the machine-learning models are calibrated on the in-service data from a ship, and then, the effect of varying parameters (cited above) are removed simply by predicting the operating point (speed and power) for the ship in a predefined ideal condition at different instants of time. The idea here is to predict the performance of the ship in the ideal condition using the underlying trend learned by the machine-learning model. The ideal condition is intentionally chosen here to be very close to the sea-trial condition so that a clear comparison can be drawn with the sea-trial data.

From the above discussion and our knowledge of the physical model, it is clear that the problem may be solved using a non-linear regression-based machine-learning method. The list of methods which can be used to accomplish such a task is still quite long, well evident from the vast amount of literature demonstrating the same. The well-known artificial neural network (ANN) is considered to be one of the best methods to handle such problems. It is even said that a particular class of feed-forward ANN, multilayer perceptron (MLP), can be considered as universal approximators, i.e., they can be used to approximate any function. But recently, ANN based models are criticized due to their esoteric nature and overfitting problem. In view of that, it is now-a-days a trend to use probabilistic machine-learning methods. Alternatively, it is also attempted to improve the existing ANN methods using probability, resulting in probabilistic ANN. One such method is used here to predict the performance of ships.

On another note, it is well-known that the hydrodynamic model of a ship is non-linear in nature, i.e., the hydrodynamic state variables are non-linearly correlated with one another. But at the same time, the ship hydrodynamics has been a research topic since several hundred years and a lot is known about the physical phenomenon, including the approximate non-linear relationships between the majority of these hydrodynamic state variables. Thus, it may be possible to use some simple non-linear transformations to model the hydrodynamic state of a ship using

a linear method. A linear method would not only results in a transparent model, but if proven good enough, it would also be preferred over the non-linear methods as it is generally recommended to solve a problem using the simplest method available.

Keeping the above in mind, a simple multivariate linear regression method based on Principal Component Analysis (PCA), known as Principal Component Regression (PCR), is adopted here. The advantage of using PCR over ordinary least squares (OLS) linear regression is that it will help address the problem of multi-collinearity, which may be important here as it is planned to use additional non-linearly transformed features here, and since PCR only uses the first few prominent Principal Components (PCs), it may inherently remove some undesired noise from the data, by way of removing the last remaining PCs representing noise in the data. Another popular multivariate linear regression method, known as Partial Least Squares Regression (PLSR), is used here. PLSR is said to be an improvement over PCR as it organizes the obtained PCs (or factors in PLSR) in the diminishing order of correlation with the target variables, generally resulting in improved performance.

3.1.5 Time-varying Performance

It is well-known that the performance of a ship varies with time due to factors like marine fouling as well as because of performing maintenance activities on the ship's hull and propeller from time to time. Such variation in performance of the ship affects the in-service data, and therefore, it should be taken into account while calibrating a data-driven model. In other words, the data-driven model must be supplied information regarding the extent of degradation of ship's hull and propeller due to the building-up of marine fouling, and it must also be informed when the hull and/or propeller of the ship is cleaned. Keeping this in mind, a fouling growth factor (FGF) is formulated as part of the current research, which is further used as an input feature (or variable) for the data-driven models.

The extent of fouling growth on a ship, and therefore, the FGF is a function of the rate of fouling growth in the geographical location where the ship is located, which in turn depends on the environmental condition at the given location at that particular time. In the absence of any well-known formulation for the fouling growth rate (FGR), a statistics-based hydrodynamic performance indicator, established during the current research, is used as an approximate measure for the fouling growth rate on the ship's hull and propeller. The performance indicator uses near-calm-water in-service data recorded onboard the ship to model the trends or rate of fouling growth on the ship. It is assumed here that the fouling growth rate for the hull and propeller at any particular time is the same.

3.2   Scope and Limitations

One of the main tasks here is to convert the high dimensional in-service data into a useful form, which can be used to calibrate machine-learning models. Thus, data cleaning, validation and processing is carried-out in order to obtain high fidelity datasets for further analysis. Several data-driven machine-learning models are calibrated to fit to the hydrodynamic state of the ships. The calibrated models are used to predict the hydrodynamic performance of sea-going ships over time and through several propeller and hull cleaning events.

The onboard recorded in-service data is supplemented by the weather hindcast data from different sources, like ECMWF, HYCOM and CMEMS, as explained in section 3.1.1. The hindcast data is interpolated to ship's given location at all the required timestamps. The interpolated data is validated to avoid any errors due to the inconsistencies in the sign and direction conventions between the hindcast and onboard recorded in-service data. The data variables obtained from hindcast sources are used to represent and estimate the environmental loads experienced by the ship.

From the hydrodynamics aspect, the scope of the project is limited to topics like prediction of ship speed-loss, increase in power demand over time, speed-powering variation and hull-propeller performance. However, in-depth analysis of propeller wake, sea keeping performance and sea state estimation from ship motions is considered out of the scope.

Research Summary

The summary of publications contributing to this thesis along with the contribution of this research to the corresponding field is presented here.

4.1 Summary of Publications

This PhD thesis is paper-based, i.e., the work done during this research is presented in the articles attached here. In total 4 articles are included here, of which 1 is conference and 3 are journal papers. The sequence of articles is almost aligned with the direction of the research, except for the article presenting the data processing framework (Article 1), which was listed as the first in the list of research objectives (chapter 2), but it is written and submitted (for publication) towards the end of this research. It should be noted here that developing a data processing framework requires time and experience, and as explained in section 3.1, the data processing framework was developed and further evolved after gaining some experience with the data. Therefore, a streamlined and well-refined data processing framework is established and submitted (for publication) towards the end of this research.

4.1.1   Article 1: Data Processing Framework

Based on the data processing experience gained here with the given datasets, a detailed data processing framework is developed and further streamlined. Article 1 presents the data processing framework as a flow diagram (shown in figure 4.1), briefly explaining all the processing steps. The data processing framework is designed to process the data obtained from different sources during a ship's voyages, like onboard recorded in-service data, AIS data and noon reports. The characteristics of these three data sources are explained briefly in Article 1 along with the common problem cited in them, demonstrated with examples from existing datasets. The paper also discusses the best practices which may be adopted for a reliable and robust ship performance analysis.

It is first recommended to divide the data into individual trips (or voyages) either using the propulsion state information (if available in the dataset) or using the shaft rpm and ship's speed-over-ground, if the port call information and GPS coordinates are not available. This would help create trip-wise visualizations and data segregation, resulting in easier data handling and interpretation of data time-series. Obtaining and interpolating weather hindcast (or metocean) data to ship's location in time is considered as an important step for data validation and estimation of environmental loads acting on the ship.

The interpolated hindcast data as well as the features (or variables) available in the in-service data may not be directly relevant for further analyses. For instance, the longitudinal and transverse wind speed components are definitely more relevant for a hydrodynamic analysis than the total wind speed and wind direction. Therefore, it may be a good idea to derive new features here which are better suited for further analyses.

The draft measurements recorded onboard the ship are known to have errors due to the Venturi effect, explained briefly in Article 4 and Article 1. Simple interpolation using the draft measurements from just before and after an individual trip, when the ship is not moving, is recommended to fix the measurements. A more complex algorithm is suggest in Article 1 for a case when the draft or trim is adjusted during a trip without reducing the vessel speed.

The resistance components corresponding to each data sample can be estimated using one of the several available physics-based and/or empirical methods. Adopting a particular method for a ship should be done after validating the applicability of the method, i.e., the method showing good agreement with the data from the ship in-service should be adopted. Here, the data from the ship in-service should be preferred over the sea-trial or model test results. Since the sea-trial is carried-
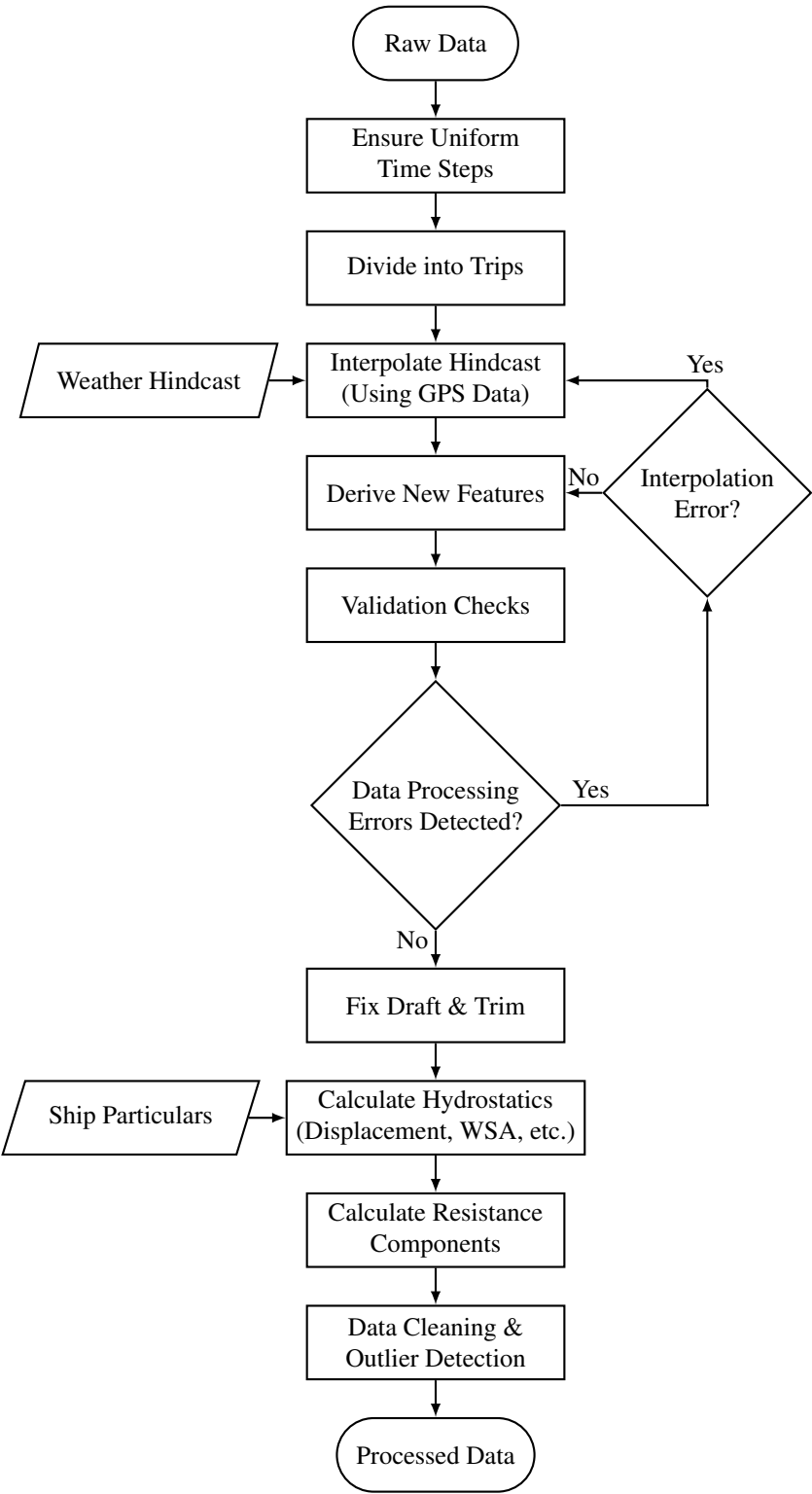
Figure 4.1: Data Processing Framework Flow Diagram.

out for only one displacement, and the model test results may not be very accurate due to scale effects, the validation with in-service data would result in a better fit for the whole speed-displacement domain for the ship.

The data processing framework presented in Article 1 (shown in figure 4.1) suggests to perform data cleaning and outlier detection towards the end of the processing. While preparing a dataset for a variety of analyses, the data cleaning may be dependent on the list of variables relevant for further analysis, and all the previous processing steps would be performed only once and does not depend on further analysis. Thus, some part of data cleaning should be performed again for a different analysis, with a different set of variables of interest. Moreover, it may be advantageous to have some additional variables, like interpolated hindcast, resistance components, etc., while analyzing suspected outliers.

4.1.2   Article 2: Data Analysis & Correlation Study

As explained in section 3.1.2, Principal Component Analysis (PCA) is used here for analyzing the data and correlation study. PCA is a matrix factorization algorithm which extracts the prominent structures or patterns from the data using the correlation between the data variables, in terms of so called Principal Components (PCs). Each of these PCs are characterized by correlation loadings (or direction cosines) and sample scores. The correlation loadings represent the direction of the PC in the high dimensional variable space, whereas the sample scores represent the distance or deviation of the sample from the PC direction. The correlation loadings can also be interpreted as the pattern extracted by the corresponding PC.
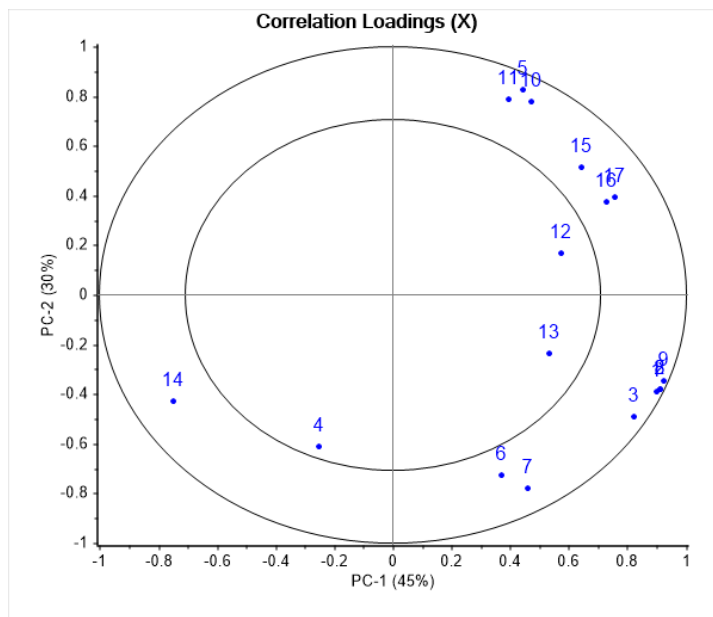
Figure 4.2: Correlation loadings for variables in PC-1 vs PC-2 space.

Traditionally, PCA is used for dimensionality reduction or data compression for easy storage or transmission over limited-bandwidth networks. In recent times, the true potential of PCA is realized, and it is demonstrated to be a one-stop shop for basic data analysis, as shown in Article 2[1]. Here, PCA is used to study the correlation between the variables and outlier detection. The correlation between the variables can be instrumental in the variable selection process for data-driven

---

[1]The copy of Article 2 attached here includes some minor corrections which are not incorporated in the published version available at the given DOI.

Table 4.1: List of variables for PCA.

Sl. No.	Variables	Sl. No.	Variables
1	ME consumed	11	Trim-by-aft
2	Shaft power	12	Long. wind speed
3	Shaft rpm	13	Trans. wind speed
4	Draft fore	14	Relative mean wave direction
5	Draft aft	15	Significant wave height
6	GPS speed	16	Mean wave direction
7	Log speed	17	Mean wave period
8	ME Load measured		
9	Shaft Torque		
10	Mean draft		

modeling. Figure 4.2 presents the correlation loadings for the variables listed in table 4.1. In figure 4.2, the horizontal axis represents PC-1, and the vertical axis represents PC-2. The percentage values in the x and y axis labels, i.e., 45% for PC-1 and 30% for PC-2, represents the amount of variance contained in the dataset which is explained by the respective Principal Component (PC). The position of the variables in the plot represents the correlation between the variables and the PCs, and the relative position of variables with respect to each other can be seen as the correlation between the variables. The variables far away from the center are strongly correlated to either one or both the PCs as well as with each other. The figure clearly shows strong correlation between the propulsive parameters, like speed, power and rpm, with environmental load variables and ship loading (draft amd trim).
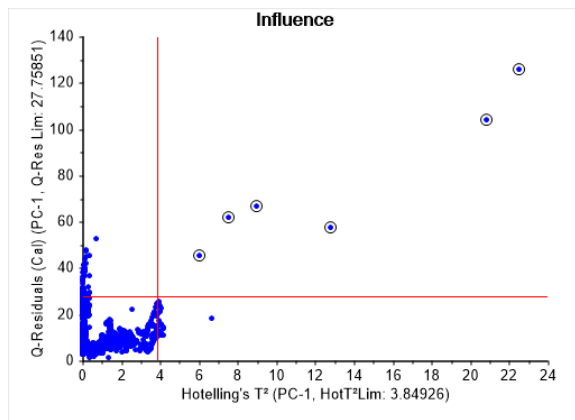
Figure 4.3: Detecting outliers using PCA.

Furthermore, Article 2 also introduces the influence plots used to detect outliers. Figure 4.3 shows the influence plot for PC-1. The horizontal axis represents the Hotelling's T-Square statistics for the data samples with respect to PC-1, and the vertical axis represents the Q-Residuals. The data samples on the top right of the red lines, representing 95% statistical limits, are detected as outliers as they have very high leverage over the model as well as high residuals. The detected outliers can be further investigated to find out the root cause for their anomalous behavior.

PCA is a simple statistics-based machine-learning method which is easy to implement as well as interpret but it is limited by the fact that it is a linear method, i.e., it can only be used to study the linear correlation between the variables. Thus, PCA, as it is, should not be used to analyse datasets with significantly non-linear relationships. As explained in section 3.1.2, the dataset used in Article 2 contains only a single voyage or trip. Therefore, the spread of the data over the high-dimensional variable space is limited, quite evident from figure 4.4, reducing the effect of non-linearities. In case of a larger, widely spread dataset, it is recommended to either use an alternate method, like neural networks based autoencoders, kernel PCA, etc., or handle the non-linearities in the dataset before applying PCA. The latter can be achieved by using some non-linear transformations, as done in the case of PCR and PLSR models in Article 4, or just dividing the data into small and linear sections, and applying PCA to them individually, similar to what is done in the case of Article 2.
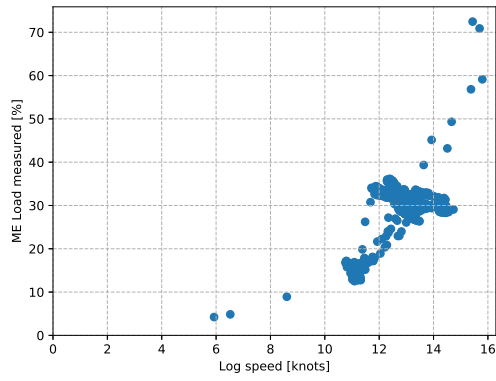
Figure 4.4: Log speed (or speed-through-water) vs Main Engine (ME) load for the data used in Article 2.

4.1.3   Article 3: Ship's Hydrodynamic Performance Indicator

During this research, the generalized form of the well-known admiralty coefficient ($\Delta^m V^n / P_s$) is depicted as the statistical performance indicator for a ship, where Δ denotes the displacement, V denotes the speed-through-water and P_s denotes the shaft power. It is demonstrated in Article 3 that the generalized admiralty coefficient can be fitted to the near-calm-water in-service data to obtain the displacement and speed exponents, i.e., m and n, respectively, for a specific ship. The obtained generalized admiralty coefficient, there after, represents the reference calm-water speed-power-displacement surface for the ship.

The distance of the ship's operating point (speed, power and displacement) from the reference calm-water surface in near-calm-water condition can be taken as a measure for the ship's hydrodynamic performance. Article 3 clarifies (in section 2.2) that the numerical values, obtained by substituting the in-service data into the above obtained generalized admiralty coefficient, represents the distance of the operating point (along the power axis) from the calm-water speed-power-displacement reference surface for the ship. Therefore, using the near-calm-water in-service data, the generalized admiralty coefficient can be used as a statistical performance indicator for a sea-going ship.

Figure 4.5(a) shows the estimated trends of hydrodynamic performance of a ship between several propeller cleaning events using the generalized admiralty coefficient ($\Delta^m V^n / P_s$). The obtained performance trends are validated by the trends obtained using the traditional method, i.e., observing the fouling friction coefficient[2] (ΔC_F; shown in figure 4.5(b)). A 'leg' in both the figures represents the duration between two consecutive propeller cleaning events. The near-calm-water in-service data is obtained here by filtering the data for total wind speed less than 5.5 m/s and significant wave height less than 1 m. The shaft power in the filtered data is further corrected for wind and wave loads using physics-based empirical methods. Each data point in figure 4.5(a) represents the mean of all the generalized admiralty coefficient values obtained for each data sample in an individual voyage (or part of a voyage), corresponding to the same ship static time. Similarly, the data points in figure 4.5(b) represents the mean of fouling friction coefficient values. The trend lines are obtained by fitting simple ordinary least squares (OLS) linear regression models in both the figures.

---

[2]Appendix B in Article 4 presents the detailed procedure for calculating the fouling friction coefficient (ΔC_F).
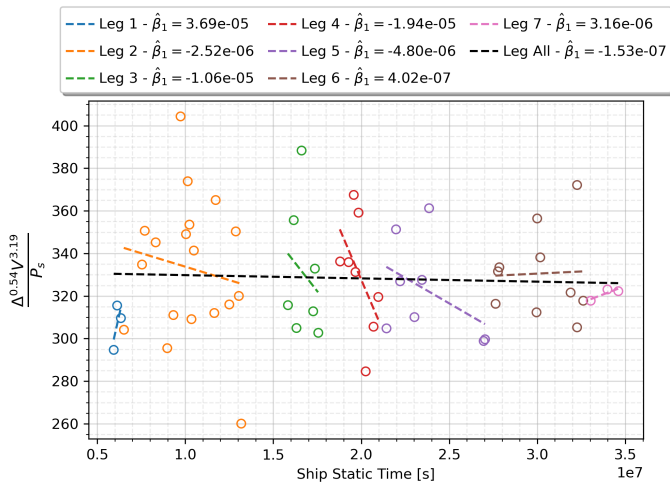
(a) Using the generalized admiralty coefficient.
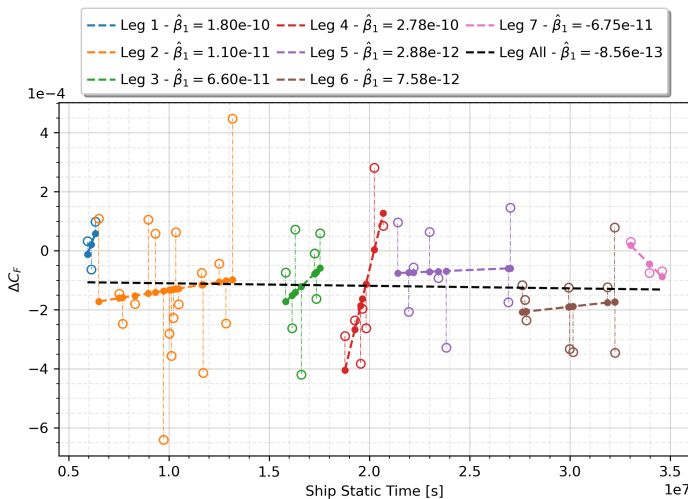
(b) Using the fouling friction coefficient (ΔC_F).

Figure 4.5: Estimated hydrodynamic performance trends of a ship.

The results presented in Article 3 are based on the onboard recorded in-service data from only a single ship. For further validation of the developed methodology, the results based on an extended dataset from the same ship and a new dataset from one of the sister ships is presented in the appendix of Article 4. The corresponding trends from the traditional method, i.e., using fouling friction coefficient (ΔC_F), are shown to be in good qualitative agreement in case of both the ships.

4.1.4   Article 4: Ship Performance Monitoring

The in-service data recorded onboard a sea-going ship can be used to monitor the hydrodynamic performance of the ship. As explained in section 3.1.4, the following three machine-learning (ML) methods are selected here to develop a data-driven model to monitor the hydrodynamic performance of a ship: (a) Principal Component Regression (PCR), (b) Partial Least Squares Regression (PLSR) and (c) Probabilistic Artificial Neural Network (Probabilistic ANN). The in-service data from two sister ships is used in Article 4 to calibrate these models.

In order to account for the variation of performance with time, a fouling growth factor (FGF) is formulated in Article 4 using the ship's cumulative static time (t_{static}) and fouling growth rate (FGR) as follows:

$$\text{FGF} = \sum_i t_{static,i}.\text{FGR}_i \qquad (4.1)$$

Based on the idea presented by Malone et al. (1981), it is assumed here that the fouling grows on the ship's hull and propeller only when it is static. The ship's cumulative static time is calculated by cumulatively adding the time (in seconds) when the speed-over-ground of the ship is less than 3 knots, as recommended by Malone et al. (1981) based on some experimental evidence. The fouling growth rate (FGR) is obtained from the trends observed in the generalized admiralty coefficient ($\Delta^m V^n / P_s$), as demonstrated in the previous section and Article 3.
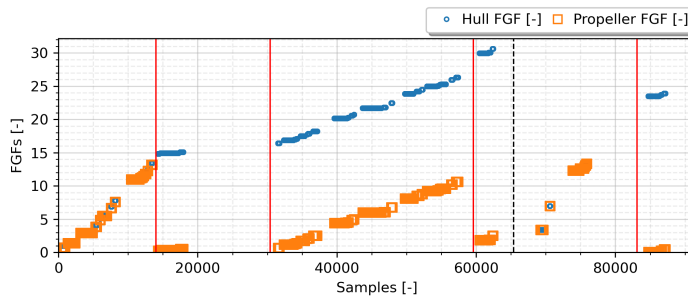
Figure 4.6: Hull and propeller fouling growth factors for a ship. The red vertical lines represents propeller cleaning events, and the black dashed line represents the hull and propeller event.

Separate FGFs are calculated in Article 4 for hull and propeller to account for fouling growth on the ship's hull and propeller, respectively. When the hull or propeller of the ship is cleaned the corresponding FGF is reset to zero, thereby,

Table 4.2: Input and target variables used by the regression models, i.e., NL-PCR, NL-PLSR and Probabilistic ANN. * marked variables are only included in NL-PCR and NL-PLSR models.

Sl. No.	Category	Variables
1		Shaft rpm, Mean draft, Trim-by-aft
2		Long. wind speed, Trans. wind speed, Long. current speed
3	Input	Significant wave height, Relative mean wave direction, Mean wave period
4		Fouling growth factor
5*		Shaft rpm^3, Mean $draft^{1/2}$, Significant wave $height^2$
6	Target	Shaft power, GPS speed, Log speed
7*		GPS $speed^3$, Log $speed^3$

incorporating the effect of cleaning events. Figure 4.6 shows the hull and propeller fouling growth factors for a ship through a hull and several propeller cleaning events.

Further, the data-driven models are calibrated using the total FGF, obtained as a summation of hull and propeller FGFs, and several other variables. Table 4.2 shows the list of input and target variables used to calibrate the above mentioned ML models. The table also shows the non-linear transformations (* marked) used to solve the non-linear problem with the linear models, i.e., PCR and PLSR, as discussed in section 3.1.4. The calibrated models are further used to extract the performance trends in calm-water condition learned by the ML models for the ship over time, as shown in figure 4.7.
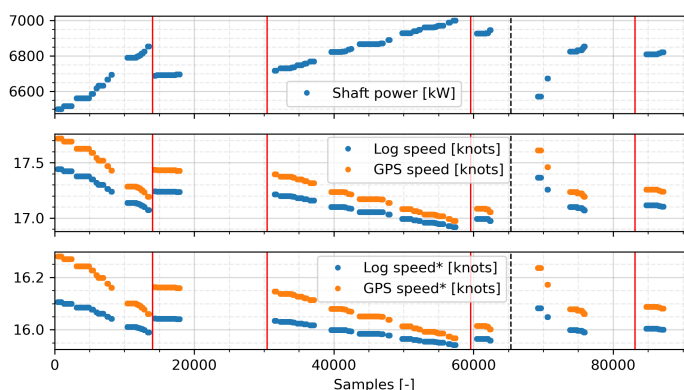
Figure 4.7: Performance trends predicted by PLSR model for a ship. The * marked speed variables are obtained from the corresponding cubic transformations.

Finally, the change in performance of the ship due to a propeller or hull cleaning activity is estimated as the change in power demand for the ship just before and after the corresponding activity, presented in Article 4 (table 5). The results indicate improvement in performance for most of the propeller and hull cleaning events for one of the ships, with the highest improvement predicted for the hull (and propeller) cleaning event, also visible in figure 4.7. Figures 4.8, 4.9 and 4.10 shows the evolution of speed-power calm-water curve of the sister ship for just before and after the hull and propeller cleaning event, predicted by PCR, PLSR and probabilistic ANN models, respectively.

The results obtained from the ML models are compared with the results (i.e., the change in power demand) obtained from the traditional method, i.e., using the fouling friction coefficient (ΔC_F). Unfortunately, the results cannot be corroborated here as the values obtained from the traditional method does not seem to be valid in almost half of the cases.
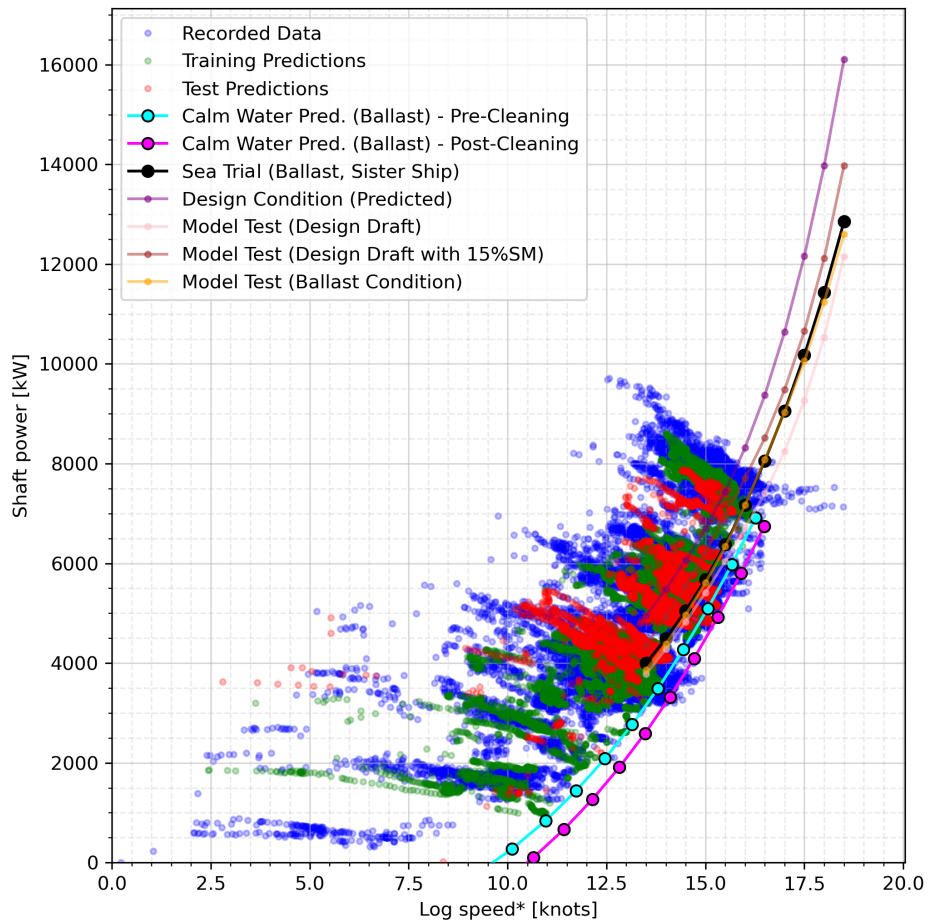
Figure 4.8: Calm-water speed-power curves predicted by PCR model for the sister ship for just before (pre-cleaning) and after (post-cleaning) the hull and propeller cleaning event.
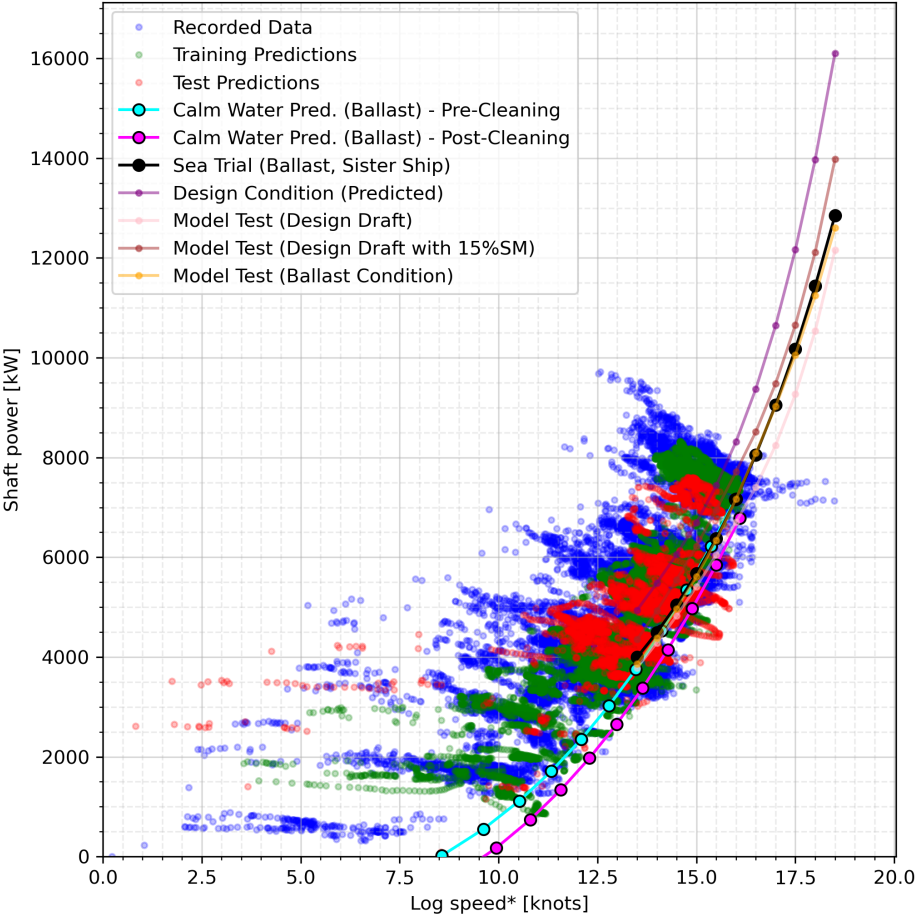
Figure 4.9: Calm-water speed-power curves predicted by PLSR model for the sister ship for just before (pre-cleaning) and after (post-cleaning) the hull and propeller cleaning event.
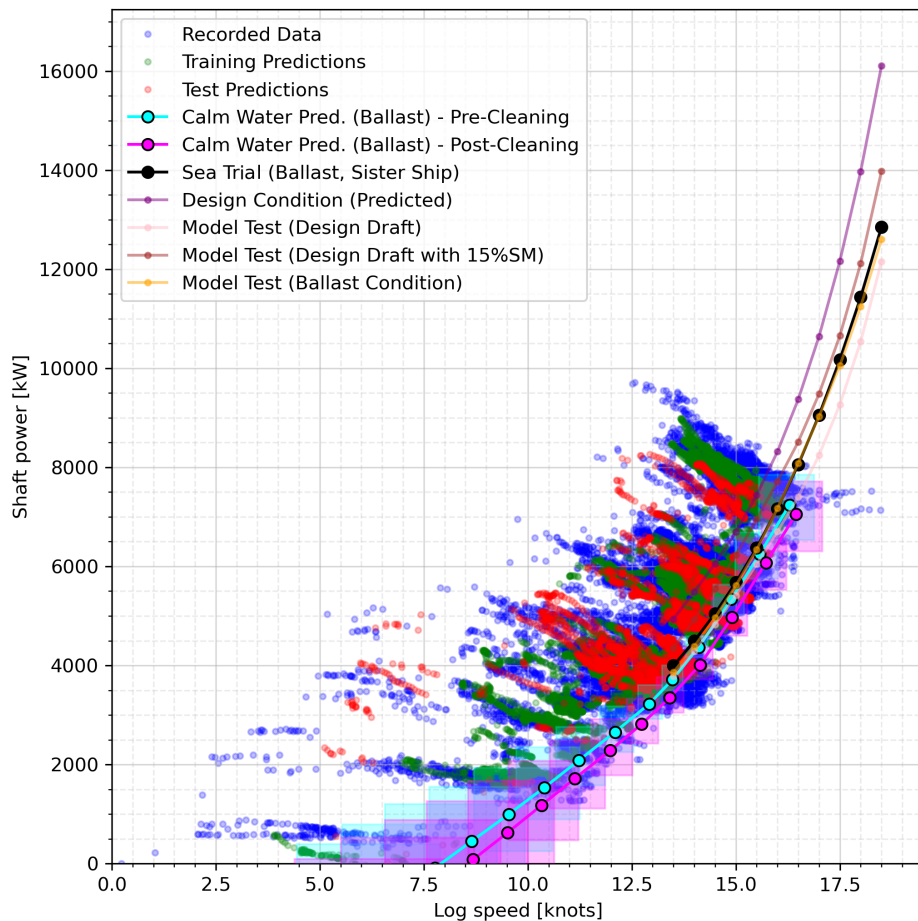
Figure 4.10: Calm-water speed-power curves predicted by probabilistic ANN models for the sister ship for just before (pre-cleaning) and after (post-cleaning) the hull and propeller cleaning event. The shaded region around the predicted calm-water curve, in case of the ANN model, presents the 95% confidence interval estimated using the approximate predictive distributions predicted for each sample.

4.2   Research Contribution

The current research has several contributions to the field of marine technology, specially from the data processing, data analysis, data-driven modeling, and ship performance monitoring point of view. Several statistics-based machine-learning methods are presented here to utilize the onboard recorded in-service data for monitoring the hydrodynamic performance of a ship. The main contributions of this research are listed as follows:

- Data-driven methods for ship performance monitoring are established based on the in-service data recorded onboard the ships.

- Linear machine-learning (ML) methods, namely, Principal Component Regression (PCR) and Partial Least Squares Regression (PLSR), are shown to be producing comparable results with a well-established non-linear method, artificial neural network (ANN), while modeling the hydrodynamic state of a ship using some simple non-linear transformations, obtained from the domain knowledge.

- Calibrated machine-learning models are demonstrated to predict the change in performance of a ship through propeller and hull cleaning events.

- A statistical hydrodynamic performance indicator, in the form of generalized admiralty coefficient ($\Delta^m V^n / P_s$), is established to monitor the hydrodynamic performance of a ship over time.

- It is clarified here that the generalized admiralty coefficient, fitted on the near-calm-water in-service data recorded onboard a ship, represents an approximated calm-water speed-power-displacement reference surface for the specific ship.

- Principal Component Analysis (PCA), a simple matrix factorization method, is established to study the correlation between data variables and perform other basic data analysis tasks, like variable selection and outlier detection.

- A semi-automatic data processing framework is developed to process the data from a ship in-service for ship performance monitoring.

- Several common problems found in the data obtained from a ship in-service are discussed and appropriate solutions are suggested.

CHAPTER 5

Conclusion

This chapter presents the conclusion of this research and ideas
for future work.

The main conclusion of the current research, like many others concerning data-driven modeling, is that the quality of results is highly dependent on the quality of data. Therefore, quality assurance and validation of datasets is quite critical, and ample time and resources should be dedicated for the same. Even though the quality of onboard recorded in-service datasets used for the current work may be considered quite good, there is still need for improvement to make them well suited for analysis. Therefore, several data cleaning and rectification methods are adopted to process the datasets for further analysis. Thus, the task of data processing is, clearly, the most challenging, critical as well as demanding, while working towards establishing data-driven models.

Reflecting on individual data variables, the usually infamous speed-through-water measurements continues to be insufficiently accurate for ship performance monitoring. In view of that, the current work shows great success in limiting the usage of speed-through-water by using the change in power demand as a measure for ship's hydrodynamic performance, instead of the commonly accepted speed-loss. It may be a good idea to continue on this path unless an improved way of measuring or obtaining the speed-though-water with higher accuracy is established. It is also observed here that, probably, enough attention has not been paid to the draft measurements recorded onboard the ship, which is shown to be detrimentally affected by the Venturi effect. Although the importance of draft measurements for ship performance monitoring is not studied here in detail, the faulty measure-

ments may induce some errors in the performance analysis, specially in case of a physics-based approach.

It should also be kept in mind that the data handling and acquisition system may also introduce some errors in the dataset, as can be observed in the case of degree measurements for 15 minutes averaged values. Therefore, a thorough examination and proper validation of data is mandatory. Moreover, gathering additional data from supplementary sources, like the publicly available weather hindcast data, should be considered a good practice in this regard. The additional data would not only provide new information, but it can also be used to validate the data recorded onboard the ship.

The extent of research is definitely limited by the quality of data. Even after extensively processing and validating the data, it is observed that the statistical noise in the data is quite substantial. Due to the same, the research cannot be further extended to adopt more sophisticated techniques, like obtaining a statistically fitted non-linear surface (in log scale) for the calm-water speed-power-displacement reference surface for a ship. The statistical noise in the data affects the reliability of results, specially while applying such sophisticated techniques. Thus, the data acquisition for ships needs to be further matured as well as the environmental load corrections needs to be improved, so that the statistical noise in the data can be subdued to a greater extent.

The current research establishes the generalized admiralty coefficient ($\Delta^m V^n / P_s$) as a statistics-based hydrodynamic performance indicator for a ship. The displacement and speed exponents in the generalized admiralty coefficient, i.e., m and n, respectively, are obtained statistically by fitting the near-calm-water in-service data recorded onboard the ship to the log-linear relation. A qualitative comparison of performance trends predicted by the generalized admiralty coefficient and the traditionally used fouling friction coefficient (ΔC_F) shows quite good agreement. Unlike ΔC_F, the generalized admiralty coefficient can be obtained and used for performance monitoring of ships without using any physics-based and/or empirical method.

Using linear methods to model the hydrodynamic state of a ship is shown to be quite promising. The trick is to either use some non-linear transformations or dividing the data into linear subsets. The former is demonstrated here, but the latter also seems feasible. The non-linear transformations can be further improved by studying the physical model in detail. Thus, it may be possible to avoid esoteric methods, like artificial neural network (ANN), and adopt transparent and interpretable methods for ship performance monitoring.

The effect of fouling growth on the hull and propeller of the ship is incorporated successfully into data-driven models using a simple formulation for fouling growth factor. The calibrated models are demonstrated to predict the performance of ships in calm-water condition, in a way separating the calm-water resistance from the total resistance. The change in performance of the ship over several propeller and hull cleaning event is also predicted effectively.

5.1   Future Work

There is quite good scope for building upon and carrying forward the current research. The following are some of the main points which can be considered while thinking about the future work:

- The current formulation for the statistical performance indicator, i.e., the generalized admiralty coefficient ($\Delta^m V^n / P_s$), assumes log-linearity for the calm-water speed-power-displacement reference surface, but the literature and some evidence clearly indicates non-linearities in the log scale. Thus, a better formulation or an alternate method to statistically obtain the reference surface from the in-service data can be developed.

- The non-linear transformations used to model the hydrodynamic state of a ship using linear methods can be improved further by studying the physical model in detail or using the correlations between the data variables.

- The simple model for fouling growth factor (FGF) is definitely an approximation, and there are several possible ways to improve it. For example, the FGF, here based on the statistical performance indicator, can also be modeled using the information regarding the fouling growth intensity for each port visited by the ship. Such information can be determined experimentally or even using a large amount of data from ships in-service.

- Although the linear models, with non-linear transformations, shows promising results, it may also be a good idea to further explore the realm of probabilistic modeling. The probabilistic method used here is just an approximation for a proper Bayesian approach, a better approach may produce better results and give more insight into the problem.

- The models developed here are based on the in-service data obtained from two sister ships. It is, of course, desired to validate the results using a variety of datasets.

- The traditional method (fouling friction coefficient, ΔC_F) used here to compare and corroborate the results from the data-driven models for ship per-

formance monitoring resulted in invalid or unexpected values in about half of the cases. Thus, a better method or reference for comparing the results should be sought. A high fidelity method, say, physically monitoring the fouling growth on the ship's hull and propeller, for performance monitoring of ships over time may help quantify the error in the predictions made using the data-driven models in the current research.

Other than the above mentioned points, there is definitely some scope for improvement in data acquisition, processing and preparation steps. The sensor technology is expected to improve in future, resulting in better data quality. New technology will present new challenges, and therefore, would need new solutions.

References

E. Cambria, G.-B. Huang, L. L. C. Kasun, H. Zhou, C. M. Vong, J. Lin, J. Yin, Z. Cai, Q. Liu, K. Li, V. C. Leung, L. Feng, Y.-S. Ong, M.-H. Lim, A. Akusok, A. Lendasse, F. Corona, R. Nian, Y. Miche, P. Gastaldo, R. Zunino, S. Decherchi, X. Yang, K. Mao, B.-S. Oh, J. Jeon, K.-A. Toh, A. B. J. Teoh, J. Kim, H. Yu, Y. Chen, and J. Liu. Extreme learning machines [trends amp; controversies]. *IEEE Intelligent Systems*, 28(6):30–59, 2013. doi: 10.1109/MIS.2013.140.

A. Carchen and M. Atlar. Four KPIs for the assessment of biofouling effect on ship performance. *Ocean Engineering*, 217:107971, 2020. ISSN 0029-8018. doi: https://doi.org/10.1016/j.oceaneng.2020.107971. URL https://www.sciencedirect.com/science/article/pii/S0029801820309239.

A. Carchen, K. Pazouki, A. Murphy, B. Aktas, and M. Atlar. Uncertainty anaysis of full-scale ship performance monitoring onboard the princess royal. 10 2017.

A. Coraddu, L. Oneto, F. Baldi, F. Cipollini, M. Atlar, and S. Savio. Data-driven ship digital twin for estimating the speed loss caused by the marine fouling. *Ocean Engineering*, 186, 2019. doi: 10.1016/j.oceaneng.2019.05.045. cited By 1.

Ø. Ø. Dalheim and S. Steen. Uncertainty in the real-time estimation of ship speed through water. *Ocean Engineering*, 235:109423, 2021. ISSN 0029-8018. doi: https://doi.org/10.1016/j.oceaneng.2021.109423. URL https://www.sciencedirect.com/science/article/pii/S0029801821008313.

K. O. Ejdfors. Use of in-service data to determine the added power of a ship due to fouling. Master's thesis, NTNU, 2019. URL http://hdl.handle.net/11250/2622960.

M. Foteinos, E. Tzanos, and N. Kyrtatos. Ship hull fouling estimation using shipboard measurements, models for resistance components, and shaft torque calcu-

lation using engine model. *Journal of Ship Research*, 61(2):64–74, 2017. doi: 10.5957/JOSR.61.2.160053. cited By 3.

ISO. ISO 19030-2:2016: Ships and marine technology — measurement of changes in hull and propeller performance — part 2: Default method, 2016. URL https://www.iso.org/standard/63775.html.

P. Karagiannidis and N. Themelis. Data-driven modelling of ship propulsion and the effect of data pre-processing on the prediction of ship fuel consumption and speed loss. *Ocean Engineering*, 222:108616, 2021. ISSN 0029-8018. doi: https://doi.org/10.1016/j.oceaneng.2021.108616. URL https://www.sciencedirect.com/science/article/pii/S0029801821000512.

Y.-R. Kim, M. Jung, and J.-B. Park. Development of a fuel consumption prediction model based on machine learning using ship in-service data. *Journal of Marine Science and Engineering*, 9(2), 2021. ISSN 2077-1312. doi: 10.3390/jmse9020137. URL https://www.mdpi.com/2077-1312/9/2/137.

Ž. Koboević, D. Bebić, and Ž. Kurtela. New approach to monitoring hull condition of ships as objective for selecting optimal docking period. *Ships and Offshore Structures*, 14(1):95–103, 2019. doi: 10.1080/17445302.2018.1481631. cited By 1.

Y. Kwon. Speed loss due to added resistance in wind and waves. *Naval Architect*, pages 14–16, 03 2008.

A. Laurie, E. Anderlini, J. Dietz, and G. Thomas. Machine learning for shaft power prediction and analysis of fouling related performance deterioration. *Ocean Engineering*, 234:108886, 2021. ISSN 0029-8018. doi: https://doi.org/10.1016/j.oceaneng.2021.108886. URL https://www.sciencedirect.com/science/article/pii/S0029801821003218.

R. Lu, O. Turan, E. Boulougouris, C. Banks, and A. Incecik. A semi-empirical ship operational performance prediction model for voyage optimization towards energy efficient shipping. *Ocean Engineering*, 110:18–28, 2015. ISSN 0029-8018. doi: https://doi.org/10.1016/j.oceaneng.2015.07.042. URL https://www.sciencedirect.com/science/article/pii/S0029801815003558. Energy Efficient Ship Design and Operations.

J. A. Malone, D. E. Little, and M. Allman. Effects of hull foulants and cleaning/coating practices on ship performances and economics. *Transactions - Society of Naval Architects and Marine Engineers*, 88:75–101, 1981. cited By 12.

T. Munk. Fuel conservation through managing hull resistance. In *Motorship Propulsion Conference, Copenhagen*, 2016. URL https://www.messe.no/ExhibitorDocuments/97726/2419/BIMCO%20Hull-Resistance.pdf.

D. R. Oliveira, L. Granhag, and L. Larsson. A novel indicator for ship hull and propeller performance: Examples from two shipping segments. *Ocean Engineering*, 205:107229, 2020. ISSN 0029-8018. doi: https://doi.org/10.1016/j.oceaneng.2020.107229. URL https://www.sciencedirect.com/science/article/pii/S0029801820302833.

M. Tsujimoto and H. Orihara. Performance prediction of full-scale ship and analysis by means of on-board monitoring (part 1 ship performance prediction in actual seas). *Journal of Marine Science and Technology*, 24, 01 2018. doi: 10.1007/s00773-017-0523-1.

B. Yoo and J. Kim. Probabilistic modeling of ship powering performance using full-scale operational data. *Applied Ocean Research*, 82:1–9, 2019. ISSN 0141-1187. doi: https://doi.org/10.1016/j.apor.2018.10.013. URL https://www.sciencedirect.com/science/article/pii/S014111871730768X.

Research Articles

Article 1

Data Processing Framework for Ship Performance
Analysis

Prateek Gupta, Young-Rong Kim, Sverre Steen, Adil Rasheed

Highlights

Data Processing Framework for Ship Performance Analysis

Prateek Gupta,Young-Rong Kim,Sverre Steen,Adil Rasheed

- Ship's hydrodynamic performance can be assessed using the data from ship-in-service

- Data can be recorded onboard the ship, obtained via AIS or as noon reports

- Gathered data needs to be cleaned and processed for performance analysis

- A standardized data processing framework for preparing the data is developed

- Data processing framework can be easily casted for processing any similar datasets

Data Processing Framework for Ship Performance Analysis

Prateek Gupta[a,*], Young-Rong Kim[a], Sverre Steen[a] and Adil Rasheed[b]

[a]Norwegian University of Science and Technology (NTNU), Department of Marine Technology, Trondheim, 7052, Sør-trondelag, Norway
[b]Norwegian University of Science and Technology (NTNU), Department of Engineering Cybernetics, Trondheim, 7034, Sør-trondelag, Norway

ARTICLE INFO

ABSTRACT

The hydrodynamic performance of a sea-going ship can be analysed using the data obtained from the ship. Such data can be gathered from different sources, like onboard recorded in-service data, AIS data, and noon reports. Each of these sources is known to have their inherent problems. The current work gives a brief introduction to these data sources as well as the common problems associated with them, along with some examples. In order to resolve most of these problems, a streamlined semi-automatic data processing framework for fast data processing is developed and presented here. The data processing framework can be used to process the data obtained from any of the above three mentioned sources. The framework incorporates processing steps like interpolating weather hindcast (metocean) data to ship's location in time, deriving additional features, validating data, estimating resistance components, data cleaning, and outlier detection. A brief description of each of the processing steps is provided with examples from existing datasets. The processed data can be further used to analyse the hydrodynamic performance of a ship.

1. Introduction

The performance of a sea-going ship is important not only to keep the fuel and operational cost in-check but also to reduce global emissions from the shipping industry. Analyzing the performance of a ship is also of great interest for charter parties to estimate the potential of a ship and the profit that can be made out of it. Therefore, driven by both the economic and social incentives, the trade of ship performance analysis and monitoring has been booming substantially in recent times. The importance of in-service data in this context is very well understood by most of the stake holders, clearly reflected by the amount of investment made by them on onboard sensors, data acquisition systems, and onshore operational performance monitoring and control centers.

The traditional way to evaluate the performance of a ship is using the noon report data provided by the ship's crew. A more exact approach, but not very feasible for commercial vessels, was suggested by Walker and Atkins (2007), conducting in-service sea trials in calm-water conditions on a regular basis. With the advent of sensor-based continuous monitoring systems, the current trend is to directly or indirectly observe the evolution of the calm-water speed-power curve over time. ISO 19030 ISO (2016) along with several researchers (Koboević et al. (2019); Coraddu et al. (2019)) recommends observing the horizontal shift (along the speed axis) of the calm-water speed-power curve, termed as the speed-loss, over time to monitor the performance of a sea-going ship using the in-service data. Alternatively, it is suggested to observe the vertical shift of the calm-water speed-power curve, often termed as the change in power demand (adopted by Gupta et al. (2021a) and Carchen and Atlar (2020)). Some researchers also formulated and used some indirect performance indicators like fuel consumption (Koboević et al. (2019)), resistance (or fouling) coefficient (Munk (2016); Foteinos et al. (2017); Carchen and Atlar (2020)), (generalized) admiralty coefficient (Ejdfors (2019); Gupta et al. (2021b)), wake fraction (Carchen and Atlar (2020)), fuel efficiency (Kim et al. (2021)), etc. In each of these cases, it is clearly seen (and most of the time acknowledged) that the results are quite sensitive to the quality of the data used to estimate the ship's performance.

The ship's performance-related data obtained from various sources usually inherits some irregularities due to several factors like sensor inaccuracies, vibration of the sensor mountings, electrical noise, variation of environment, etc., as pointed out in the Guide for Smart Functions for Marine Vessels and Offshore Units (Smart Guide) published recently by American Bureau of Shipping (2020). The quality of data used to carry-out ship performance analysis

*Corresponding author
✉ prateek.gupta@ntnu.no (P. Gupta); youngrong.kim@ntnu.no (Y. Kim); sverre.steen@ntnu.no (S. Steen); adil.rasheed@ntnu.no (A. Rasheed)
ORCID(s): 0000-0001-7147-0868 (P. Gupta)

and the results obtained further can be significantly improved by adopting some rational data processing techniques, as shown by Liu et al. (2020) and Kim et al. (2020). Another important factor is the source of data as it may also be possible to obtain such datasets using the publicly available AIS data (You et al. (2017)). Dalheim and Steen (2020b) presented a data preparation toolkit based on the in-service data recorded onboard 2 ships. The presented toolkit was developed for a specific type of dataset, where the variables were recorded asynchronously and had to be synchronized before carrying-out ship performance analysis. The current work would rather focus on challenges faced while processing an already synchronized dataset.

The current paper presents a review of different data sources used for ship performance analysis and monitoring, namely, onboard recorded in-service data, AIS data, and noon reports, along with the characteristics for each of these data sources. Finally, a data processing framework is outlined which can be used to prepare these datasets for ship performance analysis and monitoring. Although the data processing framework is developed for the performance monitoring of ships, it may easily be casted for several other purposes. With the easy availability of data from ships, the concept of creating digital twins for sea-going ships is becoming quite popular. Major et al. (2021) presented the concept of digital twin for a ship and the cranes onboard it. The digital twin established by Major et al. (2021) can be used to perform three main offshore operations, including remote monitoring of the ship, maneuvering in harsh weather and crane operations, from an onshore control center. Moreover, as pointed out by Major et al. (2021), the digital twin technology can also be adopted for several other purposes, like predictive maintenance, ship autonomy, etc. Nevertheless, the data processing framework presented here can also be used to process the real-time data obtained to create digital twins for ships in an efficient manner.

The following section discusses the art of ship performance analysis and the bare minimum characteristics of a dataset required to do such an analysis. Section 3 presents the above mentioned sources of data used for ship performance analysis, their characteristics, and the tools required to process these datasets. Section 4 presents the data processing framework which can be used to process and prepare these datasets for ship performance monitoring. Finally, section 5 finishes the paper with concluding remarks.

2. Ship Performance Analysis

The performance of a ship-in-service can be assessed by observing its current performance and, then, comparing it to a benchmarking standard. There are several ways to establish (or obtain) a benchmarking standard, like model test experiments, full-scale sea trials, CFD analysis, etc. It may even be possible to establish a benchmarking standard using the in-service data recorded onboard a newly built ship, as suggested by Coraddu et al. (2019) and Gupta et al. (2021b). On the other hand, evaluating the current performance of a ship requires a good amount of data processing as the raw data collected during various voyages of a ship is susceptible to noise and errors. Moreover, the benchmarking standard is, generally, established for only a given environmental condition, most likely the calm-water condition. In order to draw a comparison between the current performance and the benchmarking standard, the current performance must be translated to the same environmental condition, therefore, increasing the complexity of the problem.

2.1. Bare Minimum Variables

For translating the current performance data to the benchmarking standard's environmental condition and carrying-out a reliable ship performance analysis, a list of bare minimum variables must be recorded (or observed) at a good enough sampling rate. The bare minimum list of variables must provide the following information about each sampling instant for the ship: (a) Operational control, (b) Loading condition, (c) Operational environment, and (d) Operating point. The variables containing the above information must either be directly recorded (or observed) onboard the ship, collected from regulatory data sources such as AIS, or may be derived using additional data sources, like the operational environment can be easily derived using the ship's location and timestamp with the help of an appropriate weather hindcast (or metocean) data repository.

The operational control information should contain the values of the propulsion-related control parameters set by the ship's captain on the bridge, like shaft rpm, rudder angle, propeller pitch, etc. The shaft rpm (or propeller pitch, in case of ships equipped with controllable pitch propellers running at constant rpm) is by far the most important variable here as it directly correlates with the ship's speed-through-water. It should be noted that even in the case of constant power or speed mode, the shaft rpm (or propeller pitch) continues to be the primary control parameter as the set power or speed is actually achieved by using a real-time optimizer (incorporated in the governor) which optimizes the shaft rpm (or propeller pitch) to get to the set power or speed. Nevertheless, in case the shaft rpm (or propeller pitch) is not

51

Table 1
The list of bare minimum data variables required for ship performance analysis.

Category	Variables
Operational Control	Shaft rpm, Rudder angle, & Propeller pitch
Loading Condition	Fore and aft draft
Operational Environment	Longitudinal and transverse wind speed, Significant wave height, Relative mean wave direction, & Mean wave period
Operating Point	Shaft power & Speed-through-water

available, it may be appropriate to use the ship's speed-through-water as an operational control parameter, as done by several researchers (Farag and Ölçer (2020); Laurie et al. (2021); Minoura et al. (2021); Liang et al. (2019)), but in this case, it should be kept in mind that, unlike the shaft rpm (or propeller pitch), the speed-through-water is a dependant variable strongly influenced by the loading condition and the operational environment.

The loading condition should contain the information regarding the ship's fore and aft draft, which can be easily recorded onboard the ship. Although the wetted surface area and under-water hull-form are more appropriate for a hydrodynamic analysis, these can be derived easily using the ship's hull form, if the fore and aft draft is known. The operational environment should at least contain variables indicating the intensity of wind and wave loads acting on the ship, like wind speed and direction, significant wave height, mean wave direction, mean wave period, etc. Finally, the operating point should contain the information regarding the speed-power operating point for the sampling instant. Table 1 presents the list of bare minimum variables required for ship performance analysis. The list given in the table may have to be modified according to ship specifications, for example, the propeller pitch is only relevant for a ship equipped with a controllable pitch propeller.

2.2. Best Practices

It is well-known that the accuracy of various measurements is not the same. It also depends on the source of the measurements. The measurements recorded using onboard sensors are generally more reliable as compared to the manually recorded noon report measurements, due to the possibility of human error in the latter. Even in the case of onboard recorded sensor measurements, the accuracy varies from sensor-to-sensor and case-to-case. Some sensors can be inherently faulty, whereas others can give incorrect measurements due to unfavorable installation and operational conditions, and even the best ones are known to have some measurement noise. Thus, it is recommended to establish and follow some best practices for a reliable and robust ship performance analysis.

The onboard measurements for shaft rpm (n) and shaft torque (τ) are generally obtained using a torsion meter installed on the propeller shaft, which is considered to be quite reliable. The shaft power (P_s) measurements are also derived from the same as the shaft power is related to the shaft rpm and torque through the following identity: $P_s = 2\pi n\tau$. It should be noted that no approximation is assumed in this formulation and, therefore, it should be validated with the data, if all three variables (n, τ, P_s) are available. On the other hand, the measurements for speed-through-water are known to have several problems, as presented by Dalheim and Steen (2021). Thus, it is recommended to use shaft rpm (and not speed-though-water) as the independent variable while creating data-driven regression models to predict the shaft power. Owing to the same reason, it may also be a good idea to quantify the change in ship's performance in terms of change in power demand rather than speed-loss (or speed-gain), as recommended by ISO 19030 ISO (2016).

Further, it is also quite common to use fuel oil consumption as a key performance indicator for ship performance analysis (Karagiannidis and Themelis (2021)). The fuel oil consumption can be easily calculated from the engine delivered torque and engine rpm, if the specific fuel consumption (SFC) curve for the engine is known. Even though the SFC curve is established and supplied by the engine manufacturer, it is only valid for a specific operating environment, and it is known to evolve over time due to engine degradation and maintenance. Thus, including the fuel oil consumption in ship performance analysis increases the complexity of the problem, which requires taking engine health into account. If the objective of ship performance analysis is also to take into account the engine performance, then it may be beneficial to divide the problem into two parts: (a) Evaluate the change in power demand (for hydrodynamic performance analysis), and (b) Evaluate the change in engine SFC (for engine performance analysis). Now, the latter can be formulated as an independent problem with a completely new set of variables-of-interest, like engine delivered torque, engine rpm, ambient air temperature, calorific value of fuel, turbocharger health, etc. This would not only improve the accuracy of ship's hydrodynamic performance analysis but would also allow the user to develop a more

comprehensive and, probably, accurate analysis model. The current work is focused on the hydrodynamic performance analysis.

2.3. Sampling Frequency

Almost all electronics-based sensors are known to have some noise in their measurements. The simplest way adopted to subdue this noise is by taking an average over a number of measurements (known as a 'sample' in statistics), recorded over a very short period of time (milliseconds). It is also known that the statistical mean of a 'sample' converges to the true mean (i.e., the mean of the entire population), thereby eliminating the noise, as the number of measurements in the 'sample' is increased, provided the observations follow a symmetrical distribution. Nevertheless, it is observed that the high frequency data still retains some noise, probably due to the fact that the number of measurements in each 'sample' is small, i.e., the measurements are obtained by averaging a small number of samples recorded over a very short period of time. On the other hand, as seen in the case of noon reports and most of the in-service datasets, time-averaging the measurements over a longer period of time obscures the effect of moderately varying influential factors, for example, instantaneous incident wind and waves, response motions, etc. Thus, a very high sampling frequency data may retain high noise, and a very low sampling frequency data, with time-averaged values, may result in obscuring important effects from the data time-series. Furthermore, in the third scenario, it may be possible that the data acquisition (DAQ) system onboard the ship is simply using low sampling frequency, recording instantaneous values instead of time-averaged ones, saving a good amount of storage and bandwidth while transmitting it to the shore-based control centers. These low frequency instantaneous values may result in an even more degraded data quality as it would contain noise as well as obscure the moderately varying effects.

The ideal sampling frequency would also depend on the objective of the analysis and the recorded variables. For example, if the objective of the analysis is to predict the motion response of a ship or analyse its seakeeping characteristics, the data should be recorded at a high enough sampling frequency such that it is able to capture such effects. Hansen et al. (2011) analyzed the ship's rudder movement and the resulting resistance, and demonstrated that if the sampling interval would be large, the overall dynamics of the rudder movement would not be captured, resulting in a difference in resistance. One criterion for selecting the data sampling rate is Nyquist frequency (Jerri (1977)), which is widely used in signal processing. According to this criterion, the sampling frequency shall be more than twice the frequency of the observed phenomenon to sufficiently capture the information regarding the phenomenon. Therefore, if the aim is not to record any information regarding the above mentioned moderately varying effects (instantaneous incident wind and waves, response motions, etc.), it may be acceptable to just obtain low frequency time-averaged values so that such effects are subdued. But it may still be useful to obtain high frequency data, in this case, as it can be advantageous from data cleaning point of view. For example, the legs of time-series showing very high variance, due to the noise or moderately varying effects, can be removed from the analysis to increase the reliability of results.

3. Data Sources, Characteristics & Processing Tools

3.1. In-service Data

The in-service data, referred to here, is recorded onboard a ship during its voyages. This is achieved by installing various sensors onboard the ship, collecting the measurements from these sensors on a regular basis (at a predefined sampling rate) using a data acquisition (DAQ) system, and fetching the collected data to onshore control centers. The two most important features of in-service data is the sampling rate (or, alternatively, sampling frequency) and the list of recorded variables. Unfortunately, there is no proper guide or standard which is followed while defining both these features for a ship. Thus, the in-service data processing has to be adapted to each case individually.

The in-service datasets used here are recorded over a uniform (across all recorded variables) and evenly-spaced sampling interval, which makes it easier to adopt and apply data processing techniques. In an otherwise case, where the data is sampled with a non-uniform and uneven sampling interval, some more pre-processing has to be done in order to prepare it for further analysis, as demonstrated by Dalheim and Steen (2020b). Dalheim and Steen (2020b) presented a detailed algorithm to deal with time vector jumps and synchronizing non-uniformly recorded data variables. The problem of synchronization can, alternatively, be looked at using the well-known dynamic time warping (DTW) technique, which is generally used for aligning the measurements taken by two sensors, measuring the same or highly correlated features. In a different approach, Virtanen et al. (2020) demonstrated that the collected data can be down-sampled or up-sampled (resampling) to obtain a uniform and evenly sampled dataset.

53

3.1.1. Inherently Faulty & Incorrect Measurements

Some of the sensors onboard a ship can be inherently faulty and provide incorrect measurements due to unfavorable installation or operational conditions. Many of these can actually be fixed quite easily. For instance, Wahl (2019) presented the case of faulty installation of the wind anemometer onboard a ship, resulting in missing measurements for head-wind condition probably due to the presence of an obstacle right in front of the sensor. Such a fault is fairly simple to deal with, say, by fixing the installation of the sensor, and it is even possible to fix the already recorded dataset using the wind measurements from one of the publicly available weather hindcast datasets. Such an instance also reflects the importance of data exploration and validation for ship performance analysis. Unlike above, the case of draft and speed-through-water measurement sensors is not as fortunate and easy to resolve.

The ship's draft is, generally, recorded using a pressure transducer installed onboard the ship. The pressure transducer measures the hydrostatic pressure acting on the bottom plate of the ship which is further converted into the corresponding water level height or the draft measurement. When the ship starts to move and the layer of water in contact with the ship develops a relative velocity with respect to the ship, the total pressure at the ship's bottom reduces due to the non-zero negative hydrodynamic pressure and, therefore, further measurements taken by the draft sensor are incorrect. This is known as the Venturi effect. It may seem like a simple case, and one may argue that the measurements can be fixed by just adding the water level height equivalent to the hydrodynamic pressure, which may be calculated using the ship's speed-through-water. Here, it should be noted that, firstly, to accurately calculate the hydrodynamic pressure, one would need the localized relative velocity of the flow (and not the ship's speed-through-water), which is impractical to measure, and secondly, the speed-though-water measurements are also known to have several sources of inaccuracy. Alternatively, it may be possible to obtain the correct draft measurements from the ship's loading computer. The loading computer can calculate the draft and trim in real-time based on the information such as the ship's lightweight, cargo weight and distribution, and ballast water loading configuration.

The state-of-the-art speed-though-water measurement device uses the Doppler acoustic speed log principle. Here, the relative speed of water around the hull (i.e., the speed-though-water) is measured by observing the shift in frequency (popularly known as the Doppler shift) of the ultrasound pulses emitted from the ship's hull, due to its motion. The ultrasonic pulses are reflected by the ocean bottom, impurities in the surrounding water, marine life, and even the liquid-liquid interface between the density difference layers in deep ocean. The speed of water surrounding the ship is influenced by the boundary layer around the hull so it is required that the ultrasonic pulses reflected only by the particles outside the boundary layer are used to estimate the speed-though-water. Therefore, a minimum pulse travelling distance has to be prescribed for the sensor. If the prescribed distance is too larger or if the ship is sailing in shallow waters, the Doppler shift is calculated using the reflection from the ocean bottom, i.e., the sensor is in ground-tracking mode, and therefore, it would clearly record the ship's speed-over-ground instead of the speed-though-water. Dalheim and Steen (2021) presented a detailed account regarding the uncertainty in the speed-though-water measurements for a ship, commenting that the speed log sensors are considered to be one of the most inaccurate ones onboard the ship.

It may also be possible to estimate the speed-though-water of a ship using the ship's speed-over-ground and incident longitudinal water current speed. The speed-over-ground of a ship is measured using a GPS sensor, which is considered to be quite accurate, but unfortunately, the water current speed is seldom recorded onboard the ship. It is certainly possible to obtain the water current speed from a weather hindcast data source, but the hindcast measurements are not accurate enough to obtain a good estimate for speed-through-water, as indicated by Antola et al. (2017). It should also be noted that the temporal and spatial resolution of weather hindcast data is relatively larger than the sampling interval of the data recorded onboard the ship. Moreover, the water current speed varies along the depth of the sea, therefore, the incident longitudinal water current speed must be calculated as an integral of the water current speed profile over the depth of the ship. Thus, in order to obtain accurate estimates of speed-though-water, the water current speed has to be measured or estimated upto a certain depth of the sea with good enough accuracy, which is not possible with the current state-of-the-art.

3.1.2. Outliers

Another big challenge with data processing is the problem of detecting and handling outliers. As suggested by Olofsson (2020), it may be possible to categorize outliers into the following two broad categories: (a) Contextual outliers, and (b) Correlation-defying outliers[1]. Dalheim and Steen (2020b) presented methods to detect and remove contextual outliers, further categorized as (i) obvious (or invalid) outliers, (ii) repeated values, (iii) drop-outs, and (iv) spikes. Contextual outliers are easily identifiable as they either violate the known validity limits of one or more

---

[1]Called collective outliers by Olofsson (2020).

recorded variables (as seen in the case of obvious outliers and spikes) or present an easily identifiable but anomalous pattern (as seen in the case of repeated values and drop-outs).

The case of correlation-defying outliers is much more difficult to handle, as they can easily blend into the cleaned data pool. The two most popular methods which can be used to identify correlation-defying outliers are Principal Component Analysis (PCA) and autoencoders. Both these methods try to reconstruct the data samples after learning the correlation between the variables. It is quite obvious that a correlation-defying outlier would result in an abnormally high reconstruction error and, therefore, can be detected using such techniques. In a recent attempt, Thomas and Judith (2021) demonstrated an ensemble method combining PCA and autoencoders coupled with isolation forest to detect such outliers.

3.1.3. Time-Averaging Problem

As aforementioned, the onboard recorded in-service data can be supplied as time-averaged values over a short period of time (generally upto around 15 minutes). Although the time-averaging method eliminates white noise and reduces the variability in the data samples, it introduces a new problem in case of angular measurements. The angular measurements are, generally, recorded in the range of 0 to 360 degrees. When the measurement is around 0 or 360 degrees, it is obvious that the instantaneous measurements, reported by the sensor, will fluctuate in the vicinity of 0 and 360 degrees. For instance, assuming that the sensor reports a value of about 0 degree for half of the averaging time and about 360 degrees for the remaining time, the time-averaged value recorded by the data acquisition (DAQ) system will be around 180 degrees, which is significantly incorrect. Most of the angular measurements recorded onboard a ship, like relative wind direction, ship heading, etc., are known to inherit this problem, and it should be noted that, unlike the example given here, the incorrect time-averaged angle can take any value between 0 and 360 degrees, depending on the instantaneous values over which the average is calculated.

Although it may be possible to fix these incorrect values using a carefully designed algorithm, there is no established method available at the moment. Thus, it is suggested to fix these measurements using an alternate source for the data variables. For example, the wind direction can be gathered easily from a weather hindcast data source. Thus, it can be used to correct or just replace the relative wind direction measurements, recorded onboard the ship. The ship's heading, on the other hand, can be estimated using the latitude and longitude measurements from the GPS sensor.

3.2. AIS Data

AIS is an automatic tracking system that uses transceivers to help ships and maritime authorities identify and monitor ship movements. It is generally used as a tool for ship transportation services to prevent collisions during navigation. Ships over 300 tons must be equipped with transponders capable of transmitting and receiving all message types of AIS under the SOLAS Convention. AIS data is divided into dynamic (position, course, speed, etc.) static (ship name, dimensions, etc.), and voyage-related data (draft, destination, ETA, etc.). Dynamic data is automatically transmitted every 2-10 seconds depending on the speed and course of the ship, and if anchored, such information is automatically transmitted every 6 minutes. On the other hand, static and voyage-related data is provided by the ship's crew, and it is transmitted every 6 minutes regardless of the ship's movement state.

Since dynamic information is automatically updated based on sensor data, it is susceptible to faults and errors, similar to those described in section 3.1.1. In addition, problems may occur even in the process of collecting and transmitting data between AIS stations, as noted by Weng et al. (2020). The AIS signal can also be influenced by external factors, such as weather conditions and Earth's magnetic field, due to their interference with the very high frequency (VHF) equipment. Therefore, some of the AIS messages are lost or get mixed. Moreover, the receiving station has a short time slot during which the data must be received, and due to heavy traffic in the region, it fails to receive the data from all the ships in that time. In some cases, small ships deliver inaccurate information due to incorrectly calibrated transmitters, as shown by Weng et al. (2020). In a case study, Harati-Mokhtari et al. (2007) observed that 2% of the MMSI (Maritime Mobile Service Identity) information was incorrect and 30% of the ships were not properly marked with the correct navigation status. In the case of ship dimensions, about 18% of the information was found to be inaccurate. Therefore, before using AIS raw data for ship performance analysis, it is necessary to check key parameters such as GPS position, speed, and course, and the data identified as incorrect must be fixed.

3.2.1. Irrational Speed Data

The GPS speed (or speed-over-ground) measurements from AIS data may contain samples that have a sudden jump compared to adjacent samples or excessively higher or lower value than the normal operating range. This type of

Table 2

Typical service speed range of different ship types, given by Solutions (2018).

Category	Type	Service speed (knot)
Tanker	Crude oil carrier	13-17
	Gas tanker/LNG carrier	16-20
	Product	13-16
	Chemical	15-18
Bulk carrier	Ore carrier	14-15
	Regular	12-15
Container	Line carrier	20-23
	Feeder	18-21
General cargo	General cargo	14-20
	Coaster	13-16
Roll-on/roll-off cargo	Ro-Ro/Ro-Pax	18-23
Passenger ship	Cruise ship	20-23
	Ferry	16-23

inaccurate data can be identified through comparison with location and speed data of adjacent samples. The distance covered by the ship at the corresponding speed during the time between the two adjacent AIS messages is calculated, and the distance between the actual two coordinates is calculated using the Haversine formula (given by equation 1) to compare the two values. If the difference between the two values is negligible, the GPS speed can be said to be normal, but if not, it is recommended to be replaced with the GPS speed value of the adjacent sample. It should be noted that if the time difference between the samples is too short, the deviation of the distance calculated through this method may be large. In such a case, it is necessary to consider the average trend for several samples. If there are no valid samples nearby or the GPS coordinate data is problematic, one can refer to the normal service speed according to the ship type, as shown in table 2, or if available, a more specific method such as normalcy box (Rhodes et al. (2005); Tu et al. (2017)), which defines the speed range of the ships according to the geographic location, may be applied.

$$D = 2r \sin^{-1} \left(\sqrt{ \sin^2 \left(\frac{y_{i+1} - y_i}{2} \right) + \cos \left(y_i \right) \cos \left(y_{i+1} \right) \sin^2 \left(\frac{x_{i+1} - x_i}{2} \right) } \right) \tag{1}$$

Where D is the distance between two coordinates (x_i, y_i) and (x_{i+1}, y_{i+1}), r is the radius of Earth, and (x_i, y_i) is the longitude and latitude at timestamp i.

3.2.2. Uncertainty due to Human Error

AIS data, excluding dynamic information, is not automatically updated by the sensors, but it is logged by the ship's crew manually, so there is a possibility of human error. This includes information such as the draft, navigation status, destination, and estimated time of arrival (ETA) of the ship. Although it is difficult to clearly distinguish the incorrectly entered information, it is possible to indirectly determine whether the manual input values have been updated using the automatically logged dynamic information. Each number in navigation status represents ship activity such as 'under way using engine (0)', 'at anchorage (1)', and 'moored (5)'. If this field is being updated normally, it should be '0' if the ship is in-trip and '5' if it is at berth. If the navigation status of the collected AIS data is '1' or '5' above a certain GPS speed (or speed-over-ground), or if the state is set to '0' even when the speed is 0 and the location is within the port, the AIS data have not been updated on time and other manually entered information should also be questioned.

3.3. Noon Report Data

Ships engaged in international navigation of more than 500 gross tons are required to send a noon report to the company, which briefly records what happened on the ship from previous noon to present noon. The noon report must basically contain sufficient information regarding the location, course, speed, and internal and external conditions affecting the vessel's voyage. Additionally, the shipping company collects information related to fuel consumption and remaining fuel onboard, propeller slip, average RPM, etc. as needed. Such information is often used as a ship's management tool and reference data, such as monitoring and evaluating ship's performance, calculating energy

efficiency operating indicators, and obtaining fuel and freshwater order information. Despite its customary use, the standardized information in the noon reports may not be sufficient to accurately assess the performance of the ship, due to several problems discussed as follows. This information is based on the average values from noon to noon. For an accurate ship performance analysis, higher frequency samples and additional data may be recommended.

3.3.1. Uncertainties due to Averaging Measurements & Human Error

Basically, information reported through the noon reports is created based on the measurement values of the onboard sensor. Therefore, it also has the possibility to involve the problem of inherently faulty sensors and incorrect measurements, as discussed in section 3.1.1. Apart from the problems caused by sensors, the noon report data may have problems caused by the use of 24-hour averaged values and human errors. The data collection interval is once a day and the average of the values recorded for 24 hours is reported, thus, significant inaccuracies may be included in the data. Aldous et al. (2015) performed a sensitivity analysis to assess the uncertainty due to the input data for ship performance analysis using continuously recorded in-service data and noon reports. It was observed here that the uncertainty of the outcome was significantly sensitive to the number of samples in the dataset. In other words, such uncertainty can be mitigated through the use of data representing longer time-series, data collection with higher frequency, and data processing. These results were also confirmed by Park et al. (2017) and Themelis et al. (2018). Park et al. (2017) demonstrated in a case study that the power consumption between the noon reports and the recorded sensor data differed by 6.2% and 17.8% in ballast and laden voyage, respectively.

Using the averaged values over a long time period, as in the case of noon reports, the variations due to acceleration/deceleration and maneuvering cannot be captured. In particular, in the case of ships that sail relatively short voyages such as feeder ships and ferries, inappropriate data for performance analysis may be provided due to frequent changes in the operational state. In the case of information regarding the weather and sea states, the information generally corresponds to the condition right before the noon report is sent from the ship, therefore, it is not easy to account for the changes in the performance of the ship due to the variation of weather conditions during the last 24 hours. In general, the information to be logged in the noon report is read and noted by a person from onboard sensors. Thus, it is possible that the time at which the values are read from the sensors everyday may be different as well as different sensors may be used for the values to be logged for the same field. In addition, there may be cases when the observed value is incorrectly entered into the noon report. Thus, if the process of preparing the noon reports is not automated, there would always be a possibility of human errors in the data.

4. Results: Data Processing Framework

The results here are presented in the form of the developed data processing framework, which can be used to process raw data obtained from one of the above mentioned data sources (in section 3) for ship performance analysis. The data processing framework is designed to resolve most of the problems cited in the above section. Figure 1 shows the flow diagram for the data processing framework. The following sections will explain briefly the consecutive processing steps of the given flow diagram. It may be possible that the user may not able to carry-out each step due to unavailability of some information or features in the dataset, for example, due to the unavailability of the GPS data (latitude, longitude and timestamp variables), it may not be possible to interpolate weather hindcast data. In such a case, it is recommended to skip the corresponding step and continue with the next one.

The data processing framework has been outlined in such a manner that, after being implemented, it can be executed in a semi-automatic manner, i.e., requiring limited intervention from the user. The semi-autonomous nature of the framework would also result in fast data processing, which can be important for very large datasets. The implementation of the framework in terms of executable code is also quite important to obtain a semi-automatic and fast implementation of the data processing framework. Therefore, it is recommended to adopt best practices and optimized algorithms for each individual processing step according to the programming language in use. On another note, the reliability of the data processing activity is also quite critical to obtain good results. Therefore, it is important to carry-out the validation of work done in each processing step by creating visualization (or plots) and inspecting them for any undesired errors. The usual practice adopted here, while processing the data using the framework, is to create several such visualizations, like time-series plots of data variables in trip-wise manner (explained later in section 4.2), at the end of each processing step and then inspecting them to validate the outcome.
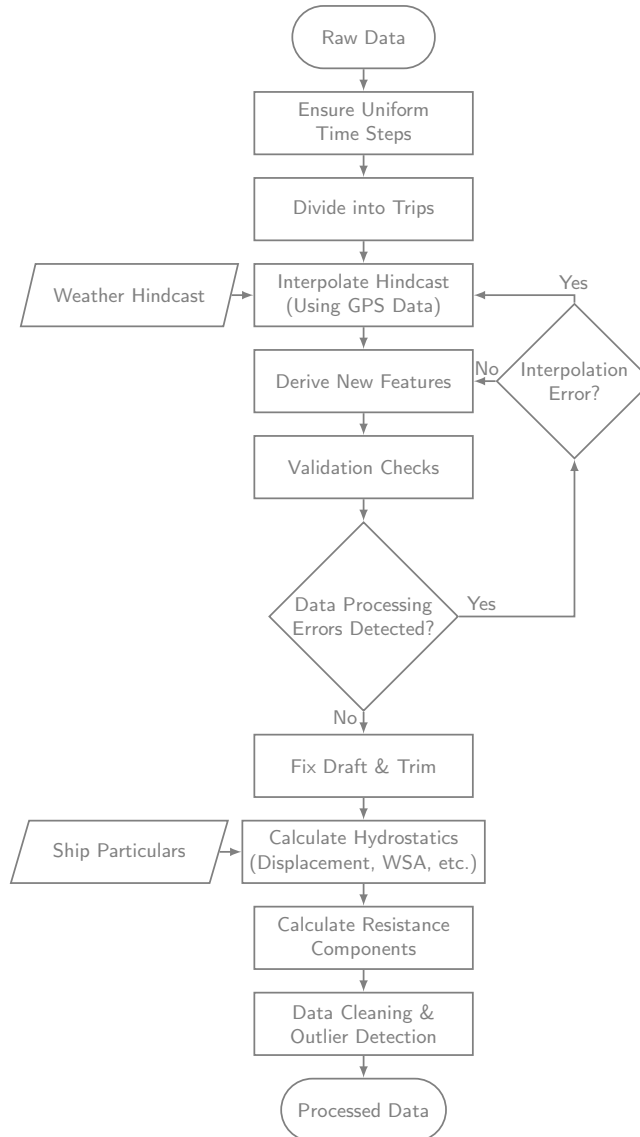
Figure 1: Data processing framework flow diagram.

4.1. Ensure Uniform Time Steps

Ensuring uniform and evenly-spaced samples would not only make it easier to apply time-gradient-based data processing or analysis steps but would also help avoid any misunderstanding while visualizing the data, by clearly showing a gap in the time-series plots (when plotted against sample numbers) and removing any abrupt jumps in the data values. Depending on the data acquisition (DAQ) system, the in-service data recorded onboard a ship is generally recorded with a uniform and evenly spaced sampling interval. Nevertheless, it is observed that the extracted sub-dataset

from the main database may contain several missing time steps (or timestamps). In such a case, it is recommended to check for such missing timestamps by simply calculating the gradient of timestamps, and for each missing timestamp, just add an empty row consisting only the missing timestamp value. Finally, the dataset should be sorted according the timestamps, resulting in a uniform and evenly-spaced list of samples.

Similar procedure can be adopted for a noon report dataset. The noon reports are generally recorded every 24 hours, but it may sometimes be more or less than 24 hours if the vessel's local time zone is adjusted, specially on the day of arrival or departure. The same procedure may not be feasible in case of AIS data, as the samples here are sporadically distributed in general. Here, the samples are collected at different frequencies depending on the ship's moving state, surrounding environment, traffic, and the type of AIS receiving station (land-based or satellite). It is observed here that the data is collected in short and continuous sections of the time-series, leaving some large gaps between samples, as shown in figure 2. Here, it is recommended to first resample the short and continuous sections of AIS data to a uniform sampling interval through data resampling techniques, i.e., up-sampling or down-sampling (as demonstrated by Virtanen et al. (2020)), and then, fill the remaining large gaps with empty rows.
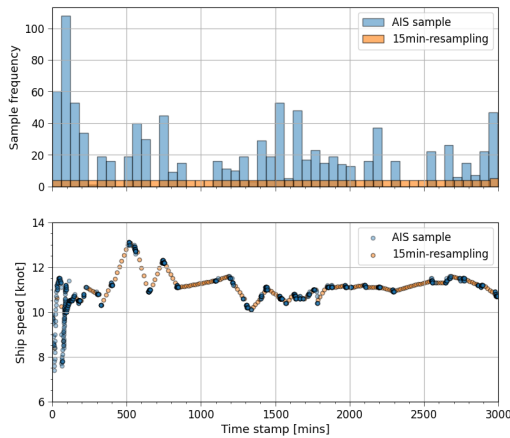
Figure 2: Down-sampling the collected AIS data to 15 minutes interval.

4.2. Divide Into Trips

Using conventional tools, data visualization becomes a challenge if the number of samples in the dataset is enormously large. It may simply not be practical to plot the whole time-series in a single plot. Moreover, dividing the time-series into individual trips may be considered as neat and help discretize the time-series into sensible sections which may be treated individually for further data processing and analysis. Plotting an individual trip would also give a complete overview of a port-to-port journey of the ship. Dividing the data into trips and at-berth legs would also make further data processing computationally less expensive as it may be possible to ignore a large number of samples (for further steps) where the ship is not in a trip. For such samples, it may not be necessary to interpolate hindcast, calculate hydrostatics, calculate resistance components, etc. Lastly, identifying individual trips would also make draft and trim correction step easier.

Dividing data into trips is substantially easier for noon reports and AIS data as they are generally supplied with a source and/or destination port name. In case of in-service data, it may be possible that no such information is available. In such a case, if the GPS data (latitude and longitudes) is available, it may be possible to just plot the samples on the world map and obtain individual trips by looking at the port calls. Alternatively, if the in-service data is supplied with a 'State' variable[2] (mentioned by Gupta et al. (2019)), indicating the propulsive state of the ship, like 'Sea Passage', 'At Berth', 'Maneuvering', etc., it is recommended to find the continuous legs of 'At Berth' state and enumerate the gaps in these legs with trip numbers, containing the rest of the states, as shown in figure 3a. Otherwise, it is recommended to

---

[2]Generally available for ships equipped with Marorka systems (www.marorka.com).

use the shaft rpm and GPS speed (or speed-over-ground) time-series to identify the starting and end of each port-to-port trip. Here, a threshold value can be adopted for the shaft rpm and GPS speed. All the samples above these threshold values (either or both) are considered to be in-trip samples, as shown in figure 3b. Thus, continuous legs of such in-trip samples can simply be identified and enumerated. It may also be possible to append few samples before and after each of these identified trips to obtain a proper trip, starting from zero and ending at zero. Such a process is designed keeping in mind the noise in the shaft rpm and GPS speed variables when the ship is actually static. Finally, if the GPS data is available, further adjustments can be done by looking at the port calls on the world map plotted with the GPS data.
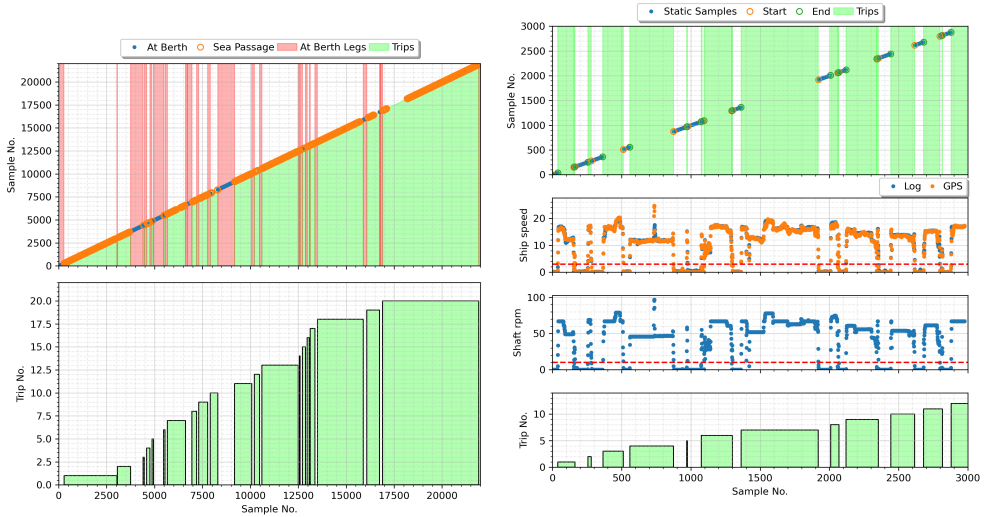
(a) Splitting time-series into trips using the 'State' variable.

(b) Splitting time-series into trips using threshold values (indicated by dashed red lines) for shaft rpm (10 rpm) and GPS speed (3 knots) variables.

Figure 3: Splitting time-series into trips.

4.3. Interpolate Hindcast & GPS Position Correction

Even if the raw data contains information regarding the state of the weather for each data sample, it may be a good idea to interpolate weather hindcast (or metocean) data available from one of the well-established sources. The interpolated hindcast data would not only provide a quantitative measure of the weather conditions (and, consequently, the environmental loads) experienced by the ship, but it would also help carry-out some important validation checks (discussed later in section 4.5). In order to interpolate hindcast data, the information regarding the location (latitude and longitude) and recording timestamp must be available in the ship's dataset. For ship performance analysis, it should be aimed that, at least, the information regarding the three main environmental load factors, i.e., wind, waves and sea currents, is gathered from the weather hindcast sources. For a further detailed analysis, it may also be a good idea to obtain additional variables, like sea water temperature (both surface and gradient along the depth of the ship), salinity, etc.

Before interpolating the weather hindcast data to the ship's location and timestamps, it is recommended to ensure that the available GPS (or navigation) data is validated and corrected (if possible) for any errors. If the GPS data is inaccurate, weather information at the wrong location is obtained, resulting in incorrect values for further analysis. For instance, the ship's original trajectory obtained from the GPS data, presented in figure 4a, shows that the ship proceeds in a certain direction while suddenly jumping to an off-route location occasionally. The ship, of course, may have gone off-route as shown here, but referring to the GPS speed and heading of the ship at the corresponding time, shown in figure 4b, it is obvious that the navigation data is incorrect. Here, such an irrational position change can be detected through the two-stage steady-state (or stationarity) filter suggested by Gupta et al. (2021b), based on the

60

method developed by Dalheim and Steen (2020a). The first stage of the filter uses a sliding window to remove unsteady samples by performing a t-test on the slope of the data values, while the second stage performs an additional gradient check for the samples failing in the first stage to retain the misidentified samples. The 'irrational position' in figure 4a shows the coordinates identified as unsteady when the above two-stage filter is applied to longitude and latitude time-series. The filtered trajectory is further obtained after removing the samples with 'irrational position' from the original data.
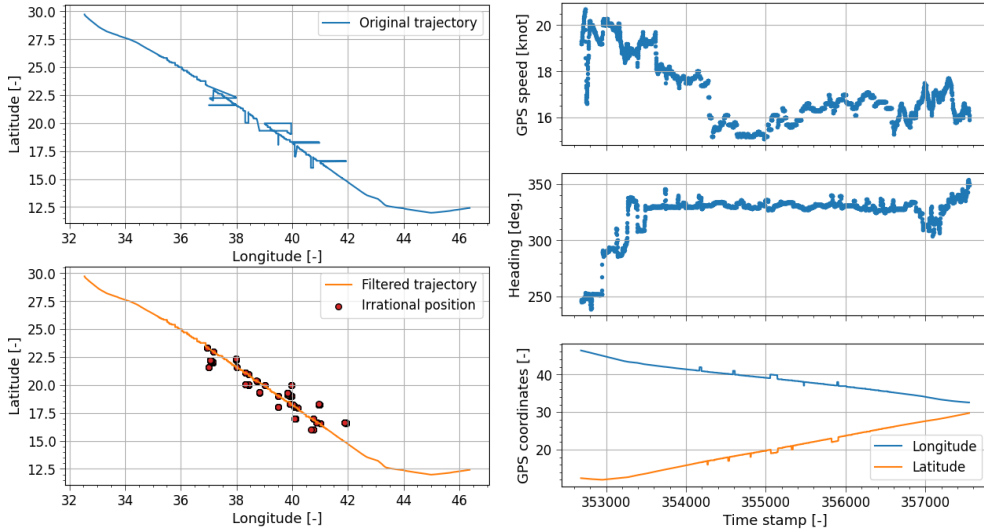
(a) Original trajectory and filtered trajectory with irrational GPS position.

(b) Trends of GPS speed, heading, and position of the ship according to the corresponding period.

Figure 4: GPS position cleaning using the steady-state detection algorithm.

The hindcast data sources generally allow downloading a subset of the variables, timestamps, and a sub-grid of latitudes and longitudes, i.e., the geographical location. Depending on the hindcast source, the datasets can be downloaded manually (by filling a form), using an automated API script, or even by directly accessing their ftp servers. It may also be possible to select the temporal and spatial resolution of the variables being downloaded. In some cases, the hindcast web servers allows the users to send a single query, in terms of location, timestamp, and list of variables, to extract the required data for an individual sample. But every query received by these servers is generally queued for processing, causing substantially long waiting times, as they are facing a good amount of traffic from all over the world. Thus, it is recommended to simply download the required subset of data on a local machine for faster interpolation.

Once the hindcast data files are available offline, the main task at hand is to understand the cryptic (but highly efficient) data packaging format. Now-a-days, the two most poplar formats for such data files are GRIdded Binary data (GRIB) and NetCDF. GRIB (available as GRIB1 or GRIB2) is the international standard accepted by World Meteorological Organization (WMO), but due to some compatibility issues with windows operating systems, it may be preferable to use the NetCDF format.

Finally, a step-by-step interpolation has to be carried-out for each data sample from the ship's dataset. Algorithm 1 shows a simple procedure for n-th order (in time) interpolation scheme. Here, the spatial and temporal interpolation is performed in steps 10 and 12, respectively. For a simple and reliable procedure, it is recommended to perform the spatial interpolation using a grid of latitudes and longitudes around the ship's location, after fitting a linear or non-linear 2D surface over the hindcast grid. It may be best to use a linear surface here as, firstly, the hindcast data may not be so accurate that performing a higher order interpolation would provide any better estimates, and secondly, in some case, higher order interpolation may result in highly inaccurate estimates, due to the waviness of the over-fitted non-linear

61

surface. Similar arguments can be given in the case of temporal interpolation, and therefore, a linear interpolation in time can also be considered acceptable. The advantage of using the given algorithm is that the interpolation steps, here, can be easily validated by plotting contours (for spatial interpolation) and time-series (for temporal interpolation).

Algorithm 1 A simple algorithm for n-th order interpolation of weather hindcast data variables.

1: $wData \leftarrow$ weather hindcast data
2: $x \leftarrow$ data variables to interpolate from hindcast
3: $wT \leftarrow$ timestamps in $wData$
4: **for all** timestamps in ship's dataset **do**
5:     $t \leftarrow$ current ship time stamp
6:     $loc \leftarrow$ current ship location (latitude & longitude)
7:     $i \leftarrow n+1$ indices of wT around t
8:     **for all** x **do**
9:         **for all** i **do**
10:             $x[i] \leftarrow$ 2D spatial interpolation at loc using $wData[x][i, :, :]$
11:         **end for**
12:         $X \leftarrow$ n-th order temporal interpolation at t using $x[i]$
13:     **end for**
14: **end for**

An important feature of hindcast datasets is masking the invalid values. For instance, the significant wave height should only be predicted by the hindcast model for the grid nodes which fall in the sea, requesting the value of such a variable on land should result in an invalid value. Such invalid values (or nodes) are by default masked in the downloaded hindcast data files, probably for an efficient storage of the data. These masked nodes may be filled with zeros before carrying-out the spatial interpolation in step 10, as one or more of these nodes may be contributing to the interpolation. Alternatively, if a particular masked node is contributing to the interpolation, it can be set to the mean of other nodes surrounding the point of interpolation, as suggested by Ejdfors (2019). It is argued by Ejdfors (2019) that this would help avoid the artificially low (zero) values during the interpolation, but if the grid resolution is fine-enough, it is expected that the calculated mean (of unmasked surrounding nodes) would also not be much higher than zero.

4.4. Derive New Features

Interpolating the weather hindcast variables to ship's location at a given time would provide the hindcast variables in the global (or the hindcast model's) reference frame. For further analysis, it may be appropriate to translate these variables to ship's frame of reference, and furthermore, it may be desired to calculate some new variables which could be more relevant for the analysis or could help validate the assimilated (ship and hindcast) dataset. The wind and sea current variables, obtained from the hindcast source and the ship's dataset, can be resolved into the longitudinal and transverse speed components for validation and further analysis. Unfortunately, the wave load variables cannot be resolved in a similar manner, but the mean wave direction should be translated into the relative mean wave direction (relative to the ship's heading or course).

4.5. Validation Checks

Although it is recommended to validate each processing step by visualizing (or plotting) the task being done, it may be a good idea to take an intermediate pause and perform all types of possible validation checks. These validation checks would not only help assess the dataset from reliability point of view but can also be used to understand the correlation between various features. The validation checks can be done top-down, starting from the most critical feature to the least one. As explained in section 2.2, the shaft power measurements can be validated against the shaft rpm and shaft torque measurements, if these are available, else just plotting the shaft rpm against the shaft power can also provide a good insight into the quality of data. For a better assessment, it is suggested to visualize the shaft rpm vs shaft power overlaid with the engine operational envelope and propeller curves, as presented by Liu et al. (2020) (in figure 11). Any sample falling outside the shaft power overload envelope (specially at high shaft rpm) should be removed from the analysis, as they may be having measurement errors. It may also be possible to make corrections, if the shaft power data seems to be shifted (up or down) with respect to the propeller curves due to sensor bias.

The quality of speed-through-water measurements can be assessed by validating it against its estimate, obtained as a difference between the speed-over-ground and longitudinal current speed. Here, it should be kept in mind that the two values may not be a very good match due to several problems cited in section 3.1.1. Visualizing the speed-though-water vs shaft power along with all the available estimates of the speed-power calm-water curve is also an important validation step (shown in figure 5). Here, the majority of measurement data should accumulate around these curves. In case of disparity between the curves, the curve obtained through the sea trial of the actual ship may take precedence.
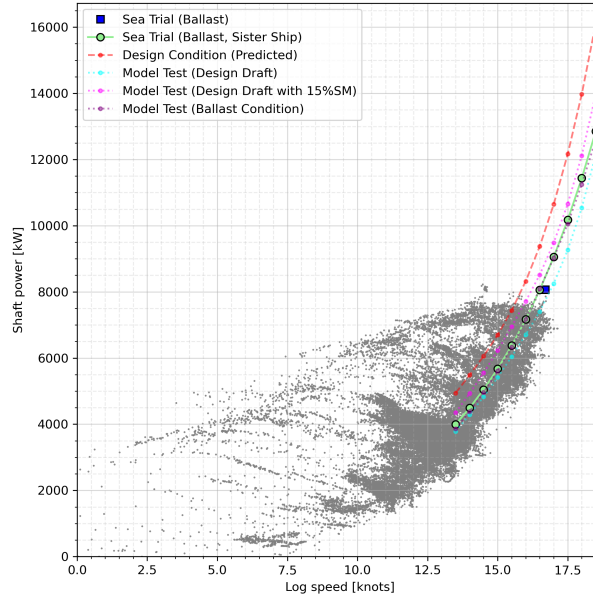
Figure 5: Speed-though-water (log speed) vs shaft power with various estimates of speed-power calm-water curves.

The interpolated weather hindcast data variables must also be validated against the measurements taken onboard the ship. This is quite critical as the sign and direction notations assumed by the hindcast models and ship's sensors (or data acquisition system) are probably not the same, which may cause mistakes during the interpolation step. Moreover, most ships are generally equipped with anemometers that can measure the actual and relative wind speed and directions, and these two modes (actual or relative) can be switched through a simple manipulation by the crew onboard. It is possible that this mode change may have occurred during the data recording duration, resulting in errors in the recorded data. In addition, there may be a difference between the reference height of the wind hindcast data and the vertical position of the installed anemometer, which may lead to somewhat different results even at the same location at sea. The wind speed at the reference height (V_{WTref}) can be corrected using the anemometer recorded wind speed (V_{WT}), assuming a wind speed profile, as follows (recommended by ITTC (2017)):

$$V_{WTref} = V_{WT} \left(\frac{Z_{ref}}{Z_a} \right)^{\frac{1}{9}} \tag{2}$$

Where Z_{ref} is the reference height above the sea level and Z_a is the height of the anemometer.

Finally, these wind measurements can be translated into the longitudinal and transverse relative components. The obtained transverse relative wind speed can be validated against the transverse wind speed, obtained from the hindcast source, as they are basically the same. Similarly, the difference between the longitudinal relative wind speed and the speed-over-ground of the ship can be validated against the longitudinal wind speed measurements from hindcast, as

shown in figure 6. In case of time-averaged in-service data, the problem of faulty averaging of angular measurements when the measurement values are near 0 or 360 degrees (i.e., the angular limits), explained in section 3.1.3, must also be verified and appropriate corrective measures should be taken. From figure 6, it can be clearly seen that the time-averaging problem (in relative wind direction) causes the longitudinal wind speed (estimated using the ship data) to jump from positive to negative, resulting in a mismatch with the corresponding hindcast values. In such a case, it is recommended to either fix these faulty measurements, which may be difficult as there is no proven way to do it, or just use the hindcast measurements for further analysis.
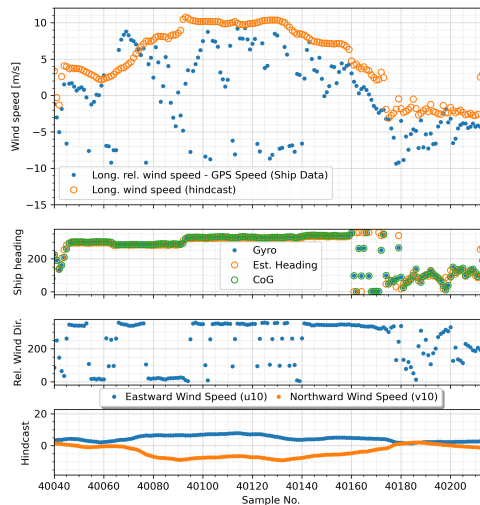
Figure 6: Validating longitudinal wind speed obtained using the ship data against the values obtained from the hindcast. The time-averaging problem with angular measurements around 0 or 360 degrees (explained in section 3.1.3) is clearly visible here.

As discussed in the case of noon reports in section 3.3.1, weather information generally refers to the state of the weather at the time when the report is logged, which is probably not the average state from noon to noon. Furthermore, the wind loads here are observed based on the Beaufort scale, therefore, the deviation may be somewhat large when converted to the velocity scale. In this case, it is recommended to consider the daily average values obtained from the weather hindcast data, over the travel region, rather than the noon report values.

4.6. Data Processing Errors

The validation step is very critical in finding out any processing mistakes or inherent problems with the dataset, as demonstrated in the previous section. Such problems or mistakes, if detected, must be corrected or amended for before moving forward with the processing and analysis. The main mistakes found at this step are generally either interpolation mistakes or incorrect formulation of the newly derived feature. These mistakes should be rectified accordingly, as shown in the flow diagram (figure 1).

4.7. Fix Draft & Trim

The draft measurements recorded onboard the ship are often found to be incorrect due to the Venturi effect, explained briefly in section 3.1.1. The Venturi effect causes the draft measurements to drop to a lower value due to a non-zero negative dynamic pressure as soon as the ship develops a relative velocity with respect of the water around the hull. Thus, the simplest solution to fix these incorrect measurements is by interpolating the draft during a voyage using the draft measured just before and after the voyage. Such a simple solution provides good results for a simple case where the draft of the ship basically remains unchanged during the voyage, except for the reduction of draft due to consumed fuel, as shown in the figure 7a.

64

(a) Simple draft correction.

(b) Complex draft correction.
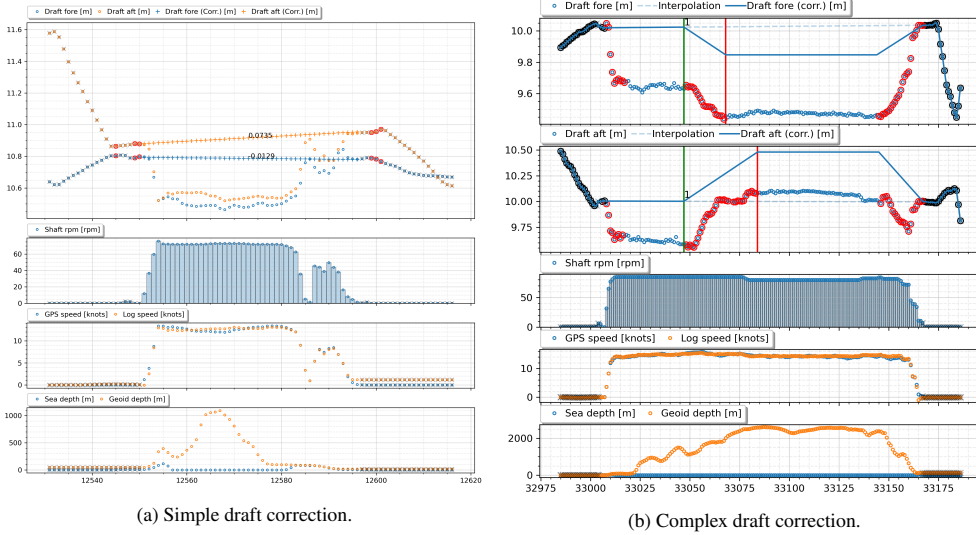
Figure 7: Correcting in-service measured draft.

In a more complex case where the draft of the ship is changed in the middle of the voyage and the ship is still moving, i.e., conducting ballasting operations or trim adjustments during transit, the simple draft interpolation would result in corrections which can be way off the actual draft of the vessel. As shown in figure 7b, the fore draft is seen to be dropping and the aft draft increasing in the middle of the voyage without much change in the vessel speed, indicating trim adjustments during transit. In this case, a more complex correction is applied after taking into account the change in draft during the transit. Here, first of all, a draft change operation is identified (marked by green and red vertical lines in figure 7b), then the difference between the measurements before and after the operation is calculated by taking an average over a number of samples. Finally, a ramp is created between the starting of the draft change operation (green line) and the end of operation (red line). The slope of the ramp is calculated using the difference between the draft measurements before and after the draft change operation. The draft change operation can either be identified manually, by looking at the time-series plots, or using the steady-state (or stationarity) filter developed by Dalheim and Steen (2020a).

In case of AIS data, Bailey et al. (2008) reported that 31% of the draft information out of the investigated AIS messages had obvious errors. The draft information from AIS data generally corresponds to the condition of ships while arriving at or departing from the port, and changes due to fuel consumption and ballast adjustment onboard are rarely updated. Since the draft obtained from the AIS as well as noon reports has a long update cycle and is acquired by humans, it is practically difficult to precisely fix the draft values as in the case of in-service data. However, by comparing the obtained draft with a reference value, it may be possible to gauge whether the obtained draft is, in fact, correct. If the obtained draft excessively deviates from the reference, it may be possible to remove the corresponding data samples from further analysis or replace the obtained draft value with a more appropriate value. Table 3 shows the results of investigating the average draft ratio, which is the ratio of the actual draft (T_c) and design draft (T_d), for various ship types from 2013 to 2015 by Olmer et al. (2017). As summarized in the table, the draft ratio varies depending on the ship type and the voyage type. By using these values as the above mentioned reference, the draft obtained from the AIS data and noon reports can be roughly checked and corrected.

4.8. Calculate Hydrostatics

Depending on the type of performance analysis, it may be necessary to have features like displacement, wetted surface area (WSA), etc. in the dataset, as they are more relevant from a hydrodynamic point of view. Moreover, most of the empirical or physics-based methods for resistance calculations (to be done in the next step) requires these

65

Table 3

Average draft ratio (T_c/T_d) for different ship types. T_c = actual draft during a voyage; T_d = design draft of the ship.

Ship types	Ballast Voyage	Laden Voyage
Liquefied gas tanker	0.67	0.89
Chemical tanker	0.66	0.88
Oil tanker	0.60	0.89
Bulk carrier	0.58	0.91
General cargo	0.65	0.89
The following ship types do not generally have ballast-only voyages.		
Container		0.82
Ro-Ro		0.87
Cruise		0.98
Ferry pax		0.90
Ferry ro-pax		0.93

Table 4

Estimation formulas for wetted surface area of different ship types.

Category	Formula	Reference
Tanker/Bulk carrier	$WSA = 0.99 \cdot (\frac{\nabla}{T} + 1.9 \cdot L_{WL} \cdot T)$	Kristensen and Bingham (2017)
Container	$WSA = 0.995 \cdot (\frac{\nabla}{T} + 1.9 \cdot L_{WL} \cdot T)$	Kristensen and Bingham (2017)
Other (General)	$WSA = 1.025 \cdot (\frac{\nabla}{T} + 1.7 \cdot L_{PP} \cdot T)$	Molland (2011)

Table 5

Typical block coefficient (C_B) range at design draft for different ship types, given by Solutions (2018).

Category	Type	Block coefficient (C_B)
Tanker	Crude oil carrier	0.78-0.83
	Gas tanker/LNG carrier	0.65-0.75
	Product	0.75-0.80
	Chemical	0.70-0.78
Bulk carrier	Ore carrier	0.80-0.85
	Regular	0.75-0.85
Container	Line carrier	0.62-0.72
	Feeder	0.60-0.70
General cargo	General cargo/Coaster	0.70-0.85
Roll-on/roll-off cargo	Ro-Ro cargo	0.55-0.70
	Ro-pax	0.50-0.70
Passenger ship	Cruise ship	0.60-0.70
	Ferry	0.50-0.70

features. Unfortunately, these feature cannot be directly recorded onboard the ship. But it is fairly convenient to estimate them using the ship's hydrostatic table or hull form (or offset table) for the corresponding mean draft and trim for each data sample. Here, it is recommended to use the corrected draft and trim values, obtained in the previous step. If the detailed hull form is not available, the wetted surface area can also be estimated using the empirical formulas shown in table 4. The displacement at design draft, on the other hand, can be estimated using the ship particulars and typical range of block coefficient (C_B), presented in table 5.

4.9. Calculate Resistance Components

There are several components of the ship's total resistance, and there are several methods to estimate each of these components. The three main resistance components which generally constitutes the majority of the ship's total resistance are calm-water, added wind, and added wave resistance. It is possible to further divide the calm-water resistance into sub-components, namely, skin friction and residual resistance. The total calm-water resistance can be calculated using one of the many well-known empirical methods, like Guldhammer and Harvald (Guldhammer

and Harvald (1970)), updated Guldhammer and Harvald (Kristensen and Bingham (2017)), Hollenbach (Hollenbach (1998)), Holtrop and Mennen (Holtrop and Mennen (1982)), etc. These empirical methods are developed using the data from numerous model test results of different types of ships, and each one is proven to be fitting well on several different ship types. The latter makes choosing the right method for a ship quite complicated.

The easiest way to choose the right calm-water resistance estimation method is to calculate the calm-water resistance from each of these methods and comparing it with the corresponding data obtained for the given ship. The calm-water data for a given ship can be obtained from the model tests, sea trial, or even filtering the operational data, obtained from one of the sources discussed here (in section 3), for near-calm-water condition. The usual practice here is to use the sea trial data as it is obtained and corrected for near-calm-water condition and do not suffer from scale effects, seen in model test results. But the sea trials are sometimes conducted at only the high range of speed and ballast displacement (as shown in figure 5). Thus, it is recommended to use the near-calm-water filtered (and corrected) operational data to choose the right method so that a good fit can be ensured for a complete range to speed and displacement.

According to ITTC (2017), the increase in resistance due to wind loads can be obtained by applying one of the three suggested methods, namely, wind tunnel model tests, STA-JIP, and Fujiwara's method. If the wind tunnel model test results for the vessel are available, it may be considered as the most accurate method for estimating added wind resistance. Otherwise, the database of wind resistance coefficients established by STA-JIP (van den Boom et al. (2013)) or the regression formula presented by Fujiwara et al. (2005) is recommended. From the STA-JIP database, experimental values according to the specific ship type can be obtained, whereas Fujiwara's method is based-on the regression analysis of data obtained from several wind tunnel model tests for different ship types.

The two main sets of parameters required to estimate the added wind resistance using any of the above three methods are incident wind parameters and information regarding the exposed area to the wind. The incident wind parameters, i.e., relative wind speed and direction, can be obtained from onboard measurements or weather hindcast data. In case of weather hindcast data, the relative wind measurements can be calculated from the hindcast values according to the formulation outlined by ITTC (2017) in section E.1, and in case of onboard measurements, the relative wind measurements should be corrected for the vertical position of the anemometer according to the instructions given by ITTC (2017) in section E.2, also explained here in section 4.5. The information regarding the exposed area to the wind can be either estimated using the general arrangement drawing of the ship or approximately obtained using a regression formula based-on the data from several ship, presented by Kitamura et al. (2017).

The added wave resistance (R_{AW}) can also be obtained in a similar manner using one of the several well-established methods for estimating R_{AW}. ITTC (2017) recommends conducting sea keeping model tests in regular waves to obtain R_{AW} transfer functions, which can further be used to estimate R_{AW} for the ship in irregular seas. To empirically obtain these transfer functions or R_{AW} for a given ship, it is possible to use physics-based empirical methods like STAWAVE1 and STAWAVE2 (recommended by ITTC (2017)). STAWAVE1 is a simplified method for directly estimating R_{AW} in head wave conditions only, and it requires limited input, including ship's waterline length, breadth, and significant wave height. STAWAVE2 is an advanced method to empirically estimate parametric R_{AW} transfer functions for a ship. The method is developed using an extensive database of sea keeping model test results from numerous ships, but unfortunately, it only provides transfer functions for approximate head wave conditions (0 to ±45 degrees from bow). A method proposed by DTU (Martinsen (2016); Taskar and Andersen (2019); Taskar and Andersen (2021)) provides transfer functions for head to beam seas, i.e., 0 to ±90 degrees from bow. Finally, for all wave heading, it may be recommended to use the newly established method by Liu et al. (2020). There have been several studies to assess and compare the efficacy of each of these methods and several other methods, but no consistent guidelines are provided regarding their applicability.

4.10. Data Cleaning & Outlier Detection

It may be argued by some that the process of data cleaning and outlier detection should be carried-out way earlier in the data processing framework, as proposed by Dalheim and Steen (2020b), but it should be noted here that all the above steps proposed here have to be performed only once for a given dataset, whereas data cleaning is done based on the features selected for further analysis. Since the same dataset can be used for several different analyses, which may be using different sets of features, some part of data cleaning has to be repeated before each analysis to obtain a clean dataset with as many data samples as possible. Moreover, the additional features acquired during the above listed processing steps may be helpful in determining to a better extent if a suspected sample is actually an outlier or not.

Nevertheless, it may be possible to reduce the work load for the above processing steps by performing some basic data cleaning before some of these steps. For instance, while calculating the resistance components for in-trip data samples, it is possible to filter-out samples with invalid values for one or more of the ship data variables used to calculate these components, like speed-though-water, mean draft (or displacement), etc. This would reduce the number of samples for which the new feature has to be calculated. It should also be noted that even if such simple data cleaning (before each step) is not performed, these invalid samples would be easily filtered-out in the present step. Thus, the reliability and efficacy of the data processing framework is not affected by performing the data cleaning and outlier detection step at the end.

Most of the methods developed for ship performance monitoring assumes that the ship is in a quasi-steady state for each data sample. The quasi-steady assumption indicates that the propulsive state of the ship remains more or less constant during the sample recording duration, i.e., the ship is neither accelerating nor decelerating. This is specially critical for aforementioned time-averaged datasets, as the averaging duration can be substantially long, hiding the effects of accelerations and decelerations. Here, the two-stage steady-state filter, explained in section 4.3, can be applied to the shaft rpm time-series to remove the samples with accelerations and decelerations, resulting in quasi-steady samples. In tandem to the steady-state filter on the shaft rpm time-series, it may also be possible to use the steady-state filter, with relaxed setting, on the speed-over-ground time-series to filter-out the sample where the GPS speed (or speed-over-ground) signal suddenly drops or recovers from a dead state, resulting in measurement errors.

As discussed in section 3.1.2, the outliers can be divided into two broad categories: (a) Contextual outliers, and (b) Correlation-defying outliers. The contextual outliers can be identified and resolved by the methods presented as well as demonstrated by Dalheim and Steen (2020b), and for correlation-defying outliers, methods like Principal Component Analysis (PCA) and autoencoders can be used. Figure 8 shows the in-service data samples recorded onboard a ship. The data here is already filtered-out for quasi-steady assumption, explained above, and contextual outliers, according to the methods suggested by Dalheim and Steen (2020b). Thus, the samples highlighted by red circles (around 6.4 MW shaft power in figure 8a) can be classified as correlation-defying outliers. The time-series plot (shown in figure 8b) clearly indicates that the detected outliers have faulty measurements for the speed-through-water (stw) and speed-over-ground (sog), defying the correlation between these variables and the rest. It is also quite surprising to notice that the same fault occurs in both the speed measurements at the same time, considering that they are probably obtained from different sensors.
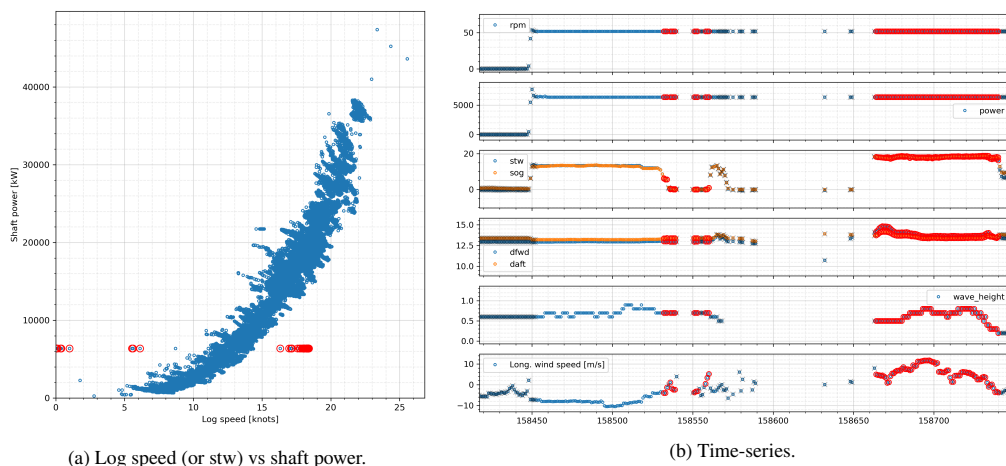

(a) Log speed (or stw) vs shaft power.

(b) Time-series.

Figure 8: Correlation-defying outliers marked with red circles.

5. Conclusion

The quality of data is very important in estimating the performance of a ship. In this study, a streamlined semi-automatic data processing framework is developed for ship performance analysis. The data processing framework can be used to process data from several different sources, like onboard recorded in-service data, AIS data and noon reports. These three data sources are discussed here in detail along with their inherent problems and associated examples. It is here recommended to use the onboard recorded in-service data for ship performance monitoring over the other data sources, as it is considered more reliable due its consistent and higher sampling rate. Moreover, the AIS data and noon reports lacks some of the critical variables required for ship performance analysis, and they are also susceptible to human error, as some of the data variables recorded here are manually logged by the ship's crew. Nevertheless, all three data sources are known to have several problems and should be processed carefully for any further analysis.

The data processing framework, presented in the current work, is designed to address and resolve most of the problems found in the above three data sources. It is first recommended to divide the data into trips so that further processing can be performed in a more systematic manner. A simple logic to divide the data into individual trips is outlined here if the port call information is not available. The weather hindcast (metocean) data is considered as an important supplementary information, which can be used for data validation and estimating environmental loads experienced by the ship. A simple algorithm to effectively interpolate the hindcast data at a specific time and location of a ship is presented within the data processing framework. The problem of erroneous draft measurements, caused due to the Venturi effect, is discussed in detail as well as simple interpolation is recommended to fix these measurements. A more complex case, where the draft or trim is voluntarily adjusted during the voyage without reducing the vessel speed, is also presented here. Such a case cannot be resolved with simple interpolation, and therefore, an alternate method is suggested for the same problem.

Choosing the most suitable methods for estimating resistance components may also be critical for ship performance analysis. It is, therefore, recommended to carry out some validation checks to find the most suitable methods before adopting them into practice. Such validation checks should be done, wherever possible, using the data obtained from the ship while in-service rather than just using the sea trial or model test results. Data cleaning and outlier detection is also considered an important step for processing the data. Since cleaning the data requires selecting a subset of features relevant for the analysis, it is recommended to perform this as the last step of the data processing framework, and some part of it should be reiterated before carrying out a new type of analysis. The presented data processing framework can be systematically and efficiently adopted to process the datasets for ship performance analysis. Moreover, the various data processing methods or steps mentioned here can also be used elsewhere to process the time-series data from ships or similar sources, which can be used further for a variety of tasks.

CRediT authorship contribution statement

Prateek Gupta: Conceptualization, Methodology, Investigation, Software, Data curation, Visualization, Writing. **Young-Rong Kim:** Conceptualization, Methodology, Investigation, Software, Data curation, Visualization, Writing. **Sverre Steen:** Conceptualization, Supervision, Resources. **Adil Rasheed:** Conceptualization, Supervision.

References

Aldous, L., Smith, T., Bucknall, R., Thompson, P., 2015. Uncertainty analysis in ship performance monitoring. Ocean Engineering 110, 29–38.

American Bureau of Shipping, 2020. Guide for smart functions for marine vessels and offshore units. ABS Guides .

Antola, M., Solonen, A., Pyorre, J., 2017. Notorious speed through water. 2nd Hull Performance & Insight Conference (HullPIC'17) , 156–165.

Bailey, N.J., Ellis, N., Sampson, H., 2008. Training and technology onboard ship: how seafarers learned to use the shipboard automatic identification system (AIS). Seafarers International Research Centre (SIRC), Cardiff University.

van den Boom, H., Huisman, H., Mennen, F., 2013. New guidelines for speed/power trials. Level playing field established for IMO EEDI. SWZ Maritime , 1–11.

Carchen, A., Atlar, M., 2020. Four KPIs for the assessment of biofouling effect on ship performance. Ocean Engineering 217, 107971. URL: https://www.sciencedirect.com/science/article/pii/S0029801820309239, doi:https://doi.org/10.1016/j.oceaneng.2020.107971.

Coraddu, A., Oneto, L., Baldi, F., Cipollini, F., Atlar, M., Savio, S., 2019. Data-driven ship digital twin for estimating the speed loss caused by the marine fouling. Ocean Engineering 186. doi:10.1016/j.oceaneng.2019.05.045. cited By 1.

Dalheim, Ø., Steen, S., 2020a. A computationally efficient method for identification of steady state in time series data from ship monitoring. Journal of Ocean Engineering and Science doi:10.1016/j.joes.2020.01.003. cited By 1.

Dalheim, Ø.Ø., Steen, S., 2020b. Preparation of in-service measurement data for ship operation and performance analysis. Ocean Engineering 212, 107730. URL: https://www.sciencedirect.com/science/article/pii/S0029801820307125, doi:https://doi.org/10.1016/j.oceaneng.2020.107730.

Dalheim, Ø.Ø., Steen, S., 2021. Uncertainty in the real-time estimation of ship speed through water. Ocean Engineering 235, 109423. URL: https://www.sciencedirect.com/science/article/pii/S0029801821008313, doi:https://doi.org/10.1016/j.oceaneng.2021.109423.

Ejdfors, K.O., 2019. Use of in-service data to determine the added power of a ship due to fouling. Master's thesis. NTNU. URL: http://hdl.handle.net/11250/2622960.

Farag, Y.B., Ölçer, A.I., 2020. The development of a ship performance model in varying operating conditions based on ann and regression techniques. Ocean Engineering 198, 106972. URL: https://www.sciencedirect.com/science/article/pii/S0029801820300536, doi:https://doi.org/10.1016/j.oceaneng.2020.106972.

Foteinos, M., Tzanos, E., Kyrtatos, N., 2017. Ship hull fouling estimation using shipboard measurements, models for resistance components, and shaft torque calculation using engine model. Journal of Ship Research 61, 64–74. URL: https://www.scopus.com/inward/record.uri?eid=2-s2.0-85024491367&doi=10.5957%2fJOSR.61.2.160053&partnerID=40&md5=4d8fedda376f0ed57cf089dbbfe28012, doi:10.5957/JOSR.61.2.160053. cited By 3.

Fujiwara, T., Ueno, M., Ikeda, Y., 2005. A new estimation method of wind forces and moments acting on ships on the basis of physical component models. Journal of the Japan Society of Naval Architects and Ocean Engineers 2, 243–255. doi:10.2534/jjasnaoe.2.243.

Guldhammer, H., Harvald, S., 1970. Ship Resistance: Effect of Form and Principal Dimensions. Akademisk Forlag.

Gupta, P., Rasheed, A., Steen, S., 2021a. Ship performance monitoring using machine-learning. arXiv:2110.03594.

Gupta, P., Steen, S., Rasheed, A., 2019. Big data analytics as a tool to monitor hydrodynamic performance of a ship. doi:10.1115/OMAE2019-95815. v07AT06A059.

Gupta, P., Taskar, B., Steen, S., Rasheed, A., 2021b. Statistical modeling of ship's hydrodynamic performance indicator. Applied Ocean Research 111, 102623. URL: https://www.sciencedirect.com/science/article/pii/S0141118721001000, doi:https://doi.org/10.1016/j.apor.2021.102623.

Hansen, S.V., Petersen, J., Jensen, J., 2011. Performance monitoring of ships. DTU Mechanical Engineering.

Harati-Mokhtari, A., Wall, A., Brooks, P., Wang, J., 2007. Automatic identification system (ais): data reliability and human error implications. The Journal of Navigation 60, 373–389.

Hollenbach, K.U., 1998. Estimating resistance and propulsion for single-screw and twin-screw ships. Ship Technology Research 45, 72–76. Cited By 21.

Holtrop, J., Mennen, G., 1982. Approximate power prediction method., pp. 166–170. URL: https://www.scopus.com/inward/record.uri?eid=2-s2.0-0002154745&doi=10.3233%2fisp-1982-2933501&partnerID=40&md5=d9302542762e00fd19dfb49dd2bd6990, doi:10.3233/isp-1982-2933501. cited By 347.

ISO, 2016. ISO 19030-2:2016: Ships and marine technology — measurement of changes in hull and propeller performance — part 2: Default method. URL: https://www.iso.org/standard/63775.html.

ITTC, 2017. Recommended procedures and guidelines 7.5-04-01-01.1: Preparation, conduct and analysis of speed/power trials. URL: https://www.ittc.info/media/7691/75-04-01-011.pdf.

Jerri, A.J., 1977. The shannon sampling theorem—its various extensions and applications: A tutorial review. Proceedings of the IEEE 65, 1565–1596.

Karagiannidis, P., Themelis, N., 2021. Data-driven modelling of ship propulsion and the effect of data pre-processing on the prediction of ship fuel consumption and speed loss. Ocean Engineering 222, 108616. URL: https://www.sciencedirect.com/science/article/pii/S0029801821000512, doi:https://doi.org/10.1016/j.oceaneng.2021.108616.

Kim, S.Y., Kim, M.S., Han, K.M., gyu Kim, J., Seo, D.W., 2020. Study on Data Analysis of On-Board Measurement Data for Ship's Speed Power Performance. URL: https://doi.org/10.1115/OMAE2020-19153, doi:10.1115/OMAE2020-19153, arXiv:https://asmedigitalcollection.asme.org/OMAE/proceedings-pdf/OMAE2020/84379/V06AT06A038/6606596/v06at06a038-omae v06AT06A038.

Kim, Y.R., Jung, M., Park, J.B., 2021. Development of a fuel consumption prediction model based on machine learning using ship in-service data. Journal of Marine Science and Engineering 9. URL: https://www.mdpi.com/2077-1312/9/2/137, doi:10.3390/jmse9020137.

Kitamura, F., Ueno, M., Fujiwara, T., Sogihara, N., 2017. Estimation of above water structural parameters and wind loads on ships. Ships and Offshore Structures 12, 1100–1108.

Koboević, Ž., Bebić, D., Kurtela, Ž., 2019. New approach to monitoring hull condition of ships as objective for selecting optimal docking period. Ships and Offshore Structures 14, 95–103. doi:10.1080/17445302.2018.1481631. cited By 1.

Kristensen, H.O.H., Bingham, H., 2017. Prediction of Resistance and Propulsion Power of Ships. Technical Report. Technical University of Denmark. URL: https://gitlab.gbar.dtu.dk/oceanwave3d/Ship-Desmo.

Laurie, A., Anderlini, E., Dietz, J., Thomas, G., 2021. Machine learning for shaft power prediction and analysis of fouling related performance deterioration. Ocean Engineering 234, 108886. URL: https://www.sciencedirect.com/science/article/pii/S0029801821003218, doi:https://doi.org/10.1016/j.oceaneng.2021.108886.

Liang, Q., Tvete, H.A., Brinks, H.W., 2019. Prediction of vessel propulsion power using machine learning on AIS data, ship performance measurements and weather data. Journal of Physics: Conference Series 1357, 012038. URL: https://doi.org/10.1088/1742-6596/1357/1/012038, doi:10.1088/1742-6596/1357/1/012038.

Liu, S., Loh, M., Leow, W., Chen, H., Shang, B., Papanikolaou, A., 2020. Rational processing of monitored ship voyage data for improved operation. Applied Ocean Research 104, 102363. URL: https://www.sciencedirect.com/science/article/pii/S0141118720309226, doi:https://doi.org/10.1016/j.apor.2020.102363.

Major, P., Li, G., Zhang, H., Hildre, H., 2021. Real-time digital twin of research vessel for remote monitoring, pp. 159–164. doi:10.7148/2021-0159.

Martinsen, M.A., 2016. An design tool for estimating the added wave resistance of container ships, et design værktøj til estimering af øget bølgemodstand for kontainerskibe.

Minoura, M., Hanaki, T., Nanjo, T., 2021. Improvement of statistical estimation of ship performance in actual seas by normalization of data unevenness using cluster analysis, in: Okada, T., Suzuki, K., Kawamura, Y. (Eds.), Practical Design of Ships and Other Floating Structures, Springer Singapore, Singapore. pp. 878–898.

Molland, A.F., 2011. The maritime engineering reference book: a guide to ship design, construction and operation. Elsevier.

Munk, T., 2016. Fuel conservation through managing hull resistance, in: Motorship Propulsion Conference, Copenhagen. URL: https://www.messe.no/ExhibitorDocuments/97726/2419/BIMCO%20Hull-Resistance.pdf.

Olmer, N., Comer, B., Roy, B., Mao, X., Rutherford, D., 2017. Greenhouse gas emissions from global shipping, 2013–2015 detailed methodology. International Council on Clean Transportation: Washington, DC, USA , 1–38.

Olofsson, R., 2020. Unsupervised anomaly detection. Master's thesis. UMEÅ University. URL: https://www.diva-portal.org/smash/get/diva2:1445794/FULLTEXT01.pdf.

Park, J., Kim, B., Jeong, S., Park, J.H., Jeong, D., Ahn, K., 2017. A comparative analysis of ship speed-power performance based on the noon reports and recorded sensor data: Overcoming sensor issues, in: OCEANS 2017-Anchorage, IEEE. pp. 1–7.

Rhodes, B.J., Bomberger, N.A., Seibert, M., Waxman, A.M., 2005. Maritime situation monitoring and awareness using learning mechanisms, in: MILCOM 2005-2005 IEEE Military Communications Conference, IEEE. pp. 646–652.

Solutions, M.E., 2018. Basic principles of ship propulsion. MAN: Augsburg, Germany .

Taskar, B., Andersen, P., 2019. Benefit of speed reduction for ships in different weather conditions .

Taskar, B., Andersen, P., 2021. Comparison of added resistance methods using digital twin and full-scale data. Ocean Engineering 229, 108710. URL: https://www.sciencedirect.com/science/article/pii/S0029801821001451, doi:https://doi.org/10.1016/j.oceaneng.2021.108710.

Themelis, N., Spandonidis, C., Christopoulos, G., Giordamlis, C., 2018. A comparative study on ship performance assessment based on noon report and continuous monitoring system datasets, in: Proceedings, pp. 55–64.

Thomas, R., Judith, J., 2021. Hybrid dimensionality reduction for outlier detection in high dimensional data. International Journal of Emerging Trends in Engineering Research 8. doi:10.30534/ijeter/2020/160892020.

Tu, E., Zhang, G., Rachmawati, L., Rajabally, E., Huang, G.B., 2017. Exploiting ais data for intelligent maritime navigation: A comprehensive survey from data to methodology. IEEE Transactions on Intelligent Transportation Systems 19, 1559–1582.

Virtanen, P., Gommers, R., Oliphant, T.E., Haberland, M., Reddy, T., Cournapeau, D., Burovski, E., Peterson, P., Weckesser, W., Bright, J., et al., 2020. Scipy 1.0: fundamental algorithms for scientific computing in python. Nature methods 17, 261–272.

Wahl, J.M., 2019. Prediction of fuel consumption of a ship in transit using machine learning. Master's thesis. NTNU. URL: https://ntnuopen.ntnu.no/ntnu-xmlui/handle/11250/2622968.

Walker, M., Atkins, I., 2007. Surface ship hull and propeller fouling managment, pp. 131–138. Cited By 3.

Weng, J., Liao, S., Wu, B., Yang, D., 2020. Exploring effects of ship traffic characteristics and environmental conditions on ship collision frequency. Maritime Policy & Management 47, 523–543.

You, Y., Kim, J., Seo, M.G., 2017. A feasibility study on the rpm and engine power estimation based on the combination of ais and ecmwf database to replace the full-scale measurement. Journal of the Society of Naval Architects of Korea 54, 501–514. doi:10.3744/SNAK.2017.54.6.501.

71

Article 2

Big Data Analytics as a Tool to Monitor Hydrodynamic Performance of a Ship
(with corrections on page 4)

Prateek Gupta, Sverre Steen, Adil Rasheed

OMAE2019-95815

BIG DATA ANALYTICS AS A TOOL TO MONITOR HYDRODYNAMIC PERFORMANCE OF A SHIP

(with corrections on page 4)

Prateek Gupta[*], **Sverre Steen**
Department of Marine Technology
Norwegian University of Science and Technology
7052 Otto Nielsens veg. 10, Trondheim
Norway

Adil Rasheed
Department of Engineering Cybernetics
Norwegian University of Science and Technology
7034 Gløshaugen, Trondheim
Norway

ABSTRACT

A modern ship is fitted with numerous sensors and Data Acquisition Systems (DAQs) each of which can be viewed as a data collection source node. These source nodes transfer data to one another and to one or many centralized systems. The centralized systems or data interpreter nodes can be physically located onboard the vessel or onshore at the shipping data control center. The main purpose of a data interpreter node is to assimilate the collected data and present or relay it in a concise manner. The interpreted data can further be visualized and used as an integral part of a monitoring and decision support system. This paper presents a simple data processing framework based on big data analytics. The framework uses Principal Component Analysis (PCA) as a tool to process data gathered through in-service measurements onboard a ship during various operational conditions. Weather hindcast data is obtained from various sources to account for environmental loads on the ship. The proposed framework reduces the dimensionality of high dimensional data and determines the correlation between data variables. The accuracy of the model is evaluated based on the data recorded during the voyage of a ship.

Keywords: Big Data, Ship Hydrodynamics, Principal Component Analysis.

[*]Corresponding author: prateek.gupta@ntnu.no

INTRODUCTION

The influence of environment on the hydrodynamic performance of a ship is a long studied subject. Estimation of added wave resistance for a ship has always been a topic of research. Moreover, the introduction of Energy Efficiency Design Index (EEDI) and Energy Efficiency Operation Index (EEOI) proposed during 58th MEPC conference is an additional push towards improving the energy efficiency and reducing emissions from shipping industry. The performance of a ship in the absence of any environmental loads can be simply evaluated based on the calm water speed-power relation for the ship. As proposed by Boom & Hout (2008) [1], the speed-power relation or curve, for near calm water condition, can be established by means of speed trials. Alternatively, it is possible to establish such a curve by analyzing the in-service data collected on-board a newly built ship. Based on this curve a simple one-to-one mathematical relation can be formulated between the speed and power consumption of the ship.

As the environment becomes significant, large deviations are observed from the well-known parabolic calm water speed-power curve. In order to explain or predict these deviations, a lot of research has been done, for example, to create prediction models for speed loss of a ship. Prpić-Oršić & Faltinsen (2012) [2] estimated the speed loss of a ship due to ship motions and propeller ventilation. Feng et al. (2010) [3] presented a procedure to predict the speed reduction of a ship accounting only for added resistance in waves. Lu et al. (2018) [4] computed the speed loss of a ship using simulations based on different numerical and

1   Copyright © 2019 ASME

mechanical approaches. Some researchers, on the other hand, predicted these deviations in terms of increased power or fuel consumption by the ship. Seo et al. (2013) [5] presented three different numerical approaches to predict the added resistance in waves and therefore, increased power consumption. Kim et al. (2017) [6] carried out the assessment of ship operating performance for a LNG ship using a power prediction model based on wave basin model test results, numerical computations and empirical formulations to account for environmental loads.

It can be clearly observed that all the above proposed procedures are either using simplified or approximated models of much more complex environmental loads or uses various different components, each one calculating an approximate correction for an individual environmental factor. Moreover, most of these methods neglect smaller influencing factors like engine-propeller degradation and fouling. The biggest advantage of a data-driven model is that it can be developed as a single component model which would be capable of including the effect of even the smallest influencing factor. The challenge here would be to correctly identify the variables which would appropriately quantify all the influencing factors which are responsible for the deviation from the basic speed-power characteristic of the ship.

With the advancement of technology, data-driven approaches have become nearly ubiquitous. Some researchers used this opportunity to develop ship performance evaluation or speed prediction models based on pure statistical or mathematical approach. Mao et al. (2016) [7] tested three different statistics based regression models, using limited/indirect information, for predicting the speed of a small size containership. Pedersen (2014) [8] illustrated the possibility of using purely data-driven method, based on Artificial Neural Networks (ANN) or Gausian Process Regression (GPR), for predicting power consumption of a ship. Gjølme (2017) [9] developed a data-driven machine learning model to predict the speed loss of a ship due to current, wind and waves. Bal Beşikçi et al. (2016) [10] presented an ANN based model to predict fuel consumption of a ship and based on that, developed a Decision Support System (DSS) for energy efficient ship operations. Perera (2017) [11] presented a study to illustrate the use of big data analytics as a data handling framework to process the large volume of data recorded onboard a ship.

The aim of this publication is to develop a data-driven mathematical model which can be used to monitor and assess the hydrodynamic performance of a ship during a sea voyage. The mathematical model is based on a selected set of variables obtained directly or indirectly via onboard measurements and weather hindcast data. The variable selection process is based on the engineering knowledge available to us as well as the results obtained from a preliminary Principal Component Analysis (PCA) model[1]. The preliminary PCA model is also used to de-

tect and understand potential outlier sample data points. Finally, a better fit PCA model is developed with minimum number of Principal Components to statistically explain the variance in the dataset.

BIG DATA ANALYTICS

Big data analytics is a data handling framework which can be used to extract meaningful information from large datasets, often termed as big data [12]. It can be used to perform tasks like data exploration, feature selection, pattern recognition, etc. Big data analytics can be implemented using various Machine Learning (ML) based methods to perform data analysis. As in the case of ML, big data analysis methodologies can also be classified as: supervised, unsupervised and semi-supervised learning.

With the advent of modern technology and automation, Machine Learning (ML) methods are becoming increasingly popular in the field of data science. ML can be said to be a subfield of Artificial Intelligence (AI), which itself is a subfield of computer science. The primary concern about such methods is that they are becoming increasingly opaque and difficult to explain. Holzinger (2018) [13] presented a discussion about the increasing need for explainable AI (XAI) instead. It is well known that a complex Artificial Neural Network (ANN) can be challenging to comprehend. The methodology used in the current work uses a simple Principal Component Analysis (PCA) model which can be quite explainable as demonstrated by Brinton (2017) [14]. The PCA model presented here is developed using a commercial application, The Unscrambler X[2].

Principal Component Analysis (PCA)

An analysis involving more than one variable, often known as multivariate analysis, is generally characterized by a number of correlated variables. Principal Component Analysis (PCA) [15] is an unsupervised machine learning or big data analysis method based on statistics that transforms the correlated multivariate data into a small number of independent and uncorrelated variables, known as Principal Components (PCs). These PCs accounts for variability in the dataset. In general, the first PC accounts for maximum variability and the succeeding PCs accounts for as much of the remaining variability as possible. PCA is also viewed as a method to reduce the dimensionality of a high dimensional dataset that retains most of the information contained in the large dataset. PCA splits the dataset matrix (X) into a modelled part (X_M) and a residual error part (E), with X_M and E having the same dimensions as X:

$$X^{m \times n} = X_M^{m \times n} + E^{m \times n} \qquad (1)$$

---

[1]Further explained in Results section.

---

[2]https://en.wikipedia.org/wiki/The_Unscrambler

Copyright © 2019 ASME

Here, superscript $m \times n$ is the dimension of the original dataset X, i.e., X has m rows and n columns. Generally, in case of a time series data, m is the number of samples and n is the number of variables in the recorded dataset. The modelled part, X_M, is expressed as a subspace with a certain complexity or dimensionality. The model dimensionality (A) represents the number of PCs used to create the model. It should be noted that the residual error E changes with varying model dimensionality. Thus, the primary aim of a PCA model is to, ideally, retain all the information in $X_{M, A}$ and discard the remaining noise in E_A.

Pre-processing.   Before establishing the model $X_{M, A}$, it is customary to pre-process the original dataset. The pre-processing involves two main steps: scaling and mean-centering the data. If variables are recorded on different scales, for example, they have different units of measurement, it is mathematically advantageous to scale these variables to the same scale. This is usually done by multiplying the recorded data matrix (X_{rec}) with a diagonal matrix (S_0) containing one scaling factor for each variable. This scaling factor is, in general, the inverse of the total standard deviation of the corresponding variable, i.e., $diag(S_0)_k = 1/std(X_{rec, k})$ where $std(X_{rec, k})$ is the standard deviation of the kth column of X_{rec}. The scaled matrix is, thus, defined as:

$$X_S^{m \times n} = X_{rec}^{m \times n} \cdot S_0^{n \times n} \qquad (2)$$

Further, it is mathematically convenient to mean-center the recorded data such that the modelled part ($X_{M, A}$) may be viewed as a Tylor's series expansion around a working point X_0. This working point (X_0) is, in general, the mean-center of the cloud formed by the data points in the given high dimensional space. If X_0 is a row matrix containing the mean of each column (or variable) in X_S and I_C is a column matrix of ones, then the mean-centered data matrix is calculated as:

$$X^{m \times n} = X_S^{m \times n} - I_C^{m \times 1} \cdot X_0^{1 \times n} \qquad (3)$$

It should be noted that scaling and mean-centering the data would not affect the final outcome of the model but, in some cases, unscaled data might introduce the rounding-off error during matrix operations [16].

Bilinear Modelling.   In PCA, the data-driven mathematical model is regarded as a sum of contributions from different functions of rows and columns. Each of these functions is simply approximated as a linear model. Thus, resulting in a bilinear model as follows:

$$X^{m \times n} = X_{M, A}^{m \times n} + E_A^{m \times n} = T_A^{m \times A} \cdot P_A'^{\,A \times n} + E_A^{m \times n} \qquad (4)$$

Here, matrix T_A contains the so-called scores and matrix P_A contains the so-called loadings with each column corresponding to a Principal Component (PC). P_A' represents the transpose of P_A matrix. The above expression can also be written as summation of A PCs:

$$X^{m \times n} = \sum_{i=1}^{A} t_i^{m \times 1} \times p_i'^{\,1 \times n} + E_A^{m \times n} \qquad (5)$$

Where t_i and p_i are column matrices or vectors containing scores and loadings of ith PC, respectively. Scores shows the patterns of co-variation among m samples whereas loadings shows the corresponding patterns of co-variation among n variables. It should be noted that the model dimensionality (A) is user-specified but is limited by the maximum number of linearly independent rows or columns in X, commonly known as the rank of the matrix, i.e., $A_{max} = rank(X)$.

Conventionally, in PCA, the score vectors (columns in T_A) are orthogonal[3] to each other and the loading vectors (columns in P_A or rows in P_A') are orthonormal[4]. The scores and loading can be estimated in many different ways. Two of the most popular methods are: Singular Value Decomposition (SVD) [17] and Nonlinear Iterative Partial Least Squares (NIPALS) algorithm [18]. SVD is a direct method which calculates the maximum number of PCs (determined by the rank of the data matrix) whereas NIPALS is an iterative method which calculates 1 PC at a time. NIPALS algorithm can be further modified to accommodate missing values in the dataset using a method given by Martens & Martens (2001) [19].

Singular Value Decomposition (SVD).   SVD is a generalization of eigen-decomposition[5] for any $m \times n$ matrix. The data matrix (X), having dimensions $m \times n$ with $m \geq n$, can be decomposed using SVD as follows:

$$X^{m \times n} = U^{m \times n} \cdot \Sigma^{n \times n} \cdot V'^{\,n \times n} \qquad (6)$$

Where U consists of n orthonormalized eigenvectors of $(X \cdot X')$, V consists of orthonormalized eigenvectors of $(X' \cdot X)$

---

[3] $T_A' \cdot T_A = \lambda$, where λ is a diagonal matrix and $diag(\lambda)_i$ is proportional to the eigenvalue associated with the ith PC.
[4] $P_A' \cdot P_A = I$ where I is an identity or unit matrix.
[5] Factorizing a diagonalizable square matrix into eigenvalues and eigenvectors.

3   Copyright © 2019 ASME

and Σ is a diagonal matrix containing non-negative square roots of the scaled eigenvalues of $(X'.X)$, also known as singular values. The columns of U and V are also known as left-singular eigenvectors and right-singular eigenvectors of X, respectively.

Comparing Equations (5) and (6), the loading vectors (p_i) corresponds to columns in V and score vectors (t_i) corresponds to columns in $(U.\Sigma)$. Moreover, for the model with maximum dimensionality, i.e., $A = A_{max}$, $P = V$ and $T = (U.\Sigma)$.

Covariance & Correlation

Variance of a data variable is an absolute measure of variability which quantifies the "spread" of the observations from the expected or mean value of the variable. It can also be interpreted as the mean of the squares of the deviations. Covariance quantifies the relation between the variability of two variables, i.e., it measures the deviation from mean for these two variables with respect to each other. The covariance between a variable and itself is the variance. Covariance is mathematically formulated as:

$$Cov(\alpha, \beta) = E\big((\alpha - \overline{\alpha})(\beta - \overline{\beta})\big) \qquad (7)$$

Where α and β are data variables. A high positive or negative value of covariance indicate a strong relationship between variables whereas zero covariance indicate that the variables may be independent of each other.

For more than two variables, the statistical relationship between variables can be quantified as the covariance between two variables at a time and can be presented in the form of a covariance matrix as:

$$Cov(X) = \begin{bmatrix} Cov(X_1,X_1) & Cov(X_1,X_2) & Cov(X_1,X_3) \\ Cov(X_2,X_1) & Cov(X_2,X_2) & Cov(X_2,X_3) \\ Cov(X_3,X_1) & Cov(X_3,X_2) & Cov(X_3,X_3) \end{bmatrix} \qquad (8)$$

Where X_1, X_2 and X_3 are data variables. It should be noted that the above matrix is symmetric about the diagonal as $Cov(X_1,X_2) = Cov(X_2,X_1)$ and the diagonal of the matrix contains the variance of the corresponding variable. If X is a mean-centered vector containing n elements or variables $(X_1, X_2,..., X_n)$, the above equation can also be written as:

$$Cov(X) = \frac{1}{m-1} X'.X \qquad (9)$$

For a better interpretation of covariance matrix, it is sensible to scale the covariance matrix. This is, generally, done by

dividing each element of matrix by the product of standard deviation of the corresponding variables. The scaled covariance is also known as the correlation between the variables, calculated as:

$$r(X_1,X_2) = \frac{Cov(X_1,X_2)}{std(X_1).\,std(X_2)} \qquad (10)$$

In case of already scaled variables, the covariance matrix is the correlation matrix. Also, the diagonal of the correlation matrix will contain 1 indicating 100% correlation between a variable and itself.

Correlation Loadings. Correlation loadings are defined as the correlation between data variables and a Principal Component (PC). The correlation loadings, thus, can be used to interpret the physical meaning of a PC and it is also useful in visualizing the relationship between individual variables. Two variables which are strongly correlated ($\sim \pm 1$ correlation) with a PC will also be strongly correlated with each other. Additionally, the correlation loadings reflects the contribution of individual variable to a PC and quantifies the amount of variability, contained in that variable, which is accounted for or absorbed by the PC.

The correlation loading matrix can be calculated as the cross-correlation between standardized data variables and standardized PCs. Using Equations (6) and (9), the correlation loading matrix can be calculated as:

$$L = \frac{1}{m-1} X'.\sqrt{m-1}\,U = \frac{1}{\sqrt{m-1}} V.\Sigma \qquad (11)$$

Thus, the correlation loading vectors are, simply, loading vectors scaled by the square root of the respective eigenvalues.

Explained Variance

Each Principal Component (PC) is characterized by three main parameters: scores, loadings and explained variance. Explained variance is a measure of the amount of variability or information, contained in all the variables, taken into account (or absorbed) by a PC. It is often quantified as the percentage of total variance in the data which is accounted for by the current PC.

The variance explained by a PC is the variance contained in the corresponding PC score vector. The total explained variance is obtained as the cumulative sum of the variance explained by consecutive PCs accepted in the model. Thus, the total explained variance represents how well the data fits the model, i.e., it measures the accuracy of the model. The explained variance and total

4   Copyright © 2019 ASME

explained variance are, in general, presented as the percentage of the total variance contained in the original dataset.

DATA

Two main datasets are used for the current work: ship in-service measurement data and weather hindcast data. These two datasets were acquired from different sources. The in-service measurement ship data contains the measurements recorded by various sensors onboard a ship whereas the weather hindcast data represents the external environmental loads that the ship was assumed to be experiencing.

Data Description

The ship data used in the analysis was recorded onboard an approximately $200m$ long general cargo ship. The ship has a installed propulsion capacity of approximately $10,000KW$ in MCR condition. The vessel is equipped with a comprehensive energy management web application, Marorka Online[6]. Marorka Online is a platform for visualizing fleet data, and it facilitates collaboration between the ship and shore, i.e., the data recorded onboard the ship is transmitted to the shore control center in real-time. The system records parameters which are relevant as performance indicators for the vessel.

Ship Data. The input ship data is about a month-long continuously recorded time series, sampled and stored at every 15 minutes. Figure 1 shows the trajectory of the ship during the voyage. The recorded data contains 26 variables. These variables are classified into different categories with each category representing the nature of the information conveyed by the variables. These categories are: ship identity, navigation, auxiliary power system, propulsion system, and environment. In addition to these categories, time is defined as an independent variable. Table 1 presents the list of categorized ship data variables.

Propulsion system variables are primarily related to the hydrodynamic performance of the ship. But some of these variables, like *State*, *Draft Fore*, and *Draft Aft*, do not directly correlate with ship performance. *State* variable indicates the operational state of the vessel. It has one of the following four values for each time step: 'At Berth', 'Manoeuvring', 'Sea Passage', or 'Anchor/Waiting'. This is used to further discretize the data and only 'Sea Passage' data is used for the analysis. *Draft Fore* and *Draft Aft* are used to introduce two additional variables: mean draft and trim-by-aft. They are more relevant from the hydrodynamics point of view. The cargo weight remained constant during the whole duration of the journey, thus, it cannot be included in the analysis.

---

[6]www.marorka.com
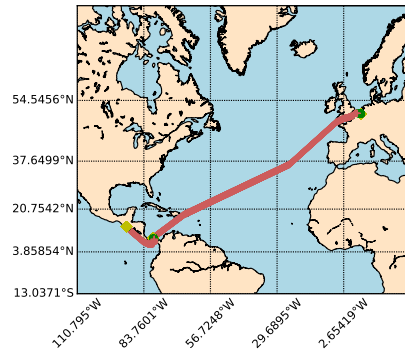
FIGURE 1: SHIP'S TRAJECTORY FOR THE MONTH LONG RECORDED VOYAGE DATA.

Environment variables represent wind loads and sea depth. Incident wind loads strongly influence the hydrodynamic performance of the ship due to air drag. From relative wind speed and direction, longitudinal and transverse incident relative wind speeds are calculated. It is quite obvious that longitudinal and transverse wind speeds would be more correlated to vessel performance. It was observed that the sea depth values were not continuously recorded probably due to the limitation of the depth sensor, so it is not included in the analysis. Navigation variables are used to interpolate hindcast weather data variables, representing environmental loads on the ship.

Ship identity and auxiliary power system variables are not used in the current analysis. As the ship is propelled by a diesel engine, auxiliary power systems hardly influence the hydrodynamic performance of the vessel. In case of an electric propulsion system this might not be the case. Also, in case of a very detailed analysis, say using a numerical model of the ship to determine its hydrodynamic properties, ship identity variables can be used to fetch the building specifications and designs of the ship. This can be very useful to theoretically or empirically predict the calm water hydrodynamic performance of the hull with varying mean draft and trim of the vessel.

Weather Data. The weather data is acquired from two sources: European Centre for Medium-Range Weather Forecast (ECMWF) [20] and Hybrid Coordinate Ocean Model (HYCOM) [21]. The ECMWF data is the ERA-Interim reanalysis data. ERA-Interim is a global atmospheric reanalysis from 1979, which is continuously updated in real time. The spatial resolution

5 Copyright © 2019 ASME

TABLE 1: CATEGORIZED LIST OF VARIABLES RECORDED ONBOARD THE SHIP. 'NAVIGATION', 'PROPULSION SYSTEM' & 'ENVIRONMENT' ARE IMPORTANT CATEGORIES FOR THE CURRENT ANALYSIS.

Ship Identity	Navigation	Auxiliary Power System	Propulsion System	Environment
Ship Name IMO Number	Latitude Longitude Gyro Heading COG Heading	Aux. Consumed Aux. Electrical Power Output DG1 Power DG2 Power DG3 Power	State ME Load Measured Shaft Power Shaft rpm Shaft Torque ME Consumed Draft Fore Draft Aft GPS Speed Log Speed Cargo Weight	Relative Wind Speed Relative Wind Direction Sea Depth

for ECMWF data, used here, is $0.75°$, i.e., approximately $80km$. It provides wave data variables every 6 hours and wind data variables every 3 hours. The data variables obtained from ECMWF includes northward and eastward wind speed $10m$ above the sea surface, significant wave height, mean wave period and mean wave direction. The data obtained from HYCOM has a spatial resolution of $1/12°$ with a sampling frequency of 1 measurement per day. The data variables obtained from HYCOM includes northward and eastward sea water speed.

The weather data variables are linearly interpolated in space and time to ship's location using the ship's navigation data. The weather data variables obtained from ECMWF and HYCOM are, further, transformed to ship's reference frame, i.e., northward and eastward wind and current speeds are transformed to longitudinal and transverse wind and current speeds using ship's gyro heading. Since the wave data variables cannot be directly transformed to ship's reference frame as in the case of wind and current, only a new variable, relative mean wave direction, is introduced using the mean wave direction and ship's gyro heading.

Data Exploration & Validation

The hydrodynamic performance of a ship is, in general, quantified as the maximum speed achievable for a given propulsive power output. The propulsive power output is, here, measured as the percentage of Maximum Continuous Rating (MCR) load and recorded as the variable *ME Load Measured*. The propulsive power output will be correlated with the measured shaft power. The measured shaft power will differ from the total propulsive power output of the main engine due to transmission losses, which may or may not vary with varying engine power output. The shaft power can be calculated from shaft torque (τ) and rpm (n) as:

$$P = \tau . \omega = \frac{2\pi n}{60} . \tau \qquad (12)$$

The acquired data includes shaft power, torque and rpm readings, but the shaft power can also be calculated from measured shaft torque and rpm (Equation (12)). Figure 2 presents the measured and calculated shaft power vs main engine load. A minor difference for a few values is noticeable but otherwise the values are in good agreement.

The main engine power output will be correlated with its fuel oil consumption. *ME Consumed* variable contains the value of fuel consumed by the main engine between the two recorded samples. The correlation between ship speed and propulsive power output will be strongly influenced by environmental loads like wind, waves and current. Figure 3 shows the correlation between ship's speed through water, i.e., log speed and main engine power output for 'Sea Passage' state only. A substantial variation of ship's speed through water for a given main engine load is observed which indicates the influence of environmental loads.

Figure 4 shows the fuel consumed by main engine for a measured instantaneous load output. It should be noted that the fuel oil consumption values are recorded as the total fuel consumed between two sampling instants, i.e., fuel consumed in past 15 minutes. Thus, it will include the dynamic effects between these sampling instants as well as the variation of engine performance with environmental loads. Minor variations in fuel oil consumption for the same engine load indicate these effects but the large deviations from the mean trend-line observed between 20% and 50% ME load cannot be explained by this. A deeper analysis into the data shows that the ME fuel consumption readings taken during the initial 24 hours shows abnormally

Copyright © 2019 ASME
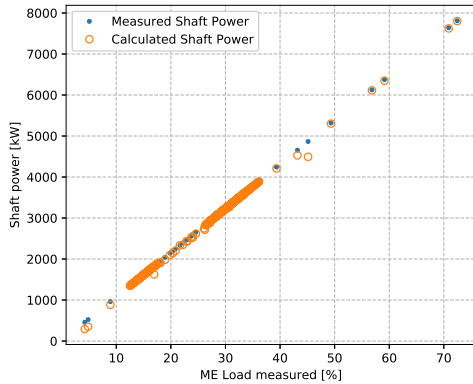
FIGURE 2: COMPARISON OF MEASURED AND CALCULATED SHAFT POWER. CALCULATED SHAFT POWER IS OBTAINED FROM MEASURED SHAFT TORQUE AND RMP.

high values due to unknown reasons. Keeping this in mind, all the data recorded for first two days are removed from the analysis.

Log speed is the measured speed of ship through water whereas GPS speed is the speed of the ship relative to the ground. In the absence of sea current, log speed will coincide with GPS speed. Thus, the difference between log speed and GPS speed is correlated with sea current speed. The difference between these two measured speeds can be considered as an estimate of sea current speed in longitudinal direction of the ship. Thus, it is possible to validate this difference with the sea current speed obtained from HYCOM data. Figure 5 shows the comparison of longitudinal current speed obtained from HYCOM data and the estimated value obtained as the difference between log speed and GPS speed of the ship for 'Sea Passage' state (the gap in the time-series is due to removal of data points when the ship was 'Manoeuvring' across Panama Canal). The two values shows quite good agreement. It should be noted here that high current speeds are well estimated by the difference between log and GPS speeds.

In the current analysis, the wind speed data is obtained from two sources: ship's data and ECMWF. It is, therefore, possible to validate these two sources by comparison. As mentioned above, the relative wind speed and direction obtained from on-board measurements are used to calculate relative longitudinal
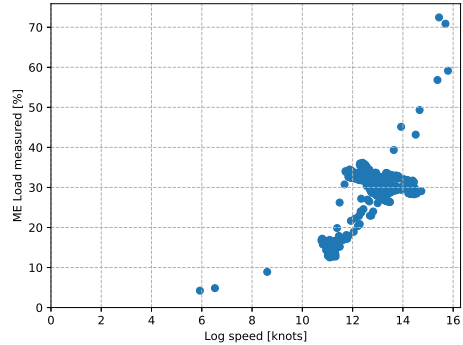
FIGURE 3: MEASURED MAIN ENGINE LOAD (ME LOAD) AS A FUNCTION OF MEASURED LOG SPEED (OR SPEED THROUGH WATER).
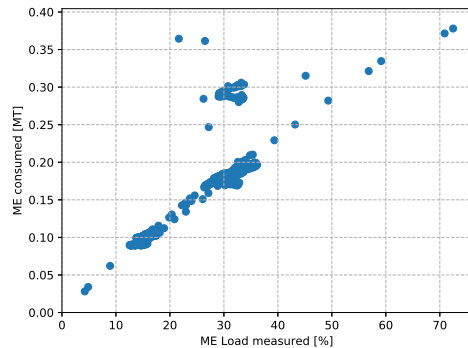
FIGURE 4: MEASURED ME FUEL CONSUMED (BETWEEN 2 SAMPLING INTERVALS) AS A FUNCTION OF MEASURED ME LOAD.

and transverse wind speeds. Also, the northward and eastward wind speeds obtained from ECMWF are transformed to longitudinal and transverse wind speeds. Assuming negligible speed of ship in transverse direction (i.e., no sway motion), the relative transverse wind speed should match with transverse wind speed.

7

81
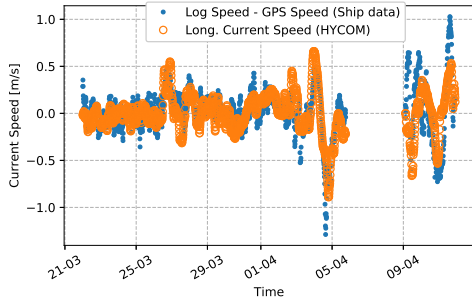
FIGURE 5: COMPARISON OF LONGITUDINAL SEA CURRENT SPEED ESTIMATED FROM SHIP DATA AND HINDCAST (HYCOM) MODEL FOR 'SEA PASSAGE' STATE.

FIGURE 6: COMPARISON OF TRANSVERSE WIND SPEED OBTAINED FROM SHIP DATA AND HINDCAST (ECMWF) MODEL FOR 'SEA PASSAGE' STATE.

Similarly, it is possible to compare the longitudinal wind speed (from ECMWF) with the difference between relative longitudinal wind speed and GPS speed (from ship's data).

Figure 6 and 7 shows the comparison for transverse and longitudinal wind speeds from the two data sources. The two sources of data are seen to be in quite good agreement but the values obtained from ship's data seems to be unreliable, specially in case of longitudinal wind speed as the wind speed is changing sign or direction without any probable cause. Thus, the

FIGURE 7: COMPARISON OF LONGITUDINAL WIND SPEED OBTAINED FROM SHIP DATA AND HINDCAST (ECMWF) MODEL FOR 'SEA PASSAGE' STATE.
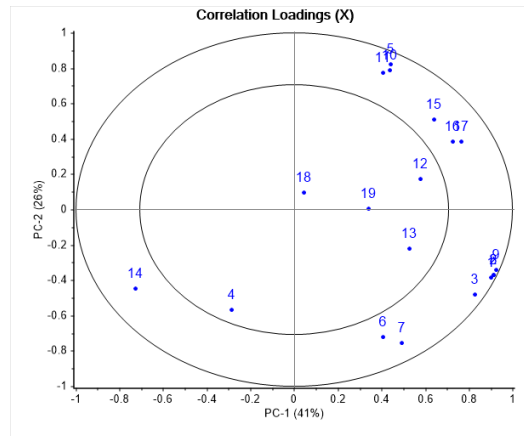
FIGURE 8: PRELIMINARY PCA MODEL: GRAPHICAL REPRESENTATION OF CORRELATION LOADINGS FOR INPUT VARIABLES (TABLE 2) IN PC-1 VS. PC-2 SPACE.

wind speed data obtained from ship's data is not included in the analysis any further.

TABLE 2: PRELIMINARY PCA MODEL: CORRELATION LOADINGS. SHOWING THE CORRELATION BETWEEN PRINCIPAL COMPONENTS AND INPUT VARIABLES. RED COLOR INDICATES STRONG CORRELATION WHILE YELLOW INDICATES NIL CORRELATION.

Sl. No.	Variables	PC-1	PC-2
1	ME consumed	0.9017	-0.3826
2	Shaft power	0.9121	-0.3727
3	Shaft rpm	0.8280	-0.4792
4	Draft fore	-0.2879	-0.5690
5	Draft aft	0.4425	0.8232
6	GPS speed	0.4075	-0.7195
7	Log speed	0.4939	-0.7568
8	ME Load measured	0.9121	-0.3727
9	Shaft Torque	0.9239	-0.3403
10	Mean draft	0.4380	0.7883
11	Trim-by-aft	0.4087	0.7724
12	Long. wind speed	0.5769	0.1749
13	Trans. wind speed	0.5277	-0.2213
14	Relative mean wave direction	-0.7242	-0.4460
15	Significant wave height	0.6416	0.5118
16	Mean wave direction	0.7243	0.3832
17	Mean wave period	0.7653	0.3862
18	Long. current speed	0.0437	0.0957
19	Trans. current speed	0.3393	0.0034

FIGURE 9: PRELIMINARY PCA MODEL: GRAPHICAL REPRESENTATION OF CORRELATION LOADINGS FOR INPUT VARIABLES (TABLE 2) IN PC-1 VS. PC-4 SPACE.

RESULTS

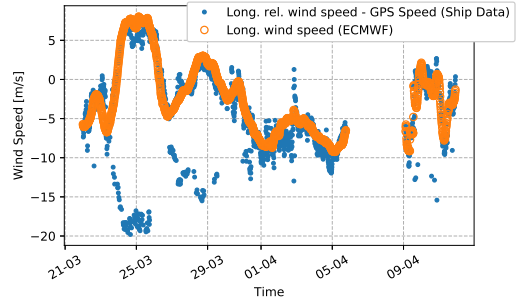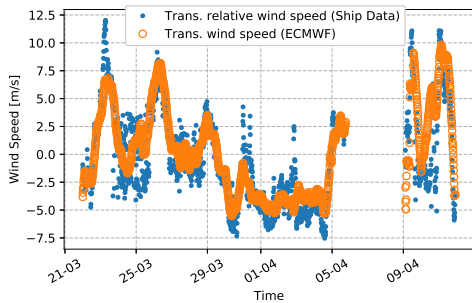Based on the available dataset and observations made during data exploration, a preliminary Principal Component Analysis (PCA) model was created including 19 variables and 1688 samples from 'Sea Passage' state only. Table 2 presents the list of variables included in the preliminary PCA model and the obtained correlation loadings for each variable with PC-1 and PC-2. Figure 8 shows the correlation loadings in graphical format. The purpose of the preliminary PCA model is to do the following: (a) Check the correlation between variables and perform variable selection for final model; (b) Detect and investigate potential outliers.

Variable Selection

From the correlation loadings (Figure 8), it can be observed that longitudinal and transverse current speeds are very loosely correlated with the PCs as well as with other variables. In other words, longitudinal and transverse current speeds do not contribute much to the model. Thus, it is better to remove these variables from the analysis to get a better fitting and compact model.

A consequence of not removing an uncorrelated variable can be understood as follows. The primary aim of a PCA model is to explain the variance in the complete dataset via minimum number of Principal Components (PCs). Therefore, the variance in any uncorrelated variable must also be explained. So as to achieve this, the model will create an extra PC just to explain the variance in this uncorrelated variable. Figure 9 shows that PC-4 is the undesirable extra PC created by the model to explain the variance in longitudinal current speed.

Outliers

Figure 10 shows the influence plot for PC-1 with 5% confidence limits. The samples marked by circles are potential outliers as they have high residuals and high influence on the model. The residuals are calculated as Q-residuals and the influence is calculated as Hotelling's T2 values. Further investigation revealed that these potential outlier are different from the rest of the sample set. They have either too low or too high shaft rpm than the rest of the samples, as shown in Figure 11. Thus, these samples are not erroneous values, rather they are very rare samples which are entirely different from the rest of the sample set.

The best way to deal with this type of problem is to gather additional samples which are similar to such rare samples. Since this is not possible here, it is better to remove these samples so

9

Copyright © 2019 ASME
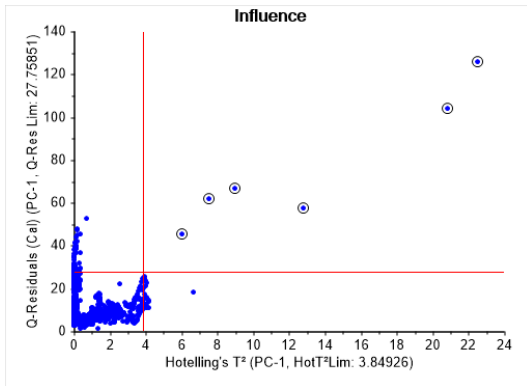
FIGURE 10: PRELIMINARY PCA MODEL: PC-1 INFLU-
ENCE PLOT WITH 5% CONFIDENCE LIMITS SHOWING
POTENTIAL OUTLIERS (MARKED BY CIRCLES TO THE
TOP-RIGHT OF RED LINES).
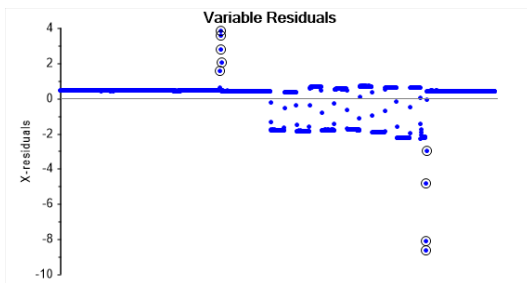
FIGURE 11: SCALED AND MEAN-CENTERED SHAFT
RMP. SAMPLES MARKED BY CIRCLE ARE RARE AS
THEY LIE FAR AWAY FROM THE MEAN (ZERO) LINE AS
COMPARED TO REST OF THE SAMPLE SET.

that the model fits better to the remaining sample set. In view
of this, all such rare samples were removed from the final PCA
model.

PCA Model
Scores & Loadings. Based on the results from the pre-
liminary PCA model, only 17 variables are included in the final
PCA model. Table 3 shows the correlation loadings for first 7
Principal Components (PCs) calculated by the model. Figure 12

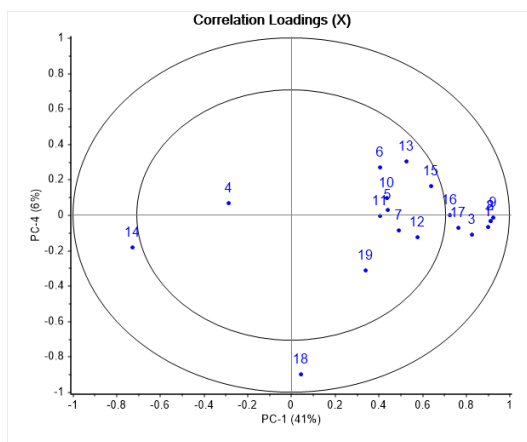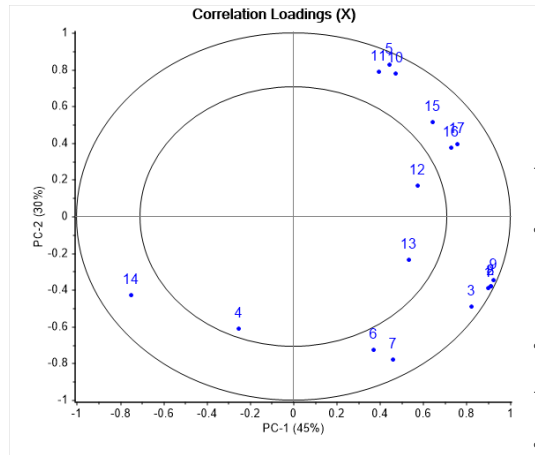**FIGURE 12**: FINAL PCA MODEL: GRAPHICAL REPRESEN-
TATION OF CORRELATION LOADINGS FOR INPUT VARI-
ABLES (TABLE 3) IN PC-1 VS. PC-2 SPACE.

presents the correlation loadings for PC-1 and PC-2 in graphical
format. It is observed that the 17 input variables are separated
into 4 main groups of strongly correlated variable: Power pa-
rameters $(1\text{-}3, 8, 9)$, wave parameters (14-17), draft parameters
$(4, 5, 10, 11)$ and speed parameters $(6, 7)$. Each of these groups
are oriented along a different direction in PC-1 vs. PC-2 space
but none of these groups are completely aligned with either PC-1
or PC-2.

Similar observations can drawn in case of PC-3. This makes
it difficult to interpret the physical meaning of these PCs. Ad-
ditionally, it should be observed that PC-5 to PC-7 do not show
good correlation with any of the variables, indicating that they
are mostly representing noise in the given dataset. Thus, it is
possible to retain only first 4 Principal Components and discard
the remaining.

From Figure 12, it is surprising to observe that transverse
wind speed (13) is correlated with PC-1 and PC-2 almost as
much as longitudinal wind speed (12). It even shows higher cor-
relation with PC-3 (refer Table 3), indicating that it is an impor-
tant parameter for this model.

Explained Variance & Validation. Figure 13 presents
the explained variance for the PCA model. The model can ex-
plain about 90% variance with just 4 PCs and further PCs do not
really contribute to the model. Thus, the model with only first 4
PCs is a very good fit for the given dataset. Figure 13 also shows

10

Copyright © 2019 ASME

TABLE 3: FINAL PCA MODEL: CORRELATION LOADINGS. SHOWING THE CORRELATION BETWEEN PRINCIPAL COMPONENTS AND INPUT VARIABLES. RED COLOR INDICATES STRONG CORRELATION WHILE YELLOW INDICATES NIL CORRELATION.

Sl. No.	Variables	PC-1	PC-2	PC-3	PC-4	PC-5	PC-6	PC-7
1	ME consumed	0.9016	-0.3893	0.1181	-0.0774	0.0127	-0.0149	0.0784
2	Shaft power	0.9126	-0.3792	0.0633	-0.0636	0.0102	-0.0245	0.0760
3	Shaft rpm	0.8247	-0.4927	0.2330	-0.0609	0.0462	-0.0039	0.0816
4	Draft fore	-0.2544	-0.6107	-0.6950	-0.0257	0.0512	-0.2620	0.0098
5	Draft aft	0.4427	0.8281	0.2983	-0.0109	-0.1109	-0.0999	0.0270
6	GPS speed	0.3706	-0.7254	0.2980	0.1898	-0.1275	-0.0730	-0.4044
7	Log speed	0.4608	-0.7770	0.3185	0.1361	0.0353	-0.0497	0.0418
8	ME Load measured	0.9126	-0.3792	0.0633	-0.0636	0.0102	-0.0245	0.0760
9	Shaft Torque	0.9226	-0.3468	0.0182	-0.0675	0.0028	-0.0304	0.0761
10	Mean draft	0.4721	0.7781	-0.0890	-0.0364	-0.1279	-0.3548	0.0484
11	Trim-by-aft	0.3965	0.7897	0.4532	0.0016	-0.0949	0.0240	0.0152
12	Long. wind speed	0.5750	0.1699	-0.2688	-0.7265	-0.0422	0.0865	-0.1020
13	Trans. wind speed	0.5333	-0.2347	-0.5990	0.2794	-0.3868	0.1609	0.0988
14	Relative mean wave direction	-0.7482	-0.4300	0.2344	0.0012	0.2447	-0.0698	0.1753
15	Significant wave height	0.6418	0.5128	-0.1387	0.4909	0.0795	-0.0085	0.0217
16	Mean wave direction	0.7295	0.3732	-0.3334	0.0717	0.3372	-0.0637	-0.1637
17	Mean wave period	0.7556	0.3947	-0.2025	0.1089	0.3138	0.1840	-0.0158

the explained variance for validation dataset. Model validation is done using cross-validation technique with 20 segments of randomly picked nonconsecutive samples, each segment containing about 145 samples. The validation dataset presents similar results as the calibration dataset.

Interpreting PCs. The simplest way to interpret Principal Components (PCs) is by looking at the correlation loadings or observing trends in sample score space, say, by means of sample grouping the scores. Sample grouping could not be used in the given case due to the complexity of PCs but by looking at correlation loadings (Table 3), it can said that PC-4 is mainly a combination of longitudinal wind speed (12) and significant wave height (15), i.e., it signifies the severity of environmental loads. Thus, a sample with high score for PC-4 would represent high environmental loads. PC-1, PC-2 and PC-3 are a combination of many variables as clearly observed from Table 3 and Figure 12.

It is also possible to understand the physical meaning of PCs from variable contributions point of view, i.e., by looking at variable residuals for all the PCs. Figure 14 shows that shaft power contributes to PC-1 and PC-2 only whereas Figure 15 shows that

trim-by-aft contributes to PC-1, PC-2 and PC-3.

CONCLUSION

A data-driven mathematical approach was used to process the high dimensional sensor data recorded onboard a ship during a sea voyage. Principal Component Analysis (PCA) was used to perform variable selection and detect potential outliers. The high dimensional dataset obtained from the sensors onboard the ship and weather hindcast, representing the hydrodynamic performance of the ship, was greatly reduced in dimensions by PCA. The PCA model achieved upto 90% explained variance with only 4 Principal Components (PCs).

Wind and sea current hindcast data, obtained from ECMWF and HYCOM respectively, was found to be in good agreement and, in some cases, more reliable than the in-service measurements recorded onboard the ship. The sea current speed variables were eliminated during the variable selection process as they did not contribute to the PCA model for the given dataset. Transverse wind speed was observed to be an important parameter for the given dataset. Investigation needs to be done on a larger dataset in order to draw any further conclusions.

11

Copyright © 2019 ASME
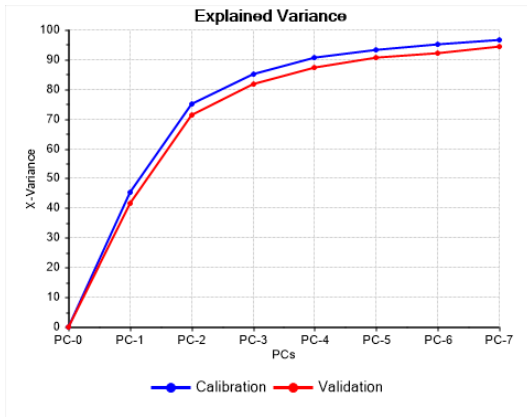
FIGURE 13: FINAL PCA MODEL: EXPLAINED VARIANCE. SHOWING THE VARIANCE IN DATASET ABSORBED BY CONSECUTIVE PCS. FIRST 4 PCS EXPLAINING ABOUT 90% VARIANCE.

FUTURE WORK

The PCA model presented in the current work is developed using the data recorded onboard a ship for about a month long period. A similar model can be easily developed on a larger set of data and for a different vessel. It would be interesting to corroborate the current findings for new and variant sets of such data.

Based on the current model, it is possible to quantify the performance of the vessel using the location of a sample in Principal Component Analysis (PCA) score space. But, in order to do so, a benchmark or standard basis needs to be established in PCA score space to mark, say, 100% performance. Alternatively, it is possible to develop a regression model based on the current analysis model, as demonstrated by Massy (1965) [22]. The regression model would be able to predict the speed or fuel consumption for a given state of the ship. Thus, it would be possible to quantify the performance of the ship in terms of speed loss or excess fuel consumption.

ACKNOWLEDGMENT
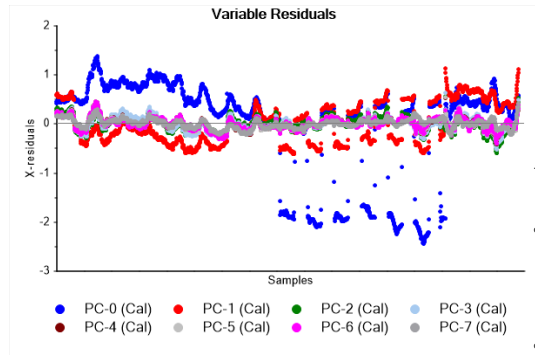
FIGURE 14: FINAL PCA MODEL: SHAFT POWER RESIDUALS. SHOWING THE VARIANCE IN SHAFT POWER ABSORBED BY CONSECUTIVE PCS. FIRST 2 PCS EXPLAINING MOST OF THE VARIANCE IN SHAFT POWER.
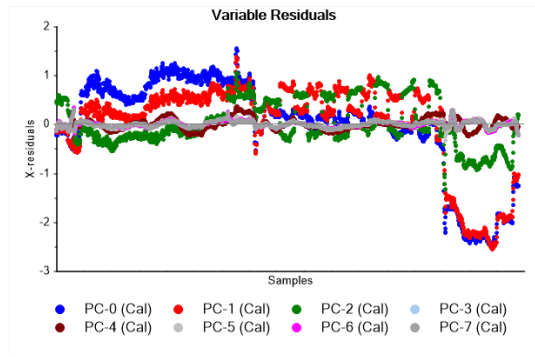
FIGURE 15: FINAL PCA MODEL: TRIM-BY-AFT RESIDUALS. SHOWING THE VARIANCE IN TRIM-BY-AFT ABSORBED BY CONSECUTIVE PCS. FIRST 3 PCS EXPLAINING MOST OF THE VARIANCE IN TRIM-BY-AFT.

REFERENCES

[1] van den Boom, H., and van der Hout, I., 2008. "Speed-power performance of ships during trials and in service".

[2] Prpić-Oršić, J., and Faltinsen, O., 2012. "Estimation of ship speed loss and associated co2 emissions in a seaway". *Ocean Engineering,* **44**, 04, pp. 1–10.

[3] Feng, P., Ma, N., and Gu, X., 2010. "Long-term prediction

of speed reduction due to waves and fuel consumption of a ship at actual seas". Vol. 4, pp. 199–208. cited By 4.

[4] Lu, L., Mao, Y.-T., and Hsin, C.-Y., 2018. "Computation of the speed loss in seaway by different approaches". Vol. 2018-June, pp. 128–134. cited By 0.

[5] Seo, M.-G., Park, D.-M., Yang, K.-K., and Kim, Y., 2013. "Comparative study on computation of ship added resistance in waves". *Ocean Engineering, 73*, pp. 1–15. cited By 33.

[6] Kim, S.-W., Kim, J.-H., Seo, M.-G., Choi, J.-W., Lee, Y.-B., and Han, S.-K., 2017. "Assessment of ship operating performance by using full scale measurement". pp. 1001–1006. cited By 0.

[7] Mao, W., Rychlik, I., Wallin, J., and Storhaug, G., 2016. "Statistical models for the speed prediction of a container ship". *Ocean Engineering, 126*, pp. 152–162. cited By 4.

[8] Pedersen, B. P., 2014. "Data-driven vessel performance monitoring". PhD thesis.

[9] Gjølme, J. C., 2017. "Estimation of Speed Loss due to Current, Wind and Waves". MS Thesis, Norwegian University of Science and Technology (NTNU), Trondheim, NO, June. "See also URL http://hdl.handle.net/11250/2453420".

[10] Bal Beşikçi, E., Arslan, O., Turan, O., and Ölçer, A., 2016. "An artificial neural network based decision support system for energy efficient ship operations". *Computers and Operations Research, 66*, pp. 393–401. cited By 23.

[11] Perera, L., 2017. "Handling big data in ship performance and navigation monitoring".

[12] Sagiroglu, S., and Sinanc, D., 2013. "Big data: A review". pp. 42–47. cited By 301.

[13] Holzinger, A., 2018. "From machine learning to explainable ai". pp. 55–66.

[14] Brinton, C., 2017. "A framework for explanation of machine learning decisions". In IJCAI 2017 Workshop on Explainable Artificial Intelligence.

[15] Jolliffe, I., 2002. *Principal Component Analysis*. Springer Series in Statistics. Springer.

[16] Turing, A., 1948. "Rounding-off errors in matrix processes". *Quarterly Journal of Mechanics and Applied Mathematics, 1*(1), pp. 287–308. cited By 157.

[17] Golub, G., and Reinsch, C., 1970. "Singular value decomposition and least squares solutions". *Numerische Mathematik, 14*(5), pp. 403–420. cited By 1464.

[18] Vandeginste, B., Sielhorst, C., and Gerritsen, M., 1988. "Nipals algorithm for the calculation of the principal components of a matrix". *TrAC - Trends in Analytical Chemistry, 7*(8), pp. 286–287. cited By 17.

[19] Martens, H., and Martens, M., 2001. *Multivariate Analysis of Quality: An Introduction*. Wiley.

[20] Dee, D., Uppala, S., Simmons, A., Berrisford, P., Poli, P., Kobayashi, S., Andrae, U., Balmaseda, M., Balsamo, G., Bauer, P., Bechtold, P., Beljaars, A., van de Berg, L., Bidlot, J., Bormann, N., Delsol, C., Dragani, R., Fuentes, M., Geer, A., Haimberger, L., Healy, S., Hersbach, H., Hólm, E., Isaksen, L., Kållberg, P., Köhler, M., Matricardi, M., Mcnally, A., Monge-Sanz, B., Morcrette, J.-J., Park, B.-K., Peubey, C., de Rosnay, P., Tavolato, C., Thépaut, J.-N., and Vitart, F., 2011. "The era-interim reanalysis: Configuration and performance of the data assimilation system". *Quarterly Journal of the Royal Meteorological Society, 137*(656), pp. 553–597. cited By 9796.

[21] Chassignet, E., Hurlburt, H., Smedstad, O., Halliwell, G., Hogan, P., Wallcraft, A., Baraille, R., and Bleck, R., 2007. "The hycom (hybrid coordinate ocean model) data assimilative system". *Journal of Marine Systems, 65*(1-4 SPEC. ISS.), pp. 60–83. cited By 362.

[22] Massy, W., 1965. "Principal components regression in exploratory statistical research". *Journal of the American Statistical Association, 60*(309), pp. 234–256. cited By 398.

13

Article 3

Statistical Modeling of Ship's Hydrodynamic Performance Indicator

Prateek Gupta, Bhushan Taskar, Sverre Steen, Adil Rasheed

Statistical modeling of Ship's hydrodynamic performance indicator

Prateek Gupta [*,a], Bhushan Taskar [c], Sverre Steen [a], Adil Rasheed [b]

[a] *Department of Marine Technology, Norwegian University of Science and Technology (NTNU), Norway*
[b] *Department of Engineering Cybernetics, Norwegian University of Science and Technology (NTNU), Norway*
[c] *Technical University of Denmark (DTU), Denmark*

ABSTRACT

The traditional method used to estimate the hydrodynamic performance of a ship uses either the model test results or one of the many empirical methods to estimate and observe the trend in fouling friction coefficient (ΔC_F) over time. The biggest weakness of this method is that the model test results as well as the empirical methods used here is sometimes not well-fitted for the full-scale ship due to several reasons like scale effects and, therefore, this method may result in an inaccurate performance prediction. Moreover, in the case of a novel ship design, it would be nearly impossible to find a well-fitting empirical method. The current method establishes a new performance indicator, formulated in the form of generalized admiralty coefficient with displacement and speed exponents statistically estimated using the in-service data recorded onboard the ship itself. The current method completely removes the dependence on empirical methods or model test results for the performance prediction of ships. It is observed here that the performance predictions using the current method and the traditional method are based on the same underlying logic as well as the results obtained from both the methods are found to be in good agreement.

1. Introduction

The in-service data recorded onboard a ship can be significantly instrumental in accurately estimating the operational performance of the ship but it comes with an inherent problem. The operational performance of a system can be easily evaluated over time by comparing the observed operational value with a previously recorded value. It is utmost important that these two values must belong to the same operational condition so that they can be considered comparable. It is very difficult to achieve this in the case of a ship as the recorded data is not only affected by the weather but it is spread over a wide range of speed-displacement operational domain of the ship.

In a simple attempt to monitor the operational performance of a ship, Walker and Atkins (2007), proposed observing the increase in power demand of the ship at a fixed speed and displacement (or loading condition). This kind of practice is quite feasible for defence ships but is rather impractical for merchant ships due to, for instance, variation in displacement between individual runs. Another solution to this problem is to do an in-direct comparison between the old and the new value using a benchmarking curve (or surface) which takes into account the variations due to speed and displacement. A conventional benchmark for a

ship's operational performance is its calm-water speed-power curve. Using the operational data recorded onboard a ship it is possible to regenerate this curve for a range of displacements, resulting in a speed-power-displacement surface which can, then, be used to monitor the performance of the ship, as we aim to demonstrate in this paper.

The aim of the current work is to establish a simple performance indicator which can be used to monitor the hydrodynamic performance of a ship using the in-service data recorded onboard it. As it may be known, the well-known admiralty coefficient is sometimes used as a hydrodynamic performance indicator for a ship. In view of that, the paper begins with an extensive literature review of the admiralty coefficient and the relationship between shaft power (P_s), speed-through-water (V) and displacement (Δ). Based on the review, a generalized form of admiralty coefficient is proposed and fitted on the in-service data recorded onboard a $\sim 200m$ ship over a duration of about 3 years. The in-service data, used for fitting the model, is corrected to remove the effect of environmental loads and marine fouling. The obtained generalized admiralty coefficient is, then, demonstrated to be used as a performance indicator for the ship. The predicted performance is, finally, validated by presenting a thorough comparison of the current method with the traditional performance prediction method for a ship, i.

* Corresponding author.
  E-mail address: prateek.gupta@ntnu.no (P. Gupta).

e., observing the trend in fouling friction coefficient (ΔC_F).

2. Ship performance indicator

As aforementioned, the admiralty coefficient ($\Delta^{2/3} V^3 / P_s$) is sometimes used an a hydrodynamic performance indicator for a ship in service. This is due to the fact that it is believed, by some, that the admiralty coefficient summarizes the relationship between the speed, power and displacement of a ship and provides a scalar value which can be compared to its future value very conveniently. The basic assumption here is that the value of admiralty coefficient is assumed to remain constant for a ship over the whole range of operational domain, i.e., for all speed-displacement combinations, of course only in calm-water condition. This assumption has been contradicted with evidence by several researchers. The following section gives a complete overview of the admiralty coefficient, its history and the criticism that it has received in the marine research community.

2.0.1. Historical overview

In the earliest stages of research and development in the field of ship design, ship model experiments were used to explore the design space. The information obtained from these experiments was stored in a concise manner. This information storage system gradually led to the development of different data presentation systems as well as now well-known empirical relations, for example, Froude number (named after William Froude, an English naval architect working at Admiralty Experiment Works (AEW), England). Around 1878, B. J. Tideman, a naval engineer from Netherlands, introduced the concept of non-dimensional presentation of ship model resistance data by presenting his model test results as resistance per displacement (R / Δ) plotted against speed per sixth root of displacement ($V/\Delta^{1/6}$) (Telfer (1963)).

Almost 10 years later, in 1888, R. E. Froude, succeeding William Froude, published the so-called "Constant System of Notation" (Froude (1888)). The constant system attempted to standardize the ship model resistance data presentation system using some non-dimensional constants. R. E. Froude, probably from his knowledge and experience, here introduced the admiralty constant defined as $\Delta^{2/3} V^3 / e.h.p.$, where e.h.p. is the effective horsepower. The idea was to plot the inverse of admiralty constant (ⓒ = e.h.p./$\Delta^{2/3} V^3$) against non-dimensional ship length (Ⓜ = $L/\nabla^{1/3}$) with discretely varying values of non-dimensional ship speed (Ⓚ = $V/\Delta^{1/6}$). Such iso-Ⓚ curves, also known as ⓒ-Ⓚ presentation, were used by ship designers to obtain an optimal ship design.

The ⓒ-Ⓚ presentation became quite popular but it was not accepted by all. Telfer (1963), criticized this presentation as being "schizophrenic", arguing that it shows one thing and generally means exactly the opposite. He stated that inspection of any iso-Ⓚ sheet will invariably show that the reduction of ⓒ requires an increase of Ⓜ which is due to the fact that a model of constant length having a smaller and smaller displacement was being run at a lower and lower speed in relation to its length. Moreover, it was argued that the penalty for "stumpiness", i.e., low Ⓜ value was, in fact, false as the longer ships will have higher wetted-surface area and, therefore, increased frictional resistance. In order to fix this issue, Telfer (1963), proposed a new system of presentation, called $R_c V_c$ presentation (demonstrated by Doust and O'Brien (1959)), where $R_c = RL/\Delta V^2$, $V_c = V/\sqrt{L}$, R is the ships total resistance and L is the ship length.

Telfer (1963), also presented an insight into the logical derivation of ⓒ (which might or might not have been used by R. E. Froude) and R_c as follows: ⓒ = $(R / \Delta)/(V/\Delta^{1/6})^n$; and $R_c = (R / \Delta)/(V/\sqrt{L})^n$ with $n = 2$.

Here, it should be noted that the former seems to be based on the same non-dimensional presentation as proposed by B. J. Tideman while the later uses William Froudes non-dimensional speed instead, i.e., Froude number. Additionally, Telfer (1963), stated that no merchant ship is ever designed to operate on a resistance varying as the square of the speed, or the power varying as the cube, i.e., the value of exponent n, used as 2 in both the presentations, can be taken as 3 for merchant ships. But unfortunately, no evidence proving the same was provided with the argument.

2.1. Admiralty coefficient: A performance indicator?

The admiralty constant ($\Delta^{2/3} V^3$/e.h.p.) as well as the resistance constant ($R_c = RL/\Delta V^2$) (proposed by Telfer (1963)) were used to model the variation in hydrodynamic performance of different ship designs. Therefore, it is quite obvious that they used only the design point values of the included parameters but not the whole range of operational domain. In other words, the speed (V), displacement (Δ), and so on, were only actually the corresponding design point values. Thus, it was never intended to use these constants to monitor the operational performance of an individual ship but rather just compare the hydrodynamic performance of different ships in their respective design conditions. It is also noteworthy that the originally proposed admiralty constant ($\Delta^{2/3} V^3$/e.h.p.) was a function of "effective" horse-power (e.h.p.) while the modern admiralty coefficient uses shaft power (P_s) instead (ITTC (2017)). Thus, the two, clearly, differ by the factor of propulsive efficiency of the ship, which is known to be varying for different operational conditions.

Thus, it can be clearly concluded that the originally proposed admiralty constant or any of its variations were actually neither intended nor proven to be an appropriate operational hydrodynamic performance indicator for a ship. It was rather developed to compare the hydrodynamic performance of different ship designs. In any case, the idea of summarizing the calm-water speed-power curve into a singular or a very few constant values can still be realized using a simple statistical analysis of the operational data recorded onboard a ship, as demonstrated in the current work. In order to do so, a thorough literature survey is presented in the following sections to understand the relationship between shaft power (P_s), speed-through-water (V) and displacement (Δ).

2.1.1. Speed exponent (n)

The relationship between speed (V) and power (P_s) is widely accepted as $P_s \propto V^n$, with $n = 3$ according to the admiralty coefficient. From the physics point of view, the value of $n = 3$ is quite appropriate for low speed range when the total resistance coefficient remains constant (and therefore, independent of ship speed) due to negligible wave resistance. Kristensen (2010), used a computer model based on updated Guldhammer and Harvald's method (Kristensen and Bingham (2017)) to estimate the value of n for container ships of different sizes and service speeds. He concluded that the cubic relationship is only valid for container ships in low speed range, Froude number (Fn)$\lesssim 0.18$, for higher speed range n can vary from 3 to 7.

In a very recent study, Taskar and Andersen (2019a), used a detailed model of ship performance to investigate fuel savings due to speed reduction for 6 hypothetical ships. The ship performance model, based on updated Guldhammer and Harvald's method, was also used to study the speed exponent n. It was concluded that n is a function of ship size, type (or hull shape) and speed of operation. Based on that, Taskar and Andersen (2019a) presented n as a function of Froude number (Fn) for all the 6 ships. In addition to that, they calculated a constant averaged value of n by curve fitting the speed-power calm-water data assuming

2

$P_s \propto V^n$. The value of n was observed to be increasing substantially (ranging between 3 to 6) above a certain Fn (depending on ship type and size) and the constant averaged values were found to be in the range of 3.3 to 4.2.

In a slightly different domain, several researchers used full-scale operational data from sea going ships to calculate the speed exponent with respect to bunker consumption. This speed exponent is further used to estimate the bunker consumption of the ship during a sea voyage. Such an estimation forms the basis of several maritime transport models used for various different purposes. The speed exponent with respect to bunker consumption will not be exactly same as n as the Specific Fuel Consumption (SFC or SFOC) of a marine engine varies with its load. But since this variation is very small, this speed exponent can be assumed to be equal to n (demonstrated by Taskar and Andersen (2019a)).

Wang and Meng (2012) estimated that the speed exponent with respect to bunker consumption for three types of container ships (3000, 5000 and 8000-TEU) using regression analysis of full-scale data from a global liner shipping company. The values of speed exponent were obtained in the range of 2.7 to 3.3. Du et al. (2011), following the recommendations of engine manufacturer MAN-Energy-Solutions (2004), used the speed exponent as 3.5, 4.0 and 4.5 for feeder, medium-sized and jumbo container ships, respectively, to calculate the bunker consumption. Psaraftis and Kontovas (2013) reviewed 40 ship-speed-based models used in maritime transportation for various purposes like weather routing, scheduling, cost optimization, fuel management, and fleet deployment. 25 models out of these 40 were established with a cubic speed exponent assumption.

2.1.2. Displacement exponent (m)

Unlike the speed exponent (n), not much attention has been paid to the displacement exponent, $m = 2/3$ according to admiralty coefficient, formulating the relationship between power (P_s) and displacement (Δ). The displacement exponent in admiralty coefficient is very commonly used to correct sea trial data but only in the limit that the difference between the trial displacement and the required displacement is less than 2% of the required displacement (ITTC (2017)). Thus, assuming $m = 2/3$ for the whole range of displacements for a ship does not seem reliable.

Tu et al. (2018), derived a new admiralty coefficient to improve the reference speed estimation for EEDI calculations for container ships. The reference speed for EEDI calculations is, generally, obtained by using the speed-power-displacement relationship given by the admiralty coefficient. Tu et al. (2018), argued that the fixed displacement exponent (m) in admiralty coefficient should be replaced by a function of the ship's hull form coefficients, namely, block coefficient (C_b), prismatic coefficient (C_p) and water-plane area coefficient (C_w). Tu et al. (2018), used the model test data of 4 container ships to calculate the new exponent using regression analysis and formulated $m = 1 - \frac{2(C_b + C_w)}{3}$. The results were obtained by using the design point values only. Thus, the results may be useful to compare different ship designs but does not seem to be valid for different draft values for the same ship.

From our physical understanding of ship hydrodynamics, it is important to realize that the displacement of the ship is not really a direct influencing parameter but rather it is being used to summarize several highly influential parameters, like the wetted-surface area and the water-plane area. The change in displacement produces a change in these influential parameters and therefore, results in the change of operational characteristics of the ship. This change significantly influences the speed-power calm-water curve, thereby stretching it in a third dimension which we are modelling using displacement. Now, fitting a constant exponent (m) over the whole range of this new dimension assumes that the trend along this dimension is continuous and follows the curve Δ^m.

The merchant ship hull forms are now-a-days optimized for best hydrodynamic performance in design draft condition by introducing features like transom stern and bulbous bow. The change in displacement also produces change in transom stern immersion and bulb immersion. The same is the case of propeller immersion, which is known to be a very influential parameter in ship hydrodynamics (Prpić-Oršić and Faltinsen (2012)). These factors would have an additional influence on the displacement exponent (m). Thus, the assumption of continuity and uniformity will probably not be valid over the whole range of displacement. Moreover, acknowledging the fact that different combinations of draft and trim may result in same displacement, and variation in speed may also influence the value of m introduces an additional complexity to the problem.

As in the case of speed exponent (n), the above discussion clearly indicates that the actual value of m over the whole range of displacement, most likely, would not be constant, and it may also vary due to the variation of ship speed for the same displacement range. But it may still be possible to either model an averaged constant value of m over the whole domain or obtain several values of m by piece-wise fitting the trend. The latter would definitely produce better results but the former would be more feasible to implement, keeping in mind the fact that the available data is generally limited to only a handful of displacement values. In general, commercial ships like bulk-carriers and tankers operates either around the full-load or the ballast displacement for most of their voyages. Thus, it would be most advantageous to establish at least 2 values of m around these two displacement ranges.

2.2. Generalized admiralty coefficient: A performance indicator?

From physics point of view, the generalized admiralty coefficient defines a log-linear relationship between speed-through-water (V), shaft power (P_s) and displacement (Δ) as follows:

$$P_s \propto \Delta^m V^n \tag{1}$$

Introducing a proportionality constant (p') and taking logarithm on both sides results in a linear equation as follows:

$$P_s = p' \Delta^m V^n \tag{2}$$

$$\ln P_s = m \cdot \ln \Delta + n \cdot \ln V + p \tag{3}$$

Fitting this relationship on the in-service calm-water data would results in the equation of a flat surface in log scale, representing the calm-water speed-power-displacement surface for the specific (consisting of speed-power calm-water curves at all the possible displacements). The exponents m and n can be statistically calculated using an ordinary least squares (OLS) regression. The in-service operational data, used to obtain the exponents, can be filtered for near-calm-water conditions, for instance, by limiting the wind speed and significant wave height below a certain critical value. It may be argued that even the remaining small variation due to the environmental loads in the filtered data may result in a bias in the estimates. An obvious solution to that would be to correct the measured shaft power to account for environmental loads using available physics-based (or empirical) methods. For the current work, both the near-calm-water filtered data and the filtered data with correction applied is used to obtain the results in order to assess if applying the environmental load corrections is really necessary.

The above method would provide an averaged constant value of m and n over the whole operational domain of the ship. Also, from Eq. 3, it can be clearly confirmed that the numerical value of the generalized admiralty coefficient ($\Delta^m V^n / P_s$) is nothing but the exponent of the

intercept ($e^{-p} = 1/p'$) of the fitted speed-power-displacement surface on the power axis (in log scale). Moreover, the numerical value of the generalized admiralty coefficient obtained after substituting an observed operational point ($\Delta_x, V_x, P_{s,x}$) is equal to the distance (along the power axis) of this operational point from a surface parallel but identical to the fitted calm-water reference surface, as shown below.

$$\frac{\Delta_x^m V_x^n}{P_{s,x}} = e^{\left(m \cdot \ln\Delta_x + n \cdot \ln V_x - \ln P_{s,x}\right)} = e^{\pm\sqrt{m^2+n^2+1}\cdot d_x} \tag{4}$$

Where $d_x = \frac{|m \cdot \ln\Delta_x + n \cdot \ln V_x - \ln P_{s,x}|}{\sqrt{m^2+n^2+1}}$ is the shortest distance between the operational point ($\Delta_x, V_x, P_{s,x}$) and the parallel surface, which is passing through the origin in log scale and identical (in shape and orientation) to the fitted calm-water reference surface. Now, it is well-known that the line representing the shortest distance between a point and a surface is perpendicular to the surface. Thus, the cosine of the angle (θ) between the line representing the shortest distance and the power axis (in log scale) is given by:

$$\cos\theta = \frac{-1}{\sqrt{m^2+n^2+1}} \tag{5}$$

Using simple geometry (shown in Fig. 1), the distance of ($\Delta_x, V_x, P_{s,x}$) from the reference parallel surface (passing through the origin) along the power axis is given by $d_x/\cos\theta = \pm\sqrt{m^2+n^2+1}\cdot d_x$. Thus, the idea of using the generalized admiralty coefficient as a hydrodynamic performance indicator is mathematically equivalent to calculating and comparing the distance (along the power axis) of the operational points from the reference calm-water surface in speed-power-displacement domain.

On a different note, the discussion presented in the previous sections indicates that the values of these exponents may vary over the speed-displacement operational domain, i.e., the actual speed-power-displacement calm-water surface is probably log-non-linear. In such a case, the above presented linear regression model may be used to piece-wise fit the available data and obtain several values of these exponents. This would be equivalent to fitting the log-non-linear reference calm-water surface by several patches of log-linear surfaces in order to account for non-linearities.[1] The results obtained using such an approach are also presented in the current work. Nevertheless, the ratio $V^n \Delta^m / P_s$, further referred to as the generalized admiralty coefficient, with an appropriate value of m and n, can be used as an operational performance indicator for the ship which can be easily monitored over time.
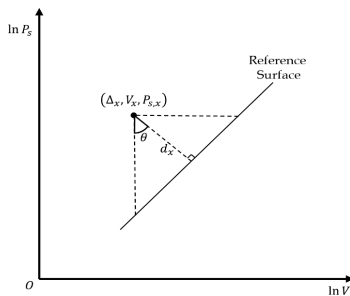
Fig. 1. Showing the angle (θ) subtended between the perpendicular dropped on the reference surface from the point ($\Delta_x, V_x, P_{s,x}$) and the line marking the distance of the point ($\Delta_x, V_x, P_{s,x}$) from the reference surface along the shaft power axis (in log scale). The figure shows the 2D projection of a 3D space, assuming that the third axis (ln Δ) is protruding out and above the 2D plane.

---

[1] All non-linear curves or surfaces are piece-wise linear.

2.3. Fouling friction coefficient (ΔC_F)

The traditional method to evaluate the performance of a ship observes the trend in fouling friction coefficient (ΔC_F) over time. The fouling friction coefficient is calculated as the difference between the total resistance coefficient ($C_{T,Data}$) obtained from the in-service data in calm-water conditions and the total resistance coefficient ($C_{T,Emp}$) obtained from a well-established empirical method or model test results.

$$\Delta C_F = C_{T,Data} - C_{T,Emp} \tag{6}$$

Multiplying the above equation with the non-dimensionalizing factor ($1/2\rho S V^2$) and again with the ship speed (V) results in an equation in terms of effective power. Further dividing the resulting equation with propulsion efficiencies would result in the same equation in terms of shaft power (P_s).

$$\Delta P_{s,F} = P_{s,Data} - P_{s,Emp} \tag{7}$$

Now, the above equation is clearly the distance (along the power axis) between the observed operational point (Δ, V, P_s) and the reference calm-water speed-power-displacement surface, determined by the adopted empirical method.

From the above and the discussion in the previous section, it is clear that the proposed method in the current work (using generalized admiralty coefficient) and the traditional method is based on the same underlying logic, i.e., observing the distance between the operational point and the reference calm-water speed-power-displacement surface. Finally, it should be noted here that the results from the traditional method would most definitely depend on how well the adopted empirical method's reference surface mimics the actual calm-water speed-power-displacement surface for the given ship. So it is critically important to validate the adopted empirical method for the given ship using the in-service data before using it for performance predictions. The new performance indicator, introduced in the current work, clearly, does not have any such problems.

3. OLS regression

A linear model, defining the relationship between a response variable and a group of independent variables, can be written in the form:

$$\mathbf{y} = \mathbf{X}\beta + \epsilon \tag{8}$$

Where $\mathbf{y}$ is the response variable, $\mathbf{X} = \begin{bmatrix} 1 & x_1 & \ldots & x_{p-1} \end{bmatrix}$ is the set of p independent variables (including the intercept), and ϵ contains the Normally distributed zero-mean residuals, i.e., $\epsilon \sim N(0, \sigma^2)$, where σ^2 is the true residual or error variance.

The coefficients, β, can be estimated using least squares regression as follows:

$$\widehat{\beta} = \left(\mathbf{X}^T\mathbf{X}\right)^{-1}\mathbf{X}^T\mathbf{y} \tag{9}$$

In an ordinary least squares (OLS) regression, the above parameter estimates ($\widehat{\beta}$) are obtained by minimizing the sum of squared residuals (SSR):

$$\arg \min \sum_{i=1}^{n} \epsilon_i^2 = \epsilon^T\epsilon = (\mathbf{y} - \mathbf{X}\beta)^T(\mathbf{y} - \mathbf{X}\beta) \tag{10}$$

The estimated parameters are statistics, and therefore, they have their corresponding sampling distributions. If the model assumptions are correct, these sampling distributions are also Normally distributed, and the estimated parameter values are the means of these sampling distributions. The variances of this sampling distribution can be calculated using the true error variance (σ^2) and the regressors ($\mathbf{X}$) as follows:

$$\sigma_{\hat{\beta}}^2 = \sigma^2 \left(\mathbf{X}^T\mathbf{X}\right)^{-1} \tag{11}$$

4

Since the true error variance (σ^2) is not known, it can be approximated by its best estimate (s^2) obtained using n samples, and it can be further used to obtain the standard errors (SE) (or standard deviations) of the estimated parameters as follows:

$$s^2 = \sum_{i=1}^{n} \frac{\epsilon_i^2}{(n-p)}$$

$$SE(\widehat{\beta}) = s\sqrt{\left(\mathbf{X}^T\mathbf{X}\right)^{-1}}$$

4. Quasi-steady filter

The current method is only applicable for data samples obtained in a quasi-steady state. In other words, the acceleration of the ship at each time step must be negligible. To ensure this, a two-stage filter is implemented to remove the samples with non-zero acceleration (further referred to as unsteady samples). The first stage of the filter uses a sliding window to remove unsteady samples as proposed by Dalheim and Steen (2020), while the second stage enforces an additional gradient check for the samples failing after the first stage.

In the first stage, a sliding window is used to observe the slope of a fitted straight line, using linear regression. Further, a student's t-test is done to check for non-zero slope (representing unsteady behavior) and a pass(1)-fail(0) test-statistic is calculated for each window. Each sample is, then, assigned a front and rear test-statistic which are obtained as the test-statistic calculated for the window when the given sample was at the front and rear end of the sliding window, respectively. It should be noted

that the front end of a window is in the direction of the motion of the window as explained in Fig. 1 in Dalheim and Steen (2020). Finally, each leg of unsteady behavior is identified as a leg starting with rear test-statistic failure and ending with front test-statistic failure.

The second stage filter calculates the backward gradient or slope only at the samples failing in the first stage and performs a students t-test, like the first stage, to check for non-zero slope. The samples indicating non-zero slope are finally removed as non-quasi-steady samples.

5. Data

The current work is based on the extended dataset obtained from the same sources as Gupta et al. (2019). The complete dataset is an assimilation of in-service measurement data recorded onboard a ship and weather hindcast data.

5.1. Ship data

The data is recorded onboard a $\sim 200m$ long general cargo ship with installed capacity of $\sim 10MW$ (MCR[2]) equipped with Marorka Online[3] web application. The data used here is recorded over a duration of about 3 years covering several voyages around the globe (shown in Fig. 2), and it contains uniformly sampled 15 minutes mean values for each recorded variable. The recorded variables are further used to calculate some additional variables, which are more appropriate for the current analysis, for instance, mean draft, trim-by-aft, displacement etc. The recorded data is filtered to extract the samples recorded during a sea voyage,
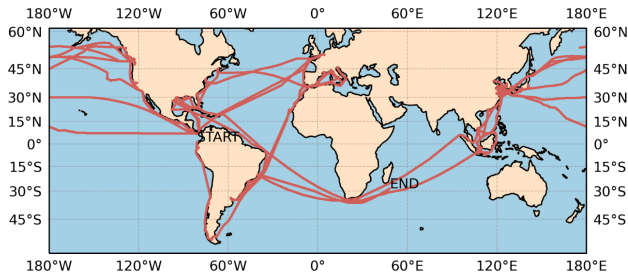
Fig. 2. Ship trajectory for the data recording duration (~ 3 years).

Table 1

Categorized list of variables recorded onboard the ship. Only 'Navigation', 'Propulsion System' & 'Environment' variables are used for the current analysis. *Abbreviations:* IMO = International Maritime Organization; COG = Center of Gravity; Aux. = Auxiliary; DG = Diesel Generator (for auxiliary power systems); ME = Main Engine (for propulsion system); GPS = Global Positioning System.

Ship Identity	Navigation	Auxiliary Power System	Propulsion System	Environment
Ship Name	Latitude	Aux. Consumed	State	Relative Wind Speed
IMO Number	Longitude	Aux. Electrical Power Output	ME Load Measured	Relative Wind Direction
	Gyro Heading	DG1 Power	Shaft Power	Sea Depth
	COG Heading	DG2 Power	Shaft rpm	
		DG3 Power	Shaft Torque	
			ME Consumed	
			Draft Fore	
			Draft Aft	
			GPS Speed	
			Log Speed	
			Cargo Weight	

---

[2] Maximum Continuous Rating of the engine.
[3] www.marorka.com

i.e., removing samples when the ship is stationary. Table 1 presents the categorized list of all the data variables recorded onboard the ship. Refer Gupta et al. (2019), for further overview of the recorded data variables as well as a brief description about the first part of preprocessing.

5.2. Hindcast data

The weather hindcast data, for wind and waves, is obtained from European Centre for Medium-Range Weather Forecast (ECMWF) (Copernicus Climate Change Service (C3S) (2017)). The ECMWF data is obtained from ERA5 HRES (High Resolution) climate reanalysis dataset. The spatial resolution of ERA5 HRES, used here, is 0.25° and temporal resolution is 1 hour. The weather data variables (presented in Table 2) are linearly interpolated in space and time to ship's location using the available navigation data. Fig. 3 shows the distribution of total wind

Table 2
Hindcast weather data variables obtained from ECMWF.

Hindcast Variables
1. Northward wind speed (10 m above the sea surface)
2. Eastward wind speed (10 m above the sea surface)
3. Significant wave height
4. Mean wave period
5. Mean wave direction
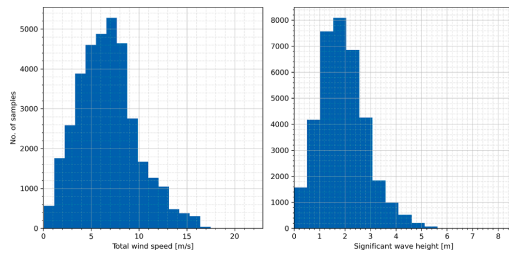
Fig. 3. Weather encountered by the ship during the data recording duration (∼ 3 years).
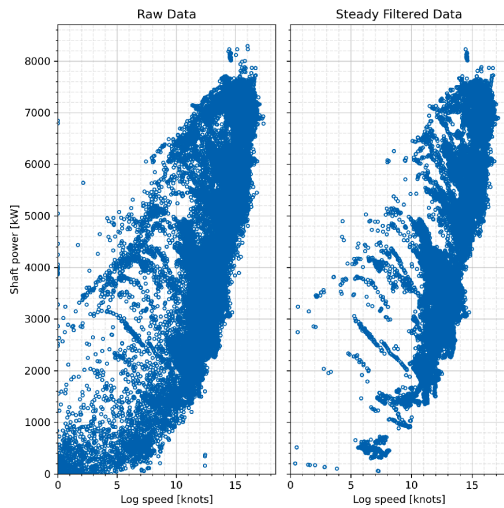
Fig. 4. Measured speed-through-water (or log speed) vs measured shaft power obtained from 3 years long time series.

speed and significant wave height encountered by the ship during the data recording duration.

5.3. Data exploration & pre-processing

Fig. 4 presents the speed-through-water (or log speed) vs shaft power from the raw data recorded over a period of 3 years onboard the ship. The figure shows a good spread over a speed range of 6 ∼ 16 knots. The design speed of the ship is 15.5 knots. In comparison to a typical calm-water curve obtained from model tests or numerical simulations, the raw data in Fig. 4 shows a good variation in power for a fixed speed. This is expected to occur due to variation in loading conditions and environmental loads. Nevertheless, this does not explain the samples with quite high shaft power at almost zero speed-through-water. A closer analysis reveals that such samples are obtained due to non-zero accelerations, i. e., periods when the ship is accelerating, for example, due to voluntary increase in shaft rpm by the ship master.

Quasi-steady filter: Although, it may be possible to use the samples with non-zero acceleration (further referred to as unsteady samples) after correcting for the effect of acceleration of the ship, it is decided to remove these samples for the current work. After removing all such samples, the ship can be assumed to be in a quasi-steady state at each observed sample. Unfortunately, the speed-through-water (or log speed) measurements cannot be used as a means to remove these samples due to several reasons. The speed-through-water measurements are quite noisy due to inadequate sensor accuracy, and the ship speed would also contain accelerations and decelerations due to changing environmental loads, which must be retained in the filtered data. But since the data here is averaged over the last 15 minutes, and 15 minutes seems to be long enough for the ship speed to catch up to the rpm change command, shaft rpm measurements can be used to remove unsteady samples. Thus, a quasi-steady filter, presented previously, is applied to the shaft rpm time series to filter out the unsteady samples.

Fig. 5 shows a small section of shaft rpm time series with quasi-steady filter in action. The figure contains two legs of unsteady behavior, one just before sample 20360 and the other around sample 20380. As clearly observed in the figure, the first (1st) stage filter also intends to removes some steady samples at the beginning and end of unsteady legs. The second stage filter helps retain these samples. The right-hand side subplot in Fig. 4 shows all the samples remaining after applying the quasi-steady filter on the raw data. Comparing the raw and the filtered data in Fig. 4, most of the points with small speed but very high shaft power are removed.

Ship heading estimation: The direction of heading of the ship is required to estimate the environmental loads acting on the ship. Although the gyro and COG headings are recorded onboard the ship (as
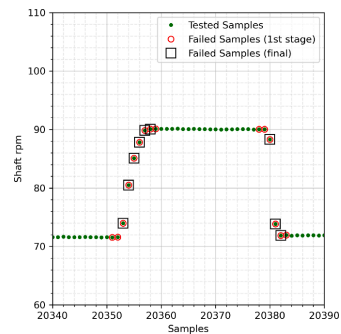
Fig. 5. Filtering out unsteady samples to ensure quasi-steady assumption.

shown in Table 1), it is observed that there were some errors in these measurements. The recorded heading variables were filled with zeros in the latter part of the time series. The ship heading is, therefore, estimated using the latitude and longitude variables recorded onboard the ship. The estimated ship heading is further validated against the first (non-zero) part of the recorded COG heading time series.

Draft correction: In general, draft measuring sensors are calibrated to convert measured pressure to water column height, resulting in draft measurements. But due to Venturi effect (or non-zero dynamic pressure), when the relative velocity between ship and fluid is non-zero, the actual measured pressure is smaller than the actual hydrostatic pressure, thus, the measured draft is smaller than the actual draft. Therefore, the draft measurements are corrected to account for this effect by interpolating the draft during an individual trip by using the initial and final draft measurements (when the ship speed is negligible).

*Displacement estimation:* Mean draft or draft at mid-ship and trim-by-aft are obtained as the mean and difference, respectively, of the above corrected aft and fore draft (assuming that the measured draft aft and draft fore are drafts at aft peak and fore peak, respectively). The mean draft and trim-by-aft are used as the input parameters to linearly interpolate the displacement for each data sample using the hydrostatics obtained from the 3D model of the ship. It is worth remembering that using the 3D model to estimate the displacement of the ship is also an approximation due to inherent discrepancies between the model and the real ship. As an estimation of error, it was observed that the displacement obtained using the 3D model, without the appendages, was about 73 tonnes more than the value reported in the sea trial report of the vessel for the same draft and trim settings. In view of this, no further corrections were made to account for an increase in displacement due to the appendages.

6. RESULTS

The results are divided in the following 4 sections. The first section presents the fouling friction coefficient (ΔC_F) calculated using the traditional method, which is further used for correcting the data for performance variation in time due to marine fouling. The next section presents the averaged constant value of displacement (m) and speed (n) exponents estimated using the in-service data recorded onboard a seagoing ship. The third section does the same but, here, the model is fitted piece-wise over the speed-displacement domain after dividing it into a regular grid, thus, presenting a grid of statistically fitted values for m and n. The final section presents a comparison of the obtained performance indicator, i.e., the generalized admiralty coefficient, with the most widely accepted performance indicator, the fouling friction coefficient (ΔC_F), as well as a demonstration regarding the use of the obtained performance indicator as a tool to monitor the hydrodynamic performance of a ship.

6.1. Calm-water in-service data

The calm-water in-service data is obtained by further filtering the steady-filtered data (shown in Fig. 4) for near-calm-water limits, total wind speed ($|V_{Wind}|$) less than 5.5 m/s (equivalent to Beaufort scale 3) and significant wave height (H_S) less than 1 m. As mentioned before, the data used here is recorded over a duration of about 3 years. The ship's propeller was cleaned 6 times in this duration. Based on these propeller cleaning events, the filtered near-clam-water data is divided into 7 legs with a propeller cleaning event falling between two consecutive legs. Fig. 6 shows the filtered near-calm-water in-service data in a log speed (or speed-through-water) vs shaft power space for all the legs. Fig. 7 shows the distribution of the filtered data in different legs as well as the distribution of data in all the legs combined (leg *All*).

6.2. Environmental load corrections

The calm-water in-service data presented in the previous section is corrected, in some cases, for wind and wave loads using empirical methods. Fujiwara's method (Fujiwara et al. (2005)) is used for wind load corrections (as recommended by ITTC (2017)), and DTU's method (Martinsen (2016), Taskar and Andersen (2021), based on an approach which uses the strip theory (Salvesen (1978)) and the asymptotic limit (Faltinsen et al. (1981)) to obtain the added wave resistance transfer functions, is used for wave load corrections. DTU's method for wave load corrections is used here with the help of ship simulation workbench (Taskar and Andersen (2019b)), and it provides added wave resistance corrections for the relative mean wave heading from head (180°) to beam seas (90°).

The total propulsive efficiency (η_D), for the given ship, is interpolated using the data available from the model test results for the ship. A linear interpolation grid is created over the speed vs mean draft domain using the model test data for interpolating η_D for each data sample. For samples outside the interpolation grid (for example, the samples with smaller ship speed which are outside the model test range), the nearest value on the grid is used.

6.3. Fouling friction coefficient (ΔC_F)

The data used for the current work is recorded over a duration of about 3 years and consists of numerous voyages. The ship, usually, re-
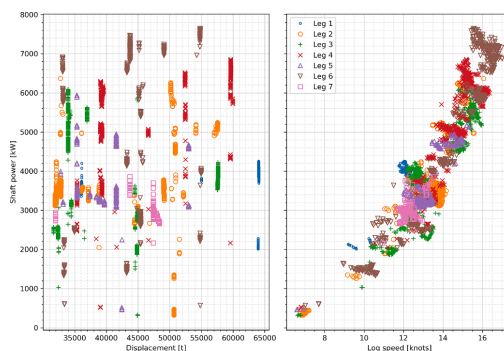
Fig. 6. Filtered near-calm-water in-service data. The time series data is divided into 7 legs with a propeller cleaning event falling between two consecutive legs.
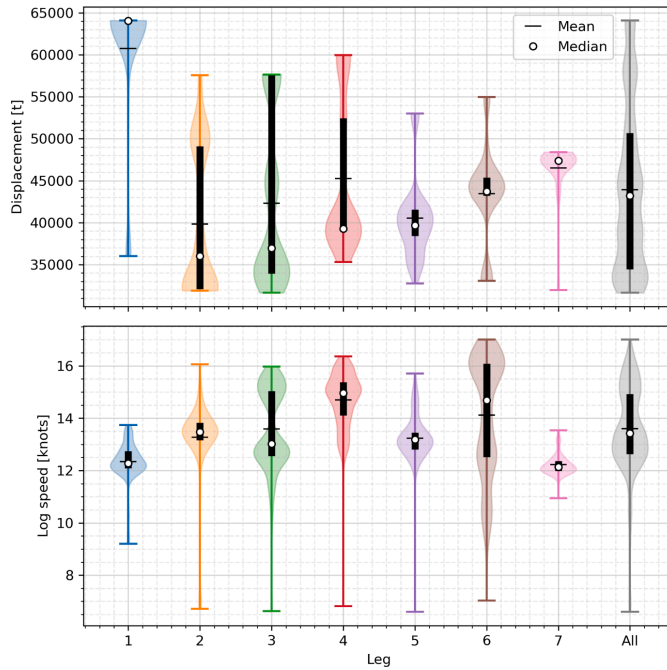
Fig. 7. Filtered near-calm-water in-service data (same as in Fig. 6) as violin plot. The thick black vertical lines stretch between 25% and 75% quantiles.

mains static for sometime between each voyage causing a build-up of marine fouling on the hull and propeller (Malone et al. (1981)). Moreover, the given data is affected by several propeller cleaning events, and a propeller cleaning activity may considerably influence the performance of a ship (Townsin (1982)). Thus, to obtain a good estimate of displacement (m) and speed (n) exponents, the data should be corrected to account for performance variation due to such phenomenon.

The shaft power measurement data is corrected for variation in performance over time due to marine fouling. These corrections are calculated by observing the trend in fouling friction coefficient (ΔC_F) with respect to the cumulative ship static time. The fouling friction coefficient (ΔC_F) is calculated using Eq. 6 with $C_{T,Data}$ calculated using the near-calm-water in-service data (presented in Section 6.1) with environmental loads corrections, using the method described in Section 6.2. The total calm-water resistance coefficient ($C_{T,Emp}$) is calculated using updated Guldhammer and Harvald's method (Kristensen and Bingham (2017)), as it is found to be fitting well for the given ship. The cumulative ship static time is calculated as the cumulative time (in seconds) for which the ship speed remains less than 3 knots (as suggested by Malone et al. (1981)). The fitted trend lines are used to calculate shaft power corrections to remove the effect of fouling, as shown in Fig. 8.

The calculated ΔC_F values shows quite small variation with time and most of the values are in the negative range. The small variation indicates little fouling build-up. This can be attributed to the fact that the

data used here is obtained from a newly-built ship (from first 3 years of service) and the anti-fouling systems are quite effective. The obtained ΔC_F values are negative likely due to the fact that the method used here to calculate $C_{T,Emp}$ is overestimating the calm-water resistance for the given ship.

6.4. Simple regression

The current section presents the averaged constant value of exponents estimated using the filtered near-calm-water in-service data (presented in Section 6.1) recorded onboard a ship over a duration of about 3 years. The following two models are used to calculate the displacement (m) and speed (n) exponents:

- **OLS:** An ordinary least squares model, based on Eq. 3, fitted to near-calm-water data, presented in Section 6.1.
- **OLS (Corr.):** An ordinary least squares model fitted to near-calm-water data corrected for environmental loads, as explained in Section 6.2.

The exponents calculated after applying corrections for variation in performance over time due to marine fouling are also presented in this section. The fouling corrections are done by subtracting the expected increase in the shaft power due to non-zero ΔC_F from the measured shaft

8
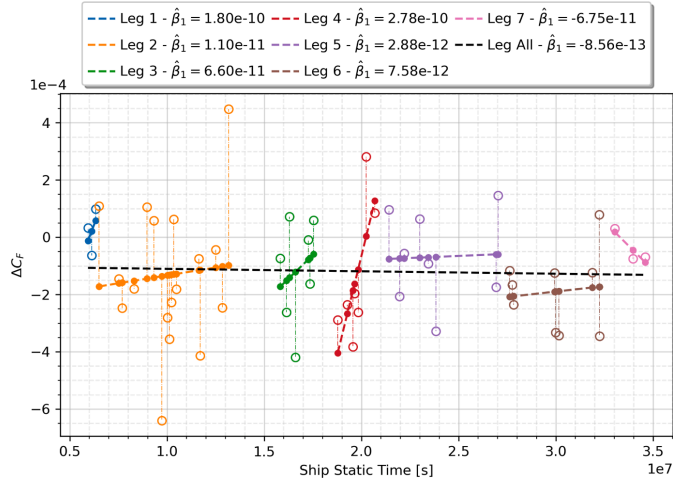
Fig. 8. Fouling friction coefficient (ΔC_F) with respect to ship static time. The trend lines are shown in dashed. The hollow circles are the calculated ΔC_F values and the filled circles are the project ΔC_F values on the fitted trend.

power, as explained in Section 6.3. As a simple cross-validation test, the exponents are also presented for the filtered but uncorrected (for fouling) legs. Finally, to draw a comparison, three well-known empirical methods are used to calculate the averaged constant value of exponents for the given ship. The data from empirical methods is obtained with the help of ship simulation workbench (Taskar and Andersen (2019b)).

Discussion: Table 3 presents the results obtained from the OLS and OLS (Corr.) models for all the legs, the complete dataset (leg *All*) and the time corrected dataset (leg *All-T*). Fig. 9 shows the estimated exponents in graphical format along with 95% confidence intervals. Fig. 10 shows the
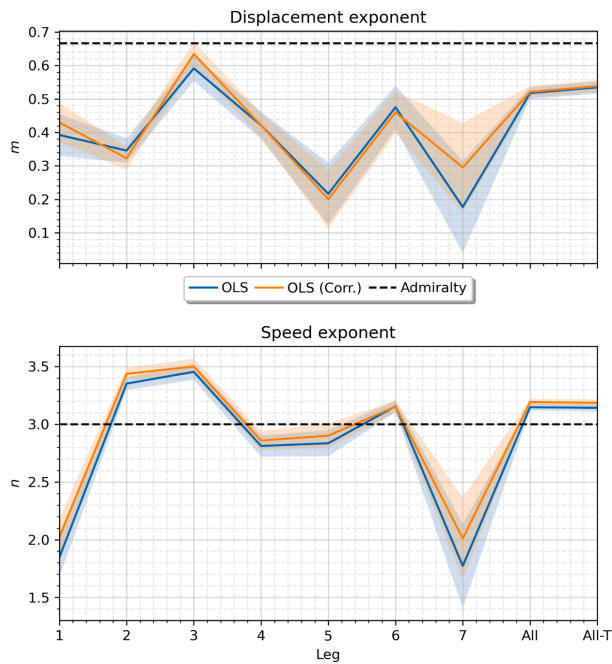
Fig. 9. Averaged constant exponents calculated using OLS and OLS (Corr.) models. Shaded regions represent 95% confidence intervals. Refer Table 3 for values.

9

Table 3

Results obtained from OLS and OLS (Corr.) regression models. The full dataset is divided to 7 legs with a propeller cleaning event fall between two consecutive legs. Leg *All* contains the full dataset (obtained after merging all the legs). Leg *All-T* also contains the full dataset but it is corrected for performance variation over time due to marine fouling.

Leg	Samples	m		n		RMSE		R2	
		OLS	OLS(Corr.)	OLS	OLS(Corr.)	OLS	OLS(Corr.)	OLS	OLS(Corr.)
1	289	0.39 ± 0.06	0.43 ± 0.06	1.85 ± 0.17	2.02 ± 0.16	318	298	0.455	0.536
2	795	0.35 ± 0.04	0.32 ± 0.03	3.35 ± 0.06	3.44 ± 0.05	368	340	0.858	0.874
3	917	0.59 ± 0.04	0.63 ± 0.04	3.45 ± 0.07	3.50 ± 0.07	389	378	0.900	0.901
4	621	0.42 ± 0.04	0.42 ± 0.04	2.81 ± 0.09	2.86 ± 0.08	419	381	0.863	0.887
5	313	0.22 ± 0.09	0.20 ± 0.09	2.84 ± 0.11	2.90 ± 0.11	328	307	0.810	0.828
6	599	0.48 ± 0.06	0.46 ± 0.06	3.16 ± 0.05	3.15 ± 0.05	443	424	0.958	0.961
7	166	0.18 ± 0.14	0.30 ± 0.13	1.77 ± 0.36	2.01 ± 0.35	205	194	0.378	0.443
All	3700	0.52 ± 0.02	0.52 ± 0.02	3.15 ± 0.03	3.19 ± 0.03	420	396	0.913	0.923
All-T	3700	0.53 ± 0.02	0.54 ± 0.02	3.14 ± 0.03	3.19 ± 0.03	455	436	0.908	0.915
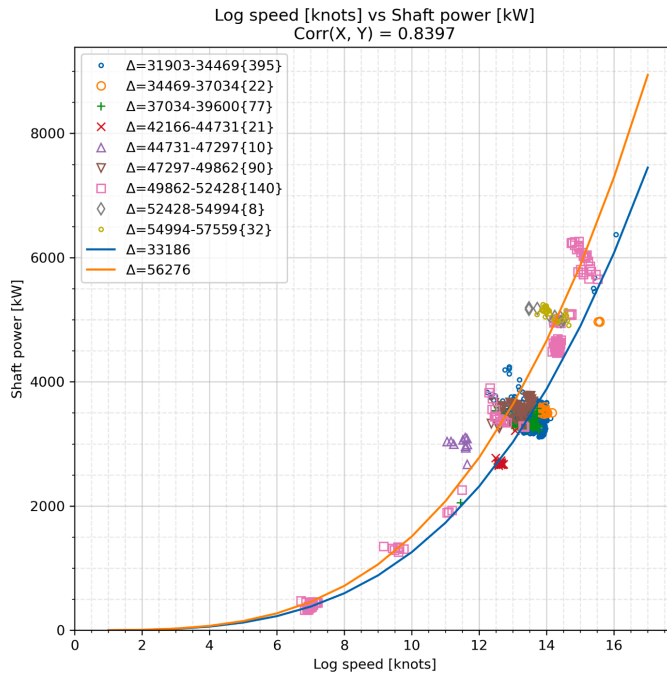
Fig. 10. Speed-power curves (indicated by solid lines) obtained using the OLS model for varying displacement (Δ) for leg 2. The fitted data is indicated by markers, divided into different categories according to the displacement, and the numbers in curly braces ({}) are the number of samples in the corresponding category.

fitted speed-power curves for the simple OLS model using the data in leg 2.

It is observed that the averaged constant displacement (m) and speed (n) exponents (shown in Table 3 and Fig. 9) obtained from the complete dataset (leg *All*) and the time-corrected dataset (leg *All-T*) are not very different. This is not surprising as the observed trends for individual legs in the fouling friction coefficient (shown in Fig. 8) are quite small, which in-turn is probably due to the fact that the current data is recorded onboard a newly-built ship. It should also be noted that applying environmental loads corrections on top of the currently employed near-calm-water filtering limits ($|V_{Wind}| < 5.5m/s$ & $H_S < 1m$), as done in the case of the OLS (Corr.) model, may not be necessary as the simple OLS model produces a good estimate for m and n as compared to the OLS (Corr.) model.

The speed exponent (n) obtained for the first and last leg (i.e., leg 1 & 7) using both the models is quite small as compared to the values in other legs. This is due to the fact that these legs consists of very few samples spread over a very limited range of speed axis (refer Figs. 6 and 7). Leg 5 is also observed to have very few samples but in this case the samples are well distributed along the speed axis. Looking at Fig. 7, it can also be said that leg 6, resulting in $n \approx 3.1$, has the best coverage over the speed-power domain. This is very close to the value obtained for complete dataset (leg *All* & *All-T*) as well as the speed exponent in the admiralty coefficient. Further, discarding the results in leg 1 & 7, it is observed that the averaged constant speed exponent (n) lies between 2.8 to 3.5 for the given ship, and 3.1 is the mean as well as the most probable value of n.

Table 4

Averaged constant displacement (m) and speed (n) exponents obtained from the conventional empirical methods for the given ship.

Method	Samples	m	n	RMSE	R2
Updated Guldhammer	990	0.69 ± 0.01	3.35 ± 0.02	147	0.997
Guldhammer	990	0.65 ± 0.01	3.21 ± 0.01	118	0.999
Hollenbach	990	0.67 ± 0.01	3.28 ± 0.02	190	0.996

The fitted displacement exponent (m) seems to be varying quite substantially for different legs. Thus, it does not seem appropriate to define a reliable range for the true value of m. Observing Fig. 7, it can be seen that the samples in legs 2, 3 & 4 has a fairly good coverage over the displacement-power domain but each of them results in a very different value. It should be noted that leg 3, which shows the best coverage over the displacement-power domain, predicts the displacement exponent to be ~ 0.6 (closest to 2/3, the exponent in the admiralty coefficient) but the results from the complete datasets (leg *All & All-T*) results in $m \approx 0.5$.

As aforementioned, the averaged constant displacement (m) and speed (n) exponents are also calculated using the data obtained from three well-known empirical methods for the given ship (shown in Table 4). The exponents obtained here seems to be on the higher side as compared to the corresponding values from in-service data, and the displacement exponent in all the three cases is quite close to $m = 2/3$, as in the case of the original admiralty coefficient. In case of empirical methods, a weighted least squares (WLS) regression model (refer Appendix A) has to be used to calculate the exponents, as explained in Appendix B.

6.5. Piece-wise regression

It may be expected that the log-linear assumption, taken in Eq. 3, would result in an inaccurate modeling of the speed-power-displacement reference surface. The extensive literature survey presented in the current work also suggests that the speed (n) and displacement (m) exponents are not constant over the complete speed-displacement domain, thus, indicating a log-non-linear relationship between speed, power and displacement. Nevertheless, acknowledging the fact that all non-linear surfaces are piece-wise linear, it is, therefore, possible to fit a log-linear relationship to a greater degree on the given data by dividing it into several small pieces over the speed-displacement domain. This is equivalent to modeling the log-non-linear surface in speed-power-displacement 3D space by several patches of log-linear surfaces.

Fig. 11 presents the displacement (m) and speed (n) exponents calculated using the calm-water data (shown by faded hollow circles) obtained, for the given ship, from updated Guldhammer and Harvald's method by piece-wise fitting the log-linear model. The data is, first, divided into rectangular blocks, shown by grid-like lines in Fig. 11, and, then, the exponents are calculated for each block by using simple OLS regression in log scale. Finally, the calculated values are used to create the m and n contours over the whole speed-displacement domain. The goodness of fit is indicated (in Fig. 11 title) by the minimum R-squared (R2) and maximum root mean square error (RMSE) obtained from the blocks in the fitted domain. The results confirm the expected log-non-linearity or non-constant and varying value for displacement (m) and speed (n) exponents over the speed-displacement domain. Observing the values in Fig. 11, it can be noted that the major area of the contours corresponds to the values of the exponents in the original admiralty coefficient.
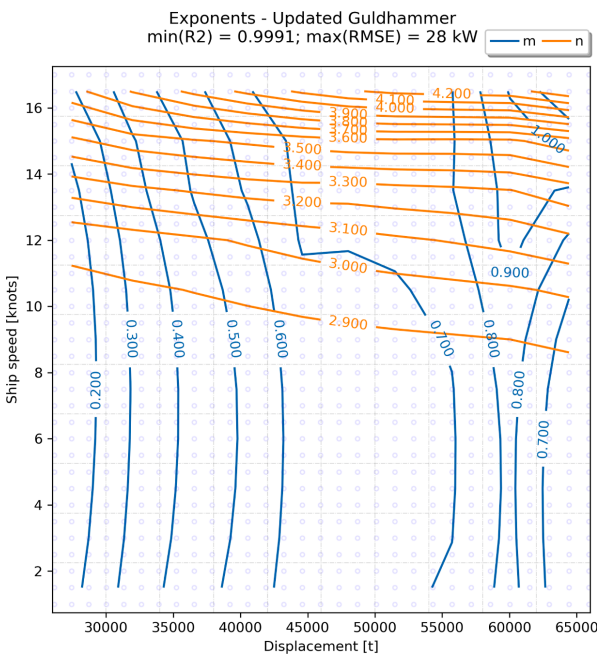
Fig. 11. Displacement and speed exponents (m and n, respectively) calculated piece-wise using the calm-water data obtained using updated Guldhammer and Harvald's method (Kristensen and Bingham (2017)) for the given ship. The data used for fitting the model is shown by faded hollow circles. The grid-like lines divide the data into pieces or blocks which are further used to carry-out log-linear OLS regression. The exponents obtained for each block are further used to obtain the contours.

Obtaining a similar contour from the in-service calm-water data is far more complicated due to several obvious reasons like sparsity of data, non-uniform distribution of data, etc. Fig. 12 shows the displacement (*m*) and speed (*n*) exponents obtained from in-service data. The data used here is corrected for both time and environmental loads (same as OLS (Corr.) model in leg *All-T* in the previous section). Although some of the obtained values are comparable with the values in Fig. 11, the values are still not consistent enough to create a contour. Moreover, it should be noted that the grid blocks used in Fig. 12 are substantially bigger than the blocks used in Fig. 11. Smaller blocks results in many more inappropriate values of *m* and *n* as the variation due to noise in the data becomes larger than the variation due to the actual trend.

The inconsistencies in the values of exponents observed in Fig. 12 indicate that the fitted patches of log-linear surfaces will not produce a very smooth speed-power-displacement surface for the ship. In view of that, the averaged constant exponents, obtained for leg *All-T* in the previous section, are used to formulate the performance indicator for the current case.

6.6. Performance indicator

As aforementioned, the underlying logic behind the traditional method for performance prediction, using the fouling friction coefficient (ΔC_F), as well as the current method is based on observing the distance (along the power axis) between an operational point (Δ, V, P_s) and the reference speed-power-displacement calm-water surface for the ship. In case of the traditional method, the reference surface is usually obtained using an empirical method (which is nothing but a regression model fitted on the model test results obtained from several generalized hull forms) or the model tests conducted for the ship during the design stage. The reference surface obtained using an empirical method may not fit well for the given ship, and the model test results may introduce unknown scale effects while estimating the reference surface for the full

scale ship. It is, therefore, critically important to validate the reference surface obtained from these sources using the in-service data recorded onboard the full scale ship. The method proposed, here, establishes the reference calm-water surface directly using the in-service data recorded onboard the ship. Thus, it does not need any further validation.

Fig. 13 shows the reference surfaces used by the traditional method (top row), i.e., the best fitted empirical method (updated Guldhammer and Harvald's method, Kristensen and Bingham (2017)) for the given ship, and the current method (bottom row). The reference surfaces in Fig. 13 are, first, divided into a number of sections based on the displacement (Δ), as indicated on the top of the subplots in the first row. The filtered near-calm-water in-service data (presented in Section 6.1), without any corrections, falling in the range of the surface section is, then, plotted with it. The vertical distance (along the power axis) between the reference surface and the in-service data samples is indicated by the color intensity of the data samples, with red being on top of the surface and blue below the surface. The goodness of fit for each surface section is indicated by RMSE and R2 parameters, shown on top of each surface section subplot. It should be noted that these subplots are projections of 3D surfaces on a 2D plane but the distance (indicated by color intensity) between the in-service data samples and the surface are calculated in 3D.

Fig. 13 clearly shows that the reference surface from the current method has a better fit for lower displacement range whereas the reference surface predicted using the updated Guldhammer and Harvald's method (Kristensen and Bingham (2017)) fits better in the higher displacement range (clearly noticeable for $\Delta = [45000, 55000]$). This can be attributed to the fact that the in-service data, used for estimating the reference surface for the current method, has more number of samples in the lower displacement range (as shown in Fig. 7). A better distribution of in-service data would result in a more accurate reference surface.

Further, the obtained reference surface can be used to predict the performance of the ship over time by calculating the value of the
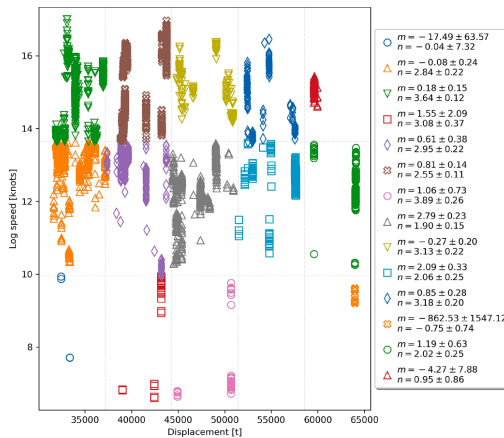
Fig. 12. Displacement and speed exponents (*m* and *n*, respectively) calculated piece-wise using the in-service calm-water data. The data used here is corrected for time as well as environmental loads.
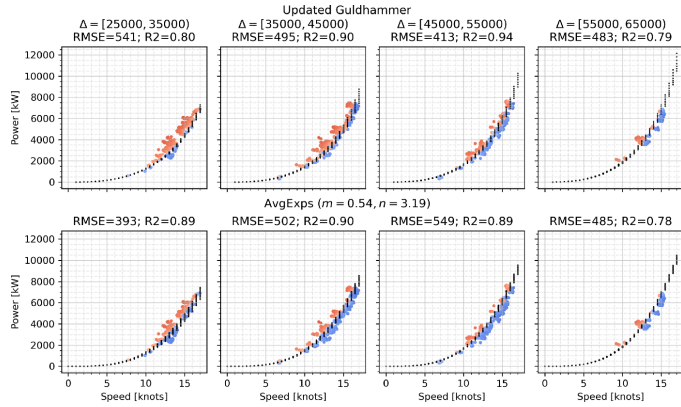
Fig. 13. Comparison between the calm-water reference surface used by the traditional method (calculating ΔC_F using the best fitting empirical method for the given ship, updated Guldhammer and Harvald's method (Kristensen and Bingham (2017))) and the current method for performance prediction.

generalized admiralty coefficient (with statistically estimated values of displacement (m) and speed (n) exponents from leg *All-T* in Table 3) using the filtered near-calm-water in-service data with environmental load corrections, explained in Section 6.2. Fig. 14 shows the evolution of obtained performance indicator with ship static time along with the trend lines. Here, each hollow circle represents the mean generalized admiralty coefficient obtained using the in-service data recorded at the corresponding ship static time. As in the case of ΔC_F method, the filtered near-calm-water in-service data used here is corrected for environmental loads, so that a clear comparison can be drawn between the current method and the performance predictions by the traditional ΔC_F method (shown in Fig. 8).

Comparing Figs. 14 and 8, it can be seen that both the methods

predict an unnatural trend in the performance change of the ship for some legs (leg 1, 6 & 7 for the current method, and leg 7 for the traditional method). Moreover, both the methods predict a drop in performance after the last propeller cleaning event (between leg 6 & 7). Looking at the slopes for each leg, it is quite noticeable that both the methods predict the biggest performance drop in leg 4 and the second biggest drop in leg 3, and the predicted performance drop in leg 2 is quite comparable. Lastly, observing the overall trend (leg *All*), the current method (generalized admiralty coefficient) seems to be predicting an appropriate trend showing a drop in performance whereas the traditional method predicts an unnatural increase in the performance of the ship over a duration of 3 years.
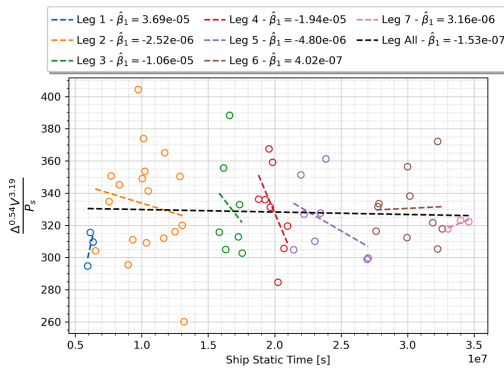
Fig. 14. Statistically obtained generalized admiralty coefficient with respect to ship static time.

13

7. Conclusion

The current work establishes a simple hydrodynamic performance indicator, in the form of generalized admiralty coefficient, to predict the change in performance over time for a sea-going ship using the in-service data recorded onboard the ship. The in-service data recorded onboard a new-built sea-going ship over a period of about 3 years is used to statistically obtain the speed and displacement exponents in the generalized admiralty coefficient for the ship. The fitted generalized admiralty coefficient represents the reference speed-power-displacement surface, in calm-water condition, for the ship.

The extensive literature review presented here indicates a log-non-linear nature of the true reference speed-power-displacement surface for modern hull forms operating in calm-water. To account for these non-linearities, the reference surface is fitted piece-wise using several log-linear surface patches but the results produced using the piece-wise approach did not produce consistent values, due to large amount of noise in the in-service data. Therefore, the reference surface, assuming a log-linear form as per the generalized admiralty coefficient, is used here for predicting the performance of the ship over time.

The fitted log-linear reference surface and the performance predictions made using the fitted surface are validated by carrying-out a thorough comparison with the traditional method, i.e., observing the trend in fouling friction coefficient (ΔC_F). The performance prediction results are found to be in good agreement with the results from the traditional method, indicating that the non-linearities in the actual reference surface are not significant.

As the results from the current method are well-validated here, it provides the ship operators with a simplistic and easily implementable method to monitor the hydrodynamic performance of a ship directly using the in-service data, thereby, removing the dependence on empirical methods or model test results. The reference speed-power-displacement surface for calm-water conditions (represented by the generalized admiralty coefficient) can be easily estimated using the in-service data without carrying-out any environmental load corrections and marine fouling corrections. The environmental load corrections can be avoided by using a near-calm-water filtering limit for the in-service data, and the data recorded onboard a new-built ship may not need fouling corrections, as indicated by the results in the current work. Thus, the performance of a ship can be simply monitored by observing the trend in the generalized admiralty coefficient (with statistically estimated exponents) using the filtered near-calm-water in-service data.

The results also indicate that the exponents used in the original admiralty coefficient are probably not valid for modern hull forms, but the log-linear relationship can still be used, as an approximation, to represent the true reference surface. It should be noted that the results obtained using the current method are highly dependent on the quality of the in-service data. Moreover, the current method requires an initial data recording time (to estimate the speed and displacement exponents) before it can be used for predicting the performance of a ship, but once the reference surface is established for a ship, using the current method, it can be used to predict the performance of the ship for the rest of its life very easily. On the other hand, the results obtained from the traditional method would surely depend on the validity (for the given ship) of the method used for calculating ΔC_F and may lead to inaccurate results due to various reasons like scale effects (as the reference surface used in that case is estimated using the data obtained from model test results of generalized hull forms or the given ship). Therefore, the current method, i.e., using the generalized admiralty coefficient statistically fitted on the in-service data recorded onboard the given ship, proves to be a more robust method for the performance prediction of the ships over time.

CRediT authorship contribution statement

Prateek Gupta: Conceptualization, Methodology, Investigation, Software, Data curation, Visualization, Writing – original draft, Writing – review & editing. **Bhushan Taskar:** Conceptualization, Investigation, Validation, Software. **Sverre Steen:** Conceptualization, Supervision, Resources. **Adil Rasheed:** Supervision.

Declaration of Competing Interest

The authors declare that they have no known competing financial interests or personal relationships that could have appeared to influence the work reported in this paper.

Appendix A. Weighted least squares (WLS) regression

In OLS regression, it is inherently assumed that all the fitted samples holds equal importance or weightage. Thus, all the samples used for fitting the model exert an equal influence over the parameters being estimated. A model that treats all of the samples equally would give less precisely measured points more influence than they should have and would give highly precise points too little influence. In statistical terms, OLS assumes that the standard deviation of error term is constant over all the values of independent variables. This assumption, however, is not valid for all the models.

In WLS regression, the fitted samples are assigned unequal weights so that the samples with higher weights exert a higher influence over the parameters being estimated. The size of the weight may also indicate the precision of the information contained in the associated observation. Here, the estimates are obtained by weighted SSR instead of ordinary SSR.

$$\arg \min \sum_{i=1}^{n} \epsilon_i^{*2} = (\mathbf{y} - \mathbf{X}\beta)^T \mathbf{W} (\mathbf{y} - \mathbf{X}\beta) \tag{A.1}$$

$$\widehat{\beta}_{WLS} = \left(\mathbf{X}^T \mathbf{W} \mathbf{X}\right)^{-1} \mathbf{X}^T \mathbf{W} \mathbf{y} \tag{A.2}$$

Where $W = diag([w_1, w_2, ..., w_n])$ is a diagonal matrix with the diagonal containing weights assigned to n given samples. The standard errors of the estimated parameters can be further calculated as follows:

$$s_{WLS}^2 = \sum_{i=1}^{n} \frac{w_i \epsilon_i^2}{(n-p)} \tag{A.3}$$

$$SE(\widehat{\beta}) = s_{WLS} \sqrt{\left(\mathbf{X}^T W \mathbf{X}\right)^{-1}} \tag{A.4}$$

14

WLS models are, generally, used to treat datasets with non-constant error variances, or heteroscedasticity, identified as a funnel shape in the residual plot (James et al. (2013)). In order to obtain the most precise parameter estimates, the weights should be as defined as inversely proportional to the variance of the quality of information in the samples. In other words, each weight should be directly proportional to the preciseness of the corresponding sample.

$$w_i \propto \frac{1}{\sigma_i^2} \tag{A.5}$$

Appendix B. Empirical methods

It is well-known that the results obtained using a statistical machine-learning method is highly susceptible to biases, mainly, due to an uneven distribution of data samples. Thus, it is considered very important to do a validation study, if possible, using a previously known and well-established method. In order to validate the above results, the displacement (m) and speed (n) exponents are also obtained for the given ship using following three empirical methods:

a) Guldhammer and Harvald's method (Guldhammer and Harvald (1970))
b) Updated Guldhammer and Harvald's method (Kristensen and Bingham (2017))
c) Hollenbach's method (Hollenbach (1998))

These three empirical methods are, first, used to calculate the calm-water resistance and the total propulsive power for the given ship over a uniform speed vs mean draft grid (keeping zero trim). An OLS regression model is, then, fitted on these calculated values as per the relation given in Eq. 3. Table 4 presents the estimated parameters obtained from all the three empirical methods. Observing the R-squared (R2) values for the OLS model, it seems to be having a very good fit but the residuals plot (shown in Fig. B.15) clearly indicate that the model does not actually fit the data well.[4]

As shown in Fig. B.15, the simple OLS model shows an increasing trend in residuals with increasing propulsive power as well as other variables. This is due to the fact that the linear regression model is being fitted in log scale and, therefore, the OLS model minimizes the sum of square residuals (SSR) in log scale. In order to obtain a better fitted linear model, a WLS regression model is used with weights as the square of propulsive power (i.e., $w_i = Y_i^2$) so as to give higher weights to higher propulsive power samples. Fig. B.16 shows the residuals for the WLS model. The WLS models is, clearly, a better fit and it results in a substantially smaller RMSE (as shown in Table B.5b).
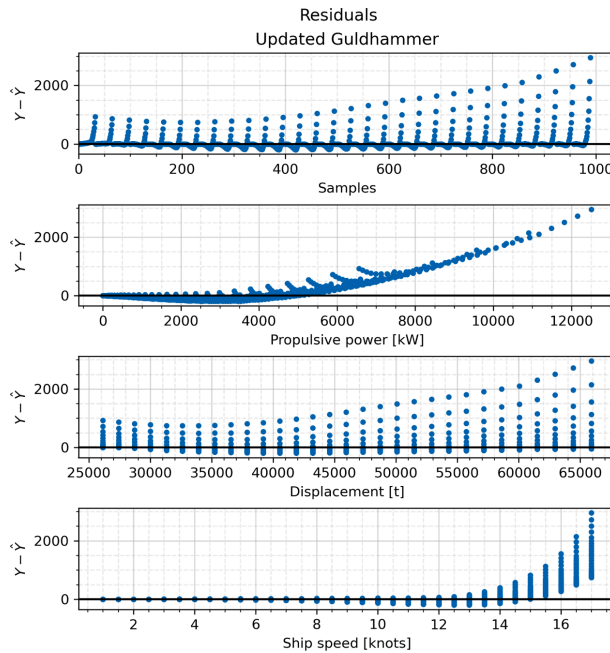
Fig. B1. Residuals for OLS model fitted on the calm-water data obtained using the updated Guldhammer and Harvald's method. Y = Propulsive power.

---

[4] It is well-known in statistical community that a thorough investigation of residuals is mandatory to judge the goodness of fit of any statistical machine-learning model, just observing the goodness of fit parameters like R2, RMSE, etc. is not sufficient.
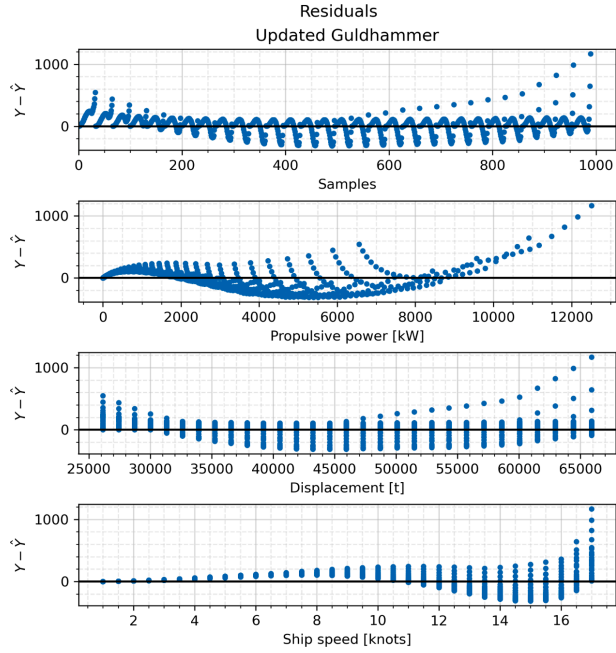
Fig. B2. Residuals for WLS model, with Y_i^2 as sample weights, fitted on the calm-water data obtained using the updated Guldhammer and Harvald's method. Y = Propulsive power.

Table B1
Results obtained from regression models (OLS and WLS) using data obtained from the conventional empirical methods for the given ship.

(a) Displacement exponent (m) and speed exponent (n). The estimated values of m and n are presented with their 95% confidence limits (assuming that the estimates are Normally distributed).

Method	Samples	m		n	
		OLS	WLS	OLS	WLS
Updated Guldhammer	990	0.574 ± 0.014	0.687 ± 0.011	2.901 ± 0.005	3.352 ± 0.020
Guldhammer	990	0.561 ± 0.011	0.650 ± 0.007	2.946 ± 0.004	3.212 ± 0.013
Hollenbach	990	0.685 ± 0.018	0.671 ± 0.013	2.700 ± 0.007	3.281 ± 0.022

(b) Goodness of fit parameters. *STDE* = Standard error, *RMSE* = Root mean square error and *R2* = Coefficient of determination (prediction).

Method	OLS			WLS		
	STDE	RMSE	R2	STDE	RMSE	R2
Updated Guldhammer	229	370	0.980	143	147	0.997
Guldhammer	181	303	0.990	116	118	0.999
Hollenbach	319	515	0.971	190	196	0.996

It should be noted that the current behavior is not observed in case of the OLS and WLS models while using the in-service data because the data samples in that case are sparsely distributed with substantially fewer samples in lower shaft power range, thereby automatically giving higher weights to samples with higher shaft power measurements. On another note, from Fig. B.15, it can be observed that trend in residuals is not linear, as one might expect assuming a log-linear relation assumed in the generalized admiralty coefficient. This is due to the fact that the data is non-linear in log scale and, therefore, the log-linear relation is a mere simplification of a more complex problem.

16

References

Copernicus Climate Change Service (C3S), 2017. ERA5: Fifth generation of ECMWF atmospheric reanalyses of the global climate. copernicus climate change service climate data store (CDS). Last Accessed: May 29th, 2019.

Dalheim, Ø., Steen, S., 2020. A computationally efficient method for identification of steady state in time series data from ship monitoring. Journal of Ocean Engineering and Science. https://doi.org/10.1016/j.joes.2020.01.003.Cited By 1

Doust, D., O'Brien, T., 1959. Resistance and propulsion of trawlers. North East Coast Institution of Engineers and Shipbuilders.

Du, Y., Chen, Q., Quan, X., Long, L., Fung, R., 2011. Berth allocation considering fuel consumption and vessel emissions. Transportation Research Part E: Logistics and Transportation Review 47 (6), 1021–1037. https://doi.org/10.1016/j.tre.2011.05.011.Cited By 138

Faltinsen, O.M., Minsaas, K.J., Liapis, N., Skjordal, S.O., 1981. Prediction of resistance and propulsion of a ship in a seaway, pp. 505–529.Cited By 178

Froude, R.E., 1888. The constant system of notation of results of experiments on models used at AEW.

Fujiwara, T., Ueno, M., Ikeda, Y., 2005. A new estimation method of wind forces and moments acting on ships on the basis of physical component models. Journal of the Japan Society of Naval Architects and Ocean Engineers 2, 243–255. https://doi.org/10.2534/jjasnaoe.2.243.

Guldhammer, H., Harvald, S., 1970. Ship resistance: Effect of form and principal dimensions. Akademisk Forlag.

Gupta, P., Steen, S., Rasheed, A., 2019. Big data analytics as a tool to monitor hydrodynamic performance of a ship. In: International Conference on Offshore Mechanics and Arctic Engineering, Volume 7A: Ocean Engineering. https://doi.org/10.1115/OMAE2019-95815.V07AT06A059

Hollenbach, K.U., 1998. Estimating resistance and propulsion for single-screw and twin-screw ships. Ship Technology Research 45 (2), 72–76.Cited By 21

ITTC, 2017. Recommended procedures and guidelines 7.5-04-01-01.1: Preparation, conduct and analysis of speed/power trials.

ITTC, 2017. ITTC symbols and terminology list.

James, G., Witten, D., Hastie, T., Tibshirani, R., 2013. An introduction to statistical learning: With applications in r. Springer New York.

Kristensen, H.O.H., 2010. Model for environmental assessment of container ship transport. Transactions - Society of Naval Architects and Marine Engineers 118, 122–139.Cited By 6

Kristensen, H.O.H., Bingham, H., 2017. Prediction of Resistance and Propulsion Power of Ships. Technical Report. Technical University of Denmark.

Malone, J.A., Little, D.E., Allman, M., 1981. Effects of hull foulants and cleaning/coating practices on ship performances and economics. Transactions - Society of Naval Architects and Marine Engineers 88, 75–101.Cited By 12

MAN-Energy-Solutions, 2004. Basic Principles of Ship Propulsion. Technical Report. MAN Energy Solutions.

Martinsen, M.A., 2016. An design tool for estimating the added wave resistance of container ships, et design vrktj til estimering af get blgemodstand for kontainerskibe.

Prpić-Oršić, J., Faltinsen, O., 2012. Estimation of ship speed loss and associated co2 emissions in a seaway. Ocean Eng. 44, 1–10. https://doi.org/10.1016/j.oceaneng.2012.01.028.

Psaraftis, H., Kontovas, C., 2013. Speed models for energy-efficient maritime transportation: a taxonomy and survey. Transportation Research Part C: Emerging Technologies 26, 331–351. https://doi.org/10.1016/j.trc.2012.09.012. Cited By 217.

Salvesen, N., 1978. Added resistance of ships in waves. J Hydronaut 12 (1), 24–34. https://doi.org/10.2514/3.63110.Cited By 61

Taskar, B., Andersen, P., 2019a. Benefit of speed reduction for ships in different weather conditions.

Taskar, B., Andersen, P., 2019b. Ship simulation workbench: User manual, Technical University of Denmark.

Telfer, E.V., 1963. The design presentation of ship model resistance data.

Taskar, Bhushan, Andersen, Poul, 2021. Comparison of added resistance methods using digital twin and full-scale data. Ocean Engg. In press.

Townsin, R.L., 1982. Estimating the technical and economic penalties of hull and propeller roughness. Transactions - Society of Naval Architects and Marine Engineers 89, 295–318.

Tu, H., Yang, Y., Zhang, L., Xie, D., Lyu, X., Song, L., Guan, Y.-M., Sun, J., 2018. A modified admiralty coefficient for estimating power curves in eedi calculations. Ocean Eng. 150, 309–317. https://doi.org/10.1016/j.oceaneng.2017.12.068. Cited By 4.

Walker, M., Atkins, I., 2007. Surface ship hull and propeller fouling managment, pp. 131–138.Cited By 3

Wang, S., Meng, Q., 2012. Sailing speed optimization for container ships in a liner shipping network. Transportation Research Part E: Logistics and Transportation Review 48 (3), 701–714. https://doi.org/10.1016/j.tre.2011.12.003.Cited By 175

Article 4

Ship Performance Monitoring using
Machine-learning

Prateek Gupta, Adil Rasheed, Sverre Steen

Highlights

Ship Performance Monitoring using Machine-learning

Prateek Gupta,Adil Rasheed,Sverre Steen

- Linear methods can model non-linear phenomena using domain knowledge

- Simple interpretable models can outperform advanced black-box methods

- In-service data can be used for continuous performance monitoring of ships

- Machine-learning can be used to monitor the hydrodynamic performance of ships

- Change in performance can be estimated for propeller and hull cleaning events

Ship Performance Monitoring using Machine-learning

Prateek Gupta[a,*], Adil Rasheed[b] and Sverre Steen[a]

[a]*Norwegian University of Science and Technology (NTNU), Department of Marine Technology, Trondheim, 7052, Sør-trondelag, Norway*
[b]*Norwegian University of Science and Technology (NTNU), Department of Engineering Cybernetics, Trondheim, 7034, Sør-trondelag, Norway*

ARTICLE INFO

ABSTRACT

The hydrodynamic performance of a sea-going ship varies over its lifespan due to factors like marine fouling and the condition of the anti-fouling paint system. In order to accurately estimate the power demand and fuel consumption for a planned voyage, it is important to assess the hydrodynamic performance of the ship. The current work uses machine-learning (ML) methods to estimate the hydrodynamic performance of a ship using the onboard recorded in-service data. Three ML methods, NL-PCR, NL-PLSR and probabilistic ANN, are calibrated using the data from two sister ships. The calibrated models are used to extract the varying trend in ship's hydrodynamic performance over time and predict the change in performance through several propeller and hull cleaning events. The predicted change in performance is compared with the corresponding values estimated using the fouling friction coefficient (ΔC_F). The ML methods are found to be performing well while modeling the hydrodynamic state of the ships with probabilistic ANN model performing the best, but the results from NL-PCR and NL-PLSR are not far behind, indicating that it may be possible to use simple methods to solve such problems with the help of domain knowledge.

1. Introduction

The hydrodynamic performance of a ship is an important factor which must be considered while working towards the green shipping future. In the ongoing development towards low-emission shipping, sparked partly by the IMO's goal of 50% reduction of greenhouse gas (GHG) emissions from global shipping within 2050, energy saving is going to be much more important, also from an economic perspective. Optimizing the hydrodynamic performance of a ship would not only lead to direct reduction of GHG, when running the ship on fossil fuels, but would also make alternative low-GHG fuel options more economically viable, as all the low-GHG alternative energy sources are significantly more expensive per unit energy than the traditional marine fuels.

The operational efficiency and, therefore, fuel or energy savings can be increased by keeping the hull and propeller smooth and clean of marine fouling (Townsin (2003)). However, cleaning very frequently is quite expensive and may also lead to increase in wear of the hull coating, which in turn may increase the resistance and fuel consumption (Munk (2016)). Conventionally, most of the ship owners perform scheduled maintenance (hull and propeller cleaning) on a regular timely basis which may not be very efficient. If the performance of the in-service ship can be efficiently and accurately monitored, the hull and propeller maintenance intervals can be optimized.

A sea-going ship is, now-a-days, equipped with numerous sensors which are continuously recording several variables, some of them representing the hydrodynamic state of the ship. These in-service recorded variables can be used to monitor the hydrodynamic performance of the ship (as suggested by Pedersen and Larsen (2009)). The objective of the current work is to use machine-learning (ML) methods to monitor the hydrodynamic performance of a ship over time using the in-service data recorded onboard the ship. Pedersen and Larsen (2009) used an artificial neural network (ANN) with just one hidden layer to model the hydrodynamic state of a ship, indicating the simplicity of the problem. Therefore, it may be possible to solve such a problem using a simple interpretable model like Principal Component Regression (PCR) or Partial Least Squares Regression (PLSR) with the help of some non-linear transformations obtained from our domain knowledge, thereby, linearizing the problem. In case of a linear problem, a simple model like PLSR is known to have outperformed ANN (Farifteh et al. (2007)).

The current work focuses on developing data-driven methods for ship performance monitoring using the in-service data recorded onboard two sister ships. It is attempted here to predict the performance of the ships using two well-known

multivariate linear regression models, namely, Principal Component Regression (PCR) and Partial Least Squares Regression (PLSR), enhanced using simple (but approximate) non-linear transformations, obtained from our domain knowledge. The enhanced models are used alongside an advanced probabilistic non-linear model, probabilistic artificial neural network (ANN), so that the performance of the enhanced models can be compared with the state-of-the-art. Moreover, a fouling growth factor is proposed to account for the growth of fouling on the ships' hull and propeller. The calibrated models are used to observe the fitted trend in the hydrodynamic state variables and predict the change in performance of the ships over time through several propeller and hull cleaning events. The predicted change is performance is compared with the corresponding values obtained from the fouling friction coefficient (ΔC_F). Finally, the evolution of calm-water speed-power curve over time for the given ships is predicted.

The following section describes the ML methods used here to model the hydrodynamic state of a ship. Section 3 contains a detailed literature survey regarding marine fouling and the formulation of the fouling growth factor used to include the effect of fouling growth on the hull and propeller of the ships. The datasets used to calibrate and validate the ML models are presented in section 4. Lastly, sections 5, 6 and 7 presents the final results, conclusion and possible future work, respectively.

2. Machine Learning (ML)

Machine-learning (ML) is a broad subject involving design and operations of a diverse set of algorithms based on statistical methods. The main purpose of a statistical model is to draw inference, i.e., trying to establish the relationship between different variables, thereby helping physics establish or verify empirical relationships. ML is based on the same principle, but it serves a different purpose. ML models are designed with focus on predictive capabilities. In order to improve the predictive capabilities of ML models, simple and interpretable statistical models are transformed into highly complex and esoteric algorithms, like neural networks. With this adaptation, some ML models becomes more obscure (leading to the creation of so-called 'black-box' models), but it should be noted that ML also contains a substantial number of transparent and interpretable algorithms. These transparent algorithms can be used to solve a wide range of problems, but the simplicity of these transparent algorithms sometimes cannot compete with the complex algorithms due the complex nature of the problem-at-hand. Thus, it should be the role of the user to find a balance between interpretability and performance while doing method selection for a complex problem. In view of above, the current work presents three different ML models with varying complexity, interpretability and performance.

2.1. Regression Modeling: Method & Variable Selection

Regression modeling is a statistics-based technique mainly used for inference and prediction. In other words, it is used to estimate the relationship between the target and input variable(s). It can thereafter be used to predict the target variable(s) from the input variable(s). One of the simplest cases of regression modeling is linear regression between a regressor (or input variable) and a regressand (or target variable). In such a simple case, it is possible to just plot the regressand against the regressor to ensure that there exists a good linear correlation between them. The performance of the regression model depends on how strong is this correlation.

In some cases, it is possible that the variation in the regressand(s) cannot be completely explained by the variation in the regressor(s), i.e., the given regressand(s) may also be dependent on some other unidentified regressor(s). Thus, the predictive performance of any regression model at least depends on the following two factors: (a) Correlation between the regressands and regressors; (b) The amount of variance in the regressands explained by the regressors. Further, it is naturally understandable that including an uncorrelated variable as an additional regressor cannot increase the model performance, rather in some cases, it may unnecessarily increase the model size and, therefore, the required computational time. Thus, variable selection is an important step in regression modeling. This is here achieved by Principal Component Analysis (PCA) (as demonstrated by Gupta et al. (2019)).

PCA is a very powerful statistical method which can be used to fulfill several different purposes at the same time. In other words, PCA can be used as a one-stop shop for basic statistical analysis. One of the biggest advantage of PCA is that it is a completely transparent and interpretable ML method. Moreover, it can be further extended to a multivariate linear regression model, known as Principal Component Regression (PCR) (Jolliffe (2002)). PCR is different from ordinary least squares (OLS) linear regression as it, first, factorizes the regressor (or input) matrix into Principal Components (PCs), and then, uses only the first few significant PCs to carry-out the least squares regression. Thus, the PCR may produce better results as it reduces the noise in the regressors, by way of filtering-out the last few insignificant PCs, and the fact that the PCs are orthogonal to each other eliminates the problem of multicollinearity

(well-known in the case of OLS regression). It should also be noted that PCR with maximum possible PCs (equal to the rank of regressor matrix) is exactly same as the OLS linear regression.

As mentioned above, PCR is a linear regression method, but it is well-known from our domain knowledge that the problem of ship propulsion is non-linear in nature. Moreover, one of the short comings of PCR is that the PC factorization of the regressor matrix is done independently from the regressands. Therefore, the sequence of PCs produced by the factorization of the regressor matrix is not always in the desired order of diminishing correlation with the regressands (Martens and Martens (2001)). This is generally resolved using a slightly modified method known as Partial Least Squares Regression (PLSR). On the other hand, to handle the non-linearities, some non-linear transformations can be used, thereby converting a non-linear problem into a linear one, and transforming PCR and PLSR into non-linear PCR (NL-PCR) and non-linear PLSR (NL-PLSR), respectively. In order to achieve the best possible results using such a method the user must be able to model all the non-linear dependencies. This is sometimes not feasible due to the complexity of the problem. Alternatively, it is possible to use a more complex non-linear model like artificial neural network (ANN) in order to better model the non-linear nature of the problem.

Considering the above, the following three supervised ML algorithms are used to create statistics-based regression models for the current work: (a) Principal Component Regression (PCR); (b) Partial Least Squares Regression (PLSR); (c) Probabilistic artificial neural network (Probabilistic ANN).

2.2. Principal Component Regression (PCR)

PCR is a linear regression model, based-on Principal Component Analysis (PCA), in which the regressors (or input variables) are the first few significant Principal Components (PCs). The mean-centered and standardized input data matrix (X) is, first, factorized using PCA as per the following equation:

$$\mathbf{X}^{m \times n} = \mathbf{T}_A^{m \times A} \cdot \mathbf{P}_A'^{A \times n} + \mathbf{E}_A^{m \times n} \tag{1}$$

Where $\mathbf{T}_A$ is PC scores' matrix and $\mathbf{P}_A$ is PC loadings' matrix with each column corresponding to a PC, and $\mathbf{E}_A$ is the residual matrix. Superscripts represent the dimensions of the matrices, and $\mathbf{P}_A'$ represents the transpose of $\mathbf{P}_A$. A is the model dimensionality or number of PCs. Further, the target variables are regressed using a linear regression model on the selected set of PC scores (T_A) as follows:

$$\mathbf{Y}^{m \times k} = \mathbf{T}_A^{m \times A} \cdot \mathbf{B}^{A \times k} + \mathbf{e}^{m \times k} \tag{2}$$

Where $\mathbf{Y}$ is the target matrix with k target variables, $\mathbf{B}$ is the regression coefficient matrix and $\mathbf{e}$ is the regression residual matrix. Ridge regression with built-in cross-validation (*RidgeCV* from *Scikit-learn* in python (Pedregosa et al. (2011))) is used here for linear regression. Finally, to account for the non-linearities, additional variables are appended to the input (X) and target (Y) matrices after applying simple non-linear transformations on one original variable at a time. The PCR model enhanced with these non-linear transformations is further referred to as NL-PCR.

2.3. Partial Least Squares Regression (PLSR)

PLSR is also a linear regression model based on the similar principle as PCR. Like PCR, it involves 2 steps: (1) Establishing a score matrix (T_A); (2) Regressing Y on T_A. But, in PLSR, T_A is derived from both the regressor (X) and regressand (Y), and it is done in a manner such that t_a vectors (comprising T_A) are produced in the desired order of diminishing correlation with the regressands (Y). Here, a simple iterative algorithm based on NIPALS (Vandeginste et al. (1988)) is carried-out as follows:

$$w_a = \frac{E_{a-1}' \cdot u_a}{||E_{a-1}' \cdot u_a||} \quad \text{and} \quad t_a = E_{a-1} \cdot w_a \tag{3}$$

$$q_a = \frac{u_a' \cdot t_a}{||u_a' \cdot t_a||} \quad \text{and} \quad u_a = F_{a-1} \cdot q_a \tag{4}$$

Where u_a is chosen as any one column of F_{a-1}, and E_{a-1} and F_{a-1} are X and Y residuals, respectively, obtained after extracting $(a-1)$ factors, therefore, $E_0 = X$ and $F_0 = Y$. The above steps are carried-out iteratively until t_a converges. The X loadings (p_a) are calculated by using the relation indicated in equation 1 as follows:

$$p_a = \frac{E_{a-1}' \cdot t_a}{||t_a' \cdot t_a||} \tag{5}$$

Further, X and Y residuals are calculated as follows, and the process is repeated to extract the next set of scores and loadings.

$$E_a = E_{a-1} - t_a . p'_a \quad \text{and} \quad F_a = F_{a-1} - u_a . q'_a \tag{6}$$

For the current work, the PLSR model is created using the *PLSRegression* function defined by *Scikit-learn* in python (Pedregosa et al. (2011)), and the non-linear variables are introduced in the same manner as explained above for the PCR model. The PLSR model enhanced with the non-linear transformations is further referred to as NL-PLSR.

2.4. Artificial Neural Network (ANN)

Originally inspired by the human brain, neural networks have proven to be excellent estimators for both classification and regression problems. Neural networks have out-competed many traditional signal processing and pattern recognition methods, becoming state-of-the-art in research fields, such as natural language processing (NLP) and computer vision (Schmidhuber (2015)). The simplest form of a neural network dates back to 1960s, called a multilayer perceptron (MLP) or a deep feed forward network (Schmidhuber (2015)). A MLP takes an input ($\mathbf{X}$) and maps it to an output ($\mathbf{Y}$) as $\mathbf{Y} = f(\mathbf{X}; \theta)$, where θ denotes the network parameters. The mapping can be seen as L nonlinear mappings applied in succession: $f(\mathbf{X}) = f^L(f^{L-1}(...f^2(f^1(\mathbf{X}))))$. Each non-linear mapping is referred to as a layer, and the number of layers is known as the depth of the network.

$$\mathbf{l}^i = \sigma^i(\mathbf{W}^i \cdot \mathbf{l}^{i-1} + \mathbf{b}^i) \tag{7}$$

The output of a layer, $\mathbf{l}^i = f^i(f^{i-1}(...f^2(f^1(\mathbf{X}))))$, is computed as shown in equation 7. First, the output of the previous layer is multiplied with a weight matrix ($\mathbf{W}^i$), and then, a bias vector ($\mathbf{b}^i$) is added to the product. The resulting vector is then fed to an activation function (σ^i) which is typically of the type sigmoid, ReLU or tanh (Goodfellow et al. (2016)). The neural network can be visualized as a graph where each node, called a neuron, outputs an element of a layer vector ($\mathbf{l}^i$). The first column of neurons simply output the value of the input vector ($\mathbf{X}$). The edges represent multiplication of the output of a neuron with an element of the weight matrix of the next layer. The products going into a neuron are summed, a bias is added and the activation function is applied. Analogous to multivariate linear regression, the model is trained to obtain an estimate of the set of model parameters (weights and biases), $\theta = [\mathbf{W}^1 \quad \mathbf{W}^2 \quad \cdots \quad \mathbf{W}^n \quad \mathbf{b}^1 \quad \cdots \quad \mathbf{b}^n]^T$, which minimizes the cost function, considering the hypothesis $\mathbf{Y} = f(\mathbf{X}; \theta)$. The most commonly used cost function is Mean Squared Error (MSE) with L_2 regularization.

$$\mathbf{J}(\theta) = \frac{1}{m}(\hat{\mathbf{Y}} - \mathbf{Y})^T(\hat{\mathbf{Y}} - \mathbf{Y}) + \lambda \sum_{i=1}^{L}(||\mathbf{W}^i||^2 + ||\mathbf{b}^i||^2) \tag{8}$$

Where m is the number of samples in $\mathbf{Y}$, $\hat{\mathbf{Y}}$ is the model prediction for $\mathbf{Y}$, and λ is the weight decay or regularization parameter.

2.4.1. Probabilistic ANN: Dropout as a Bayesian Approximation

It is well-known that a deep neural network is susceptible to over-fitting. Applying additional dropout layers while training the model helps avoid this problem (Srivastava et al. (2014)). Dropout refers to dropping-out units in a neural network. The units to be dropped-out are chosen randomly with a probability, known as the dropout probability (p_{drop}). This is mathematically equivalent to multiplying a vector, obtained from a Bernoulli distribution with success rate $(1 - p_{\text{drop}})$, with the selected weight matrix ($\mathbf{W}^i$). Thus, the dropped-out units are not considered during a particular forward and backward pass. Once the model is trained, the dropout layers are removed, and the model can be used to obtain point predictions, hereafter referred to as *Standard dropout* predictions.

The reliability of predictions from a deep neural network model is also a well debated topic. Two main reasons for this debate are: (1) The esoteric or black-box nature of the model; (2) The lack of information about the uncertainty in the predictions. A statistics-based Bayesian model uses probability to represent all uncertainty within the model. In other words, a Bayesian model also estimates the uncertainty (or confidence) with which the model is making a prediction, thus, providing a better way for the end user to gauge the reliability of results. Gal and Ghahramani (2016) claimed that a neural network with a dropout layer applied before each network layer, named as dropout neural network, can be treated as a Bayesian approximation for the probabilistic deep Gaussian process (Damianou and Lawrence (2012)).

115

The dropout neural network used for the current work is based on the framework developed by Gal and Ghahramani (2016). The model uncertainty is obtained by performing T stochastic forward passes through the already-trained network (with dropout layers still active) and averaging the results. Thus, calculating a Monte Carlo mean of the predictions (hereafter referred to as *MC dropout* predictions), along with an approximate predictive probability distribution.

$$\hat{\mathbf{Y}} = \frac{1}{T} \sum_{t=1}^{T} \hat{\mathbf{Y}}_t(\mathbf{X}, \mathbf{W}_t^1, \mathbf{W}_t^2, ..., \mathbf{W}_t^L) \tag{9}$$

The approximate predictive distribution can be further used to calculate the predictive variance. A small predictive variance corresponds to a strong or high confidence prediction, whereas a large variance represents high uncertainty in the model prediction.

2.5. Model selection

In case of NL-PCR and NL-PLSR models, it is crucial to decide the model dimensionality, i.e., the number of Principal Components (PCs, for NL-PCR) or factors (for NL-PLSR) included in the regression model. In this case, the model selection is done by "sequential mode" cross-validation (CV) scheme, proposed by Wold et al. (2001). Here, first, the dataset is divided into 20 slices or continuous folds, then, 20 CV models are trained with leave-one-fold-out scheme. The prediction residuals are calculated for each CV model only using the corresponding left-out fold. These prediction residuals from all the CV models are, then, collected to calculate the prediction residual sum of squares (PRESS), which represents the predictive ability of the model.

Parallelly, a fitted residual sum of squares (SS) is calculated for each model dimensionality using the full model (trained on the full dataset). Finally, the ratio $\text{PRESS}_a/\text{SS}_{a-1}$ is calculated of each model complexity (a) and a component or factor is considered significant if this ratio is smaller than around 0.9 for at least one of the target variables. Once a non-significant component or factor is observed, all the further PCs or factors are dropped, and the model dimensionality is set to $a-1$. It should be noted that, in the ratio $\text{PRESS}_a/\text{SS}_{a-1}$, PRESS_a is calculated for the model with 'a' number of PCs or factors, but SS_{a-1} is calculated for the model with '$a-1$' number of PCs or factors.

Model selection in the case of artificial neural networks (ANN) is a tedious process which involves searching for an optimum model in a multi-dimensional hyper-parameter space. In other words, it is required to find a set of hyper-parameter values which produces the optimum model. Table 1 shows the list of hyper-parameters selected here for the probabilistic ANN model. The model precision (τ), length scale (l) and dropout probability (p_{drop}) are further used to calculate the regularization parameter (λ) as follows (Gal and Ghahramani (2016)):

$$\lambda = \frac{l^2(1 - p_{\text{drop}})}{2n\tau} \tag{10}$$

where n is the number of training samples. As indicated above, some of these hyper-parameters are obtained by searching for an optimum model. Therefore, the last 4 hyper-parameters (in table 1), from 8 to 11, are obtained after testing several model architectures over a grid of length scale and dropout probability (further explained in section 5.2). The remaining hyper-parameters are assumed to be constant.

The optimization algorithm, loss function and activation function are set to stochastic gradient descent (Adam), MSE (Mean Squared Error) and ReLU (Rectified Linear Unit), respectively, as generally recommended for ANN models for regression-based problems (Goodfellow et al. (2016)). Adam is a highly efficient optimization algorithm (Ruder (2016)) used to adaptively vary the learning rate over the epochs to ensure fast and smooth convergence. The two most popular activation functions used for regression-based problems are hyperbolic tangent (tanh) and ReLU. ReLU is known to have several advantages over the other, like avoiding the problem of vanishing gradients (Glorot et al. (2011)).

3. Marine Fouling

As discussed by Yebra et al. (2004), the growth rate of biofouling on marine structures is dependent on many factors like water temperature, salinity, solar radiation, water depth, nutrients, etc. Additionally, the ability of these organisms to remain attached to the hull depends on the shear force acting on the hull (and, consequently, the ship speed) and the type of anti-fouling coating, as demonstrated by Fabbri et al. (2018) in an experimental study. Unfortunately, with the

116

Table 1
Hyper-parameters for the probabilistic ANN model.

Sl. No.	Hyper-parameter	Value
1	Optimization algorithm	Stochastic gradient descent (Adam)
2	Loss function	Mean Squared Error (MSE)
3	Activation function	Rectified Linear Unit (ReLU)
4	Batch size	5% of the training samples
5	No. of epochs	2000
6	No. of stochastic forward passes (T)	10,000
7	Model precision (τ)	1.0
8	Length scale (l)	10.0
9	Dropout probability (p_{drop})	0.2
10	No. of hidden layers	1
11	No. of neurons in hidden layer	50

current state of technological advancements, it is not practical to have continuous visual monitoring of the hull surface to determine the extent of marine growth on the ship[1]. Therefore, the extent of fouling growth is here estimated using the in-service data recorded onboard the ship.

Based on the final objective, most of the prominent research in this field can be broadly categorized into following two types of methods: (i) Detection of marine fouling; (ii) Finding trend in ship's performance. The first type of methods includes the use of anomaly detection methods (Coraddu et al. (2019a); Logan (2012)). These methods are, unfortunately, only demonstrated to differentiate between the clean hull and a fouled one. They seem to be unable to quantify the extent of fouling growth. The second type of methods includes studies where researchers observed a trend in ship performance varying over time. In these methods, the authors used one or several of the following parameters, representing the performance of the ship: (a) Increased power demand (Walker and Atkins (2007); Ejdfors (2019)); (b) Speed-loss (Koboević et al. (2019); Coraddu et al. (2019b)); (c) Admiralty coefficient (Ejdfors (2019)); (d) Resistance or resistance coefficient (Munk (2016); Foteinos et al. (2017); Ejdfors (2019)).

Ejdfors (2019) presented a comparison between three of the above mentioned alternatives (a, c and d) and concluded that using the admiralty coefficient produces the most logically-correct results[2]. Ejdfors (2019) assumed the admiralty coefficient to be constant for a given ship over a range of speed-power-displacement, therefore, it could be perceived as a summarized calm-water speed-power curve for a given displacement. Gupta et al. (2021) analysed this assumption and concluded that this assumption only holds good for a generalized form of admiralty coefficient as the speed and displacement exponents in the original admiralty coefficient are not valid for modern hull forms. Gupta et al. (2021), therefore, proposed to use the generalized admiralty coefficient ($\Delta^m V^n / P_s$) as the statistical hydrodynamic performance indicator for a ship, with displacement and speed exponents, i.e., m and n, respectively, obtained statistical using the in-service data recorded onboard the ship. The current work uses the generalized admiralty coefficient to formulate the variable used to account for the growth of marine fouling on the ships over time.

3.1. Statistical Modeling of Marine Fouling: Fouling Growth Factor

In order to account for the change in hydrodynamic performance of a ship due to fouling growth in a data-driven model, it is required to statistically model the extent of fouling growth on the ship's hull and propeller over time. It may be possible to do it using the factors affecting the fouling growth (listed by Yebra et al. (2004)) but that would require observing and recording all these factors over the data recording duration to a good enough accuracy. Moreover, a well-established formulation may be required to calculate the extent of fouling growth at any point of time based on these factors. In the absence of any such information, it may be possible to fit a simpler expression which may be able to account for fouling growth on ship's hull and propeller over time.

Malone et al. (1981) presented a computer program for Hull Performance Assessment Model (HPAM) which can be used to compare and optimize hull surface management practices. The HPAM evaluates the performance of a ship over time after taking into account the operational variation in the ship's resistance due to environmental loads and

---

[1]In future, it is possible to produce an AI-assisted drone or AUV which can obtain unbiased continuous estimates of fouling growth, say, on a scale something similar to NSTM rating (Schultz (2007)), as proposed in INCASS project by Lazakis et al. (2016).

[2]At this point, the authors would like to remind the reader that with this type of analysis there is no direct way to evaluate which method is most accurate as there is no direct way to continuously monitor and measure the actual phenomenon.

hull roughness. Here, Malone et al. (1981) estimated the total hull roughness as a sum of 4 contributing components: steel plate roughness, coating system roughness, corrosion roughness, and fouling roughness. The hull roughness due to each of these components is quantified in terms of a mean apparent amplitude (MAA), representing the average peak-to-trough vertical distance in the given area of hull surface.

Malone et al. (1981) estimated the hull fouling roughness based on the effective life of antifouling coating, ship's static time in port and port fouling severities. It was assumed that no fouling occurs while the ship is underway (over 3 knots) based on the test results from rotating drums immersed in salt water in several different port environments[3]. Therefore, the change in hull roughness due to marine fouling or hull fouling roughness was estimated as a function of cumulative static time the ship is subjected to a given in-port fouling severity. In the current approach, fouling roughness is represented by a fouling growth factor (FGF) calculated as the cumulative static time (t_{static}) during which the ship's speed is recorded to be less than 3 knots multiplied by a fouling growth rate (FGR) as follows:

$$\text{FGF} = \sum_i t_{static,i}.\text{FGR}_i \tag{11}$$

The fouling growth rate (FGR) is estimated as the trend in generalized admiralty coefficient (as demonstrated by Gupta et al. (2021)). It should be noted that two variables are calculated here to account for the fouling growth on the hull and propeller assuming the same fouling growth rate (FGR), and each time the hull or the propeller is cleaned the corresponding FGF is reset to zero, as shown later in figure 4. The total fouling growth factor (FGF), used to calibrate the models, is calculated as the sum of hull and propeller FGFs.

4. Data

The in-service data used for the current work is obtained from 2 sister ships. One of the sister ships, further mentioned as the original ship, is the same ship presented by Gupta et al. (2019) and Gupta et al. (2021), but the dataset from the original ship, used here, is recorded over a slightly longer duration (3 years). The dataset from the sister ship, further referred to as the sister ship, is recorded over a duration of about 2.5 years. The data used to calibrate the machine-learning models is an assimilation of in-service measurement data recorded onboard a ship and weather hindcast data.

4.1. Ship Data

The ships are $\sim 200m$ long general cargo ship with installed capacity of approximately $10MW$ (MCR[4]) supplied with Marorka Online[5] web application. The original and sister ship datasets are recorded over a duration of 3 years and about 2.5 years, respectively. In case of both the ships, each sample is obtained by averaging over a period of 15 minutes. Table 2 presents the categorized list of all the ship data variables recorded onboard the ships.

4.2. Weather Hindcast Data

The weather hindcast data is obtained from European Centre for Medium-Range Weather Forecast (ECMWF) (Copernicus Climate Change Service (C3S) (2017)), Hybrid Coordinate Ocean Model (HYCOM) (Chassignet et al. (2007)) and Copernicus Marine Environment Monitoring Service (CMEMS) (Global Monitoring and Forecasting Center (2018)). The ECMWF data, used for the current analysis, is obtained from ERA5 HRES (High Resolution) climate reanalysis dataset. The spatial resolution of ERA5 HRES is 0.25°, and the temporal resolution is 1 hour. ECMWF dataset is used to obtain northward and eastward wind speeds 10 m above the sea surface, significant wave height, mean wave period and mean wave direction. HYCOM dataset, used here, has a spatial resolution of 1/12° with a sampling frequency of 1 measurement per day, and CMEMS dataset has the same spatial resolution but a sampling frequency of 1 measurement per hour. HYCOM and CMEMS datasets are used here to obtain northward and eastward sea water speed for the original ship and sister ship, respectively. The weather data variables are linearly interpolated in space and time to ship's location using the available navigation data.

4.3. Data Exploration & Pre-processing

Figure 1 presents the speed-through-water (log speed) vs shaft power from the raw data recorded over a period of 3 years onboard the original ship and about 2.5 years onboard the sister ship. The design speed of both the ships is 15.5

---

[3]It should be noted that some fouling may still occurs in case of full hull form ships (like tankers) sailing at slow speed but greater than 3 knots as the local flow speed, past certain parts of the hull, can be less than 3 knots (Malone et al. (1981)).

[4]Maximum Continuous Rating of the main engine.

[5]www.marorka.com

Table 2
Categorized list of variables recorded onboard the ships. Only 'Navigation', 'Propulsion System' & 'Environment' variables are used for the current analysis. *Abbreviations:* IMO = International Maritime Organization; COG = Center of Gravity; Aux. = Auxiliary; DG = Diesel Generator (for auxiliary power systems); ME = Main Engine (for propulsion system); GPS = Global Positioning System. * marked variables are only recorded for the original ship, whereas ** marked variables are only recorded for the sister ship.

Ship Identity	Navigation	Auxiliary Power System	Propulsion System	Environment
Ship Name	Latitude	Aux. Consumed	State	Relative Wind Speed
IMO Number	Longitude	Aux. Electrical Power Output	ME Load Measured	Relative Wind Direction
	Gyro Heading	DG1 Power	Shaft Power	Sea Depth*
	COG Heading	DG2 Power	Shaft rpm	Under Keel Clearance**
		DG3 Power	Shaft Torque	
			ME Consumed	
			Draft Fore	
			Draft Aft	
			GPS Speed	
			Log Speed	
			Cargo Weight	

(a) Original ship.   (b) Sister ship.

Figure 1: Measured speed-through-water (or log speed) vs measured shaft power obtained from both the ships. The subplot on the left shows the raw data, and the subplot on the right shows the samples remaining after data cleaning. The numbers shown in curly brackets ({}) in the title of each subplot is the number of samples in the corresponding subplot.

knots. In comparison to a typical calm-water curve, the raw data subplots (in figure 1) shows a good variation in power for a fixed speed as expected due variation in loading conditions as well as environmental loads. But nevertheless, this does not explain the samples with quite high shaft power at almost zero speed-through-water. A closer analysis reveals that such samples are obtained due to non-zero accelerations, i.e., periods when the ship is accelerating or decelerating.

Although it is possible to use these samples, but only after including a variable representing the rpm increase (or decrease) by the ship master, it is decided to remove these samples for the current work. After removing all the samples associated with non-zero accelerations (further referred to as unsteady samples), the ship can be assumed to be in a quasi-steady state at each observed sample. A quasi-steady filter, explained by Gupta et al. (2021), is applied to the shaft rpm and GPS speed time series to filter out these unsteady samples.
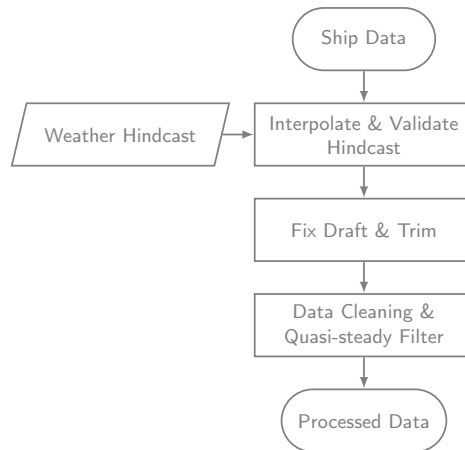
Figure 2: Main data pre-processing and validation steps.

Figure 2 shows the main steps of data pre-processing and validation. Here, the draft and trim measurements are corrected for Venturi effect, as explained by Gupta et al. (2021), and the hindcast validation is performed as explained in the following section. The processed data is further used to calibrate, validate and test the machine-learning models.

4.4. Data Validation

Speed-through-water or speed-over-ground? It is often a question about whether to use speed-though-water (log speed) or speed-over-ground (GPS speed) for an analysis. It is well-known that the GPS speed measurements are more reliable, as the GPS sensors are very accurate these days, but the log speed is more relevant for a hydrodynamic analysis, as it represents the actual speed of the ship through the surrounding water which in-turn is directly correlated with the effective power at the propeller. The difference between the GPS and log speed is caused due to the longitudinal water current speed. In the absence of any water current, the GPS and log speeds are the same. The given ships are equipped with Doppler sonar sensors for log speed measurements. The Doppler-based log speed measurements may not be accurate enough to carry-out a hydrodynamic analysis, as pointed out by Dalheim and Steen (2021). Thus, it may be useful to include GPS speed measurements in the analysis along with the longitudinal water current speed from the hindcast.

Weather hindcast data. While using an external data source like hindcast, it is important to validate the interpolated data from the external source with the onboard recorded in-service data. Several such validations are carried-out in the current case as some of these hindcast variables are also recorded directly or in-directly onboard the ship. All the ships are generally equipped with anemometers, therefore, it is possible to validate the wind speed and direction obtained from the hindcast with the onboard measurements. Similarly, as mentioned above, the difference between the GPS and log speed (recorded onboard the ship) is the longitudinal water current speed, which is validated against the corresponding values obtained using the hindcast.

5. RESULTS

This section presents the results obtained from the three regression models, NL-PCR, NL-PLSR and Probabilistic ANN. Table 3 shows the input and target variables used to calibrate these regression models. The data used to calibrate these models is obtained from two sister ship, as presented in section 4. The datasets from both the ships is split into training (80%) and test (20%) datasets to check for model performance. In case of ANN, 10% of the training dataset is used for validation during model calibration. Further, the calibrated machine-learning models are used to predict the change in performance of both the ships over time through several propeller and hull cleaning events. The predicted change in performance is, finally, compared with the change in performance estimated using the fouling

Table 3

Input and target variables used by the regression models, i.e., NL-PCR, NL-PLSR and Probabilistic ANN. * marked variables are only included in NL-PCR and NL-PLSR models.

Sl. No.	Category	Variables
1		Shaft rpm, Mean draft, Trim-by-aft
2		Long. wind speed, Trans. wind speed, Long. current speed
3	Input	Significant wave height, Relative mean wave direction, Mean wave period
4		Fouling growth factor
5*		Shaft rpm^3, Mean draft$^{1/2}$, Significant wave height^2
6	Target	Shaft power, GPS speed, Log speed
7*		GPS speed^3, Log speed^3

friction coefficient (ΔC_F), calculated using the in-service data. The detailed procedure for calculating ΔC_F is presented in appendix B.

5.1. Fouling Growth Factor (FGF)

As mentioned in section 3.1, the fouling growth factor (FGF), included as an input variable (shown in table 3) to represent the added resistance due to fouling growth on the hull and propeller of the ship, is calculated as the summation of two fouling growth factors, hull and propeller FGFs. The hull and propeller FGFs are calculated according to equation 11, where the fouling growth rate (FGR) is estimated using the trends in generalized admiralty coefficient, refer Gupta et al. (2021) regarding the detailed procedure for calculating the trends in the generalized admiralty coefficient. Appendix A presents the validation of the trends obtained using the generalized admiralty coefficient for both the ships by comparing them to the trends obtained from the traditional method, i.e., the fouling friction coefficient (ΔC_F).

Following the method given by Gupta et al. (2021), first, the generalized admiralty coefficient ($\Delta^m V^n / P_s$) is obtained for the ships by statistically fitting the displacement and speed exponents (i.e., m and n, respectively) to the near-calm-water filtered and corrected in-service data, and then, the trend lines are fitted between each propeller and/or hull cleaning event (as shown in figure 3). It should be noted that each data point in figure 3 represents the mean of all the generalized admiralty coefficient values calculated for an individual voyage (or part of a voyage), obtained at the same ship static time. Therefore, it should not be surprising that some of the trends observed here are opposite to the expectations, as the data is noisy and the methods used to correct the filtered data for near-calm-water conditions, i.e., added wind and wave resistance estimation methods, are known to have some uncertainty. Nevertheless, for calculation purpose, the abnormal trends observed in leg 1 and 6 for the original ship, and leg 2 and 6 for the sister ship (refer figure 3) were replaced by the least growth trend (observed in leg 7 for the original ship and leg 3 for the sister ship) so that the resulting FGFs remain logical.

(a) Original ship.

(b) Sister ship.
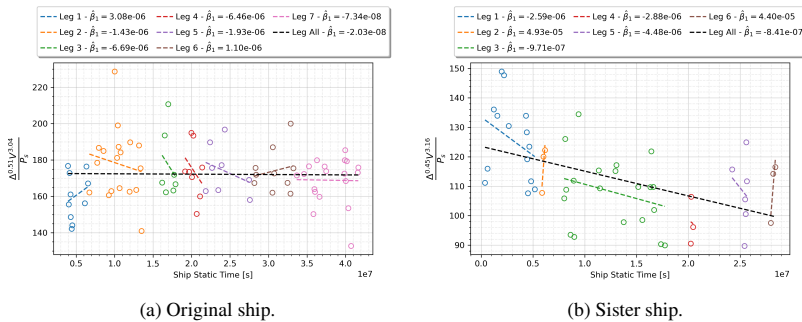
Figure 3: Trends in generalized admiralty coefficient used to estimate the fouling growth factors.

Figure 4 shows the hull and propeller FGFs calculated for the given time-series. The propeller of both the ships was cleaned several times during the data recording duration (marked by red vertical lines in figure 4), therefore, the

(a) Original ship.

(b) Sister ship.
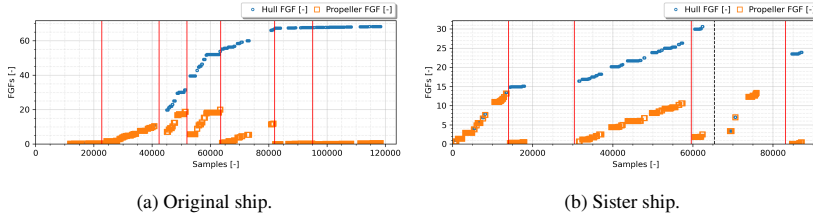
Figure 4: Fouling growth factors for hull and propeller calculated using equation 11. The red and dashed black vertical lines mark the propeller and hull cleaning events, respectively, occurring during the recorded time series.

Table 4
Model dimensionality (number of PCs or factors) for PCR and PLSR models, obtained from the cross-validation results (shown in figure 5 for the sister ship).

	NL-PCR	NL-PLSR
Original Ship	5	4
Sister Ship	8	3

propeller FGF is reset to zero just after each of these cleaning activities. Moreover, the hull was never cleaned for the original ship, but it was cleaned once for the sister ship (marked by the dashed black vertical line in figure 4b) during the data recording duration. Therefore, the hull FGF remains monotonically increasing for the original ship but is reset to zero once for the sister ship.

5.2. Regression Modeling

Model selection. For NL-PCR and NL-PLSR models, the model selection is done using the "sequential mode" cross-validation (CV), as explained in section 2.5. Figure 5 shows the cross-validation results for the sister ship. From the results of CV, the model dimensionalities, i.e., the number of Principal Components (PCs) in NL-PCR or factors in NL-PLSR, are obtained as follows (also shown in table 4): (a) Original ship: 5 PCs for NL-PCR and 4 factors for NL-PLSR; (b) Sister ship: 8 PCs for NL-PCR and 3 factors for NL-PLSR.
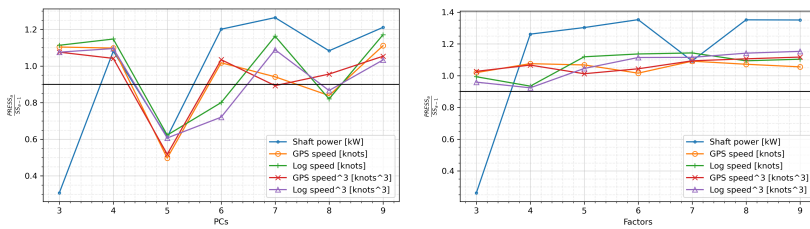
Figure 5: NL-PCR and NL-PLSR model cross-validation results for the sister ship.

For ANN, the model selection is done keeping in mind the following factors: a) Validation loss; b) Difference between the training and validation loss; c) Number of model parameters (i.e., the size of the network). In general practice, the model with minimum validation loss is chosen, as it indicates a good predictive performance, but the difference between the training and validation loss is also important as it indicates if the model is underfitted or overfitted. A good model should present comparable performance on both the training and validation datasets. Finally, the size of the network (or number of model parameters) represents the model complexity and computational resources required to calibrate the model.

Comparing 12 different network architectures with up to 5 hidden layers and 100 neurons (in a hidden layer) over a grid of dropout probability and model length scale, the model with just 1 hidden layer containing 50 neurons satisfied

all the three above mentioned conditions as well as it performed very well on the datasets from both the ships. Thus, the final results here are presented based on a single hidden layer ANN model containing 50 neurons with 0.2 dropout probability and 10.0 length scale (as presented in table 1).

Training, validation and test split. In all the cases, 80% of the data time-series is used for training the models, and 20% of the time-series is used to test the predictive performance of the models and, therefore, check for model overfitting and generalization. In case of ANN, as an additional check for model overfitting, 10% of the training set is used for validation while training the model. Although the 80/20 split, used here, is quite popular in machine-learning domain, there is no universal rule to decide the data splitting ratio. Some researchers use the 80/20 split based on the Pareto principle, which says that roughly 80% of consequences come from 20% of causes. Another way to decide the splitting ratio is using the scaling law introduced by Guyon (1997), but the scaling law does not seem appropriate to some researchers as it defines the splitting ratio based on the number of input (or independent) features instead of the number of samples and the quality of data. It seems more appropriate to split the data in such a manner that the samples in the training set contains all the important patters which should be learned by the model, but it should not result in overfitting the model. Thus, as long as the training set contains enough samples to confidently estimate all the model parameters (weights and biases) and satisfy the above criterion, the exact ratio would not matter.

Furthermore, it is generally recommended to obtain the train-validation-test split using random picking, but in the case of propulsion data from cargo ships, it should be noted that this strategy would most probably not be satisfactory. Cargo ships are generally propelled at an unchanged rpm or speed, in slowly varying weather conditions, for substantial durations of time, thereby resulting in consecutive replicated data samples in the time-series. A random selection of validation and test sets would produce a vast majority of these replicated samples which are already present in the training set. The validation and test datasets are required to check for model overfitting and generalization. Therefore, it is required for validation and test sets to contain samples which are not replicated from the training set. Rather, the validation and test sets should contain a majority of new untouched samples which can check if the model has properly generalized over the whole range of all the input variables. Thus, the train-validation-test split is done here by slicing-out sections of the time-series.

The current work aims to predict the change in performance of the ships through each propeller and hull cleaning event. Therefore, the training data should contain enough samples before and after each of these cleaning events in order to experience the change in performance through the corresponding event. Thus, the data splitting is done keeping in mind the occurrence of these cleaning events with respect to the time-series. Figure 6 presents the data division for both the ship used to calibrate and test the regression models. For the original ship, one-third of the test data is taken from the starting of the time-series and the remaining two-third is taken from the end of the time-series. For the sister ship, one-fourth of the test data is taken from the starting and end of the time-series, and the remaining half of the test data is taken from the middle of the time-series. The validation data (only used in case of the ANN model) is taken from the middle of the training data time-series in both the cases.
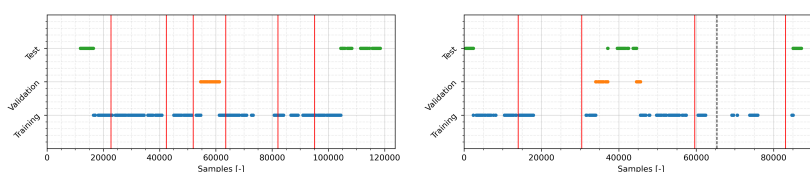
Figure 6: Data division used to calibrate and test the regression models for the original ship (left) and sister ship (right). Validation is only done for the ANN model, therefore, the validation set remained as a part of the training set in the case of NL-PCR and NL-PLSR models. The red and dashed black vertical lines represents the propeller and hull cleaning events, respectively.

Model calibration and testing. All the regression models are calibrated using the data obtained from both the ships, presented in section 4. Table 3 presents the input and target variables used to calibrate the models. The goodness of fit is assessed using the following three well known parameters: MAE (Mean Absolute Error), RMSE (Root Mean Squared Error) and R2 (R-squared score or coefficient of determination). Table 5 shows the results for all three regression models. Figure 7 shows the calibration results for the shaft power variable using the NL-PLSR and ANN models for

123

Table 5

Calibration results for regression models for both the ships. The * marked target variables are the non-linear transformed variables (number 7 in table 3) used in NL-PCR and NL-PLSR models. The 'ANN (MC dropout)' column presents the results using the Monte Carlo dropout estimates from the probabilistic ANN, as explained in section 2.4.1.

Target Variable	NL-PCR			NL-PLSR			ANN			ANN (MC dropout)		
	MAE	RMSE	R2	MAE	RMSE	R2	MAE	RMSE	R2	MAE	RMSE	R2
Original Ship - Training												
Shaft power [kW]	245.81	311.06	0.95	258.99	337.34	0.94	144.45	194.62	0.98	144.46	194.64	0.98
GPS speed [knots]	0.61	0.83	0.78	0.48	0.66	0.86	0.39	0.53	0.91	0.39	0.53	0.91
Log speed [knots]	0.41	0.60	0.87	0.35	0.51	0.91	0.20	0.29	0.97	0.20	0.29	0.97
GPS speed* [knots]	0.63	1.08	0.62	0.54	1.22	0.52	-	-	-	-	-	-
Log speed* [knots]	0.45	1.08	0.59	0.39	1.15	0.54	-	-	-	-	-	-
Original Ship - Test												
Shaft power [kW]	298.64	367.74	0.83	273.94	350.76	0.84	250.35	314.45	0.88	250.37	314.46	0.88
GPS speed [knots]	0.48	0.63	0.81	0.42	0.56	0.85	0.39	0.52	0.87	0.39	0.52	0.87
Log speed [knots]	0.37	0.48	0.87	0.28	0.38	0.92	0.23	0.30	0.95	0.23	0.30	0.95
GPS speed* [knots]	0.51	0.66	0.79	0.43	0.59	0.84	-	-	-	-	-	-
Log speed* [knots]	0.38	0.50	0.87	0.29	0.40	0.91	-	-	-	-	-	-
Sister Ship - Training												
Shaft power [kW]	216.75	277.31	0.97	249.38	312.59	0.96	144.99	191.58	0.99	144.99	191.61	0.99
GPS speed [knots]	0.41	0.59	0.90	0.44	0.61	0.89	0.33	0.48	0.92	0.33	0.48	0.92
Log speed [knots]	0.35	0.53	0.91	0.41	0.59	0.89	0.23	0.36	0.95	0.23	0.36	0.95
GPS speed* [knots]	0.51	1.40	0.41	0.52	1.39	0.42	-	-	-	-	-	-
Log speed* [knots]	0.41	1.30	0.47	0.43	1.21	0.54	-	-	-	-	-	-
Sister Ship - Test												
Shaft power [kW]	293.80	365.69	0.91	313.48	376.62	0.90	211.19	269.22	0.95	211.18	269.20	0.95
GPS speed [knots]	0.57	0.76	0.81	0.56	0.76	0.81	0.50	0.66	0.86	0.50	0.66	0.86
Log speed [knots]	0.52	0.72	0.81	0.57	0.85	0.73	0.39	0.59	0.87	0.39	0.59	0.87
GPS speed* [knots]	0.70	1.53	0.21	0.68	1.47	0.27	-	-	-	-	-	-
Log speed* [knots]	0.58	1.42	0.26	0.55	0.87	0.72	-	-	-	-	-	-

the original ship. In all the cases, the ANN model presents the best performance, but the results from the NL-PCR and NL-PLSR models are not marginally different from the ANN model.

From table 5, it seems like the non-linear transformed target variables (* marked), used in NL-PCR and NL-PLSR models, do not fit well, but a closer look at the prediction plots (refer figure 8) indicates that the poor RMSE and R2 score for these variables is due to a very poor fit for small numerical value samples. This is due to the fact that the data is sparse for small ship speeds (as evident from figure 1), and the non-linear transformations used in the NL-PCR and NL-PLSR models are, in fact, approximations, causing a not so well fit in the data tails. Nevertheless, the non-linear transformed target variables seems to be fitting well enough in the high speed range.

5.3. Ship's Hydrodynamic Performance Trend

While doing machine-learning (ML), it is often considered a good practice to carry-out several generalization checks to understand the final state of the model. A ML model represents nothing but a mapping between the input and target variable space. Thus, it seems to be an interesting idea to question the calibrated model and understand the trends to which the model is fitted. The current section aims to use this idea in order to see the hydrodynamic performance trends learned by each of the currently used ML models.

Let us assume that the ships are being driven at a constant rpm, say, the NCR[6] rated rpm, in completely calm-water condition (no wind, wave and current loads) at a constant even draft (no trim) for the whole duration of the time-series. Now, it is first of all expected that the shaft power demand for the ships in the given condition would increase over time due to the growth of marine fouling. Further, it is expected that right after each cleaning event this power demand would suddenly drop. An opposite trend is expected from the ship speed. Here, both GPS and log speeds should give the same

---

[6]Normal Continuous Rating, i.e., the rpm at which the ship should to be normally driven during the service.
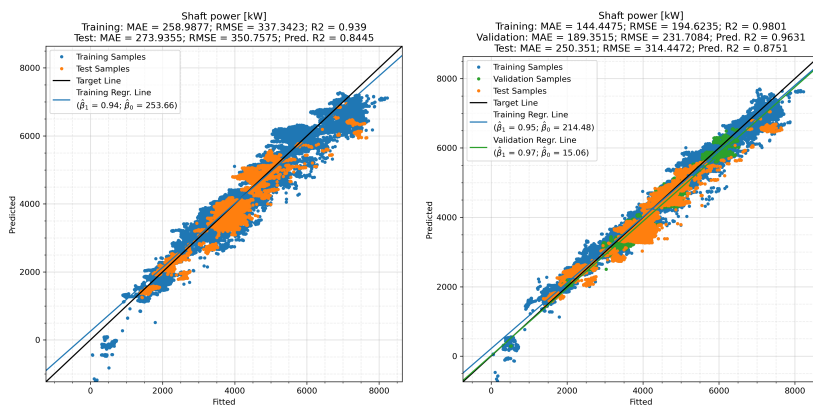
Figure 7: Shaft power calibration results using NL-PLSR (left) and ANN (right) models for the original ship.
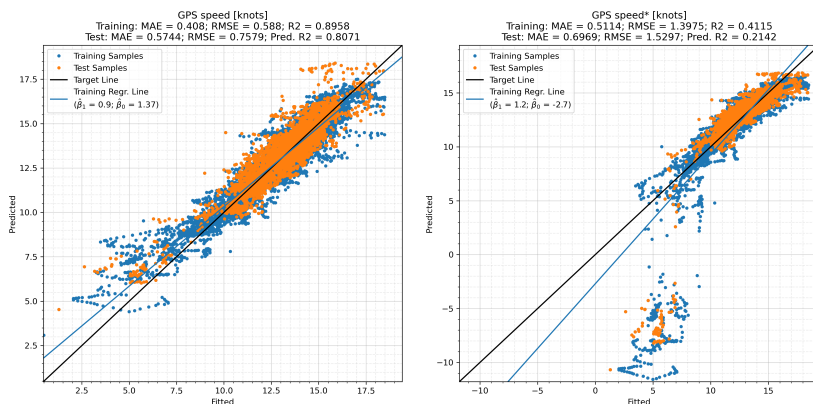
Figure 8: Calibration result plots for linear and non-linear GPS speed variables using NL-PCR model for the sister ship.

results as the water current is assumed to be absent. In order to check for these expected performance trends in the speed and power variables, an input data time-series, representing the assumed scenario, is fabricated and predictions are obtained from all the calibrated models.

Figure 9 presents the predicted performance trends for both the ships from NL-PCR and NL-PLSR models, and figure 10 presents the trends predicted by the ANN model. The red and dashed black vertical lines represent the propeller and hull cleaning events, respectively. In all the cases, the shaft power predictions shows the expected trend with a substantially big drop in power demand, i.e., a substantial hydrodynamic performance improvement, just after the hull cleaning event in the case of the sister ship. The GPS and log speeds also shows the expected trends but only in the case of the sister ship. For the original ship, the NL-PCR and ANN models did not predict the expected trend for the ship speed variables and rather shows the opposite trend indicating a drop in hydrodynamic performance after each cleaning event, but the NL-PLSR model shows the expected trend using the GPS speed variable.

5.4. Ship Performance Monitoring & Calm-Water Curves

The performance of a sea going ship is generally evaluated with respect to a reference point on its calm-water speed-power curve. For example, the drop in hydrodynamic performance of a ship has been reported either in terms

125
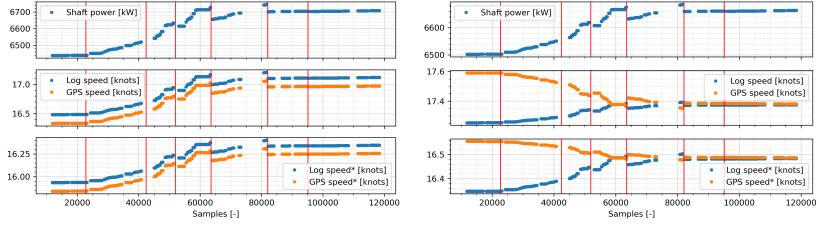
(a) Performance trends predicted by NL-PCR (left) and NL-PLSR (right) model for the original ship.
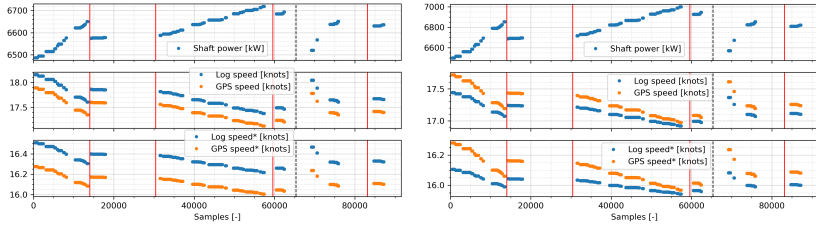
(b) Performance trends predicted by NL-PCR (left) and NL-PLSR (right) model for the sister ship.

Figure 9: Performance trends predicted by NL-PCR and NL-PLSR model for the original ship (top) and the sister ship (bottom). The red and dashed black vertical lines represents the propeller and hull cleaning events, respectively.
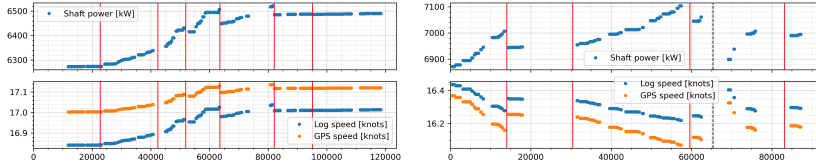
Figure 10: Performance trends predicted by ANN model for the original ship (left) and the sister ship (right). The red and dashed black vertical lines represents the propeller and hull cleaning events, respectively.

of an increase in power demand for a given ship speed (Walker and Atkins (2007); Ejdfors (2019)) or sometimes in terms of the speed-loss at a given shaft power (Koboević et al. (2019); Coraddu et al. (2019b)). Similar estimates can be predicted using the calibrated machine-learning (ML) models to quantify the hydrodynamic performance of the ships. The current section presents the results in terms of the change in power demand of the ships, at the service speed, predicted through each propeller and hull cleaning event as well as for the starting and end of the time-series. The latter represents the change in hydrodynamic performance of the ships though the entire data recording duration. Here, the predicted change in power demand is calculated as the difference between the shaft power predicted for just before and after the corresponding event at the service speed of the ship.

Table 6 shows the predicted change in the power demand at the service speed for all the cleaning events and for the starting and end of the time-series for both the ships. A reduction in power demand (negative value with green cell color) indicates an improvement in the hydrodynamic performance of the ship whereas an increase in power demand (positive value with reddish cell color) indicates performance degradation. As a reference, the change in power demand for each case is also estimated using the fouling friction coefficient (ΔC_F), presented in the rightmost column in table 6.

The predicted change in power demand (presented in table 6) for the sister ship shows an improvement in the hydrodynamic performance in all the cases except for the 2nd propeller cleaning event (*Prop. 2*). This may be due to a large section of unavailable data in the time-series just before the 2nd propeller cleaning event (as shown in figure 9).

Table 6
Performance prediction results showing the predicted change in power demand (in kW), through all the cleaning events and the starting and end of the time-series, using the regression models for both the ships. 'Prop.' stands for Propeller. The * marked target variables are the non-linear transformed variables (variable numbers 17 and 18 in table 3) used in NL-PCR and NL-PLSR models. The green colored cells indicate performance improvement and the reddish ones indicate drop in performance.

Cleaning Event	Change in Power demand [kW]										Using ΔC_F
	NL-PCR				NL-PLSR				ANN		
	Using GPS speed	Using Log speed	Using GPS speed*	Using Log speed*	Using GPS speed	Using Log speed	Using GPS speed*	Using Log speed*	Using GPS speed	Using Log speed	
	Original Ship										
Prop. 1	0.01	0.01	0.01	0.01	-0.01	0.00	-0.01	0.00	0.00	0.00	-716.03
Prop. 2	-27.31	-24.92	-27.52	-25.46	28.22	4.81	21.42	-1.97	-0.20	-3.73	-247.98
Prop. 3	23.58	21.52	24.59	20.21	-24.37	-4.16	-18.47	1.79	-5.23	-1.55	-930.51
Prop. 4	86.83	79.23	83.43	76.64	-89.74	-15.31	-67.95	6.85	-20.31	-7.29	-652.87
Prop. 5	54.21	49.46	52.77	48.49	-56.03	-9.56	-42.40	4.35	-12.99	-4.89	-274.52
Prop. 6	1.34	1.22	1.29	1.19	-1.38	-0.24	-1.05	0.11	-0.32	-0.12	534.02
After 3 yrs	-330.58	-301.68	-329.82	-299.47	341.72	58.25	259.16	-24.45	33.74	-14.62	-464.61
	Sister Ship										
Prop. 1	-308.67	-308.25	-220.64	-232.30	-390.39	-324.00	-332.12	-253.17	-192.33	-158.05	777.26
Prop. 2	39.00	39.00	27.83	29.49	49.39	40.99	41.52	32.06	24.79	20.49	291.27
Prop. 3	-137.30	-137.25	-101.66	-102.05	-173.44	-143.95	-150.14	-112.16	-98.60	-74.09	32.90
Hull & Prop. 4	-703.66	-702.93	-508.24	-529.98	-889.62	-738.71	-759.10	-577.31	-454.95	-374.73	-1286.20
Prop. 5	-82.89	-82.68	-60.06	-62.09	-104.71	-86.91	-91.14	-67.85	-53.17	-43.21	313.39
After ~2.5 yrs	605.29	605.01	432.85	458.78	765.45	635.93	647.93	497.69	408.91	348.46	568.17

Moreover, as expected, the biggest improvement is predicted for the hull and propeller cleaning event (*Hull & Prop. 4*). For the original ship, the values predicted by the NL-PCR model shows performance degradation in all the cases except for the 2nd propeller cleaning event (*Prop. 2*). This is probably due to the fact that the NL-PCR model mapped a performance degradation trend for speed variables, as shown in figure 9. The ANN model also predicted a performance degradation trend for speed variables, but it still managed to predict a very small performance improvement for almost all the cleaning events. Here, the NL-PLSR model predicts the highest performance improvement using the linear and non-linear (* marked) GPS speed variables, due to favorable trends shown for these variables in figure 9.

Comparing with the change in power demand predicted using the fouling friction coefficient (ΔC_F), all the values predicted by the machine-learning (ML) models are highly under-estimated except for the starting and end of the time-series for the sister ship (*After ~2.5 yrs*), only in this case the values seems to be in the same range. But the values obtained using ΔC_F shows unexpected drop in the hydrodynamic performance of the ship for all the propeller cleaning events for the sister ship and the last propeller cleaning event (*Prop. 6*) for the original ship. Moreover, the change in power demand predicted for the starting and end of the time-series for the original ship (*After 3 yrs*) using ΔC_F shows improvement in the performance of the ship, which is highly unexpected. Finally, using ΔC_F, a drop in power demand by about 1300 kW is predicted for the hull and propeller cleaning event for the sister ship (*Hull & Prop. 4*) whereas the values predicted using the ML models is in the range of 375 to 890 kW, of which the ANN model predicted the lowest and the NL-PLSR model predicted the highest.

Overall, a clear assessment of the quality of the results cannot be obtained here as the traditional method (using ΔC_F) itself does not seem to be predicting the expected results in about half of the cases, and there is no alternative method available to make a better quantitative assessment. Nevertheless, the results obtained from all the ML models seems to be qualitatively good, at least in the case of the sister ship. This may be attributed to the fact that the in-service data obtained from the original ship, being newly-built around the data recording duration, has a small correlation with the fouling growth factor (FGF), but the sister ship has a stronger correlation with the FGF, and therefore, shows better results using the ML models.
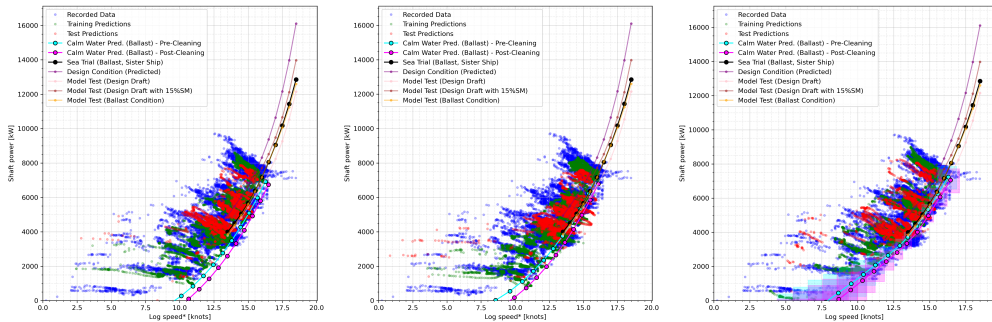
Figure 11: Calm-water speed-power curves predicted by NL-PCR (left), NL-PLSR (center) and probabilistic ANN (right) models for the sister ship for just before (pre-cleaning) and after (post-cleaning) the hull and propeller cleaning event (*Hull & Prop. 4*). The shaded region around the predicted calm-water curve, in case of the ANN model, presents the 95% confidence interval estimated using the approximate predictive distributions predicted for each sample.

Further, it is also possible to predict the whole calm-water speed-power curve for the ships for before and after each of the propeller and hull cleaning events as well as for the starting and end of the time-series. Predicting the calm-water speed-power curve would also act as a generalization check, showing the underlying mapping to which each machine-learning (ML) model is fitted. Moreover, the predicted curve can be compared with experimentally obtained calm-water speed-power curves, for example, the model test and sea-trial results. Figure 11 shows the improvement in hydrodynamic performance of the sister ship by predicting the calm-water speed-power curves (for ballast draft and trim) before and after the hull and propeller cleaning event (*Hull & Prop. 4*) using all the three models. The values in table 6 are actually the distance between these predicted calm-water curves along the shaft power axis at the service speed of the ship.

In figure 11, the speed-power curves, obtained using the NL-PCR and NL-PLSR models, are cubic in nature due to the non-linear (cubic) transformation adopted for the speed variables. It is expected that the post-cleaning curve should almost match with the sea-trial curve (in figure 11), but this is not observed here. This may be attributed to the fact that the sea trial curve (presented in figure 11) are obtained for another sister ship (not the here referred sister ship). Nevertheless, the shifting of the calm-water speed-power curve (pre- and post-cleaning) shows a substantial improvement in the hydrodynamic performance of the ship. Further, it is observed that the predicted curves do not pass through the origin (0, 0), most definitely due to the sparsity of data in the lower speed-power range. The probabilistic ANN model also predicts a higher uncertainty (presented by the shaded region around the predicted points in figure 11) for the lower speed-power range due to the same reason. A better curve may be obtained using a more balanced dataset.

Figure 12 shows the calm-water speed-power curves predicted for the starting and end of the time-series for the original ship using the ANN model. Here, the curve is predicted using the GPS speed variable, but it should match with the log speed variable as the water current is assumed to be absent while making these predictions. In this case, it is observed that the speed-power curve is well below the sea-trial and model test curves. This may be due to an extrapolation on the draft axis as the in-service data contains a very small amount of data in the ballast daft range, in the case of the original ship, as evident from figure 13. Again, a better curve may be obtained using a more balanced dataset.

6. Conclusion

The current work presents a novel method to monitor the hydrodynamic performance of a sea-going ship using the in-service data recorded onboard the ship. The in-service data from two sister ships, complemented with weather hindcast data, is used to calibrate three machine-learning (ML) models, namely, non-linear Principal Component Regression (NL-PCR), non-linear Partial Least Squares Regression (NL-PLSR) and probabilistic artificial neural network (ANN), through several propeller and hull cleaning events. A fouling growth factor (FGF) is included in the ML models to incorporate the effect of fouling growth on the hull and propeller of the ships. The FGF is formulated

128
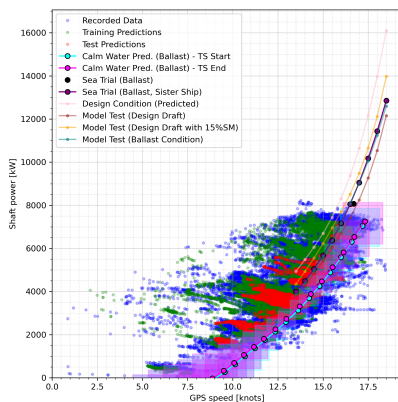
Figure 12: Calm-water speed-power curve predicted (using the GPS speed variable) by probabilistic ANN model for the original ship for the starting and end of the time-series (*After 3 yrs*). The shaded region around the predicted calm-water curve presents the 95% confidence interval estimated using the approximate predictive distributions predicted for each sample.
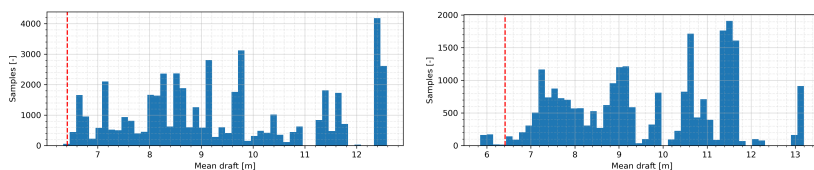
Figure 13: Distribution of mean draft for the original ship (left) and the sister ship (right). The dashed red vertical line indicates the ballast draft of the ship.

using the ships' static time in water and the fouling trends obtained using the generalized admiralty coefficient for the ships.

The results indicate that it may be possible to use simple interpretable ML models, like NL-PCR and NL-PLSR, instead of a highly complex black-box model, like ANN, to model the hydrodynamic state of a sea-going ship. PCR and PLSR are basically linear models but empowered by some approximate non-linear transformations, obtained from our domain knowledge, produced results comparable to the ANN model in the given case. These models can be further improved by using a set of more accurate non-linear transformations. Further, it is also shown in the current work that it may be necessary to use a balanced dataset to predict an accurate calm-water speed-power curve over the whole range of speed and power. The in-service datasets used here are sparse in the lower speed range, as is generally seen in most of the ship propulsion datasets, resulting in a poor prediction in that range.

The fouling friction coefficient (ΔC_F) fails as a reference for validation as the change in performance predicted by using ΔC_F does not seem to be valid in about half of the cases. Thus, the change in performance predicted by the ML models could not be validated here, but the results for at least one ship indicate an improvement in the hydrodynamic performance of the ship for almost all the propeller and hull cleaning events, with the highest improvement predicted for the hull cleaning event, which is as expected.

7. Future Work

As compared to the fouling growth model presented by Malone et al. (1981), the fouling growth factor (FGF) formulated here is quite simplified. Most importantly, it is assumed here that the fouling grows at the same rate for each unit static time between any two cleaning events, reflected by using the same fouling growth rate (FGR) in

equation 11, for all the samples between two cleaning events. The FGR here is estimated as the slope of the mean generalized admiralty coefficient (shown in figure 3). In a more accurate approach, the FGR should be estimated for each individual port visit as the FGR depends on the water conditions in which the ship is static, explained in section 3. Due to substantial noise in the mean generalized admiralty coefficient values (as seen in figure 3), it is not possible to estimate a set of logically valid FGRs for each port visit using this approach. Thus, an alternate method or approach needs to be defined to get a better FGF.

On another note, it may also be a good idea to use a different set of machine-learning (ML) models for the given case. Although ANN is still considered as one of the best ML models, there are several other ML models which are known to have outperformed ANN in different scenarios. Moreover, the probabilistic ANN model used here is an approximation for a true Bayesian model, a full Bayesian approach would probably produce better estimation of the uncertainties in the predictions. It would, therefore, be interesting to see if a different ML model can be used to solve this problem more efficiently. Finally, the current work is only validated for two sister ships. It would most definitely be desired to validate this approach on a more variant group of datasets.

A. Validation of Generalized admiralty coefficient as a Ship's hydrodynamic performance indicator.

Gupta et al. (2021) proposed to use a generalized form of admiralty coefficient as a statistical performance indicator for a ship. The paper presented the validation of the method for a new-built ship (here referred to as the original ship). This appendix present the validation of the same method using an extended dataset from the original ship as well as for its sister ship. It should be noted that the data obtained from the sister ship is recorded after a few years of service and includes a hull cleaning (dry-docking) event whereas the data from the original ship only includes propeller cleaning events. Thus, the sister ship is expected to show a greater extent of fouling.

First of all, a generalized admiralty coefficient is obtained, in much the same way as presented by Gupta et al. (2021), for each ship by statistically fitting the generalized admiralty coefficient formula ($\Delta^m V^n / P_s$) to the near-calm-water filtered and corrected in-service data, and then, the fouling growth rate is estimated as the trend in the obtained generalized admiralty coefficient for all the legs between each propeller and/or hull cleaning events. Finally, in order to validate the method, the fouling growth rate predicted by the obtained generalized admiralty coefficient is compared, qualitatively, with the fouling growth rate predicted by the traditional method, i.e., the fouling friction coefficient (ΔC_F).

The near-calm-water in-service data is obtained by, first, filtering the recorded in-service data for small wind and wave load conditions (total wind speed < 5.5 m/s and significant wave height < 1 m) and, then, correcting the shaft power measurements in the filtered dataset for wind and wave loads. The wind loads are estimated using Fujiwara's method (Fujiwara et al. (2005)), as recommended by ITTC (2017), and the wave loads are estimated using Liu and Papanikolaou's method (Liu and Papanikolaou (2020)). Unlike DTU's method (Martinsen (2016), Taskar and Andersen (2021); used by Gupta et al. (2021)), which provides added wave resistance estimates for mean wave heading from head seas to beam seas only, Liu and Papanikolaou's method (Liu and Papanikolaou (2020)), used here, provides the estimated added wave resistance for all the wave headings, including the following waves.

Figures 14 and 15 presents the validation of the generalized admiralty coefficient method for both the original ship (also presented by Gupta et al. (2021)) as well as its sister ship.

B. Calculating Fouling Friction Coefficient (ΔC_F)

The fouling friction coefficient (ΔC_F) is calculated as the difference between the total resistance coefficient ($C_{T,Data}$) obtained from the in-service data in calm-water conditions and the total resistance coefficient ($C_{T,Emp}$) obtained from well-established empirical methods or model test results.

$$\Delta C_F = C_{T,Data} - C_{T,Emp} \tag{12}$$

The total resistance coefficient ($C_{T,Data}$) from in-service data can be obtained as follows:

$$C_{T,Data} = \frac{R_{T,Data}}{0.5\rho S V^2} = \frac{P_s}{0.5\rho S V^3 \eta_T} \tag{13}$$

(a) Trends in fouling friction coefficient (ΔC_F).   (b) Trends in generalized admiralty coefficient.

Figure 14: Original ship.

(a) Trends in fouling friction coefficient (ΔC_F).   (b) Trends in generalized admiralty coefficient.
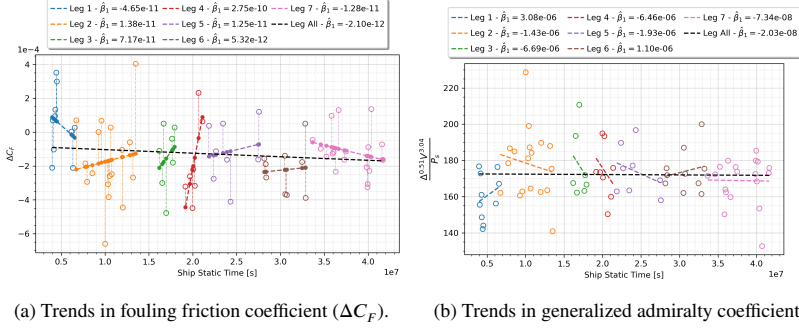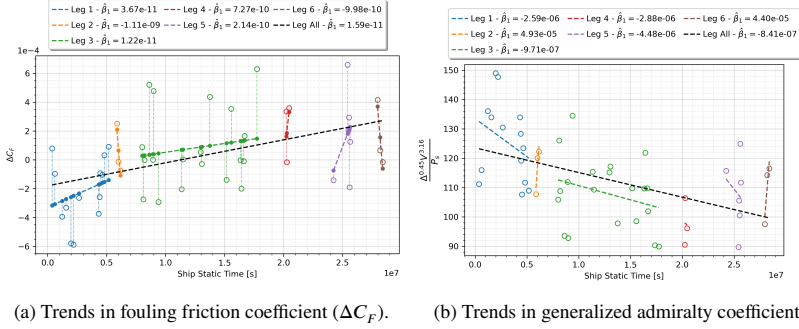
Figure 15: Sister ship.

Where $R_{T,Data}$ is the total resistance (from data), ρ is the density of sea water, S is the wetted surface area (WSA), V is the log speed (measured), P_s is the shaft power (measured) and η_T is the total propulsive efficiency. Here, the WSA can be estimated using the hull form (or offset table) of the ship for the corresponding mean draft and trim. The total propulsive efficiency (η_T) can be estimated empirically or using the model test results. In the above formula, special attention should be paid towards the units of contributing variables, for example, the unit of log speed should be m/s if the unit of shaft power is watt or kilowatt.

Further, the empirically obtained total resistance coefficient ($C_{T,Emp}$) can be dividing into individual resistance components as follows:

$$C_{T,Emp} = \frac{R_{T,Emp}}{0.5\rho SV^2} = \frac{R_{Calm} + R_{Wind} + R_{Wave} + R_{Others}}{0.5\rho SV^2} \tag{14}$$

Where $R_{T,Emp}$ is the total resistance (from empirical methods), R_{Calm} is the calm water resistance, R_{Wind} is the added wind resistance, R_{Wave} is the added wave resistance and R_{Others} is the resistance from other effects. These individual resistance components can be further estimated using different physics-based and/or empirical methods. R_{Others} can include the effect of transom stern, appendages and so on.

CRediT authorship contribution statement

Prateek Gupta: Conceptualization, Methodology, Investigation, Software, Data curation, Visualization, Writing. **Adil Rasheed:** Conceptualization, Supervision, Writing. **Sverre Steen:** Conceptualization, Supervision, Resources.

References

Chassignet, E., Hurlburt, H., Smedstad, O., Halliwell, G., Hogan, P., Wallcraft, A., Baraille, R., Bleck, R., 2007. The hycom (hybrid coordinate ocean model) data assimilative system. Journal of Marine Systems 65, 60–83. URL: https://www.scopus.com/inward/record.uri?eid=2-s2.0-33846918130&doi=10.1016%2fj.jmarsys.2005.09.016&partnerID=40&md5=30d5612192b816c6b80d9b08d4ed32ea, doi:10.1016/j.jmarsys.2005.09.016. cited By 362.

Copernicus Climate Change Service (C3S), 2017. ERA5: Fifth generation of ECMWF atmospheric reanalyses of the global climate. copernicus climate change service climate data store (CDS). URL: https://cds.climate.copernicus.eu/cdsapp#!/home. last Accessed: May 29th, 2019.

Coraddu, A., Lim, S., Oneto, L., Pazouki, K., Norman, R., Murphy, A., 2019a. A novelty detection approach to diagnosing hull and propeller fouling. Ocean Engineering 176, 65–73. URL: https://www.scopus.com/inward/record.uri?eid=2-s2.0-85061732869&doi=10.1016%2fj.oceaneng.2019.01.054&partnerID=40&md5=c00c03be845a94a8e6417bcfdf4ca5e7, doi:10.1016/j.oceaneng.2019.01.054. cited By 2.

Coraddu, A., Oneto, L., Baldi, F., Cipollini, F., Atlar, M., Savio, S., 2019b. Data-driven ship digital twin for estimating the speed loss caused by the marine fouling. Ocean Engineering 186. URL: https://www.scopus.com/inward/record.uri?eid=2-s2.0-85067817812&doi=10.1016%2fj.oceaneng.2019.05.045&partnerID=40&md5=e6c7526182fdda475ef44c15e4c4c103, doi:10.1016/j.oceaneng.2019.05.045. cited By 1.

Dalheim, y.k., Steen, S., 2021. Uncertainty in the real-time estimation of ship speed through water. Ocean Engineering 235, 109423. URL: https://www.sciencedirect.com/science/article/pii/S0029801821008313, doi:https://doi.org/10.1016/j.oceaneng.2021.109423.

Damianou, A.C., Lawrence, N.D., 2012. Deep gaussian processes. arXiv:1211.0358.

Ejdfors, K.O., 2019. Use of in-service data to determine the added power of a ship due to fouling. URL: http://hdl.handle.net/11250/2622960.

Fabbri, S., Dennington, S., Price, C., Stoodley, P., Longyear, J., 2018. A marine biofilm flow cell for in situ screening marine fouling control coatings using optical coherence tomography. Ocean Engineering 170, 321–328. URL: https://www.scopus.com/inward/record.uri?eid=2-s2.0-85057170760&doi=10.1016%2fj.oceaneng.2018.10.030&partnerID=40&md5=72ae24398b3da22fb10a31d6eb4b81d0, doi:10.1016/j.oceaneng.2018.10.030. cited By 2.

Farifteh, J., Van der Meer, F., Atzberger, C., Carranza, E., 2007. Quantitative analysis of salt-affected soil reflectance spectra: A comparison of two adaptive methods (plsr and ann). Remote Sensing of Environment 110, 59–78. URL: https://www.sciencedirect.com/science/article/pii/S003442570700082X, doi:https://doi.org/10.1016/j.rse.2007.02.005.

Foteinos, M., Tzanos, E., Kyrtatos, N., 2017. Ship hull fouling estimation using shipboard measurements, models for resistance components, and shaft torque calculation using engine model. Journal of Ship Research 61, 64–74. URL: https://www.scopus.com/inward/record.uri?eid=2-s2.0-85024491367&doi=10.5957%2fJOSR.61.2.160053&partnerID=40&md5=4d8fedda376f0ed57cf089dbbfe28012, doi:10.5957/JOSR.61.2.160053. cited By 3.

Fujiwara, T., Ueno, M., Ikeda, Y., 2005. A new estimation method of wind forces and moments acting on ships on the basis of physical component models. Journal of the Japan Society of Naval Architects and Ocean Engineers 2, 243–255. doi:10.2534/jjasnaoe.2.243.

Gal, Y., Ghahramani, Z., 2016. Dropout as a bayesian approximation: Representing model uncertainty in deep learning, in: 33rd International Conference on Machine Learning, ICML 2016, pp. 1651–1660. URL: https://www.scopus.com/inward/record.uri?eid=2-s2.0-84998879817&partnerID=40&md5=97ece85c772ca3f556cc3844daee3080. cited By 170.

Global Monitoring and Forecasting Center, 2018. GLORYS12V1 - global ocean physical reanalysis product, e.u. copernicus marine service information [data set]. URL: https://resources.marine.copernicus.eu/?option=com_csw&view=details&product_id=GLOBAL_REANALYSIS_PHY_001_030. last Accessed: Dec 16th, 2020.

Glorot, X., Bordes, A., Bengio, Y., 2011. Deep sparse rectifier neural networks, in: Gordon, G., Dunson, D., Dudík, M. (Eds.), Proceedings of the Fourteenth International Conference on Artificial Intelligence and Statistics, PMLR, Fort Lauderdale, FL, USA. pp. 315–323. URL: https://proceedings.mlr.press/v15/glorot11a.html.

Goodfellow, I., Bengio, Y., Courville, A., 2016. Deep Learning. MIT Press. http://www.deeplearningbook.org.

Gupta, P., Steen, S., Rasheed, A., 2019. Big data analytics as a tool to monitor hydrodynamic performance of a ship, in: International Conference on Offshore Mechanics and Arctic Engineering. URL: https://doi.org/10.1115/OMAE2019-95815, doi:10.1115/OMAE2019-95815, arXiv:https://asmedigitalcollection.asme.org/OMAE/proceedings-pdf/OMAE2019/58844/V07AT06A059/6443926/v07at06a059-omae v07AT06A059.

Gupta, P., Taskar, B., Steen, S., Rasheed, A., 2021. Statistical modeling of ship's hydrodynamic performance indicator. Applied Ocean Research 111, 102623. URL: https://www.sciencedirect.com/science/article/pii/S0141118721001000, doi:https://doi.org/10.1016/j.apor.2021.102623.

Guyon, I., 1997. A scaling law for the validation-set training-set size ratio, in: AT & T Bell Laboratories.

ITTC, 2017. Recommended Procedures and Guidelines 7.5-04-01-01.1: Preparation, Conduct and Analysis of Speed/Power Trials. Technical Report. ITTC. URL: https://www.ittc.info/media/7691/75-04-01-011.pdf.

Jolliffe, I., 2002. Principal Component Analysis. Springer Series in Statistics, Springer. URL: https://books.google.no/books?id=_olByCrhjwIC.

Koboević, ., Bebić, D., Kurtela, ., 2019. New approach to monitoring hull condition of ships as objective for selecting optimal docking period. Ships and Offshore Structures 14, 95–103. URL: https://www.scopus.com/inward/record.uri?eid=2-s2.0-85048357528&doi=10.1080%2f17445302.2018.1481631&partnerID=40&md5=96400904abd0f2b6359e1ef13f81212b, doi:10.1080/17445302.2018.1481631. cited By 1.

Lazakis, I., Dikis, K., Michala, A.L., Theotokatos, G., 2016. Advanced ship systems condition monitoring for enhanced inspection, maintenance and decision making in ship operations. Transportation Research Procedia 14, 1679 – 1688. URL: http://www.sciencedirect.com/science/

132

article/pii/S235214651630134X, doi:https://doi.org/10.1016/j.trpro.2016.05.133. transport Research Arena TRA2016.

Liu, S., Papanikolaou, A., 2020. Regression analysis of experimental data for added resistance in waves of arbitrary heading and development of a semi-empirical formula. Ocean Engineering 206, 107357. URL: https://www.sciencedirect.com/science/article/pii/S0029801820303887, doi:https://doi.org/10.1016/j.oceaneng.2020.107357.

Logan, K., 2012. Using a ships propeller for hull condition monitoring. Naval Engineers Journal 124, 71–87. URL: https://www.ingentaconnect.com/content/asne/nej/2012/00000124/00000001/art00012.

Malone, J.A., Little, D.E., Allman, M., 1981. Effects of hull foulants and cleaning/coating practices on ship performances and economics. Transactions - Society of Naval Architects and Marine Engineers 88, 75–101. Cited By 12.

Martens, H., Martens, M., 2001. Multivariate Analysis of Quality: An Introduction. Wiley. URL: https://books.google.no/books?id=aqpoh41CjtEC.

Martinsen, M.A., 2016. An design tool for estimating the added wave resistance of container ships, Et design værktøj til estimering af øget bølgemodstand for kontainerskibe. Ph.D. thesis. Technical University of Denmark (DTU).

Munk, T., 2016. Fuel conservation through managing hull resistance, in: Motorship Propulsion Conference, Copenhagen. URL: https://www.messe.no/ExhibitorDocuments/97726/2419/BIMCO%20Hull-Resistance.pdf.

Pedersen, B., Larsen, J., 2009. Modeling of ship propulsion performance, in: World Maritime Technology Conference. Modeling of Ship Propulsion Performance ; Conference date: 01-01-2009.

Pedregosa, F., Varoquaux, G., Gramfort, A., Michel, V., Thirion, B., Grisel, O., Blondel, M., Prettenhofer, P., Weiss, R., Dubourg, V., Vanderplas, J., Passos, A., Cournapeau, D., Brucher, M., Perrot, M., Duchesnay, E., 2011. Scikit-learn: Machine learning in Python. Journal of Machine Learning Research 12, 2825–2830.

Ruder, S., 2016. An overview of gradient descent optimization algorithms. CoRR abs/1609.04747. URL: http://arxiv.org/abs/1609.04747, arXiv:1609.04747.

Schmidhuber, J., 2015. Deep learning in neural networks: An overview. Neural networks 61, 85–117.

Schultz, M., 2007. Effects of coating roughness and biofouling on ship resistance and powering. Biofouling 23, 331–341. URL: https://www.scopus.com/inward/record.uri?eid=2-s2.0-34548601800&doi=10.1080%2f08927010701461974&partnerID=40&md5=fcb1c15ee2a44a867289956ee616bab5, doi:10.1080/08927010701461974. cited By 375.

Srivastava, N., Hinton, G., Krizhevsky, A., Sutskever, I., Salakhutdinov, R., 2014. Dropout: A simple way to prevent neural networks from overfitting. Journal of Machine Learning Research 15, 1929–1958. URL: https://www.scopus.com/inward/record.uri?eid=2-s2.0-84904163933&partnerID=40&md5=b865fd654b3befc5d829dbe5d42b80c3. cited By 7845.

Taskar, B., Andersen, P., 2021. Comparison of added resistance methods using digital twin and full-scale data. Ocean Engineering 229, 108710. URL: https://www.sciencedirect.com/science/article/pii/S0029801821001451, doi:https://doi.org/10.1016/j.oceaneng.2021.108710.

Townsin, R., 2003. The ship hull fouling penalty. Biofouling 19, 9–15. URL: https://www.scopus.com/inward/record.uri?eid=2-s2.0-0037380142&doi=10.1080%2f0892701021000060833&partnerID=40&md5=658629ee2fcf85475cd807eca7937b95, doi:10.1080/0892701021000060833. cited By 284.

Vandeginste, B., Sielhorst, C., Gerritsen, M., 1988. Nipals algorithm for the calculation of the principal components of a matrix. TrAC - Trends in Analytical Chemistry 7, 286–287. URL: https://www.scopus.com/inward/record.uri?eid=2-s2.0-0024071733&doi=10.1016%2f0165-9936%2888%2980007-4&partnerID=40&md5=2087dda2e566521f91090ce3619d1cbf, doi:10.1016/0165-9936(88)80007-4. cited By 17.

Walker, M., Atkins, I., 2007. Surface ship hull and propeller fouling managment, in: RINA, Royal Institution of Naval Architects International Conference - Warship 2007: The Affordable Warship - Papers, pp. 131–138. URL: https://www.scopus.com/inward/record.uri?eid=2-s2.0-56149088666&partnerID=40&md5=bd182d30bc8526b6d9d21d537c85f442. cited By 3.

Wold, S., Sjöström, M., Eriksson, L., 2001. Pls-regression: A basic tool of chemometrics. Chemometrics and Intelligent Laboratory Systems 58, 109–130. doi:10.1016/S0169-7439(01)00155-1. cited By 5920.

Yebra, D.M., Kiil, S., Dam-Johansen, K., 2004. Antifouling technology—past, present and future steps towards efficient and environmentally friendly antifouling coatings. Progress in Organic Coatings 50, 75 – 104. URL: http://www.sciencedirect.com/science/article/pii/S0300944003001644, doi:https://doi.org/10.1016/j.porgcoat.2003.06.001.

Previous PhD theses published at the Department of Marine Technology

Norwegian University of Science and Technology

Previous PhD theses published at the Department of Marine Technology
(earlier: Faculty of Marine Technology)
NORWEGIAN UNIVERSITY OF SCIENCE AND TECHNOLOGY

Report No.	Author	Title
	Kavlie, Dag	Optimization of Plane Elastic Grillages, 1967
	Hansen, Hans R.	Man-Machine Communication and Data-Storage Methods in Ship Structural Design, 1971
	Gisvold, Kaare M.	A Method for non-linear mixed -integer programming and its Application to Design Problems, 1971
	Lund, Sverre	Tanker Frame Optimalization by means of SUMT-Transformation and Behaviour Models, 1971
	Vinje, Tor	On Vibration of Spherical Shells Interacting with Fluid, 1972
	Lorentz, Jan D.	Tank Arrangement for Crude Oil Carriers in Accordance with the new Anti-Pollution Regulations, 1975
	Carlsen, Carl A.	Computer-Aided Design of Tanker Structures, 1975
	Larsen, Carl M.	Static and Dynamic Analysis of Offshore Pipelines during Installation, 1976
UR-79-01	Brigt Hatlestad, MK	The finite element method used in a fatigue evaluation of fixed offshore platforms. (Dr.Ing. Thesis)
UR-79-02	Erik Pettersen, MK	Analysis and design of cellular structures. (Dr.Ing. Thesis)
UR-79-03	Sverre Valsgård, MK	Finite difference and finite element methods applied to nonlinear analysis of plated structures. (Dr.Ing. Thesis)
UR-79-04	Nils T. Nordsve, MK	Finite element collapse analysis of structural members considering imperfections and stresses due to fabrication. (Dr.Ing. Thesis)
UR-79-05	Ivar J. Fylling, MK	Analysis of towline forces in ocean towing systems. (Dr.Ing. Thesis)
UR-80-06	Nils Sandsmark, MM	Analysis of Stationary and Transient Heat Conduction by the Use of the Finite Element Method. (Dr.Ing. Thesis)
UR-80-09	Sverre Haver, MK	Analysis of uncertainties related to the stochastic modeling of ocean waves. (Dr.Ing. Thesis)
UR-81-15	Odland, Jonas	On the Strength of welded Ring stiffened cylindrical Shells primarily subjected to axial Compression
UR-82-17	Engesvik, Knut	Analysis of Uncertainties in the fatigue Capacity of

Welded Joints

UR-82-18	Rye, Henrik	Ocean wave groups
UR-83-30	Eide, Oddvar Inge	On Cumulative Fatigue Damage in Steel Welded Joints
UR-83-33	Mo, Olav	Stochastic Time Domain Analysis of Slender Offshore Structures
UR-83-34	Amdahl, Jørgen	Energy absorption in Ship-platform impacts
UR-84-37	Mørch, Morten	Motions and mooring forces of semi submersibles as determined by full-scale measurements and theoretical analysis
UR-84-38	Soares, C. Guedes	Probabilistic models for load effects in ship structures
UR-84-39	Aarsnes, Jan V.	Current forces on ships
UR-84-40	Czujko, Jerzy	Collapse Analysis of Plates subjected to Biaxial Compression and Lateral Load
UR-85-46	Alf G. Engseth, MK	Finite element collapse analysis of tubular steel offshore structures. (Dr.Ing. Thesis)
UR-86-47	Dengody Sheshappa, MP	A Computer Design Model for Optimizing Fishing Vessel Designs Based on Techno-Economic Analysis. (Dr.Ing. Thesis)
UR-86-48	Vidar Aanesland, MH	A Theoretical and Numerical Study of Ship Wave Resistance. (Dr.Ing. Thesis)
UR-86-49	Heinz-Joachim Wessel, MK	Fracture Mechanics Analysis of Crack Growth in Plate Girders. (Dr.Ing. Thesis)
UR-86-50	Jon Taby, MK	Ultimate and Post-ultimate Strength of Dented Tubular Members. (Dr.Ing. Thesis)
UR-86-51	Walter Lian, MH	A Numerical Study of Two-Dimensional Separated Flow Past Bluff Bodies at Moderate KC-Numbers. (Dr.Ing. Thesis)
UR-86-52	Bjørn Sortland, MH	Force Measurements in Oscillating Flow on Ship Sections and Circular Cylinders in a U-Tube Water Tank. (Dr.Ing. Thesis)
UR-86-53	Kurt Strand, MM	A System Dynamic Approach to One-dimensional Fluid Flow. (Dr.Ing. Thesis)
UR-86-54	Arne Edvin Løken, MH	Three Dimensional Second Order Hydrodynamic Effects on Ocean Structures in Waves. (Dr.Ing. Thesis)
UR-86-55	Sigurd Falch, MH	A Numerical Study of Slamming of Two-Dimensional Bodies. (Dr.Ing. Thesis)
UR-87-56	Arne Braathen, MH	Application of a Vortex Tracking Method to the Prediction of Roll Damping of a Two-Dimension Floating Body. (Dr.Ing. Thesis)

UR-87-57	Bernt Leira, MK	Gaussian Vector Processes for Reliability Analysis involving Wave-Induced Load Effects. (Dr.Ing. Thesis)
UR-87-58	Magnus Småvik, MM	Thermal Load and Process Characteristics in a Two-Stroke Diesel Engine with Thermal Barriers (in Norwegian). (Dr.Ing. Thesis)
MTA-88-59	Bernt Arild Bremdal, MP	An Investigation of Marine Installation Processes – A Knowledge - Based Planning Approach. (Dr.Ing. Thesis)
MTA-88-60	Xu Jun, MK	Non-linear Dynamic Analysis of Space-framed Offshore Structures. (Dr.Ing. Thesis)
MTA-89-61	Gang Miao, MH	Hydrodynamic Forces and Dynamic Responses of Circular Cylinders in Wave Zones. (Dr.Ing. Thesis)
MTA-89-62	Martin Greenhow, MH	Linear and Non-Linear Studies of Waves and Floating Bodies. Part I and Part II. (Dr.Techn. Thesis)
MTA-89-63	Chang Li, MH	Force Coefficients of Spheres and Cubes in Oscillatory Flow with and without Current. (Dr.Ing. Thesis
MTA-89-64	Hu Ying, MP	A Study of Marketing and Design in Development of Marine Transport Systems. (Dr.Ing. Thesis)
MTA-89-65	Arild Jæger, MH	Seakeeping, Dynamic Stability and Performance of a Wedge Shaped Planing Hull. (Dr.Ing. Thesis)
MTA-89-66	Chan Siu Hung, MM	The dynamic characteristics of tilting-pad bearings
MTA-89-67	Kim Wikstrøm, MP	Analysis av projekteringen for ett offshore projekt. (Licenciat-avhandling)
MTA-89-68	Jiao Guoyang, MK	Reliability Analysis of Crack Growth under Random Loading, considering Model Updating. (Dr.Ing. Thesis)
MTA-89-69	Arnt Olufsen, MK	Uncertainty and Reliability Analysis of Fixed Offshore Structures. (Dr.Ing. Thesis)
MTA-89-70	Wu Yu-Lin, MR	System Reliability Analyses of Offshore Structures using improved Truss and Beam Models. (Dr.Ing. Thesis)
MTA-90-71	Jan Roger Hoff, MH	Three-dimensional Green function of a vessel with forward speed in waves. (Dr.Ing. Thesis)
MTA-90-72	Rong Zhao, MH	Slow-Drift Motions of a Moored Two-Dimensional Body in Irregular Waves. (Dr.Ing. Thesis)
MTA-90-73	Atle Minsaas, MP	Economical Risk Analysis. (Dr.Ing. Thesis)
MTA-90-74	Knut-Aril Farnes, MK	Long-term Statistics of Response in Non-linear Marine Structures. (Dr.Ing. Thesis)
MTA-90-75	Torbjørn Sotberg, MK	Application of Reliability Methods for Safety Assessment of Submarine Pipelines. (Dr.Ing.

Thesis)

MTA-90-76	Zeuthen, Steffen, MP	SEAMAID. A computational model of the design process in a constraint-based logic programming environment. An example from the offshore domain. (Dr.Ing. Thesis)
MTA-91-77	Haagensen, Sven, MM	Fuel Dependant Cyclic Variability in a Spark Ignition Engine - An Optical Approach. (Dr.Ing. Thesis)
MTA-91-78	Løland, Geir, MH	Current forces on and flow through fish farms. (Dr.Ing. Thesis)
MTA-91-79	Hoen, Christopher, MK	System Identification of Structures Excited by Stochastic Load Processes. (Dr.Ing. Thesis)
MTA-91-80	Haugen, Stein, MK	Probabilistic Evaluation of Frequency of Collision between Ships and Offshore Platforms. (Dr.Ing. Thesis)
MTA-91-81	Sødahl, Nils, MK	Methods for Design and Analysis of Flexible Risers. (Dr.Ing. Thesis)
MTA-91-82	Ormberg, Harald, MK	Non-linear Response Analysis of Floating Fish Farm Systems. (Dr.Ing. Thesis)
MTA-91-83	Marley, Mark J., MK	Time Variant Reliability under Fatigue Degradation. (Dr.Ing. Thesis)
MTA-91-84	Krokstad, Jørgen R., MH	Second-order Loads in Multidirectional Seas. (Dr.Ing. Thesis)
MTA-91-85	Molteberg, Gunnar A., MM	The Application of System Identification Techniques to Performance Monitoring of Four Stroke Turbocharged Diesel Engines. (Dr.Ing. Thesis)
MTA-92-86	Mørch, Hans Jørgen Bjelke, MH	Aspects of Hydrofoil Design: with Emphasis on Hydrofoil Interaction in Calm Water. (Dr.Ing. Thesis)
MTA-92-87	Chan Siu Hung, MM	Nonlinear Analysis of Rotordynamic Instabilities in Highspeed Turbomachinery. (Dr.Ing. Thesis)
MTA-92-88	Bessason, Bjarni, MK	Assessment of Earthquake Loading and Response of Seismically Isolated Bridges. (Dr.Ing. Thesis)
MTA-92-89	Langli, Geir, MP	Improving Operational Safety through exploitation of Design Knowledge - an investigation of offshore platform safety. (Dr.Ing. Thesis)
MTA-92-90	Sævik, Svein, MK	On Stresses and Fatigue in Flexible Pipes. (Dr.Ing. Thesis)
MTA-92-91	Ask, Tor Ø., MM	Ignition and Flame Growth in Lean Gas-Air Mixtures. An Experimental Study with a Schlieren System. (Dr.Ing. Thesis)
MTA-86-92	Hessen, Gunnar, MK	Fracture Mechanics Analysis of Stiffened Tubular Members. (Dr.Ing. Thesis)

MTA-93-93	Steinebach, Christian, MM	Knowledge Based Systems for Diagnosis of Rotating Machinery. (Dr.Ing. Thesis)
MTA-93-94	Dalane, Jan Inge, MK	System Reliability in Design and Maintenance of Fixed Offshore Structures. (Dr.Ing. Thesis)
MTA-93-95	Steen, Sverre, MH	Cobblestone Effect on SES. (Dr.Ing. Thesis)
MTA-93-96	Karunakaran, Daniel, MK	Nonlinear Dynamic Response and Reliability Analysis of Drag-dominated Offshore Platforms. (Dr.Ing. Thesis)
MTA-93-97	Hagen, Arnulf, MP	The Framework of a Design Process Language. (Dr.Ing. Thesis)
MTA-93-98	Nordrik, Rune, MM	Investigation of Spark Ignition and Autoignition in Methane and Air Using Computational Fluid Dynamics and Chemical Reaction Kinetics. A Numerical Study of Ignition Processes in Internal Combustion Engines. (Dr.Ing. Thesis)
MTA-94-99	Passano, Elizabeth, MK	Efficient Analysis of Nonlinear Slender Marine Structures. (Dr.Ing. Thesis)
MTA-94-100	Kvålsvold, Jan, MH	Hydroelastic Modelling of Wetdeck Slamming on Multihull Vessels. (Dr.Ing. Thesis)
MTA-94-102	Bech, Sidsel M., MK	Experimental and Numerical Determination of Stiffness and Strength of GRP/PVC Sandwich Structures. (Dr.Ing. Thesis)
MTA-95-103	Paulsen, Hallvard, MM	A Study of Transient Jet and Spray using a Schlieren Method and Digital Image Processing. (Dr.Ing. Thesis)
MTA-95-104	Hovde, Geir Olav, MK	Fatigue and Overload Reliability of Offshore Structural Systems, Considering the Effect of Inspection and Repair. (Dr.Ing. Thesis)
MTA-95-105	Wang, Xiaozhi, MK	Reliability Analysis of Production Ships with Emphasis on Load Combination and Ultimate Strength. (Dr.Ing. Thesis)
MTA-95-106	Ulstein, Tore, MH	Nonlinear Effects of a Flexible Stern Seal Bag on Cobblestone Oscillations of an SES. (Dr.Ing. Thesis)
MTA-95-107	Solaas, Frøydis, MH	Analytical and Numerical Studies of Sloshing in Tanks. (Dr.Ing. Thesis)
MTA-95-108	Hellan, Øyvind, MK	Nonlinear Pushover and Cyclic Analyses in Ultimate Limit State Design and Reassessment of Tubular Steel Offshore Structures. (Dr.Ing. Thesis)
MTA-95-109	Hermundstad, Ole A., MK	Theoretical and Experimental Hydroelastic Analysis of High Speed Vessels. (Dr.Ing. Thesis)
MTA-96-110	Bratland, Anne K., MH	Wave-Current Interaction Effects on Large-Volume Bodies in Water of Finite Depth. (Dr.Ing. Thesis)
MTA-96-111	Herfjord, Kjell, MH	A Study of Two-dimensional Separated Flow by a Combination of the Finite Element Method and

Navier-Stokes Equations. (Dr.Ing. Thesis)

MTA-96-112	Æsøy, Vilmar, MM	Hot Surface Assisted Compression Ignition in a Direct Injection Natural Gas Engine. (Dr.Ing. Thesis)
MTA-96-113	Eknes, Monika L., MK	Escalation Scenarios Initiated by Gas Explosions on Offshore Installations. (Dr.Ing. Thesis)
MTA-96-114	Erikstad, Stein O., MP	A Decision Support Model for Preliminary Ship Design. (Dr.Ing. Thesis)
MTA-96-115	Pedersen, Egil, MH	A Nautical Study of Towed Marine Seismic Streamer Cable Configurations. (Dr.Ing. Thesis)
MTA-97-116	Moksnes, Paul O., MM	Modelling Two-Phase Thermo-Fluid Systems Using Bond Graphs. (Dr.Ing. Thesis)
MTA-97-117	Halse, Karl H., MK	On Vortex Shedding and Prediction of Vortex-Induced Vibrations of Circular Cylinders. (Dr.Ing. Thesis)
MTA-97-118	Igland, Ragnar T., MK	Reliability Analysis of Pipelines during Laying, considering Ultimate Strength under Combined Loads. (Dr.Ing. Thesis)
MTA-97-119	Pedersen, Hans-P., MP	Levendefiskteknologi for fiskefartøy. (Dr.Ing. Thesis)
MTA-98-120	Vikestad, Kyrre, MK	Multi-Frequency Response of a Cylinder Subjected to Vortex Shedding and Support Motions. (Dr.Ing. Thesis)
MTA-98-121	Azadi, Mohammad R. E., MK	Analysis of Static and Dynamic Pile-Soil-Jacket Behaviour. (Dr.Ing. Thesis)
MTA-98-122	Ulltang, Terje, MP	A Communication Model for Product Information. (Dr.Ing. Thesis)
MTA-98-123	Torbergsen, Erik, MM	Impeller/Diffuser Interaction Forces in Centrifugal Pumps. (Dr.Ing. Thesis)
MTA-98-124	Hansen, Edmond, MH	A Discrete Element Model to Study Marginal Ice Zone Dynamics and the Behaviour of Vessels Moored in Broken Ice. (Dr.Ing. Thesis)
MTA-98-125	Videiro, Paulo M., MK	Reliability Based Design of Marine Structures. (Dr.Ing. Thesis)
MTA-99-126	Mainçon, Philippe, MK	Fatigue Reliability of Long Welds Application to Titanium Risers. (Dr.Ing. Thesis)
MTA-99-127	Haugen, Elin M., MH	Hydroelastic Analysis of Slamming on Stiffened Plates with Application to Catamaran Wetdecks. (Dr.Ing. Thesis)
MTA-99-128	Langhelle, Nina K., MK	Experimental Validation and Calibration of Nonlinear Finite Element Models for Use in Design of Aluminium Structures Exposed to Fire. (Dr.Ing. Thesis)
MTA-99-	Berstad, Are J., MK	Calculation of Fatigue Damage in Ship Structures.

129		(Dr.Ing. Thesis)
MTA-99-130	Andersen, Trond M., MM	Short Term Maintenance Planning. (Dr.Ing. Thesis)
MTA-99-131	Tveiten, Bård Wathne, MK	Fatigue Assessment of Welded Aluminium Ship Details. (Dr.Ing. Thesis)
MTA-99-132	Søreide, Fredrik, MP	Applications of underwater technology in deep water archaeology. Principles and practice. (Dr.Ing. Thesis)
MTA-99-133	Tønnessen, Rune, MH	A Finite Element Method Applied to Unsteady Viscous Flow Around 2D Blunt Bodies With Sharp Corners. (Dr.Ing. Thesis)
MTA-99-134	Elvekrok, Dag R., MP	Engineering Integration in Field Development Projects in the Norwegian Oil and Gas Industry. The Supplier Management of Norne. (Dr.Ing. Thesis)
MTA-99-135	Fagerholt, Kjetil, MP	Optimeringsbaserte Metoder for Ruteplanlegging innen skipsfart. (Dr.Ing. Thesis)
MTA-99-136	Bysveen, Marie, MM	Visualization in Two Directions on a Dynamic Combustion Rig for Studies of Fuel Quality. (Dr.Ing. Thesis)
MTA-2000-137	Storteig, Eskild, MM	Dynamic characteristics and leakage performance of liquid annular seals in centrifugal pumps. (Dr.Ing. Thesis)
MTA-2000-138	Sagli, Gro, MK	Model uncertainty and simplified estimates of long term extremes of hull girder loads in ships. (Dr.Ing. Thesis)
MTA-2000-139	Tronstad, Harald, MK	Nonlinear analysis and design of cable net structures like fishing gear based on the finite element method. (Dr.Ing. Thesis)
MTA-2000-140	Kroneberg, André, MP	Innovation in shipping by using scenarios. (Dr.Ing. Thesis)
MTA-2000-141	Haslum, Herbjørn Alf, MH	Simplified methods applied to nonlinear motion of spar platforms. (Dr.Ing. Thesis)
MTA-2001-142	Samdal, Ole Johan, MM	Modelling of Degradation Mechanisms and Stressor Interaction on Static Mechanical Equipment Residual Lifetime. (Dr.Ing. Thesis)
MTA-2001-143	Baarholm, Rolf Jarle, MH	Theoretical and experimental studies of wave impact underneath decks of offshore platforms. (Dr.Ing. Thesis)
MTA-2001-144	Wang, Lihua, MK	Probabilistic Analysis of Nonlinear Wave-induced Loads on Ships. (Dr.Ing. Thesis)
MTA-2001-145	Kristensen, Odd H. Holt, MK	Ultimate Capacity of Aluminium Plates under Multiple Loads, Considering HAZ Properties. (Dr.Ing. Thesis)
MTA-2001-146	Greco, Marilena, MH	A Two-Dimensional Study of Green-Water

Loading. (Dr.Ing. Thesis)

MTA-2001-147	Heggelund, Svein E., MK	Calculation of Global Design Loads and Load Effects in Large High Speed Catamarans. (Dr.Ing. Thesis)
MTA-2001-148	Babalola, Olusegun T., MK	Fatigue Strength of Titanium Risers – Defect Sensitivity. (Dr.Ing. Thesis)
MTA-2001-149	Mohammed, Abuu K., MK	Nonlinear Shell Finite Elements for Ultimate Strength and Collapse Analysis of Ship Structures. (Dr.Ing. Thesis)
MTA-2002-150	Holmedal, Lars E., MH	Wave-current interactions in the vicinity of the sea bed. (Dr.Ing. Thesis)
MTA-2002-151	Rognebakke, Olav F., MH	Sloshing in rectangular tanks and interaction with ship motions. (Dr.Ing. Thesis)
MTA-2002-152	Lader, Pål Furset, MH	Geometry and Kinematics of Breaking Waves. (Dr.Ing. Thesis)
MTA-2002-153	Yang, Qinzheng, MH	Wash and wave resistance of ships in finite water depth. (Dr.Ing. Thesis)
MTA-2002-154	Melhus, Øyvin, MM	Utilization of VOC in Diesel Engines. Ignition and combustion of VOC released by crude oil tankers. (Dr.Ing. Thesis)
MTA-2002-155	Ronæss, Marit, MH	Wave Induced Motions of Two Ships Advancing on Parallel Course. (Dr.Ing. Thesis)
MTA-2002-156	Økland, Ole D., MK	Numerical and experimental investigation of whipping in twin hull vessels exposed to severe wet deck slamming. (Dr.Ing. Thesis)
MTA-2002-157	Ge, Chunhua, MK	Global Hydroelastic Response of Catamarans due to Wet Deck Slamming. (Dr.Ing. Thesis)
MTA-2002-158	Byklum, Eirik, MK	Nonlinear Shell Finite Elements for Ultimate Strength and Collapse Analysis of Ship Structures. (Dr.Ing. Thesis)
IMT-2003-1	Chen, Haibo, MK	Probabilistic Evaluation of FPSO-Tanker Collision in Tandem Offloading Operation. (Dr.Ing. Thesis)
IMT-2003-2	Skaugset, Kjetil Bjørn, MK	On the Suppression of Vortex Induced Vibrations of Circular Cylinders by Radial Water Jets. (Dr.Ing. Thesis)
IMT-2003-3	Chezhian, Muthu	Three-Dimensional Analysis of Slamming. (Dr.Ing. Thesis)
IMT-2003-4	Buhaug, Øyvind	Deposit Formation on Cylinder Liner Surfaces in Medium Speed Engines. (Dr.Ing. Thesis)
IMT-2003-5	Tregde, Vidar	Aspects of Ship Design: Optimization of Aft Hull with Inverse Geometry Design. (Dr.Ing. Thesis)
IMT-	Wist, Hanne Therese	Statistical Properties of Successive Ocean Wave

2003-6		Parameters. (Dr.Ing. Thesis)
IMT-2004-7	Ransau, Samuel	Numerical Methods for Flows with Evolving Interfaces. (Dr.Ing. Thesis)
IMT-2004-8	Soma, Torkel	Blue-Chip or Sub-Standard. A data interrogation approach of identity safety characteristics of shipping organization. (Dr.Ing. Thesis)
IMT-2004-9	Ersdal, Svein	An experimental study of hydrodynamic forces on cylinders and cables in near axial flow. (Dr.Ing. Thesis)
IMT-2005-10	Brodtkorb, Per Andreas	The Probability of Occurrence of Dangerous Wave Situations at Sea. (Dr.Ing. Thesis)
IMT-2005-11	Yttervik, Rune	Ocean current variability in relation to offshore engineering. (Dr.Ing. Thesis)
IMT-2005-12	Fredheim, Arne	Current Forces on Net-Structures. (Dr.Ing. Thesis)
IMT-2005-13	Heggernes, Kjetil	Flow around marine structures. (Dr.Ing. Thesis
IMT-2005-14	Fouques, Sebastien	Lagrangian Modelling of Ocean Surface Waves and Synthetic Aperture Radar Wave Measurements. (Dr.Ing. Thesis)
IMT-2006-15	Holm, Håvard	Numerical calculation of viscous free surface flow around marine structures. (Dr.Ing. Thesis)
IMT-2006-16	Bjørheim, Lars G.	Failure Assessment of Long Through Thickness Fatigue Cracks in Ship Hulls. (Dr.Ing. Thesis)
IMT-2006-17	Hansson, Lisbeth	Safety Management for Prevention of Occupational Accidents. (Dr.Ing. Thesis)
IMT-2006-18	Zhu, Xinying	Application of the CIP Method to Strongly Nonlinear Wave-Body Interaction Problems. (Dr.Ing. Thesis)
IMT-2006-19	Reite, Karl Johan	Modelling and Control of Trawl Systems. (Dr.Ing. Thesis)
IMT-2006-20	Smogeli, Øyvind Notland	Control of Marine Propellers. From Normal to Extreme Conditions. (Dr.Ing. Thesis)
IMT-2007-21	Storhaug, Gaute	Experimental Investigation of Wave Induced Vibrations and Their Effect on the Fatigue Loading of Ships. (Dr.Ing. Thesis)
IMT-2007-22	Sun, Hui	A Boundary Element Method Applied to Strongly Nonlinear Wave-Body Interaction Problems. (PhD Thesis, CeSOS)
IMT-2007-23	Rustad, Anne Marthine	Modelling and Control of Top Tensioned Risers. (PhD Thesis, CeSOS)
IMT-2007-24	Johansen, Vegar	Modelling flexible slender system for real-time simulations and control applications
IMT-2007-25	Wroldsen, Anders Sunde	Modelling and control of tensegrity structures.

(PhD Thesis, CeSOS)

IMT-2007-26	Aronsen, Kristoffer Høye	An experimental investigation of in-line and combined inline and cross flow vortex induced vibrations. (Dr. avhandling, IMT)
IMT-2007-27	Gao, Zhen	Stochastic Response Analysis of Mooring Systems with Emphasis on Frequency-domain Analysis of Fatigue due to Wide-band Response Processes (PhD Thesis, CeSOS)
IMT-2007-28	Thorstensen, Tom Anders	Lifetime Profit Modelling of Ageing Systems Utilizing Information about Technical Condition. (Dr.ing. thesis, IMT)
IMT-2008-29	Refsnes, Jon Erling Gorset	Nonlinear Model-Based Control of Slender Body AUVs (PhD Thesis, IMT)
IMT-2008-30	Berntsen, Per Ivar B.	Structural Reliability Based Position Mooring. (PhD-Thesis, IMT)
IMT-2008-31	Ye, Naiquan	Fatigue Assessment of Aluminium Welded Box-stiffener Joints in Ships (Dr.ing. thesis, IMT)
IMT-2008-32	Radan, Damir	Integrated Control of Marine Electrical Power Systems. (PhD-Thesis, IMT)
IMT-2008-33	Thomassen, Paul	Methods for Dynamic Response Analysis and Fatigue Life Estimation of Floating Fish Cages. (Dr.ing. thesis, IMT)
IMT-2008-34	Pákozdi, Csaba	A Smoothed Particle Hydrodynamics Study of Two-dimensional Nonlinear Sloshing in Rectangular Tanks. (Dr.ing.thesis, IMT/ CeSOS)
IMT-2007-35	Grytøyr, Guttorm	A Higher-Order Boundary Element Method and Applications to Marine Hydrodynamics. (Dr.ing.thesis, IMT)
IMT-2008-36	Drummen, Ingo	Experimental and Numerical Investigation of Nonlinear Wave-Induced Load Effects in Containerships considering Hydroelasticity. (PhD thesis, CeSOS)
IMT-2008-37	Skejic, Renato	Maneuvering and Seakeeping of a Singel Ship and of Two Ships in Interaction. (PhD-Thesis, CeSOS)
IMT-2008-38	Harlem, Alf	An Age-Based Replacement Model for Repairable Systems with Attention to High-Speed Marine Diesel Engines. (PhD-Thesis, IMT)
IMT-2008-39	Alsos, Hagbart S.	Ship Grounding. Analysis of Ductile Fracture, Bottom Damage and Hull Girder Response. (PhD-thesis, IMT)
IMT-2008-40	Graczyk, Mateusz	Experimental Investigation of Sloshing Loading and Load Effects in Membrane LNG Tanks Subjected to Random Excitation. (PhD-thesis, CeSOS)
IMT-2008-41	Taghipour, Reza	Efficient Prediction of Dynamic Response for Flexible amd Multi-body Marine Structures. (PhD-

thesis, CeSOS)

IMT-2008-42	Ruth, Eivind	Propulsion control and thrust allocation on marine vessels. (PhD thesis, CeSOS)
IMT-2008-43	Nystad, Bent Helge	Technical Condition Indexes and Remaining Useful Life of Aggregated Systems. PhD thesis, IMT
IMT-2008-44	Soni, Prashant Kumar	Hydrodynamic Coefficients for Vortex Induced Vibrations of Flexible Beams, PhD thesis, CeSOS
IMT-2009-45	Amlashi, Hadi K.K.	Ultimate Strength and Reliability-based Design of Ship Hulls with Emphasis on Combined Global and Local Loads. PhD Thesis, IMT
IMT-2009-46	Pedersen, Tom Arne	Bond Graph Modelling of Marine Power Systems. PhD Thesis, IMT
IMT-2009-47	Kristiansen, Trygve	Two-Dimensional Numerical and Experimental Studies of Piston-Mode Resonance. PhD-Thesis, CeSOS
IMT-2009-48	Ong, Muk Chen	Applications of a Standard High Reynolds Number Model and a Stochastic Scour Prediction Model for Marine Structures. PhD-thesis, IMT
IMT-2009-49	Hong, Lin	Simplified Analysis and Design of Ships subjected to Collision and Grounding. PhD-thesis, IMT
IMT-2009-50	Koushan, Kamran	Vortex Induced Vibrations of Free Span Pipelines, PhD thesis, IMT
IMT-2009-51	Korsvik, Jarl Eirik	Heuristic Methods for Ship Routing and Scheduling. PhD-thesis, IMT
IMT-2009-52	Lee, Jihoon	Experimental Investigation and Numerical in Analyzing the Ocean Current Displacement of Longlines. Ph.d.-Thesis, IMT.
IMT-2009-53	Vestbøstad, Tone Gran	A Numerical Study of Wave-in-Deck Impact usin a Two-Dimensional Constrained Interpolation Profile Method, Ph.d.thesis, CeSOS.
IMT-2009-54	Bruun, Kristine	Bond Graph Modelling of Fuel Cells for Marine Power Plants. Ph.d.-thesis, IMT
IMT 2009-55	Holstad, Anders	Numerical Investigation of Turbulence in a Sekwed Three-Dimensional Channel Flow, Ph.d.-thesis, IMT.
IMT 2009-56	Ayala-Uraga, Efren	Reliability-Based Assessment of Deteriorating Ship-shaped Offshore Structures, Ph.d.-thesis, IMT
IMT 2009-57	Kong, Xiangjun	A Numerical Study of a Damaged Ship in Beam Sea Waves. Ph.d.-thesis, IMT/CeSOS.
IMT 2010-58	Kristiansen, David	Wave Induced Effects on Floaters of Aquaculture Plants, Ph.d.-thesis, CeSOS.

IMT 2010-59	Ludvigsen, Martin	An ROV-Toolbox for Optical and Acoustic Scientific Seabed Investigation. Ph.d.-thesis IMT.
IMT 2010-60	Hals, Jørgen	Modelling and Phase Control of Wave-Energy Converters. Ph.d.thesis, CeSOS.
IMT 2010- 61	Shu, Zhi	Uncertainty Assessment of Wave Loads and Ultimate Strength of Tankers and Bulk Carriers in a Reliability Framework. Ph.d. Thesis, IMT/ CeSOS
IMT 2010-62	Shao, Yanlin	Numerical Potential-Flow Studies on Weakly-Nonlinear Wave-Body Interactions with/without Small Forward Speed, Ph.d.thesis,CeSOS.
IMT 2010-63	Califano, Andrea	Dynamic Loads on Marine Propellers due to Intermittent Ventilation. Ph.d.thesis, IMT.
IMT 2010-64	El Khoury, George	Numerical Simulations of Massively Separated Turbulent Flows, Ph.d.-thesis, IMT
IMT 2010-65	Seim, Knut Sponheim	Mixing Process in Dense Overflows with Emphasis on the Faroe Bank Channel Overflow. Ph.d.thesis, IMT
IMT 2010-66	Jia, Huirong	Structural Analysis of Intect and Damaged Ships in a Collission Risk Analysis Perspective. Ph.d.thesis CeSoS.
IMT 2010-67	Jiao, Linlin	Wave-Induced Effects on a Pontoon-type Very Large Floating Structures (VLFS). Ph.D.-thesis, CeSOS.
IMT 2010-68	Abrahamsen, Bjørn Christian	Sloshing Induced Tank Roof with Entrapped Air Pocket. Ph.d.thesis, CeSOS.
IMT 2011-69	Karimirad, Madjid	Stochastic Dynamic Response Analysis of Spar-Type Wind Turbines with Catenary or Taut Mooring Systems. Ph.d.-thesis, CeSOS.
IMT - 2011-70	Erlend Meland	Condition Monitoring of Safety Critical Valves. Ph.d.-thesis, IMT.
IMT – 2011-71	Yang, Limin	Stochastic Dynamic System Analysis of Wave Energy Converter with Hydraulic Power Take-Off, with Particular Reference to Wear Damage Analysis, Ph.d. Thesis, CeSOS.
IMT – 2011-72	Visscher, Jan	Application of Particla Image Velocimetry on Turbulent Marine Flows, Ph.d.Thesis, IMT.
IMT – 2011-73	Su, Biao	Numerical Predictions of Global and Local Ice Loads on Ships. Ph.d.Thesis, CeSOS.
IMT – 2011-74	Liu, Zhenhui	Analytical and Numerical Analysis of Iceberg Collision with Ship Structures. Ph.d.Thesis, IMT.
IMT – 2011-75	Aarsæther, Karl Gunnar	Modeling and Analysis of Ship Traffic by Observation and Numerical Simulation. Ph.d.Thesis, IMT.

148

Imt – 2011-76	Wu, Jie	Hydrodynamic Force Identification from Stochastic Vortex Induced Vibration Experiments with Slender Beams. Ph.d.Thesis, IMT.
Imt – 2011-77	Amini, Hamid	Azimuth Propulsors in Off-design Conditions. Ph.d.Thesis, IMT.
IMT – 2011-78	Nguyen, Tan-Hoi	Toward a System of Real-Time Prediction and Monitoring of Bottom Damage Conditions During Ship Grounding. Ph.d.thesis, IMT.
IMT-2011-79	Tavakoli, Mohammad T.	Assessment of Oil Spill in Ship Collision and Grounding, Ph.d.thesis, IMT.
IMT-2011-80	Guo, Bingjie	Numerical and Experimental Investigation of Added Resistance in Waves. Ph.d.Thesis, IMT.
IMT-2011-81	Chen, Qiaofeng	Ultimate Strength of Aluminium Panels, considering HAZ Effects, IMT
IMT-2012-82	Kota, Ravikiran S.	Wave Loads on Decks of Offshore Structures in Random Seas, CeSOS.
IMT-2012-83	Sten, Ronny	Dynamic Simulation of Deep Water Drilling Risers with Heave Compensating System, IMT.
IMT-2012-84	Berle, Øyvind	Risk and resilience in global maritime supply chains, IMT.
IMT-2012-85	Fang, Shaoji	Fault Tolerant Position Mooring Control Based on Structural Reliability, CeSOS.
IMT-2012-86	You, Jikun	Numerical studies on wave forces and moored ship motions in intermediate and shallow water, CeSOS.
IMT-2012-87	Xiang ,Xu	Maneuvering of two interacting ships in waves, CeSOS
IMT-2012-88	Dong, Wenbin	Time-domain fatigue response and reliability analysis of offshore wind turbines with emphasis on welded tubular joints and gear components, CeSOS
IMT-2012-89	Zhu, Suji	Investigation of Wave-Induced Nonlinear Load Effects in Open Ships considering Hull Girder Vibrations in Bending and Torsion, CeSOS
IMT-2012-90	Zhou, Li	Numerical and Experimental Investigation of Station-keeping in Level Ice, CeSOS
IMT-2012-91	Ushakov, Sergey	Particulate matter emission characteristics from diesel enignes operating on conventional and alternative marine fuels, IMT
IMT-2013-1	Yin, Decao	Experimental and Numerical Analysis of Combined In-line and Cross-flow Vortex Induced Vibrations, CeSOS

IMT-2013-2	Kurniawan, Adi	Modelling and geometry optimisation of wave energy converters, CeSOS
IMT-2013-3	Al Ryati, Nabil	Technical condition indexes doe auxiliary marine diesel engines, IMT
IMT-2013-4	Firoozkoohi, Reza	Experimental, numerical and analytical investigation of the effect of screens on sloshing, CeSOS
IMT-2013-5	Ommani, Babak	Potential-Flow Predictions of a Semi-Displacement Vessel Including Applications to Calm Water Broaching, CeSOS
IMT-2013-6	Xing, Yihan	Modelling and analysis of the gearbox in a floating spar-type wind turbine, CeSOS
IMT-7-2013	Balland, Océane	Optimization models for reducing air emissions from ships, IMT
IMT-8-2013	Yang, Dan	Transitional wake flow behind an inclined flat plate-----Computation and analysis, IMT
IMT-9-2013	Abdillah, Suyuthi	Prediction of Extreme Loads and Fatigue Damage for a Ship Hull due to Ice Action, IMT
IMT-10-2013	Ramìrez, Pedro Agustìn Pèrez	Ageing management and life extension of technical systems- Concepts and methods applied to oil and gas facilities, IMT
IMT-11-2013	Chuang, Zhenju	Experimental and Numerical Investigation of Speed Loss due to Seakeeping and Maneuvering. IMT
IMT-12-2013	Etemaddar, Mahmoud	Load and Response Analysis of Wind Turbines under Atmospheric Icing and Controller System Faults with Emphasis on Spar Type Floating Wind Turbines, IMT
IMT-13-2013	Lindstad, Haakon	Strategies and measures for reducing maritime CO_2 emissons, IMT
IMT-14-2013	Haris, Sabril	Damage interaction analysis of ship collisions, IMT
IMT-15-2013	Shainee, Mohamed	Conceptual Design, Numerical and Experimental Investigation of a SPM Cage Concept for Offshore Mariculture, IMT
IMT-16-2013	Gansel, Lars	Flow past porous cylinders and effects of biofouling and fish behavior on the flow in and around Atlantic salmon net cages, IMT
IMT-17-2013	Gaspar, Henrique	Handling Aspects of Complexity in Conceptual Ship Design, IMT
IMT-18-2013	Thys, Maxime	Theoretical and Experimental Investigation of a Free Running Fishing Vessel at Small Frequency of Encounter, CeSOS
IMT-19-2013	Aglen, Ida	VIV in Free Spanning Pipelines, CeSOS

IMT-1-2014	Song, An	Theoretical and experimental studies of wave diffraction and radiation loads on a horizontally submerged perforated plate, CeSOS
IMT-2-2014	Rogne, Øyvind Ygre	Numerical and Experimental Investigation of a Hinged 5-body Wave Energy Converter, CeSOS
IMT-3-2014	Dai, Lijuan	Safe and efficient operation and maintenance of offshore wind farms ,IMT
IMT-4-2014	Bachynski, Erin Elizabeth	Design and Dynamic Analysis of Tension Leg Platform Wind Turbines, CeSOS
IMT-5-2014	Wang, Jingbo	Water Entry of Freefall Wedged – Wedge motions and Cavity Dynamics, CeSOS
IMT-6-2014	Kim, Ekaterina	Experimental and numerical studies related to the coupled behavior of ice mass and steel structures during accidental collisions, IMT
IMT-7-2014	Tan, Xiang	Numerical investigation of ship's continuous- mode icebreaking in leverl ice, CeSOS
IMT-8-2014	Muliawan, Made Jaya	Design and Analysis of Combined Floating Wave and Wind Power Facilities, with Emphasis on Extreme Load Effects of the Mooring System, CeSOS
IMT-9-2014	Jiang, Zhiyu	Long-term response analysis of wind turbines with an emphasis on fault and shutdown conditions, IMT
IMT-10-2014	Dukan, Fredrik	ROV Motion Control Systems, IMT
IMT-11-2014	Grimsmo, Nils I.	Dynamic simulations of hydraulic cylinder for heave compensation of deep water drilling risers, IMT
IMT-12-2014	Kvittem, Marit I.	Modelling and response analysis for fatigue design of a semisubmersible wind turbine, CeSOS
IMT-13-2014	Akhtar, Juned	The Effects of Human Fatigue on Risk at Sea, IMT
IMT-14-2014	Syahroni, Nur	Fatigue Assessment of Welded Joints Taking into Account Effects of Residual Stress, IMT
IMT-1-2015	Bøckmann, Eirik	Wave Propulsion of ships, IMT
IMT-2-2015	Wang, Kai	Modelling and dynamic analysis of a semi-submersible floating vertical axis wind turbine, CeSOS
IMT-3-2015	Fredriksen, Arnt Gunvald	A numerical and experimental study of a two-dimensional body with moonpool in waves and current, CeSOS
IMT-4-2015	Jose Patricio Gallardo Canabes	Numerical studies of viscous flow around bluff bodies, IMT

IMT-5-2015	Vegard Longva	Formulation and application of finite element techniques for slender marine structures subjected to contact interactions, IMT
IMT-6-2015	Jacobus De Vaal	Aerodynamic modelling of floating wind turbines, CeSOS
IMT-7-2015	Fachri Nasution	Fatigue Performance of Copper Power Conductors, IMT
IMT-8-2015	Oleh I Karpa	Development of bivariate extreme value distributions for applications in marine technology,CeSOS
IMT-9-2015	Daniel de Almeida Fernandes	An output feedback motion control system for ROVs, AMOS
IMT-10-2015	Bo Zhao	Particle Filter for Fault Diagnosis: Application to Dynamic Positioning Vessel and Underwater Robotics, CeSOS
IMT-11-2015	Wenting Zhu	Impact of emission allocation in maritime transportation, IMT
IMT-12-2015	Amir Rasekhi Nejad	Dynamic Analysis and Design of Gearboxes in Offshore Wind Turbines in a Structural Reliability Perspective, CeSOS
IMT-13-2015	Arturo Jesùs Ortega Malca	Dynamic Response of Flexibles Risers due to Unsteady Slug Flow, CeSOS
IMT-14-2015	Dagfinn Husjord	Guidance and decision-support system for safe navigation of ships operating in close proximity, IMT
IMT-15-2015	Anirban Bhattacharyya	Ducted Propellers: Behaviour in Waves and Scale Effects, IMT
IMT-16-2015	Qin Zhang	Image Processing for Ice Parameter Identification in Ice Management, IMT
IMT-1-2016	Vincentius Rumawas	Human Factors in Ship Design and Operation: An Experiential Learning, IMT
IMT-2-2016	Martin Storheim	Structural response in ship-platform and ship-ice collisions, IMT
IMT-3-2016	Mia Abrahamsen Prsic	Numerical Simulations of the Flow around single and Tandem Circular Cylinders Close to a Plane Wall, IMT
IMT-4-2016	Tufan Arslan	Large-eddy simulations of cross-flow around ship sections, IMT

IMT-5-2016	Pierre Yves-Henry	Parametrisation of aquatic vegetation in hydraulic and coastal research,IMT
IMT-6-2016	Lin Li	Dynamic Analysis of the Instalation of Monopiles for Offshore Wind Turbines, CeSOS
IMT-7-2016	Øivind Kåre Kjerstad	Dynamic Positioning of Marine Vessels in Ice, IMT
IMT-8-2016	Xiaopeng Wu	Numerical Analysis of Anchor Handling and Fish Trawling Operations in a Safety Perspective, CeSOS
IMT-9-2016	Zhengshun Cheng	Integrated Dynamic Analysis of Floating Vertical Axis Wind Turbines, CeSOS
IMT-10-2016	Ling Wan	Experimental and Numerical Study of a Combined Offshore Wind and Wave Energy Converter Concept
IMT-11-2016	Wei Chai	Stochastic dynamic analysis and reliability evaluation of the roll motion for ships in random seas, CeSOS
IMT-12-2016	Øyvind Selnes Patricksson	Decision support for conceptual ship design with focus on a changing life cycle and future uncertainty, IMT
IMT-13-2016	Mats Jørgen Thorsen	Time domain analysis of vortex-induced vibrations, IMT
IMT-14-2016	Edgar McGuinness	Safety in the Norwegian Fishing Fleet – Analysis and measures for improvement, IMT
IMT-15-2016	Sepideh Jafarzadeh	Energy effiency and emission abatement in the fishing fleet, IMT
IMT-16-2016	Wilson Ivan Guachamin Acero	Assessment of marine operations for offshore wind turbine installation with emphasis on response-based operational limits, IMT
IMT-17-2016	Mauro Candeloro	Tools and Methods for Autonomous Operations on Seabed and Water Coumn using Underwater Vehicles, IMT
IMT-18-2016	Valentin Chabaud	Real-Time Hybrid Model Testing of Floating Wind Tubines, IMT
IMT-1-2017	Mohammad Saud Afzal	Three-dimensional streaming in a sea bed boundary layer
IMT-2-2017	Peng Li	A Theoretical and Experimental Study of Wave-induced Hydroelastic Response of a Circular Floating Collar
IMT-3-2017	Martin Bergström	A simulation-based design method for arctic maritime transport systems

153

IMT-4-2017	Bhushan Taskar	The effect of waves on marine propellers and propulsion
IMT-5-2017	Mohsen Bardestani	A two-dimensional numerical and experimental study of a floater with net and sinker tube in waves and current
IMT-6-2017	Fatemeh Hoseini Dadmarzi	Direct Numerical Simualtion of turbulent wakes behind different plate configurations
IMT-7-2017	Michel R. Miyazaki	Modeling and control of hybrid marine power plants
IMT-8-2017	Giri Rajasekhar Gunnu	Safety and effiency enhancement of anchor handling operations with particular emphasis on the stability of anchor handling vessels
IMT-9-2017	Kevin Koosup Yum	Transient Performance and Emissions of a Turbocharged Diesel Engine for Marine Power Plants
IMT-10-2017	Zhaolong Yu	Hydrodynamic and structural aspects of ship collisions
IMT-11-2017	Martin Hassel	Risk Analysis and Modelling of Allisions between Passing Vessels and Offshore Installations
IMT-12-2017	Astrid H. Brodtkorb	Hybrid Control of Marine Vessels – Dynamic Positioning in Varying Conditions
IMT-13-2017	Kjersti Bruserud	Simultaneous stochastic model of waves and current for prediction of structural design loads
IMT-14-2017	Finn-Idar Grøtta Giske	Long-Term Extreme Response Analysis of Marine Structures Using Inverse Reliability Methods
IMT-15-2017	Stian Skjong	Modeling and Simulation of Maritime Systems and Operations for Virtual Prototyping using co-Simulations
IMT-1-2018	Yingguang Chu	Virtual Prototyping for Marine Crane Design and Operations
IMT-2-2018	Sergey Gavrilin	Validation of ship manoeuvring simulation models
IMT-3-2018	Jeevith Hegde	Tools and methods to manage risk in autonomous subsea inspection,maintenance and repair operations
IMT-4-2018	Ida M. Strand	Sea Loads on Closed Flexible Fish Cages
IMT-5-2018	Erlend Kvinge Jørgensen	Navigation and Control of Underwater Robotic Vehicles

IMT-6-2018	Bård Stovner	Aided Intertial Navigation of Underwater Vehicles
IMT-7-2018	Erlend Liavåg Grotle	Thermodynamic Response Enhanced by Sloshing in Marine LNG Fuel Tanks
IMT-8-2018	Børge Rokseth	Safety and Verification of Advanced Maritime Vessels
IMT-9-2018	Jan Vidar Ulveseter	Advances in Semi-Empirical Time Domain Modelling of Vortex-Induced Vibrations
IMT-10-2018	Chenyu Luan	Design and analysis for a steel braceless semi-submersible hull for supporting a 5-MW horizontal axis wind turbine
IMT-11-2018	Carl Fredrik Rehn	Ship Design under Uncertainty
IMT-12-2018	Øyvind Ødegård	Towards Autonomous Operations and Systems in Marine Archaeology
IMT-13-2018	Stein Melvær Nornes	Guidance and Control of Marine Robotics for Ocean Mapping and Monitoring
IMT-14-2018	Petter Norgren	Autonomous Underwater Vehicles in Arctic Marine Operations: Arctic marine research and ice monitoring
IMT-15-2018	Minjoo Choi	Modular Adaptable Ship Design for Handling Uncertainty in the Future Operating Context
MT-16-2018	Ole Alexander Eidsvik	Dynamics of Remotely Operated Underwater Vehicle Systems
IMT-17-2018	Mahdi Ghane	Fault Diagnosis of Floating Wind Turbine Drivetrain- Methodologies and Applications
IMT-18-2018	Christoph Alexander Thieme	Risk Analysis and Modelling of Autonomous Marine Systems
IMT-19-2018	Yugao Shen	Operational limits for floating-collar fish farms in waves and current, without and with well-boat presence
IMT-20-2018	Tianjiao Dai	Investigations of Shear Interaction and Stresses in Flexible Pipes and Umbilicals
IMT-21-2018	Sigurd Solheim Pettersen	Resilience by Latent Capabilities in Marine Systems
IMT-22-2018	Thomas Sauder	Fidelity of Cyber-physical Empirical Methods. Application to the Active Truncation of Slender Marine Structures
IMT-23-2018	Jan-Tore Horn	Statistical and Modelling Uncertainties in the Design of Offshore Wind Turbines

IMT-24-2018	Anna Swider	Data Mining Methods for the Analysis of Power Systems of Vessels
IMT-1-2019	Zhao He	Hydrodynamic study of a moored fish farming cage with fish influence
IMT-2-2019	Isar Ghamari	Numerical and Experimental Study on the Ship Parametric Roll Resonance and the Effect of Anti-Roll Tank
IMT-3-2019	Håkon Strandenes	Turbulent Flow Simulations at Higher Reynolds Numbers
IMT-4-2019	Siri Mariane Holen	Safety in Norwegian Fish Farming – Concepts and Methods for Improvement
IMT-5-2019	Ping Fu	Reliability Analysis of Wake-Induced Riser Collision
IMT-6-2019	Vladimir Krivopolianskii	Experimental Investigation of Injection and Combustion Processes in Marine Gas Engines using Constant Volume Rig
IMT-7-2019	Anna Maria Kozlowska	Hydrodynamic Loads on Marine Propellers Subject to Ventilation and out of Water Condition.
IMT-8-2019	Hans-Martin Heyn	Motion Sensing on Vessels Operating in Sea Ice: A Local Ice Monitoring System for Transit and Stationkeeping Operations under the Influence of Sea Ice
IMT-9-2019|	Stefan Vilsen	Method for Real-Time Hybrid Model Testing of Ocean Structures – Case on Slender Marine Systems
IMT-10-2019	Finn-Christian W. Hanssen	Non-Linear Wave-Body Interaction in Severe Waves
IMT-11-2019	Trygve Olav Fossum	Adaptive Sampling for Marine Robotics
IMT-12-2019	Jørgen Bremnes Nielsen	Modeling and Simulation for Design Evaluation
IMT-13-2019	Yuna Zhao	Numerical modelling and dyncamic analysis of offshore wind turbine blade installation
IMT-14-2019	Daniela Myland	Experimental and Theoretical Investigations on the Ship Resistance in Level Ice
IMT-15-2019	Zhengru Ren	Advanced control algorithms to support automated offshore wind turbine installation
IMT-16-2019	Drazen Polic	Ice-propeller impact analysis using an inverse propulsion machinery simulation approach
IMT-17-2019	Endre Sandvik	Sea passage scenario simulation for ship system performance evaluation

IMT-18-2019	Loup Suja-Thauvin	Response of Monopile Wind Turbines to Higher Order Wave Loads
IMT-19-2019	Emil Smilden	Structural control of offshore wind turbines – Increasing the role of control design in offshore wind farm development
IMT-20-2019	Aleksandar-Sasa Milakovic	On equivalent ice thickness and machine learning in ship ice transit simulations
IMT-1-2020	Amrit Shankar Verma	Modelling, Analysis and Response-based Operability Assessment of Offshore Wind Turbine Blade Installation with Emphasis on Impact Damages
IMT-2-2020	Bent Oddvar Arnesen Haugaløkken	Autonomous Technology for Inspection, Maintenance and Repair Operations in the Norwegian Aquaculture
IMT-3-2020	Seongpil Cho	Model-based fault detection and diagnosis of a blade pitch system in floating wind turbines
IMT-4-2020	Jose Jorge Garcia Agis	Effectiveness in Decision-Making in Ship Design under Uncertainty
IMT-5-2020	Thomas H. Viuff	Uncertainty Assessment of Wave-and Current-induced Global Response of Floating Bridges
IMT-6-2020	Fredrik Mentzoni	Hydrodynamic Loads on Complex Structures in the Wave Zone
IMT-7-2020	Senthuran Ravinthrakumar	Numerical and Experimental Studies of Resonant Flow in Moonpools in Operational Conditions
IMT-8-2020	Stian Skaalvik Sandøy	Acoustic-based Probabilistic Localization and Mapping using Unmanned Underwater Vehicles for Aquaculture Operations
IMT-9-2020	Kun Xu	Design and Analysis of Mooring System for Semi-submersible Floating Wind Turbine in Shallow Water
IMT-10-2020	Jianxun Zhu	Cavity Flows and Wake Behind an Elliptic Cylinder Translating Above the Wall
IMT-11-2020	Sandra Hogenboom	Decision-making within Dynamic Positioning Operations in the Offshore Industry – A Human Factors based Approach
IMT-12-2020	Woongshik Nam	Structural Resistance of Ship and Offshore Structures Exposed to the Risk of Brittle Failure
IMT-13-2020	Svenn Are Tutturen Værnø	Transient Performance in Dynamic Positioning of Ships: Investigation of Residual Load Models and Control Methods for Effective Compensation
IMT-14-2020	Mohd Atif Siddiqui	Experimental and Numerical Hydrodynamic Analysis of a Damaged Ship in Waves
IMT-15-2020	John Marius Hegseth	Efficient Modelling and Design Optimization of Large Floating Wind Turbines

IMT-16-2020	Asle Natskår	Reliability-based Assessment of Marine Operations with Emphasis on Sea Transport on Barges
IMT-17-2020	Shi Deng	Experimental and Numerical Study of Hydrodynamic Responses of a Twin-Tube Submerged Floating Tunnel Considering Vortex-Induced Vibration
IMT-18-2020	Jone Torsvik	Dynamic Analysis in Design and Operation of Large Floating Offshore Wind Turbine Drivetrains
IMT-1-2021	Ali Ebrahimi	Handling Complexity to Improve Ship Design Competitiveness
IMT-2-2021	Davide Proserpio	Isogeometric Phase-Field Methods for Modeling Fracture in Shell Structures
IMT-3-2021	Cai Tian	Numerical Studies of Viscous Flow Around Step Cylinders
IMT-4-2021	Farid Khazaeli Moghadam	Vibration-based Condition Monitoring of Large Offshore Wind Turbines in a Digital Twin Perspective
IMT-5-2021	Shuaishuai Wang	Design and Dynamic Analysis of a 10-MW Medium-Speed Drivetrain in Offshore Wind Turbines
IMT-6-2021	Sadi Tavakoli	Ship Propulsion Dynamics and Emissions
IMT-7-2021	Haoran Li	Nonlinear wave loads, and resulting global response statistics of a semi-submersible wind turbine platform with heave plates
IMT-8-2021	Einar Skiftestad Ueland	Load Control for Real-Time Hybrid Model Testing using Cable-Driven Parallel Robots
IMT-9-2021	Mengning Wu	Uncertainty of machine learning-based methods for wave forecast and its effect on installation of offshore wind turbines
IMT-10-2021	Xu Han	Onboard Tuning and Uncertainty Estimation of Vessel Seakeeping Model Parameters
IMT-01-2022	Ingunn Marie Holmen	Safety in Exposed Aquacultrue Operations
IMT-02-2022	Prateek Gupta	Ship Performance Monitoring using In-service Measurements and Big Data Analysis Methods